

Experimental and Computational Approaches to Predict Glucuronidation of Phenolics

A Dissertation Presented to the

Faculty of the Department of Pharmacological and Pharmaceutical Sciences

College of Pharmacy, University of Houston

In Partial Fulfillment of

the Requirements for the Degree of

Doctor of Philosophy

By

Baojian Wu

December, 2011

Acknowledgements

I would like to take this opportunity to acknowledge many people who have made my stay at the College of Pharmacy memorable.

Special thanks are reserved for my advisor Dr. Ming Hu, who helped and encouraged me all through my graduate years and continues to support, inspire and guide me. I know I will continue to lean on you for supports wherever my career takes me to. Thank you for taking me as your student.

I would also like to sincerely thank my dissertation committee members, Drs. Diana Chow, Romi Ghose, Vincent Tam, and Shuxing Zhang for their continuous supports and valuable inputs.

I have to also thank Dr. Xiaoqiang Wang from Noble foundation, and Mr. John Morrow from The University of Texas MD Anderson Cancer Center. They provided excellent comments and suggestions to this thesis work.

I also want to thank fellow graduate students, especially Rashim Singh, Wen Jiang, Zhen Yang, Sumit Basu, and Tao Niu of the Department of Pharmacological and Pharmaceutical Sciences for all the supports you gave me.

Lastly, thank you my wife Dong Dong for being there and absorbing all my pains and worries when things did not seem to be moving, for that I will always love you.

Abstract

[Purpose] UDP-glucuronosyltransferases (UGTs) catalyze the glucuronidation reaction which has been increasingly recognized as an important metabolic and detoxification pathway. Contrasting with the functional significance of UGTs, little is known about the molecular mechanisms of how UGT recognizes its substrates. Therefore, the overall goal of this thesis is to elucidate the catalytic selectivity of human UGTs. To approach this goal, three specific aims are 1) to determine the regioselectivity of UGT1A isoforms via kinetic profiling (a) and to identify two *in vitro* probes for hepatic UGT1A1 based on the enzyme's regioselectivity (b); 2) to determine the UGT1A9-mediated glucuronidation parameters for selected flavonols (n=30) and establish a pharmacophore-based *in silico* model using this dataset; 3) to determine UGT1A9-mediated glucuronidation parameters for a large class of structurally diverse phenolics (n=145) and to establish a more generalized *in silico* model based on this large database.

[Methods] In the absence of a three-dimensional structure of the full-length enzyme, we employed a ligand-based QSAR approach in combination with experimentally determined “expert” knowledge. “Expert” knowledge was incorporated into a model to tackle the challenges in model construction and to ensure model quality. On the experimental side, the interaction of UGT-substrate was characterized by kinetic determination, which involves measuring glucuronidation rates at various concentrations of a substrate, and deriving the kinetic parameters (K_m , V_{max} , and CL_{int}) by model fitting. On the *in silico* side, powerful QSAR techniques (Comparative Molecular Field Analysis (CoMFA) and/or Comparative Molecular Similarity Indices Analysis (CoMSIA)) combined

with protein homology modeling were used to analyze the structure-activity relationships and uncover the structural features for good or poor UGT substrates.

[Results] 1a) UGT1A1 and 1A3 regioselectively metabolize 7-OH of flavonols, whereas UGT1A7, 1A8, 1A9 and 1A10 prefer to glucuronidate 3-OH group. UGT1A1 and 1A9 are the most efficient conjugating enzymes with K_m values of $\leq 1 \mu\text{M}$. **1b)** UGT1A1 and 1A9 are the main isoforms for glucuronidating the two flavonoid probes 3,3',4'-trihydroxyflavone (33'4'THF) and 3,6,4'-trihydroxyflavone (364'THF), where UGT1A1 accounts for $92 \pm 7 \%$ and $91 \pm 10 \%$ of 4'-O-glucuronidation of 33'4'THF and 364'THF, respectively, and UGT1A9 accounts for most of the 3-O-glucuronidation. Highly significant correlations ($R^2_{\text{adj}} > 0.944$, $p < 0.0001$) between the rates of flavonoids 4'-O-glucuronidation and that of estradiol-3-glucuronidation or SN-38 glucuronidation are observed across 12 human liver microsomes (HLMs). **2)** The derived CoMFA models for 30 flavonols possess good internal and external consistency and show statistical significance and substantive predictive abilities (V_{max} model: $q^2 = 0.738$, $r^2 = 0.976$, $r^2_{\text{pred}} = 0.735$; CL_{int} model: $q^2 = 0.561$, $r^2 = 0.938$, $r^2_{\text{pred}} = 0.630$). The contour maps derived from CoMFA modeling clearly indicate structural characteristics associated with rapid or slow 3-O-glucuronidation of flavonols. **3)** The 3D-QSAR analyses based on 145 phenolics produce statistically reliable models with good predictive power (CoMFA: $q^2 = 0.548$, $r^2 = 0.949$, $r^2_{\text{pred}} = 0.775$; CoMSIA: $q^2 = 0.579$, $r^2 = 0.876$, $r^2_{\text{pred}} = 0.700$). The contour coefficient maps generated from CoMFA/CoMSIA are applied to elucidate structural features among substrates that are responsible for the selectivity differences. Furthermore, the contour coefficient maps are overlaid in the catalytic pocket of a

homology model of UGT1A9; this enabled us to identify the UGT1A9 catalytic pocket with a high degree of confidence.

[Conclusion] The extensive kinetic characterization on the formation of multiple glucuronides from a UGT substrate indicates that multiple distinct binding modes within the catalytic domain are possible for a substrate molecule. Interestingly, in our study, formation of 4'-O-glucuronides from 3,3',4',4'-THF and 3,6,4'-THF is proven to be the excellent markers for hepatic UGT1A1, and for UGT1A1-mediated glucuronidation of SN-38. Further, we for the first time demonstrate that the approach of coupling CoMFA analysis with a pharmacophore-based structural alignment is viable for constructing a predictive model for regiospecific glucuronidation of flavonols by UGT1A9. In addition, based on a large set of structurally diverse molecules (including those with multiple glucuronidation sites), the 3D-QSAR techniques CoMFA/CoMSIA can be used to predict the substrate selectivity of UGT1A9. Our findings also provide a possible molecular basis for understanding UGT1A9 functions and its substrate selectivity.

List of Tables

Table 1.	Normalized catalytic efficiencies (based on the relative UGT1A expression levels) of six recombinant human UGT1As in glucuronidation of flavonoids. Relative catalytic efficiency ($V_{\max}/K_m = 1.0$) was arbitrarily assigned for the 3-O-glucuronidation of 3,7DHF by UGT1A1.....	52
Table 2.	Flavonols used in the work (see Figure.28 for chemical structures).....	97
Table 3.	Kinetics parameters of UGT1A9 mediated 3-O-glucuronidation with flavonols, together with the predicted V_{\max} and CL_{int} values from their respective CoMFA models.	102
Table 4.	Summary of modeling parameters from CoMFA analysis	104
Table 5.	Experimentally determined kinetic parameters for UGT1A9-mediated glucuronidation of 145 compounds, including 2 catechins (No.1-2), 5 chalcones (No.3-7), 1 chromone (No.8), 6 coumarins (No.9-14), 3 curcumins (No.15-17), 6 aromatic hydrocarbons (No.18-23), 4 flavanones (No.24-27), 31 flavones (No.28-58), 36 flavonols (No.59-94), 3 hydroxycinnamic acids (No.95-97), 11 isoflavones (No.98-108), 27 phenols (No.109-135), and 7 other compounds (No.136-145). The chemical structures of all compounds are shown in Appendix A. The site of glucuronidation is indicated in the parenthesis. For a compound with multiple glucuronides generated, a lower-case letter is appended for a distinction.	138
Table 6.	Summary of modeling parameters from CoMFA and CoMSIA analyses.....	147

List of Figures

Figure 1.	The glucuronidation reaction catalyzed by UGT	2
Figure 2.	Phylogenetic tree of human UGT enzymes showing evolutionary distances between different isoforms	6
Figure 3.	Relative mRNA distribution level between human UGT1A isoforms (left) and between 2B isoforms (right) in human liver (A/B), small intestine (C/D) and colon (E/F)	8
Figure 4.	Schematic representation of human UGT topology	10
Figure 5.	Cartoon representation of glycosyltransferase GT-A (a) and GT-B (b) folds..	12
Figure 6.	Two main catalytic mechanisms of glycosyltransferases: retention (a) or inversion (b) of the anomeric configuration.	13
Figure 7.	Schematic representation of proposed catalytic mechanisms for human UGTs using UGT1A10 as an example	18
Figure 8.	Sequential kinetic mechanisms involving two substrate and two products.....	20
Figure 9.	Phosphorylation sites of UGT isoforms and their locations in UGT homology structure	22
Figure 10.	Schematic presentation of the enteric and hepatoenteric recycling in glucuronidation pathway (D, aglycone; M, glucuronide).....	31
Figure 11.	General research strategy	37
Figure 12.	A structural comparison of the model flavonols in Study I	43
Figure 13.	Relative protein quantification of UGT isoforms	47
Figure 14.	Kinetic profiles for UGT1A1-mediated glucuronidation of four flavonols (3,7DHF, 3,5,7THF, 3,7,4'THF and 3,5,7,4'QHF)	49
Figure 15.	Kinetic profiles for UGT1A3-mediated glucuronidation of three flavonols (3,7DHF, 3,5,7THF and 3,5,7,4'QHF)	51
Figure 16.	Kinetic profiles for UGT1A7-mediated glucuronidation of three flavonols (3,7DHF, 3,5,7THF and 3,5,7,4'QHF).	53
Figure 17.	Kinetic profiles for UGT1A8-mediated glucuronidation of three flavonols (3,7DHF, 3,5,7THF and 3,5,7,4'QHF).	55
Figure 18.	Kinetic profiles for UGT1A9-mediated glucuronidation of four flavonols (3,7DHF, 3,5,7THF, 3,7,4'THF and 3,5,7,4'QHF).	57
Figure 19.	Kinetic profiles of UGT1A10-mediated glucuronidation of three flavonols (3,7DHF, 3,5,7THF and 3,5,7,4'QHF).	58

Figure 20.	Phenotyping of 33'4'THF (top) and 364'THF (bottom) using 12 recombinant UGTs	74
Figure 21.	Kinetic profiles (panel a) and parameters (panel b) of glucuronidation derived from incubation of 3,3',4'-trihydroxyflavone (33'4'THF) with pooled human liver microsomes (pHLM), recombinant UGT1A1 and UGT1A9.....	76
Figure 22.	Kinetic profiles (top) and parameters (bottom) of glucuronidation of estradiol (a) and propofol (b) using recombinant UGTs and pooled human liver microsomes,	77
Figure 23.	Kinetic profiles (panel a) and parameters (panel b) of glucuronidation derived from incubation of 3,6,4'-trihydroxyflavone (364'THF) with pooled human liver microsomes (pHLM), recombinant UGT1A1 and UGT1A9.....	79
Figure 24.	Expression-activity correlation for UGT1A1 in human livers.....	80
Figure 25.	UGT1A1 activity correlation between flavonoid-4'-O-glucuronidation (top: 33'4'THF; bottom: 364'THF) and estradiol-3-glucuronidation in a bank of HLMS (n=12).	82
Figure 26.	Rate correlations between SN-38 glucuronidation and flavonoid glucuronidation (4'-OH)	83
Figure 27.	UGT1A9 activity correlation between flavonoid-3-O-glucuronidation (top: 33'4'THF; bottom: 364'THF) and propofol glucuronidation in a bank of HLMS (n=12).	87
Figure 28.	Backbone of flavonol structures (See Table 2 for the definitions of the substituents).....	96
Figure 29.	Structural modifications affect the K_m values of UGT1A9-mediated 3-O-glucuronidation.	103
Figure 30.	Two hypothetically distinct flavonol orientations that are required to generate 3-O-glucuronide (panel 1 or 3) and 7-O-glucuronide (panel 2 or 4).	106
Figure 31.	3-OH specific pharmacophore model	108
Figure 32.	Structural alignment for constructing 3D-QSAR CoMFA model generated from the 3-OH specific pharmacophore.	109
Figure 33.	Correlation between the experimental glucuronidation parameters and the predicted ones from the CoMFA models for the training and test sets (a, V_{max} ; b, CL_{int}).	111
Figure 34.	Steric and electrostatic maps from the UGT1A9 CoMFA model of V_{max}	112
Figure 35.	Steric and electrostatic maps from the UGT1A9 CoMFA model of CL_{int}	116
Figure 36.	Representative fitting of the model equations (eqs.1-3) to kinetic data of UGT1A9 with its substrates.....	131

Figure 37.	A flexible alignment of three most active substrates (66: 3-hydroxy-6-methylflavone, 140: entacapone; 52: chrysin).....	133
Figure 38.	A wide diversity in both chemical structure (a) and activity (b) for UGT1A9 substrates in this study.....	134
Figure 39.	Correlations between the experimental glucuronidation parameters and the predicted ones from the 3D-QSAR models	148
Figure 40.	Field contribution maps from the CoMFA analysis.	150
Figure 41.	Field contribution maps from the CoMSIA analysis.....	151
Figure 42.	Three-dimensional model of the UGT1A9-kaempferol (88.a) complex.	154
Figure 43.	Superposition of the CoMFA/CoMSIA contour maps over the binding site of a homology-modeled UGT1A9 structure based on a simulated binding model of kaempferol (3-OH).	156

List of Abbreviations

2D/3D	2-Dimensional/3-Dimensional
Å	Ångström, 10^{-10} m
ADME	Absorption, Distribution, Metabolism, and Elimination;
AT _{ER}	ER-localized organic anion transporters
CAZy	Carbohydrate-Active enZymes database
cDNA	Complementary DNA
CL _{int}	Intrinsic clearance
CN-I	Crigler-Najjar syndrome type I
CN-II	Crigler-Najjar syndrome type II
CoMFA	Comparative molecular field analysis;
CoMSIA	Comparative Molecular Similarity Indices Analysis;
CYPs	Cytochrome P450;
DHF	Dihydroxyflavone
DHMF	Dihydroxy- methoxyflavone
DMHF	Dimethoxy- hydroxyflavones
Don & Acc	Hydrogen bond donor and acceptor
ER	Endoplasmic reticulum
FDA	Food and Drug Administration
GT1	Family 1 of glycosyltransferases
GTs	Glycosyltransferases
HF	Hydroxyflavone
HLM	Human Liver Microsomes
HNF-1	hepatocyte nuclear factor
K _{i,app}	Apparent inhibitor constant
K _m	Michaelis constant
MHF	Methoxy-hydroxyflavone
MS	Mass spectroscopy
NMR	Nuclear magnetic resonance
NSTs	nucleotide sugar transporters
pHLM	Pooled Human Liver Microsomes
PKC	protein kinase C

PLS	Partial Least Squares
QHF	Tetrahydroxyflavone
QSAR	Quantitative Structure Activity Relationship;
RAF	Relative Activity Factor
S _N 2	Bimolecular nucleophilic substitution
SN-38	7-Ethyl-10-hydroxycamptothecin
SrcTK	Src tyrosine kinase
THF	Trihydroxyflavone
UDPGA	Uridine diphosphoglucuronic acid
UDPGlcNAC	UDP-N-acetyl glucosamine
UGT	UDP-glucuronosyltransferase
UGT71G1	Triterpene/flavonoid glycosyltransferase from the legume <i>Medicago truncatula</i>
UPLC	Ultra performance liquid chromatography
UPLC	Ultra performance liquid chromatography;
V _{max}	Maximum velocity
VvGT1	UPD-glucose: flavonoid 3-O-glucosyltransferase from red grape (<i>Vitis vinifera</i>)

Amino acids

A	Ala	Alanine
R	Arg	Arginine
N	Asn	Asparagine
D	Asp	Aspartate
C	Cys	Cysteine
E	Glu	Glutamate
Q	Gln	Glutamine
G	Gly	Glycine
H	His	Histidine
I	Ile	Isoleucine
L	Leu	Leucine
K	Lys	Lysine
M	Met	Methionine
F	Phe	Phenylalanine
P	Pro	Proline
S	Ser	Serine
T	Thr	Threonine
W	Trp	Tryptophan
Y	Tyr	Tyrosine
V	Val	Valine

Contents

Acknowledgements	i
Abstract	ii
List of Tables	v
List of Figures	vi
List of Abbreviations	ix
Chapter 1 Review of the literature	1
1.1. Introduction to the project	1
1.2. Hyperbilirubinemia	3
1.3. UDP-Glucuronosyltransferases	4
1.3.1. The human UGT superfamily	4
1.3.2. Distribution of UGTs in GI tract and liver	5
1.3.3. Topology of UGTs in ER membrane	9
1.3.4. Structure and catalytic mechanisms	11
1.3.5. Homology structure models of UGTs	15
1.3.6. Catalytic mechanism	17
1.3.7. Regulation of UGTs by phosphorylation	21
1.4. Glucuronidation of phenolics	23
1.4.1. Species-dependent glucuronidation	24
1.4.2. Gender-dependent glucuronidation	24
1.4.3. Intestinal vs. hepatic glucuronidation	25
1.4.4. Isoform-specific glucuronidation	26
1.4.5. Compensation between UGT1As and 2Bs	27
1.4.6. Regioselective glucuronidation	27
1.5. Enteric and hepatoenteric recycling	30
1.6. Deglucuronidation by β -glucuronidase	32
1.7. Structure-glucuronidation relationships	33
1.8. Summary	34
Chapter 2 Hypotheses and specific aims	35

2.1. Central hypothesis	35
2.2. Specific aims	35
2.2.1. Aim I (Studies I + II)	35
2.2.2. Aim II (Study III)	35
2.2.3. Aim III (Study IV).....	36
2.2.4. General strategy	36
Chapter 3 Regioselective glucuronidation of flavonols by six human UGT1A isoforms (Study I).....	38
3.1. Abstract	38
3.2. Introduction.....	39
3.3. Materials and methods	42
3.3.1. Materials	42
3.3.2. Immunoblotting	42
3.3.3. UGTs kinetics.....	44
3.3.4. UPLC analysis of flavonols and glucuronides:.....	44
3.3.5. Glucuronide structure identification.....	44
3.3.6. Data analysis	45
3.3.7. Statistical analysis.....	46
3.4. Results.....	46
3.4.1. Relative expression level between the UGT1A enzymes	46
3.4.2. Regioselective glucuronidation of flavonols by UGT1A1	46
3.4.3. Regioselective glucuronidation of flavonols by UGT1A3	50
3.4.4. Regioselective glucuronidation of flavonols by UGT1A7	50
3.4.5. Regioselective glucuronidation of flavonols by UGT1A8	54
3.4.6. Regioselective glucuronidation of flavonols by UGT1A9	56
3.4.7. Regioselective glucuronidation of flavonols by UGT1A10	56
3.4.8. Relative catalytic efficiencies between UGT1A enzymes	59
3.5. Discussion	60
Chapter 4 Evaluation of 3,3',4'-trihydroxyflavone and 3,6,4'-trihydroxyflavone as the in vitro functional markers for hepatic UGT1A1 (Study II).....	65
4.1. Abstract	65

4.2. Introduction	66
4.3. Materials and methods	69
4.3.1. Materials	69
4.3.2. Immunoblotting	70
4.3.3. Glucuronidation assay and kinetics	70
4.3.4. UPLC analysis:	71
4.3.5. Identification of the structure of flavonoid glucuronide	71
4.3.6. Data analysis	72
4.3.7. UGT1A1 and 1A9 relative activity factor determination	72
4.4. Results.....	73
4.4.1. UGTs involved in 33'4'THF and 364'THF glucuronidation.....	73
4.4.2. Contribution of UGT1A1 and 1A9 to metabolism of 33'4'THF in pHLM.....	75
4.4.3. Contribution of UGT1A1 and 1A9 to metabolism of 364'THF in pHLM.....	78
4.4.4. Expression-activity correlation for UGT1A1 in human livers.....	78
4.4.5. UGT1A1 activity correlation analysis	81
4.5. Discussion	84
Chapter 5 3D-QSAR studies on UGT1A9-mediated 3-O-glucuronidation of flavonols using a pharmacophore-based CoMFA model (Study III).....	90
5.1. Abstract	90
5.2. Introduction.....	91
5.3. Materials and methods	95
5.3.1. Materials	95
5.3.2. UGT1A9 enzyme kinetics	98
5.3.3. UPLC analysis of flavonols and their glucuronides:	98
5.3.4. Glucuronide structure confirmation	98
5.3.5. Kinetics analysis	99
5.3.6. Pharmacophore generation and conformation search.....	99
5.3.7. Comparative molecular field analysis (CoMFA).....	100
5.4. Results.....	101
5.4.1. Kinetic parameters for UGT1A9-mediated 3-O-glucuronidation	101
5.4.2. Pharmacophore modeling.....	105

5.4.3. CoMFA models	107
5.4.4. V_{\max} CoMFA model of UGT1A9	110
5.4.5. CL_{int} CoMFA model of UGT1A9	114
5.5. Discussion	117
Chapter 6 Accurate prediction of glucuronidation of structurally diverse phenolics by human UGT1A9 using combined experimental and in silico approaches (Study IV)....	123
6.1. Abstract	123
6.2. Introduction	124
6.3. Materials and methods	127
6.3.1. Materials	127
6.3.2. Enzyme Assays	128
6.3.3. UPLC analysis	128
6.3.4. Identification of glucuronide and glucuronidation site	128
6.3.5. Kinetics analysis	129
6.3.6. Molecular Alignment	130
6.3.7. CoMFA and CoMSIA analyses	132
6.3.8. Homology modeling and molecular docking	135
6.4. Results.....	136
6.4.1. Experimental dataset	136
6.4.2. Predictive power of the analyses	137
6.4.3. CoMFA model	146
6.4.4. CoMSIA model.....	149
6.4.5. Exploring UGT1A9 catalytic pocket using a homology model and CoMFA/CoMSIA maps.....	153
6.5. Discussion	155
Chapter 7 Summary	162
Appendix A: Chemical structures of 145 UGT1A9 substrates in this thesis.....	166
Appendix B: UPLC conditions used for glucuronidation assay and kinetic analysis	171
Appendix C Representative chromatograms	172
References	187

Chapter 1 Review of the literature

1.1. Introduction to the project

UDP-glucuronosyltransferases (UGTs) catalyzed glucuronidation represents an important metabolic and detoxification pathway for numerous endogenous and exogenous compounds, including drugs (e.g., SN-38, mycophenolic acid, and raloxifene), dietary chemicals (e.g., hydroxycinnamic acids and flavonoids), environmental toxins (e.g., benzo(α)pyrene and nitrosamines), bile acids, and steroid hormones. In the glucuronidation reaction, glucuronic acid derived from the cofactor UDP-glucuronic acid (UDPGA) is conjugated to a functional group, mostly a hydroxyl, carboxyl, amine, or thiol group on the substrate (or aglycone), leading to the formation of O-, N-, S-glucuronides, respectively (Figure 1). Although it is rare, the acidic carbon can also be glucuronidated (e.g., sulfinpyrazone and phenylbutazone) (Kerdpin *et al.*, 2006; Nishiyama, *et al.*, 2008).

Due to the nature of the reaction, UGT isoforms have a wide variety of different types (structurally unrelated) of substrates. In addition, one substrate is usually glucuronidated by several isoforms (i.e., overlapping substrate specificity). This kind of promiscuity is advantageous for enzymes involved in detoxification, but it poses significant challenges in identifying a selective UGT probe and in understanding of the mechanisms responsible for the substrate selectivity. In the present thesis, we found that various UGT isoforms display distinct regioselectivity towards flavonols (**Study I**), and then used the regiospecific glucuronidation of (two) flavonols to probe the activity of hepatic UGT1A1

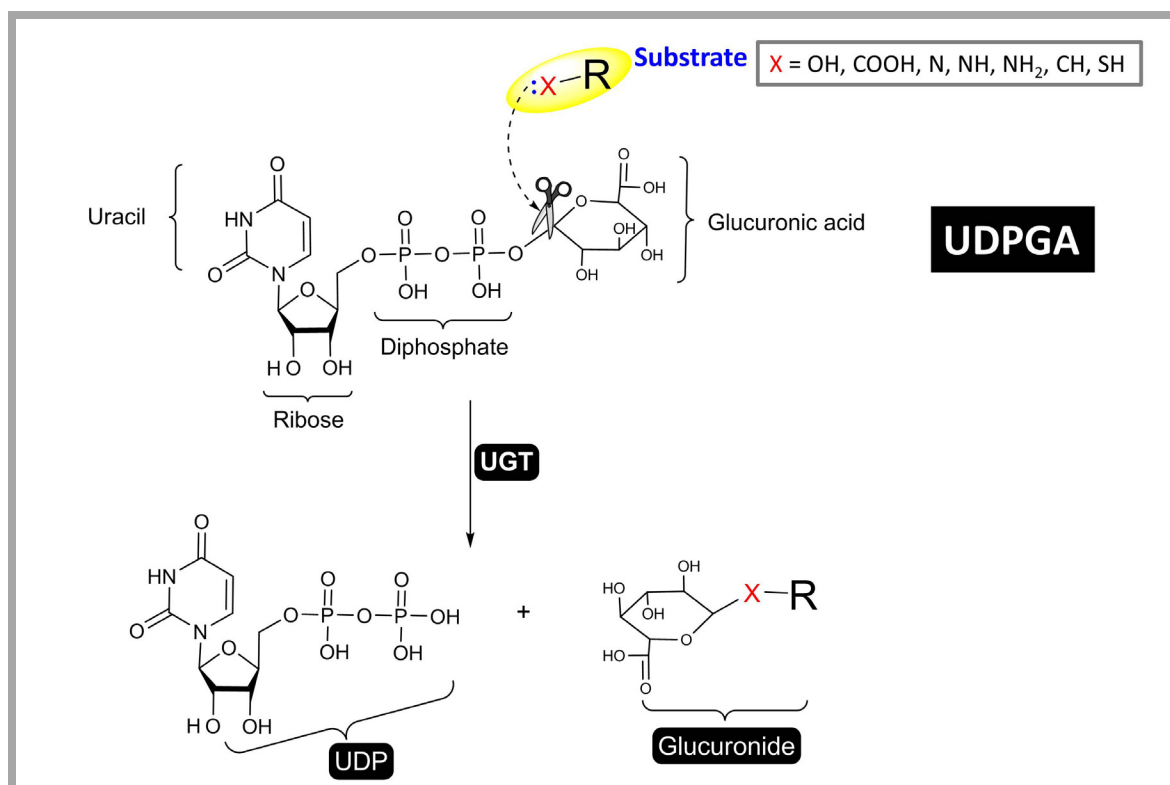


Figure 1. The glucuronidation reaction catalyzed by UGT

(**Study II**). To elucidate the molecular mechanisms for the substrate selectivity, kinetic measurements, 3D-QSAR techniques, and homology modeling were employed (**Studies III and IV**). We have identified the chemical features (i.e., steric and electrostatic properties) for good or poor UGT1A9 substrates, and deduced a binding pocket for UGT1A9 that is largely consistent with experimental data (**Studies III and IV**).

Glucuronidation is an important defense mechanism detoxifying drugs and protecting humans against toxic agents. However, extensive first-pass glucuronidation (or premature clearance by UGTs) can be a significant barrier to oral bioavailability of many phenolics including therapeutic drugs (e.g., phenylephrine and raloxifene) and dietary polyphenols (e.g., stilbenes and flavonoids) with “claimed” health benefits (Hu, 2007; Crozier *et al.*, 2009). One major purpose of the studies in the present thesis is to establish *in silico* models that can be used to predict UGT1A9-mediated glucuronidation and to design a poor substrate with possibly improved bioavailability (**Studies III and IV**).

1.2. Hyperbilirubinemia

Glucuronidation should be the only clearance pathway for bilirubin, the neurotoxic product of hemoglobin. Approximately 250-350 mg/day of bilirubin is produced in human body (Kuntz and Kuntz, 2008). This bilirubin is transported to the liver, where it is conjugated with glucuronic acid prior to excretion into bile. UGT1A1 has been recognized as the main isoform responsible for glucuronidation of bilirubin (Beutler *et al.*,

1998). Elevated levels of free (unconjugated) bilirubin in the serum result in jaundice and a disease state known as hyperbilirubinemia.

At least three forms of hyperbilirubinemia have been classified on the basis of residual UGT1A1 activity or bilirubin level in the serum: Gilbert syndrome and two types of Crigler-Najjar syndrome, CN-I and CN-II (Bosma, 2003). Gilbert syndrome is a mild but very common form (with a penetration rate of 5-10% in Caucasians) of hyperbilirubinemia (Strassburg, 2008). A major cause of this syndrome is the UGT1A1 polymorphism (also known as UGT1A1*28 allele) which has additional TA insertions in the promoter region. This allele reduces gene transcription and UGT1A1 activity to about 20% and 30% of the normal levels, respectively (Bosma, 2003). CN-1 is a very rare, but life-threatening form of hyperbilirubinemia, in which UGT1A1 activity is undetectable. By contrast, CN-2 is a milder hyperbilirubinemia, in which UGT1A1 activity is below 10% of the normal level. Both CN-type are inherited and caused by mutations in UGT1A1 coding exons.

1.3. UDP-Glucuronosyltransferases

1.3.1. The human UGT superfamily

Human UGTs are classified into four families: UGT1, UGT2, UGT3, and UGT8, on the basis of amino acid sequence identity (Mackenzie *et al.*, 2005). The most important drug-conjugating UGTs belong to UGT1 and UGT2 subfamilies or alternatively UGT1A, UGT2A, and UGT2B subfamilies. The human UGT1A gene cluster, located on chromosome 2q37, spans approximately 200 kb. It contains 13 distinct individual promoters/first exons and shared exons 2–5. Each exon 1 spliced to the same exons 2–

5 is regarded as a unique gene which translates to the corresponding active UGT1A proteins excluding the pseudogenes (i.e., UGT1A2p, UGT1A11p, UGT1A12p and UGT1A13p). Since C-terminal half of the protein is encoded by exons 2–5, thus is identical between all UGT1A enzymes. On the other hand, the UGT2B subfamily isoforms are encoded individually and each consists of six exons clustered on chromosome 4q13 ([Mackenzie et al., 2005](#)). At present, 19 human UGT isoforms from UGT1 and UGT2 has been identified; their sequence comparison is presented (Figure 2).

1.3.2. Distribution of UGTs in GI tract and liver

Human liver, as the major metabolic organ, are reported to express a panel of UGT isoforms, including UGT1A1, 1A3, 1A4, 1A5, 1A6, 1A8, 1A9, 2B4, 2B7, 2B10, 2B11, 2B15, and 2B17 ([Tukey and Strassburg, 2000](#)). Recently, mRNA expression level of UGT isoforms in various human tissues was determined and quantitatively compared using an exhaustive (RT-PCR) method. The results (Figure 3) were generally consistent with previous findings, although the authors acknowledged some minor differences due to high inter-individual variability and perhaps low amplification efficiency ([Ohno and Nakajin, 2009](#)). Compared to UGT1As, UGT2Bs are much more abundantly expressed in the liver. Among UGT2Bs, UGT2B4 has the highest expression, followed closely by UGT2B15, which, respectively, had ~9 and 4~ times greater expression than UGT2B7 (Figure 3). Among UGT1A isoforms, 1A1 and 1A9 are most abundantly expressed isoforms in the liver. By contrast, UGT1A10 and 2B17 were found predominantly in the intestines and colon. It is interesting to note that UGT1A7 is expressed only in the

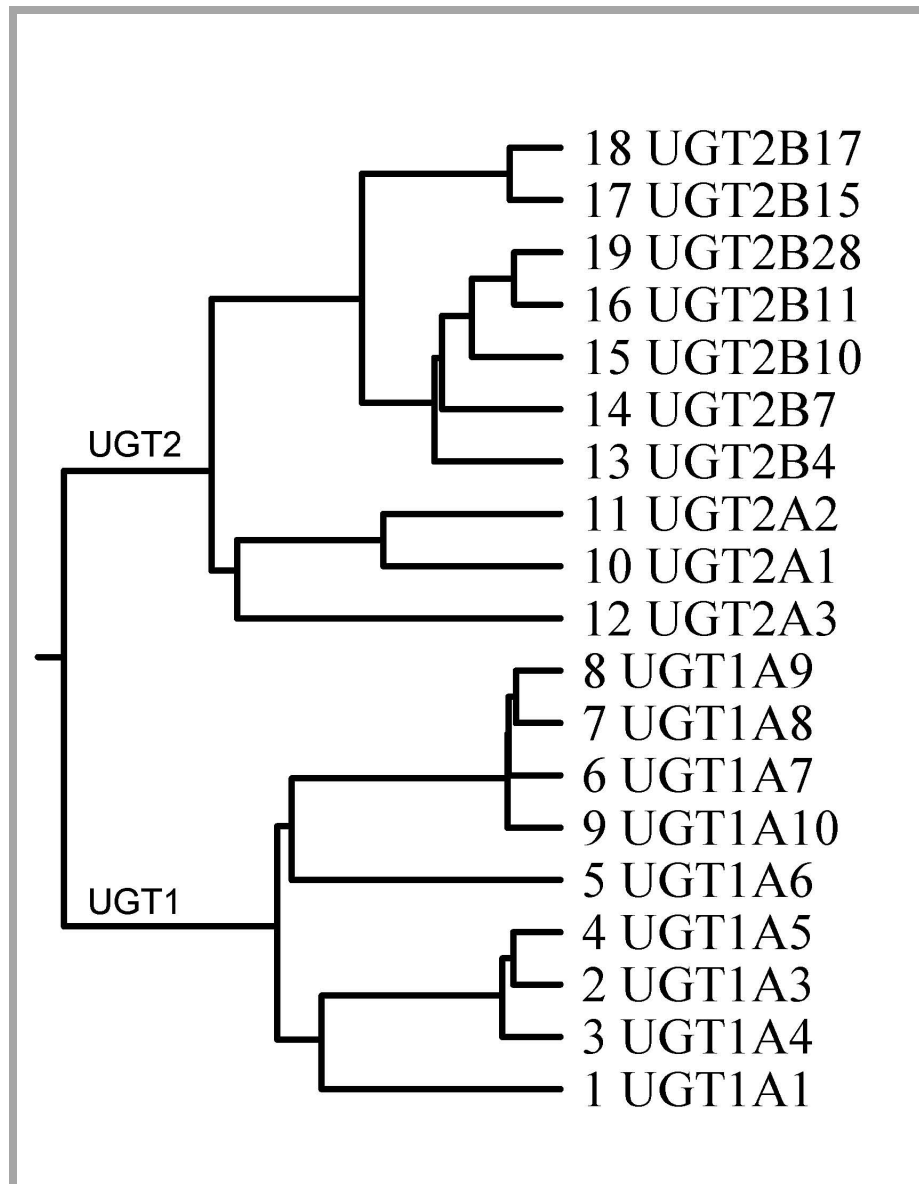


Figure 2. Phylogenetic tree of human UGT enzymes showing evolutionary distances between different isoforms

The sequence alignment was made by ClustalW (Larkin, et al., 2007) and the tree was constructed with the evolutionary Trace Server, TraceSuite II (Innis, et al., 2000).

proximal tissues of the gastrointestinal tract, such as the esophagus and stomach (Ohno and Nakajin, 2009). However, one should be more careful when interpreting data using the mRNA expression level, since one study showed that poor or no correlations were observed between the protein and mRNA levels of UGT isoforms (Izuka *et al.*, 2009).

A panel of 10 Ugt1as (Ugt1a1, 1a2, 1a3, 1a4, 1a5, 1a6, 1a7, 1a8, 1a9, and 1a10) are expressed in rats (Mackenzie *et al.*, 2005; Owens *et al.*, 2005). Rat 2b subfamily consists of six members: Ugt2b1, 2b2, 2b3, 2b6, 2b8, and 2b12. The mRNA expression of rat Ugt1a isoforms is more predominant in both liver and intestine in comparison with other tissues (Shelby *et al.*, 2003). Ugt isoforms in rat liver include Ugt1a1, 2b1, 2b2, 2b3, 2b6, and 2b12. In contrast to the Ugt1 family, a few Ugt2b subfamily members are found in rat intestine. Ugt isoforms in rat intestine mainly include Ugt1a1, 1a2, 1a6, 1a7, and 2b8 (Shelby *et al.*, 2003).

In mice, the Ugt1a subfamily contains 14 first exons, coding nine enzymes (Ugt1a1, 2, 5, 6a, 6b, 7c, 8, 9, and 10) and five pseudogenes (Ugt1a3, 4, 7a, 7b, and 11) (Mackenzie *et al.*, 2005; Owens *et al.*, 2005). The seven Ugt2b genes in mice include Ugt2b1, 2b5, 2b34, 2b35, 2b36, 2b37, and 2b38. UGT gene expression profiles in mice were determined by Buckley and Klaassen (2007). All 2b members, as well as Ugt1a1, 1a5, 1a6, 1a9, are highly expressed in mouse liver. Several Ugt isoforms were expressed in the gastrointestinal tract, including Ugt1a6, 1a7c, 2a3, 2b34, and 2b35. (Buckley and Klaassen, 2007)

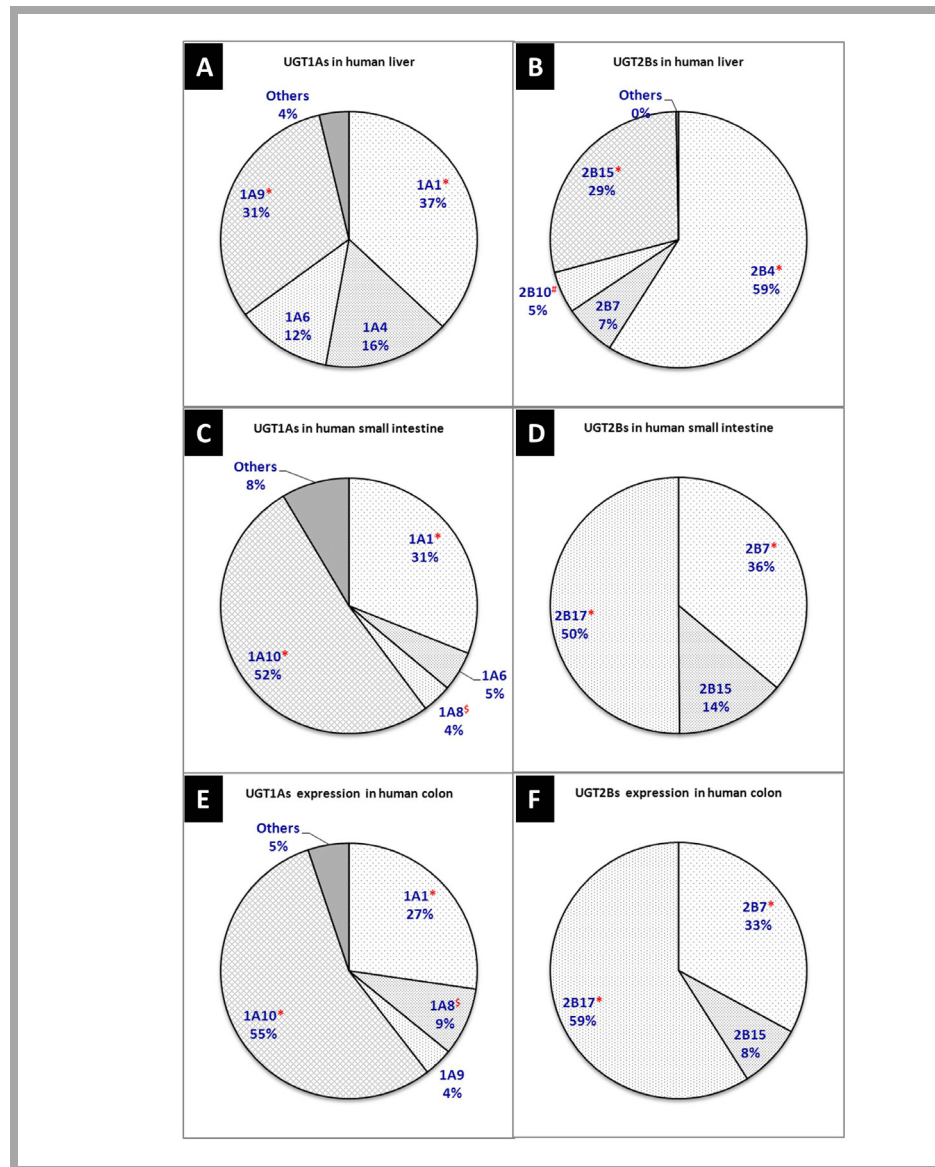


Figure 3. Relative mRNA distribution level between human UGT1A isoforms (left) and between 2B isoforms (right) in human liver (A/B), small intestine (C/D) and colon (E/F)

**The two most abundant isoforms in the organs. #The unique isoform in liver. \$The unique isoform in GI tract.*

1.3.3. Topology of UGTs in ER membrane

Human UGT proteins are around 530 amino acids in length, consisting of two approximately similar-sized domains. The C-terminal domain binds the aglycone and the N-terminal domain the UDPGA ([Mackenzie, 1990](#)). UGT active site faces the lumen of endoplasmic reticulum (ER) where the conjugation occurs, different from CYP enzymes whose active site faces the cytosolic side ([Magdalou *et al.*, 2010](#)). While the lipophilic compounds usually can passively permeate through ER membrane to access the active site of the enzyme, UDPGA is transported into the ER lumen using nucleotide sugar transporters (NSTs) (Figure 4A) ([Kobayashi *et al.*, 2005](#)). NSTs act as antiporters requiring the counter-transport of UDP-N-acetyl glucosamine (UDPGlcNAC), which is a known positive, allosteric modulator of UGTs ([Zakim and Dannenberg, 1992](#); [Bossuyt and Blanckaert, 1995](#)). The translocation of the formed glucuronide(s) to the cytosol domain appeared to be mediated by ER-localized organic anion transporters (AT_{ER}), which do not need ATP, but transport organic anions through ER membrane by facilitated diffusion (Figure 4C) ([Csala *et al.*, 2004](#)).

As shown in Figure 4B, a UGT monomer consists of the N-terminal aglycone substrate binding domain (or half) and the C-terminal UDP-glucuronic acid binding domain, and the latter contains one transmembrane fragment and a cytosolic tail. The membrane attached region in N-terminal domain is thought to facilitate the entry of aglycone to the active site ([Radomska-Pandya *et al.*, 2005](#); [Finel and Kurkela, 2008](#)). Single UGT enzyme has been demonstrated to operate by forming dimeric structures (either homodimers or heterodimers) ([Radomska-Pandya *et al.*, 2005](#); [Finel and](#)

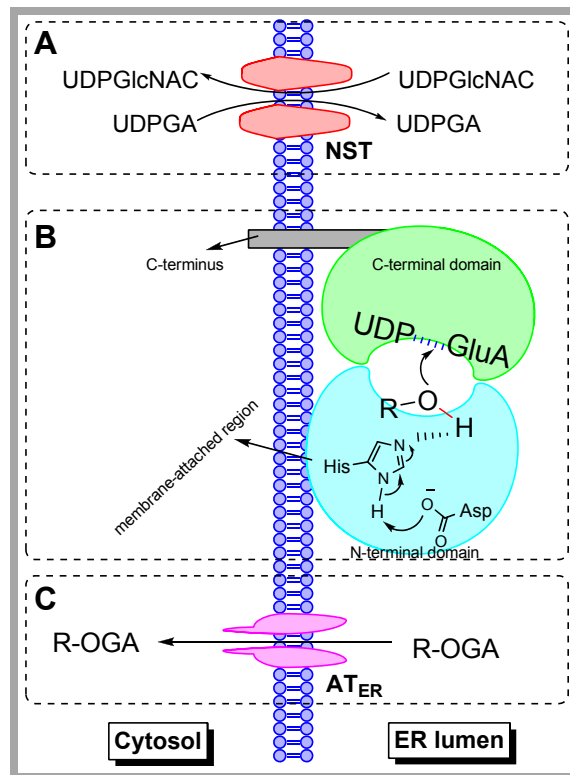


Figure 4. Schematic representation of human UGT topology

UGTs consist of two domains (panel B) and are predicted to function as dimers or oligomers. The amino-terminal domain binds the aglycone and the carboxy-terminal domain binds the UDPGA cofactor; the catalytic site is placed between the two domains. Most of the enzyme mass is located on the luminal side of the endoplasmic reticulum and the carboxy-terminal tail is on the cytosolic side of the membrane.

Kurkela, 2008). The tetramers of UGT dimers may also be formed to generate diglucuronide of bilirubin, benzo(α)pyrene and chrysene-3,6-quinols, as suggested from the radiation target analysis (Bock and Köhle, 2009). It was reasoned that, in the formation of diglucuronide, dimers may loosely interact in ER membrane to form tetramers, which generate a compartment between two dimers in which monoglucuronides reach high enough levels to facilitate diglucuronide formation (Bock and Köhle, 2009). Whether these enzymes actually form such dimeric or oligomeric structures within the ER membrane is unproven, and more work is needed to characterize these homo- and hetero-oligomers and their functional implications.

1.3.4. Structure and catalytic mechanisms

Human UGTs belong to family 1 of glycosyltransferases (GTs) according to the CAZy database (<http://www.cazy.org>). Enzymes in GT1 adopt GT-B fold (i.e., consist of two $\alpha/\beta/\alpha$ or Rossmann fold domains) (Figure 5) and an inverting catalytic mechanism (Figure 6). Approximately 50% of the GT1 family shares a highly conserved motif in the C-terminal domain, denoted as the UGT defining sequence or the UGT signature motif (Paquette *et al.*, 2003; Bowles *et al.*, 2006). Unlike mammalian UGTs, which are membrane-bound proteins, most plant or bacterial GT1 enzymes are soluble (Ross *et al.*, 2001). Because of the exceeding difficulties in purifying them in an active form, there is no complete three-dimensional structure of any mammalian UGTs. Though, a partial crystal structure (C-terminal or UDPGA binding domain) of human UGT2B7 was determined and found to be consistent with other GT-B structures (Miley *et al.*, 2007). In contrast to human UGTs, several complete 3D crystal structures of UGTs derived from

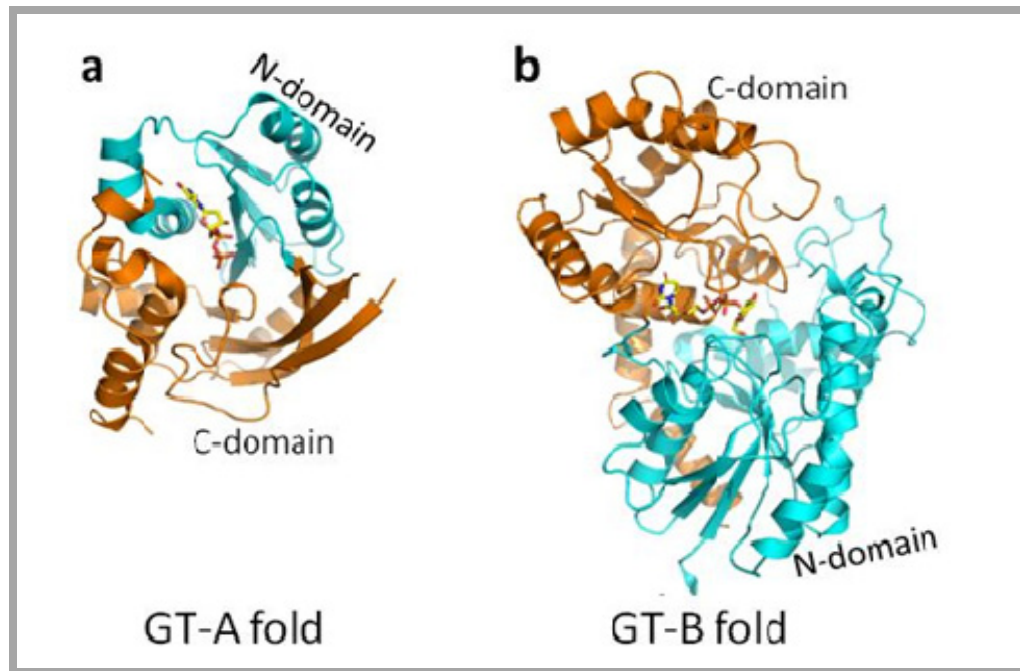


Figure 5. Cartoon representation of glycosyltransferase GT-A (a) and GT-B (b) folds

N-terminal domain is colored cyan, C-terminal domain orange. a. Nucleotide-diphospho-sugar transferase SpsA from Bacillus subtilis (PDB code: 1H7L). b. Triterpene UDP-glucosyl transferase UGT71G1 from Medicago truncatula (PDB code: 2ACW).

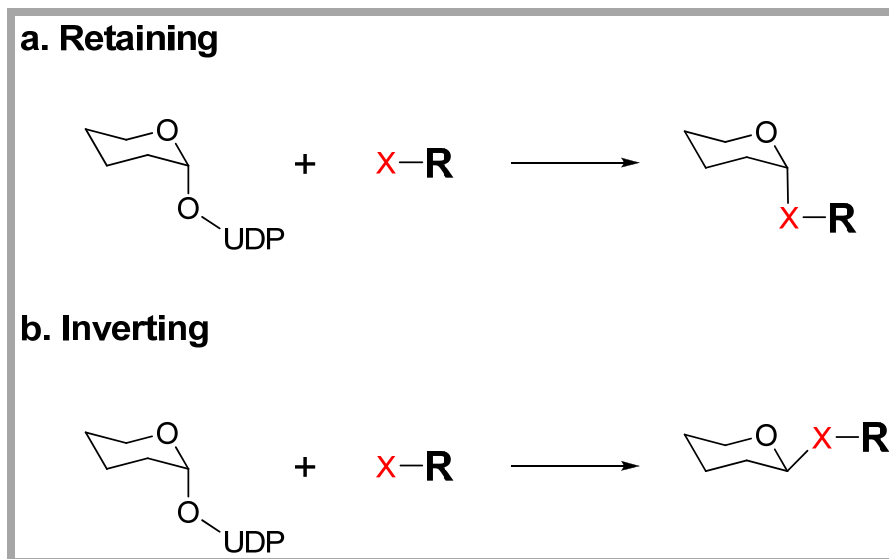


Figure 6. Two main catalytic mechanisms of glycosyltransferases: retention (a) or inversion (b) of the anomeric configuration.

Human UGTs are inverting glycosyltransferases, like all other members of the GT1 family. X = -OH, -COOH, -NH, -NH₂, or -SH.

other organisms have been reported, including five from plants (Shao *et al.*, 2005; Offen *et al.*, 2006; Li *et al.*, 2007a; Brazier-Hicks *et al.*, 2007; Modolo *et al.*, 2009) and seven from bacteria (Mulichak *et al.*, 2001, 2003, 2004; Bolam *et al.*, 2007; Mittler *et al.*, 2007; Zhang *et al.*, 2008).

Numerous studies have been conducted to explore the nature of UDPGA or aglycone binding to mammalian UGTs in last decades. Understanding of the UDPGA binding has been significantly advanced with the aid of crystal structure of UGT2B7 C-terminal. The UDPGA binding site is formed mainly by the residues from the signature motif in C-terminal domain (Radomska-Pandya *et al.*, 1999, 2005, 2010). The sugar donor binding pocket is composed of three clusters: the residues interacting with 1) nucleotide, 2) diphosphate, or 3) glucuronic acid (Radomska-Pandya *et al.*, 1999, 2005, 2010). It was noted that mutations at one of the residues interacting with the nucleotides had less effects on enzyme function than those interacting with diphosphate or glucuronic acid moieties.

In contrast to the sound understanding of UDPGA binding, knowledge about the residues interacting with the (acceptor) substrate is rather limited, mostly due to the lack of a N-terminal crystal structure. Various biochemical methods such as chemical modification, and application of technologies such photo-affinity labeling and site-mutagenesis had identified some key amino acids that govern the substrate specificity of the enzymes. Among these, the mutagenesis and activity assays suggested Phe117 of UGT1A9 participates in 1-naphthol binding (Itäaho *et al.*, 2010). The four amino acid motif of UGT1A10 [F(90)-M(91)-V(92)-F(93)] was identified as a key determinant of the

binding of phenolic substrates (Xiong *et al.*, 2006; Starlard-Davenport *et al.*, 2007). On the other hand, the presence of an aromatic amino acid residue at position 33 was important for the activity and substrate specificity of both UGT2B4 and 2B7 (Barre *et al.*, 2007).

1.3.5. Homology structure models of UGTs

For a better understanding of the UGT-substrate binding and of the reaction mechanism, scientists have simulated human UGT structures via homology modeling (or comparative modeling) using glycosyltransferases from plants or bacteria with solved crystal structures. Presently, four 2-domain homology models have been published for human UGTs: three for the human UGT1A1, and one for the human UGT1A9 (Li and Wu, 2007; Locuson and Tracy, 2007; Laakkonen and Finel, 2010; Fujiwara *et al.*, 2009).

1.3.5.1 Sequence alignment

Due to their low sequence identity (~13%), human UGT1A1 sequence were aligned to the plant UGT templates with the aids of predicted secondary structures (Li and Wu, 2007; Locuson and Tracy, 2007; Laakkonen and Finel, 2010; Fujiwara *et al.*, 2009). Major portions of the human UGT sequences were highly conserved and easily matched to the plant UGTs. However, there are two regions presumed to make contact with the (acceptor) substrates are highly variable: the N α 3 helix and a region between N α 5 and N β 6 that was defined as “loop 5” by Laakkonen and Finel (2010). In contrast to plant UGTs which have one relatively short helix N α 3, the N α 3 of human UGTs was divided into three helices (designated as N α 3-1 N α 3-2 and N α 3-3). It was reasoned that N α 3-1

may be more properly anchored at the interface between the N- and C-domains, and N α 3-2 should be matched to the N α 3 of plant UGTs (Laakkonen and Finel, 2010). The helices N α 3-1 and N α 3-3 were not modeled in the work of Locuson and Tracy (2007), and were shown as the random coils in the final generated structures. However, this sequence aligning approach was not favored by Li and Wu (2007), who match the N α 3-1 (and a part of N α 3-2) to plant N α 3. The helix N α 3-1 was predicted to isolate the reaction site from bulk water, and move concertedly to allow the exit of the products; whereas it was thought that helix N α 3-3 packs to N α 4 and N α 5-2 (Laakkonen and Finel, 2010). In terms of “loop 5”, bacterial UGTs (1iir or 1rrv) were used as the extra templates in earlier works (Locuson and Tracy, 2007; Laakkonen and Finel, 2010). Since the predicted helical pattern immediately upstream of N β 6 agrees well with the bacterial UGT proteins but not with the plant UGTs, Li and Wu (2007) relied more on sequence similarity in handing alignment for “loop 5”. It is recognized that the secondary structure of this area is the most divergent not only among the 5 plant UGTs with known structures, but also when compared to and between other GT-B fold GTs (Osmani *et al.*, 2009).

1.3.5.2 Substrate binding implications from the UGT1A1 homology models

The substrate binding pocket was almost entirely formed by the N-terminal residues, although some C-terminal residues also contributed to the formation of the pocket (Li and Wu, 2007; Locuson and Tracy, 2007; Laakkonen and Finel, 2010; Fujiwara *et al.*, 2009). The pocket was primarily formed by LoopN1, N α 1, N α 3-2, LoopN4, N α 5-1, N α 5-2, Loop C1 and Loop C5, which was consistent with the topological arrangement of β strands (3-2-1-4-5-6-7) of the enzymes. N β 2, N β 3, N β 6 and N β 7 twisted far away from

the core N β 1 where the catalytic histidine is situated. The residues predicted to be in contact with aglycones were mainly hydrophobic, suggesting that hydrophobicity is one key characteristic for substrate recognition by the enzyme. The latter agrees well with the QSAR regression models (Sorich *et al.*, 2002).

The volume of UGT1A1 model binding pocket is estimated to be 700 Å³, which is ~ 2 times as large as the biggest substrates such as bilirubin (~400 Å³) or ~4 times as large as the smaller flavonol myricetin (~170 Å³), respectively. The large aglycone-binding domain might serve as the molecular basis for the generation of multiple metabolites from a single substrate (e.g, multi-hydroxyl flavonoids), because the sufficient space can permit multiple binding modes (distinct orientations) of the acceptor substrate for region-specific catalysis.

1.3.6. Catalytic mechanism

Human UGTs are proposed to use a serine hydrolase-like mechanism for catalysis (Radomska-Pandya *et al.*, 2010). In this mechanism (Figure 7), a basic residue (usually histidine) deprotonates the nucleophilic group (e.g., -OH) of the substrate bound in the active site, which at the same time is stabilized by a neighboring acidic acid (usually aspartic acid) (Radomska-Pandya *et al.*, 2010). The deprotonated substrate then attacks at the anomeric carbon (C1) of UDPGA, and completes the conjugative reaction. This is consistent with the fact that all known mutations of the two catalytic residues (also called “His-Asp” diad) abolish the UGT activity (Li *et al.*, 2007b; Miley *et al.*, 2007; Radomska-Pandya *et al.*, 2010). On the other hand, it is found that UGT1A4 and 2B10 do not have the equivalent histidine (replaced by proline and leucine,

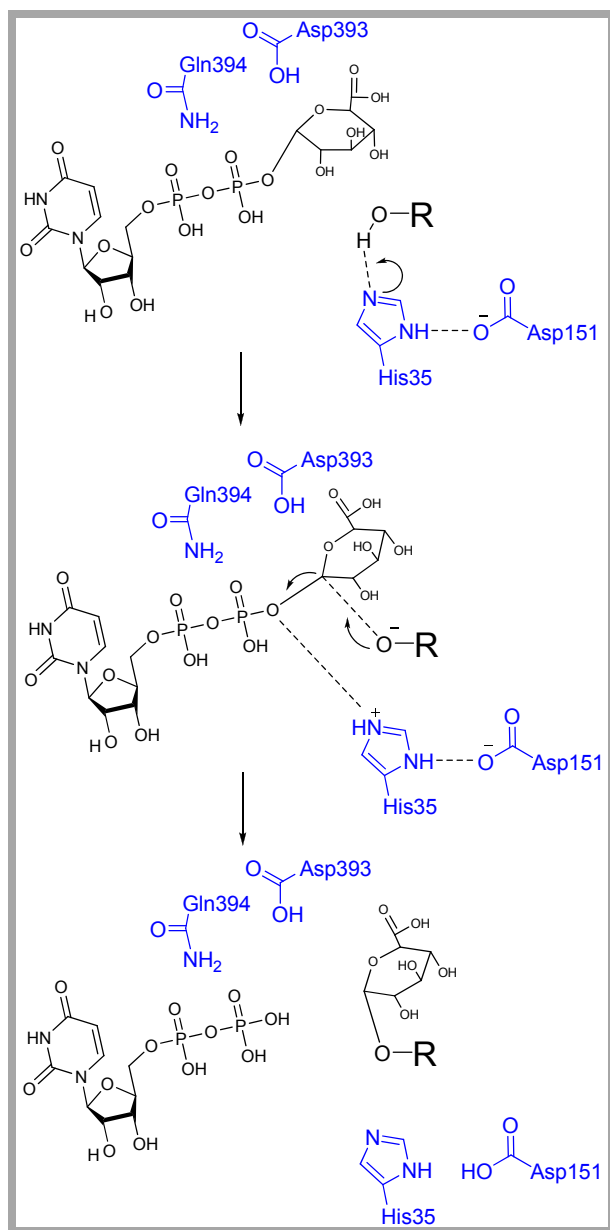


Figure 7. Schematic representation of proposed catalytic mechanisms for human UGTs using UGT1A10 as an example

R-OH, the substrates with a hydroxyl group for conjugation

respectively), and tend to specifically catalyze N-glucuronidation using a distinct catalytic mechanism (Patana *et al.*, 2008; Kerdpin *et al.*, 2009; Kaivosaaari *et al.*, 2011). The N-nucleophiles are suggested to develop a formal positive charge during the N-glucuronidation, and thus require a negatively charged (i.e., aspartic acid) residue to stabilize the transition state (Patana *et al.*, 2008; Kerdpin *et al.*, 2009).

It is well established that glucuronidation reaction involves the formation of a ternary complex, namely, the complex of [enzyme•UDPGA•substrate] prior to product release (Figure 8). Furthermore, a compulsory ordered bi bi (i.e., two substrates and two products) kinetic mechanism was proposed based on the product and dead-end inhibition studies of expressed human UGT isoforms (Luukkanen *et al.*, 2005). In this mechanism, UDPGA binds first to the enzyme, followed by the binding of aglycone substrate (Figure 8A). However, alternative mechanisms such as random ordered bi bi mechanism (Figure 8B) were also reported under similar experiments when partially purified rat UGTs were used (Yin *et al.*, 1994). In this mechanism, binding of the substrate to the enzyme does not require prior binding of UDPGA. The above two mechanistic studies of UGTs using similar experiments provided two different catalytic mechanisms that are in conflict with each other (compulsory vs. random bi bi mechanism). Based on the analyses of Luukkanen *et al.* (2005), these ambiguous results were largely due to the presence of multiple UGT enzymes and/or inactivated UGT enzyme in the latter study.

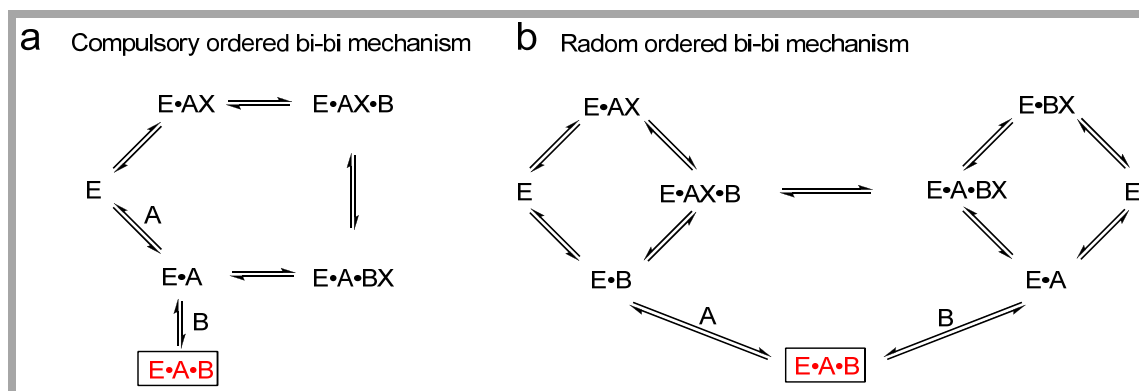


Figure 8. Sequential kinetic mechanisms involving two substrate and two products.

Panel a presents a compulsory ordered bi bi mechanism and **panel b** a random ordered bi bi mechanism. E = UGT, X = glucuronic acid, AX = UDP-glucuronic acid (UDPGA), B = aglycone substrate, BX = glucuronide or sulfate. Formation of the ternary dead-end complex of $[E \cdot A \cdot B]$ (in box) contributes to the substrate inhibition displayed by UGT enzymes.

1.3.7. Regulation of UGTs by phosphorylation

UGT gene expression is known to be regulated by a number of transcription factors including hepatocyte HNF1 and HNF2, Ah receptor, and nuclear receptors ([Mackenzie et al., 2003](#); [Zhou et al., 2005](#)). The contribution of those regulators to the large inter-individual variation of hepatic UGT levels has been discussed ([Bock, 2010](#)). In recent years, it is becoming increasingly evident that UGT enzymes are also regulated via phosphorylation mediated by protein kinase C (PKC) or Src tyrosine kinase (SrcTK) ([Basu et al., 2008](#); [Mitra et al., 2010](#)). Phosphorylation at serine/threonine by PKC is required for UGT1A activity, whereas tyrosine phosphorylation regulates UGT2B activity ([Basu et al., 2003, 2004, 2005](#)). The phosphorylation sites for UGT isoforms are summarized and their locations in UGT structure (UGT1A1 homology model from [Laakkonen and Finel, 2010](#)) are shown in Figure 9. It is not surprising that the phosphorylation sites all appear on the surface of the protein.

In addition to the activity abolishment, it is also found that the PKC-mediated phosphorylation in UGT regulates substrate specificity; mutation of PKC sites in UGT1A7 demonstrated that S432G-UGT1A7 caused a major shift in the enzyme's pH 8.5 optimum to 6.4 with new substrate preferences, including 17 β -estradiol ([Mitra et al., 2010](#)). Alteration of the substrate selection by phosphorylation was also observed for UGT2B7. Non-Src phosphorylated 2B7 metabolizes both 4-OH-estradiol and 4-OH-estrone, while Src-dependent phosphorylation of 2B7 allows metabolism of the former chemical, but not the latter ([Mitra et al., 2009](#)).

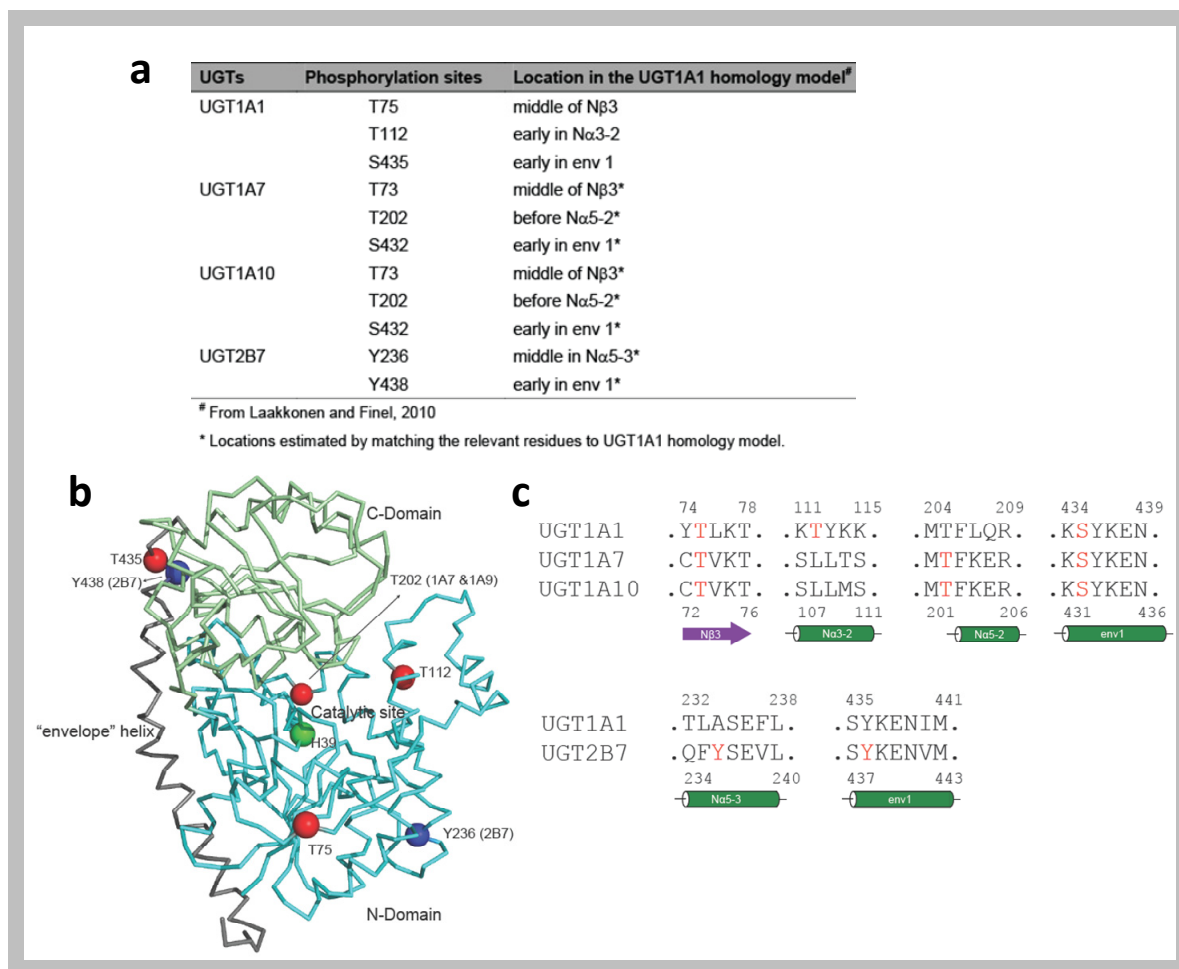


Figure 9. Phosphorylation sites of UGT isoforms and their locations in UGT homology structure

Panel a: The phosphorylation sites for UGT isoforms are summarized. **Panel b:** locations of phosphorylation sites in UGT 3D structure (UGT1A1 homology model). Green sphere: catalytic residue (histidine 39); red spheres: protein kinase C (PKC) mediated phosphorylation sites; blue spheres: Src tyrosine kinase (SrcTK) mediated phosphorylation sites. **Panel c:** alignment of UGT sequences, showing the phosphorylation amino acids (in red) in secondary structures. Sequence alignment was performed using Clustal W (<http://www.clustal.org/>)

Inhibition of UGT phosphorylation by PKC inhibitor(s) may represent a novel mechanism for drug-drug interactions (Volak *et al.*, 2010). PKC-mediated inhibition of human UGT1A6 using different PKC inhibitors was characterized; PKC delta inhibitors could interfere with UGT1A6-mediated glucuronidation of several substrates (Volak *et al.*, 2010). In addition, the inhibitors of UGT phosphorylation may be applied to reduce the magnitude of first-pass glucuronidation, thus improving the oral bioavailability. A study by Basu *et al.* (2007) represented the first work to show that targeted inhibition of glucuronidation could lead to enhanced drug (i.e., mycophenolic acid) uptake and efficacy. The authors successfully utilized curcumin (a protein kinase C inhibitor) to down-regulate UGT phosphorylation reversibly, thus, suppress glucuronidation; and demonstrated between a 6- and 9-fold improvement in free-drug (mycophenolic acid) uptake and therapeutic efficacy (Basu *et al.*, 2007).

1.4. Glucuronidation of phenolics

Phenolics refer to a very wide variety of compounds which structurally possess aromatic hydroxyl group(s), including the chemotherapeutic agents (e.g., SN-38 and flavopiridol), non-chemotherapeutic drugs (e.g., raloxifene and ezetimibe), and bioactive natural polyphenols (e.g., hydroxycinnamic acids and flavonoids). The complexity of UGT-mediated metabolism of phenolics is highlighted with species-, gender-, organ- isoform- and region-dependent specificity, as well as functional compensation between UGT1A and 2B subfamily.

1.4.1. Species-dependent glucuronidation

Species difference in glucuronidation activity was observed with human jejunum microsomes higher than rat intestinal microsomes for all hydroxyl-flavones except for 3,7-dihydroxyflavone (Zhang *et al.*, 2006). Glucuronidation of the isoflavone prunetin (CL_{int}) in human intestinal microsomes was 3~6-fold higher than that in rat intestinal microsomes, but was similar in liver microsomes (Joseph *et al.*, 2007). In addition, rat Ugt1a1 might be able to produce an unusually prunetin C-glucuronide (Joseph *et al.*, 2007). Emodin glucuronidation in liver microsomes was species dependent among mice, rats, guinea pigs, dogs, and humans, and K_m values varied 5.7-fold (3.2–18.2 μ M) in males and 2.8-fold (4.6–13.0 μ M) in females (Liu *et al.*, 2010). The male intrinsic clearance (CL_{int}) values differed by 5-fold (27.6–138.3 ml/h/mg protein), and female CL_{int} values differed by 4.3-fold (24.3–103.5 ml/h/mg protein). Raloxifene has a much lower bioavailability in humans (2%) than in rats (39%), which can be largely explained by the glucuronidation difference in the intestine. CL_{int} value for raloxifene glucuronidation was 7.5-fold (Dalvie *et al.*, 2008) or 2~5-fold (Jeong *et al.*, 2005a) higher in the human intestine as compared to rats. Also, it was shown that UGT1A10 (highly expressed in human intestine) is very proficient in glucuronidating raloxifene (Jeong *et al.*, 2005a). Glucuronidation of acetaminophen was relatively slow in ferret livers compared with livers from all other species except cat (Court, 2001).

1.4.2. Gender-dependent glucuronidation

Liu *et al.* (2010) studied the disposition of emodin using rat intestine perfusion model, excretion rates of emodin-3-O-glucuronide were significantly different ($p < 0.05$) in four

regions of the intestine and were higher in males than in females ($p < 0.01$). Similarly, the same group of investigators found duodenal excretion of glucuronide was significantly higher in male than female rats for the isoflavone daidzein ($p < 0.05$), which coincided with a higher absorption of the parent compound in duodenum (Wu *et al.*, 2011). In contrast, biliary excretion of the glucuronide is significantly higher in female than male rats ($p < 0.05$). Gender differences were also apparent in glucuronidation of acetaminophen, with intrinsic clearance values (CL_{int}) significantly higher in male compared with female ferret livers (Court, 2001). In mice model, the biliary excretion rate constant was 7-fold higher in males than in females for acetaminophen glucuronide (Lee *et al.*, 2009).

1.4.3. Intestinal vs. hepatic glucuronidation

In rats or mice, intestine probably plays a more significant role than liver in first-pass disposition of flavonoids via glucuronidation (Chen *et al.*, 2003). Glucuronidation of flavonoids using rat intestinal microsomes often times show higher catalytic efficiency than that using rat liver microsomes. In human, intestinal disposition may also be more important than hepatic disposition, because human intestinal microsomes were more efficient than liver microsomes in glucuronidating phenolic compound such as prunetin and raloxifene (Joseph *et al.*, 2007; Mizuma, 2009).

Regioselective glucuronidation differences were observed between human intestine and liver. Human intestine microsomes preferred to generate 4'-O-glucuronide for prunetin, while 5-O-glucuronide was mainly formed by human liver microsomes. In stereo- and region- glucuronidation studies of resveratrol (Aumont *et al.*, 2001; Brill *et*

[al., 2006](#)), experiments using human intestine microsomes generated 3-O- and 4'-O-glucuronide for both cis-resveratrol and trans-resveratrol, whereas those using human liver microsomes tend to form 3-O-glucuronides only.

1.4.4. Isoform-specific glucuronidation

The UGT isoforms that are responsible for glucuronidating phenolics are generally from UGT1A subfamily, especially, 1A1, 1A3, and 1A7~1A10 ([Zhou *et al.*, 2010](#); [Tang *et al.*, 2010](#)). Substrate specificity of the six main contributors often exhibits significant overlaps.

For prunetin, UGT1A7, 1A8, and 1A9 were mainly responsible for the formation of 5-O-glucuronide, whereas UGT1A1, 1A8, and 1A10 were mainly responsible for the formation of 4'-O-glucuronide ([Joseph *et al.*, 2007](#)). UGT1A10 was also shown to be responsible metabolizing 4'-OH of raloxifene. UGT1A1 appears to be more selective on certain position of a phenolic molecule. For example, UGT1A1 predominantly metabolized the 3'-OH group of flavones or flavonols ([Davis and Brodbelt, 2008](#)), and 3-OH of trans-resveratrol ([Aumont *et al.*, 2001](#); [Brill *et al.*, 2006](#)). The strict regiospecificity was also observed with UGT1A9, which predominantly catalyzed glucuronidation at the 3-OH group of either trans- or cis-resveratrol.

Even though that the quantitative UGT protein level in the intestine and liver is unknown, investigators ([Zhou *et al.*, 2010](#); [Tang *et al.*, 2010](#)) made attempts to correlate the isoform- with organ-specific glucuronidation rates considering the predominant isoforms only (intestine: UGT1A1, 1A8 and 1A10; liver: UGT1A1 and 1A9). Interestingly,

good correlations were observed in these studies. The results suggest that the differences in intestinal and hepatic glucuronidation might be ascribed to the presence of the organ-specific UGT isoforms (intestine: UGT1A8 and 1A10; liver: UGT1A9).

1.4.5. Compensation between UGT1As and 2Bs

Wang *et al.* (2009) showed that flavonoids (i.e., apigenin and genistein) are efficiently metabolized by Ugt1a-deficient Gunn rats at a comparable or even higher level, in contrast to the control Wistar rats. The equivalent or increased glucuronidation in Gunn rats was ascribed to the compensatory up-regulation of intestinal Ugt2bs and hepatic anion efflux transporters (Wang *et al.*, 2009). This was the first report to show that activities of other Ugt isoforms (2b isoforms) had changed (i.e., elevated) to compensate for Ugt1a deficiency.

1.4.6. Regioselective glucuronidation

Regioselectivity refers to the preference for formation of one glucuronide isomer over another, when a substrate possesses more than one possible glucuronidation site. Regioselectivity of various UGTs has been examined for a number of compounds such as estradiol, estrone, morphine (Lépine *et al.*, 2004; Ohno *et al.*, 2008). Elucidation of UGTs regioselectivity would facilitate the understanding of UGT-substrates interaction with respect to binding property and catalytic mechanisms. In addition, typical generation of a particular glucuronide isomer from a substrate was used to probe UGT activity in human tissues in vitro. For example, β -estradiol 3-glucuronidation is considered an excellent marker of UGT1A1 activity (Court, 2005; Donato *et al.*, 2010), and morphine 6-

glucuronidation may be used as a selective probe for UGT2B7 activity (Stone *et al.*, 2003).

1.4.6.1 Ester-acylglucuronidation vs. ether-O-glucuronidation

Ester-acylglucuronidation occurs at the carboxylic acid group (e.g., bilirubin), resulting in an acyl-linked glucuronide, whereas ether-O-glucuronidation occurs at a hydroxyl group (e.g., phenolics). Selectivity between ester-acylglucuronidation and ether-O-glucuronidation appears to be substrate- and isoform-dependent. Mouse ugt1a1 predominantly generated ether-O-glucuronide from mycophenolic acid (Basu *et al.*, 2007). By contrast, glucuronidation of (-)-11-nor-9-carboxy-tetrahydrocannabinol only occurs at the carboxylic acid group (Mazur *et al.*, 2009); the highest activity towards THC-COOH was observed with UGT1A3, though UGT1A1 and human liver microsomes (HLMs) also showed a significant amount of activity towards this substrate. An examination of kinetic parameters revealed that ferulic acid was mainly glucuronidated by UGT1A1 at the two nucleophilic groups (i.e., carboxylic acid and hydroxyl group) (Li *et al.*, 2011). UGT1A3 was able to glucuronidate the two positions at about the same rate, but with a low efficiency. UGT1A6 and 1A8 were strictly involved in the formation of the ether glucuronide, whereas UGT1A7, 1A10 and 2B7 were principally responsible for glucuronidation of the carboxyl group (Li *et al.*, 2011).

1.4.6.2 Phenolic oxygen is more favored for glucuronidation

It is generally agreed that phenolic hydroxyl groups are more prone to glucuronidation than alcoholic hydroxyl groups. When both phenolic and alcoholic hydroxyl groups are present in the structure, glucuronidation occurs primarily at the phenolic (-OH) groups.

This can be seen from the glucuronidation of a variety of UGT substrates such as SN38, ezetimibe and estradiol ([Hanioka *et al.*, 2001](#); [Ghosal *et al.*, 2004](#); [Soars *et al.*, 2003](#)).

1.4.6.3 Regioselective glucuronidation of phenolics

Caffeic acid is a hydroxycinnamic acid that can be found in majority of plants. UGT1A1 and UGT1A9 were active in glucuronidation of caffeic acid (50 μ M), albeit at a low rate of 4 ~ 8 pmol/min/mg ([Wong *et al.*, 2010](#)). UGT1A1 specifically catalyzed the formation of caffeic acid-4-O-glucuronide, whereas UGT1A9 conjugated both 3-OH and 4-OH groups of caffeic acid ([Wong *et al.*, 2010](#)). Furthermore, kinetic profiling demonstrated that UGT1A1 and UGT1A9 had lower affinity and activity towards caffeic acid, compared to its analogs such as ferulic and isoferulic acids ([Wong *et al.*, 2010](#)).

(-)-Epigallocatechin (EGC) and (-)-epigallocatechin gallate (EGCG) are major green tea polyphenols with antioxidant and anticancer activities. Lu *et al.* ([2003](#)) studied glucuronidation of EGC and EGCG in human, mouse, and rat liver microsomes and in 9 human UGT isoforms expressed in insect cells. EGCG-4''-O-glucuronide was the major EGCG glucuronide formed in all incubations, whereas EGC-3'-O-glucuronide was the major EGC glucuronide formed in all incubations. UGT1A1, 1A8 and 1A9 displayed high glucuronidation activities towards EGCG. Interestingly, UGT1A8 had the highest V_{\max}/K_m value with EGCG but low activity with EGC ([Lu *et al.*, 2003](#)).

Emodin is a major active anthraquinone present in the rhubarb. Emodin 3-O-glucuronide was the only glucuronide formed, when incubating emodin with a panel of microsomal fractions prepared from mice, rats, guinea pigs, dogs, and humans ([Liu *et*](#)

[al., 2010](#)). The 1-OH and 8-OH groups of emodin were not metabolized at all, probably due to the formation of an intramolecular hydrogen bond between the neighboring carbonyl and 1-OH or 8-OH groups.

Daphnetin is a dihydroxycoumarin that is being used in China for the treatment of coagulation disorders. UGT1A6 and UGT1A9 can rapidly conjugate both hydroxyl groups and generate 7-O-glucuronide and 8-O-glucuronide ([Liang *et al.*, 2010](#)). Although less efficient, UGT1A3, 1A4, 1A7, 1A8, and 1A10 selectively metabolized the 7-OH position of daphnetin ([Liang *et al.*, 2010](#)).

1.5. Enteric and hepatoenteric recycling

It is becoming evident that glucuronidation *in vivo* is a complex process involving three key players, namely, UGT enzymes, efflux transporters, and β -glucuronidase ([Jeong *et al.*, 2005b](#); [Liu and Hu, 2007](#)). Interactions between these players render the intricate phenomena, enteric and hepatoenteric recycling (illustrated in Figure 10). Consequently, first-pass metabolism of phenolics does not result in complete drug elimination. Rather, their apparent terminal elimination half-lives are significantly prolonged (~ 6-8 hours) despite of their poor bioavailabilities *in vivo* (< 5%).

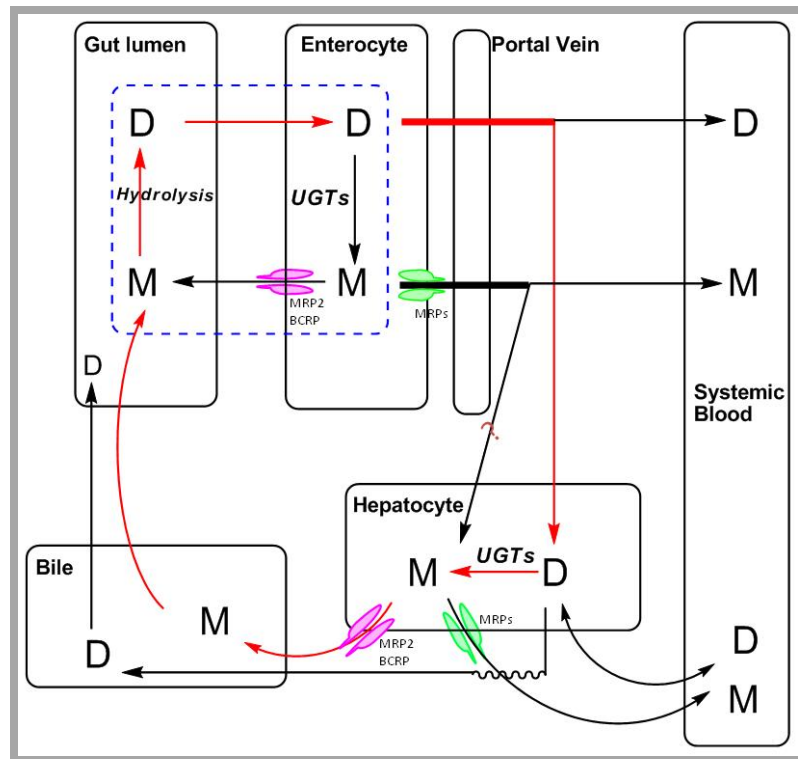


Figure 10. Schematic presentation of the enteric and hepatoenteric recycling in glucuronidation pathway (D, aglycone; M, glucuronide)

Enteric recycling (highlighted in the dashed box) is resulted from the interactions between enteric glucuronidation, glucuronide efflux, and glucuronide hydrolysis. For hepatoenteric recycling (indicated in red arrows), glucuronide formation occurs in the hepatocytes. The glucuronide is excreted into bile and reach the gut lumen following the bile flow. Question mark denotes whether glucuronide (produced from intestinal glucuronidation) can enter hepatocytes is uncertain. UGTs, UDP-glucuronosyltransferases; BCRP, breast cancer resistance protein; MRPs, multidrug resistance proteins.

1.6. Deglucuronidation by β -glucuronidase

For the majority of dietary polyphenols, it remains unclear that their glucuronide still retain the biological functions in vivo. However, accumulating evidence suggests that β -glucuronidase-mediated deglucuronidation can occur in vivo, which converts the glucuronides back to free aglycones. This process was proposed to assist in the uptake, transport of the polar metabolite, and more importantly make the inactive metabolite active (Shimoi and Nakayama, 2005; Lee-Hilz *et al.*, 2008). Deglucuronidation had been frequently reported in the gut contributing to the enteric/enterohepatic recycling (Liu and Hu, 2002; Jeong *et al.*, 2005b; Liu and Hu, 2007), where the glucuronides excreted from enterocytes can be hydrolyzed by intestinal bacteria that have β -glucuronidase. Hepatic and/or renal deglucuronidation might also contribute to disposition of acetaminophen (Bohnenstengel *et al.*, 1999). In the study of O'Leary *et al.* (2003), HepG2 cells can absorb and turnover quercetin glucuronides, and β -glucuronidase activity could modulate the intracellular biological activities of dietary antioxidant flavonoids.

Shimoi *et al.* systematically investigated the β -glucuronidase activity in inflammation (Shimoi *et al.*, 2000, 2001; Shimoi and Nakayama, 2005). Supernatants obtained from the neutrophils stimulated with ionomycin/cytochalasin B hydrolyzed luteolin (5,7,3',4'-tetrahydroxyflavone) monoglucuronide to free luteolin, suggesting that the β -glucuronidase was secreted from the stimulated neutrophils (Shimoi *et al.*, 2000, 2001). The β -glucuronidase activity in rat and mouse plasma also increased after iv injection of lipopolysaccharide (LPS) (Shimoi and Nakayama, 2005). Therefore, there is a possibility that the inactive glucuronides of exogenous compounds formed in vivo can be converted

back to the active parent compounds at the sites of inflammation (Mochizuki *et al.*, 2004). In addition, Caco-2 cells also showed a significant level of β -glucuronidase activity, suggesting that expression level of β -glucuronidase is higher in this cancerous cell (Shimoi and Nakayama, 2005). This finding and its metabolic implications remain to be confirmed. Nevertheless, the deglucuronidation process is less noted in Caco-2 transport experiment (Sun *et al.*, 2008), probably because the formed glucuronide is rapidly pumped out of the cells by efflux transporters. The efficient removal of glucuronide might preclude the occurrence of reverse reaction to a significant extent.

1.7. Structure-glucuronidation relationships

The significance pertaining structure-glucuronidation relationship is emphasized by Wong *et al* (2009). Briefly, the knowledge can usually be used to (but not limited to): (a) predict glucuronidation-mediated drug interactions that include both xenobiotics or endogenous compounds; (b) screen for compounds that are exclusively metabolized by a particular UGT isoform, which might be utilized as probe substrates for a particular UGT isoform; and (c) assist in the biosynthesis of flavonoid (or other compounds) glucuronides conjugated at desired position(s) for pharmaceutical and/or analytical purpose.

The existence of structure-glucuronidation relationship for flavonoids was first noted in the study of Chen *et al.* (2005a), which showed that the intestinal glucuronidation is slower in isoflavones without an additional A-ring substitution (electro-donating groups: -OH or -OCH₃). Zuo and coworkers further evaluated the glucuronidation of mono- and

di-hydroxyflavones using intestinal microsomes and S9 fraction (Zhang *et al.*, 2006; Wong *et al.*, 2009). Glucuronidation activity of 6- and 3'-mono-hydroxyflavones was much greater than that of 3-, 4'-, 7- and 2'-HF, with 5-HF to be the lowest (Zhang *et al.*, 2006). Increasing the number of hydroxyl groups on A- or B-ring (except for 4'-OH) would enhance the glucuronidation activity of flavones, whereas adding a 3-OH group on C-ring might not (Zhang *et al.*, 2006). Furthermore, the existence of a hydroxyl group at the 3' position may enhance the glucuronidation activity of flavonoids (Zhang *et al.*, 2006).

1.8. Summary

This survey of the literature reveals that glucuronidation is a metabolic reaction of great importance and limits the bioavailability of many phenolics. The high complexity of glucuronidation has also been widely recognized. Most notably, the patterns in substrate selection for UGT isoforms are difficult to decipher. For example, there is no explanation yet for the distinct position preference displayed by UGT isoforms. The reasons why divergent activities are observed for UGTs towards structurally similar chemical analogs are largely unknown. In the absence of a UGT 3D structure, attempts to solving this problem have been made using 2D/3D-QSAR techniques, pharmacophore models, and crystal structures of plant UGTs. However, the resulting models are insufficient to explain experimental data. Therefore, a better methodology to unraveling the mechanisms for substrate recognition by UGTs is of considerable interest in this context.

Chapter 2 Hypotheses and specific aims

2.1. Central hypothesis

Glucuronidation is a major determinant of the *in vivo* fate of phenolics. Understanding the mechanisms of drug recognition by UGTs can help identify a structure with favorable pharmacokinetics. We hypothesize that 3D-quantitative structure activity relationship (QSAR) techniques, and protein homology modeling can be employed to elucidate UGT-phenolics interactions. 3D-QSAR models that are statistically significant with a predictive power can be established.

2.2. Specific aims

2.2.1. Aim I (Studies I + II)

To determine the regioselectivity of various UGT isoforms via kinetic profiling and identify the main isoform(s) responsible for glucuronidation of flavonoids (with multiple hydroxyl groups (-OHs)) (Study I). We will also use regioselective glucuronidation of flavonoids to probe activity of hepatic UGT1A1. It is hypothesized that a regioselective pattern exists for each UGT isoform.

2.2.2. Aim II (Study III)

To determine UGT1A9-mediated glucuronidation parameters for selected flavonols (n=30) and to establish a pharmacophore-based CoMFA model using this dataset. In this aim, we will focus on UGT1A9-mediated glucuronidation at the 3-OH position of flavonols. It is hypothesized that flavonols use a unique binding mode for 3-O-glucuronidation that differs from those for glucuronidation at other positions (e.g., 7-OH).

2.2.3. Aim III (Study IV)

To determine glucuronidation parameters for a large class of structurally diverse phenolics (n=145) and to establish a more generalized computational model based on this large database. It is hypothesized that multiple binding modes are adopted by a same substrate (with multiple hydroxyl groups (-OH)) to form multiple glucuronides. Predictive models derived from QSAR analyses can be established.

2.2.4. General strategy

Due to the lack of a complete crystal structure of human UGTs, we proposed a ligand-based approach combined with “expert” knowledge to elucidate the mechanisms of substrate recognition by the enzymes. In **aim 1**, glucuronidation of several polyphenolic compounds (flavonoids) by human UGT1A isoforms is evaluated experimentally. The finding that UGT isoforms display distinct regioselectivity were subsequently explored and applied in the identification of probe substrates for UGT1A1. Further, the “expert” knowledge indicated from the kinetic characterization of regioselective metabolism in **aim 1**, namely, a multi-hydroxyl substrate uses multiple binding models to generate different glucuronide isomers, is used to guide model construction in **aims 2 and 3** (Figure 11). This enables us to derive the predictive molecular field (i.e., CoMFA and/or CoMSIA) models, and a possible protein binding pocket for UGT1A9.

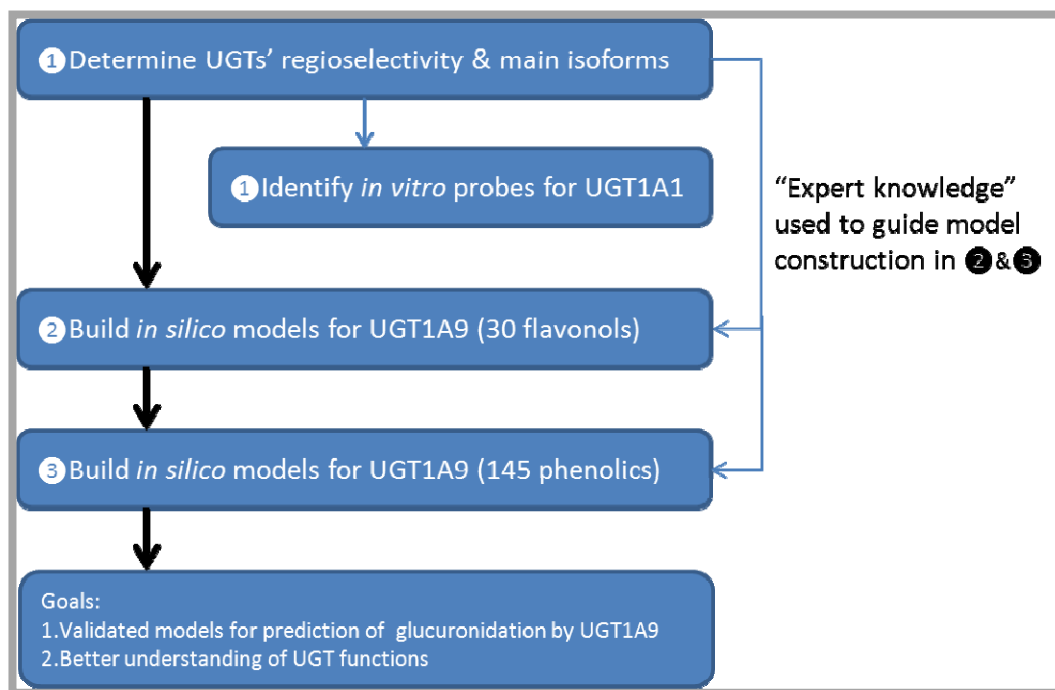


Figure 11. General research strategy

The numbers ① ② ③ are aims.

Chapter 3 Regioselective glucuronidation of flavonols by six human UGT1A isoforms (Study I)

3.1. Abstract

Flavonols, a class of polyphenols, show a variety of biological activities such as antioxidant and anticancer. However, rapid *in vivo* O-glucuronidation posed a challenge to develop them as therapeutic agents. The objective of this study is to determine the regioselective glucuronidation of flavonols by UGT1A isoforms (i.e., UGT1A1, 1A3, 1A7, 1A8, 1A9 and 1A10). The kinetics of UGT1A1-, 1A3-, 1A7-, 1A8-, 1A9- and 1A10-mediated metabolisms of four flavonols that contain 7-OH group were characterized and kinetic parameters (K_m , V_{max} and $CL_{int} = V_{max}/K_m$) were determined. UGT1A1 and 1A3 regioselectively metabolized 7-OH, whereas UGT1A7, 1A8, 1A9 and 1A10 preferred to glucuronidate 3-OH group. UGT1A1 and 1A9 were the most efficient conjugating enzymes with K_m values of $\leq 1 \mu M$ and relative catalytic efficiency ratio of ≥ 5.5 . Additionally, the four flavonols generally strongly self-inhibited the UGT1A1-mediated glucuronidation, with K_{si} (substrate inhibition constant) of $\leq 5.4 \mu M$. In conclusion, UGT1A isoforms displayed distinct positional preferences between 3-OH and 7-OH in the glucuronidation of flavonols. The differentiated kinetics properties between 3-O- and 7-O- glucuronidation indicated that the at least two distinct binding modes within the catalytic domain were responsible for the formation of these two glucuronide isomers.

3.2. Introduction

Dietary flavonoids such as flavonols, flavones and isoflavones are linked to health benefits against ailments such as cancer and heart diseases (Birt *et al.*, 2001; Ross and Kasum, 2002). However, rapid glucuronidation of flavonoid in both liver and intestine leads to dominant presence of phase II conjugates such as glucuronides and sulfates rather than the parent compound in the systemic circulation (Chen *et al.*, 2003). As a consequence, flavonoids have very poor (less than 5%) in vivo bioavailabilities in animals and humans (Setchell *et al.*, 2001; Busby *et al.*, 2002), which limit their uses as therapeutic agents.

Glucuronidation is a major metabolic pathway either as a primary or secondary (sequential) process in the disposition of xenobiotics (Tukey and Strassburg, 2000). It is catalyzed by UDP-glucuronosyltransferases (UGTs), following a S_N2 mechanism (Radomska-Pandya *et al.*, 2005). On the basis of amino acid sequence identity, human UGTs are classified into four families: UGT1, UGT2, UGT3, and UGT8 (Mackenzie *et al.*, 2005). The most important drug-conjugating UGTs belong to UGT1 and UGT2 families. The human UGT1A gene cluster, located on chromosome 2q37, spans approximately 200 kb. It contains 13 individual promoters/first exons and shared exons 2–5. Each exon 1 spliced to exons 2–5 is regarded as a unique gene which translates to the corresponding active UGT1A isoform excluding the pseudogenes (i.e., UGT1A2p, UGT1A11p, UGT1A12p and UGT1A13p). Among the UGT1A family, 1A8 and 1A10 are expressed almost exclusively in the gastrointestinal tract, 1A3, 1A4 and 1A9 are primarily present in liver, and 1A7 is mainly distributed in stomach or esophagus. In

contrast, 1A1 and 1A6 are ubiquitously present in many tissues including liver and gastrointestinal tract (Fisher *et al.*, 2001; Ohno and Nakajin, 2009).

Glucuronidation phenotyping using recombinant UGT isoforms had been widely applied in variety of areas: (a) determining the major metabolic pathway of a particular drug (Miners *et al.*, 2006, 2010); (b) identifying the main isoform(s) responsible for glucuronidation of a drug (Aprile *et al.*, 2010); (c) correlating glucuronidation between organ and isoform levels (Tang *et al.*, 2009; Zhou *et al.*, 2010); and (d) in silico modeling of various UGT isoforms and discovering the critical structural characteristics of the substrates that recognized by the isoforms (Sorich *et al.*, 2008). The QSAR regression models indicated that substrate hydrophobicity was essential for glucuronidation, which agreed with the location of UGT on the luminal side of endoplasmic reticulum (Sorich *et al.*, 2002). Pharmacophore models identified two key hydrophobic regions adjacent from the site of glucuronidation as the substrate features for UGTs recognition (Smith *et al.*, 2003).

UGT1A subfamily (except UGT1A4 and 1A6) was mainly responsible for glucuronidating flavonoids and the substrate specificities showed extensive overlaps (Tang *et al.*, 2009, 2010). UGT1A4 exclusively metabolized amines containing compounds (Chohan *et al.*, 2006), whereas UGT1A6 exhibit limited substrate specificity for flavonoids (Wong *et al.*, 2009). UGTs biotransform flavonoids into their metabolic derivatives (i.e. glucuronides) by transferring glucuronic acid from the cofactor UDP-glucuronic acid (UDPGA) to the nucleophilic oxygen in the hydroxyl group of the aglycones. Mono-glucuronide isomers are often generated from single flavonoid that

bears more than one conjugation site (Boersma *et al.*, 2002; Davis and Brodbelt, 2008), because the aglycone-binding domain might permit multiple binding modes of the acceptor substrate (Miners *et al.*, 2004). Some key structural features that govern regioselectivity had also been uncovered. For example, 3'-OH group is the major determinant of the regioselectivity of flavonoid glucuronidation by UGT1A1. Flavonoids lacking a 3'-hydroxyl were glucuronidated only at position 7, while those containing this group also formed 3'-O-glucuronides and sometimes 4'-O-glucuronides (Davis and Brodbelt, 2008). Consistent with this observation, human intestine UGTs including UGT1A1 and 1A8 were especially effective in conjugating the 3',4' catechol unit of flavonoids (Boersma *et al.*, 2002).

Most of flavonoids bear more than one potential glucuronidation sites (i.e., aromatic hydroxyl groups), which challenges the computational modeling of substrate specificity in UGT metabolism. More efforts will be needed to clarify the differences between isoform-specific metabolism (including regioselectivity) of flavonoids (so called "expert knowledge"), which can be used to guide the predictive model establishment in UGT metabolism. As a part of the continuing efforts, this study investigated the kinetics of six important UGT1A isoforms (UGT1A1, 1A3, 1A7, 1A8, 1A9 and 1A10) using selected flavonoids having both 3-OH and 7-OH groups. Substrate specificities and regioselectivity were evaluated for each UGT isoform on the basis of the derived kinetics parameters (Zhou *et al.*, 2010; Tang *et al.*, 2009, 2010).

3.3. Materials and methods

3.3.1. Materials

Expressed human UGT isoforms (Supersomes™, i.e., UGT1A1, 1A3, 1A7~1A10) were purchased from BD Biosciences (Woburn, MA). Rabbit anti-human UGT1A polyclonal antibody (H-300) and rabbit anti-goat IgG-HRP were purchased from Santa Cruz Biotechnology (Santa Cruz, CA). Uridine diphosphoglucuronic acid (UDPGA), alamethicin, D-saccharic-1,4-lactone monohydrate, and magnesium chloride were purchased from Sigma-Aldrich (St Louis, MO). Ammonium acetate was purchased from J.T. Baker (Phillipsburg, NJ). Four (4) flavonols (Figure 12) containing both 3-OH and 7-OH groups (i.e., 3,7-dihydroxyflavone (3,7DHF), 3,5,7-trihydroxyflavone, (3,5,7THF) 3,7,4'-trihydroxyflavone (3,7,4'THF), and 3,5,7,4'-tetrahydroxyflavone(3,5,7,4'QHF)) were purchased from Indofine Chemicals (Somerville, NJ). All other materials (typically analytical grade or better) were used as received.

3.3.2. Immunoblotting

The recombinant UGT Supersomes (20 µg) were analyzed by SDS-polyacrylamide gel electrophoresis (10% acrylamide gels) and transferred onto PVDF membranes (Millipore, Bedford, MA). Blots were probed with anti-UGT1A antibody (H-300) (Santa Cruz Biotechnology, Santa Cruz, CA), followed by horseradish peroxidase-conjugated rabbit anti-goat IgG (Santa Cruz Biotechnology, Santa Cruz, CA). Membranes were analyzed on FluorChem FC Imaging system (Alpha Innotech), and intensities of UGT bands were measured by densitometry using the AlphaEase software.

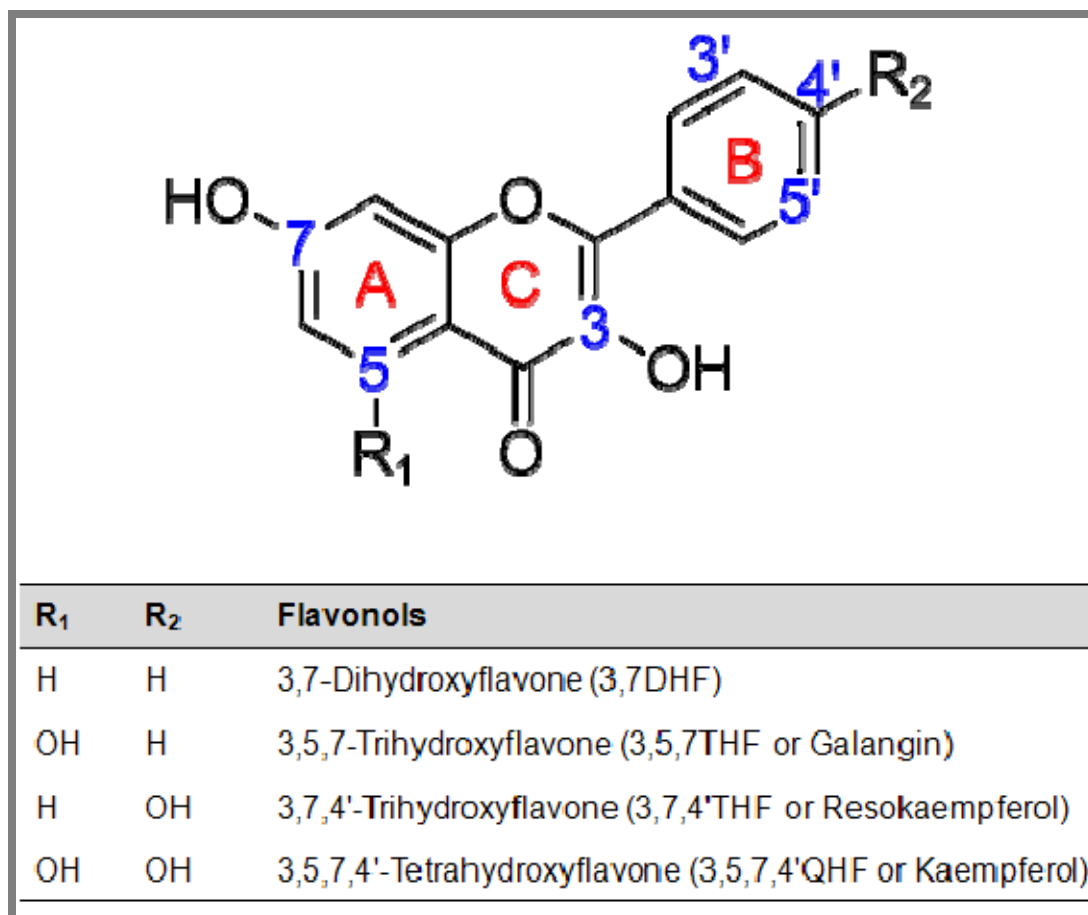


Figure 12. A structural comparison of the model flavonols in Study I

3-OH of C-ring and 7-OH of A-ring are the more favorable positions for glucuronidation by UGT1As.

3.3.3. UGTs kinetics

Enzyme kinetics parameters of glucuronidation by selected UGT1A isoforms (i.e., UGT1A1, 1A3, 1A7, 1A8, 1A9, and 1A10) were determined by measuring initial glucuronidation rates of flavonols at a series of concentrations. The experimental procedures of UGT assays were exactly the same as our previous publications (Tang *et al.*, 2009, 2010). Glucuronide(s) formation was verified to be linear with respect to incubation time and protein concentration. Glucuronidation rates were calculated as nmol glucuronide(s) formed per Supersomes protein amount per reaction time (in unit of nmol/mg protein/min), as the actual enzyme concentration is unknown. The aglycone substrate concentrations in the range of 0.039–40 μ M were used unless method sensitivity or substrate solubility necessitated otherwise. All experiments were performed in triplicates.

3.3.4. UPLC analysis of flavonols and glucuronides:

The Waters ACQUITY UPLC (Ultra performance liquid chromatography) system was used to analyze the parent compounds and the formed glucuronides (see AppendixB/C).

3.3.5. Glucuronide structure identification

Glucuronide structures were identified via a 3-step process as summarized in our earlier publication (Singh *et al.*, 2010). First, the glucuronides were hydrolyzed by β -D-glucuronidase to the aglycones. Second, the glucuronides were identified as mono-glucuronides which showed mass of [(aglycone's mass)+176] Da using UPLC/MS/MS. 176 Da is the mass of single glucuronic acid. Finally, the sites of glucuronidation were confirmed by the "UV spectrum maxima (λ_{max}) shift method". In general, if a 3-, 5- or 4'-

hydroxyl group on the flavonol nucleus was glucuronidated, hypsochromic shifts (i.e. to shorter wavelength) were observed in either Band I (300~380nm) or Band II (240~280 nm). The shift in Band I associated with the substitution of 3-hydroxyl group was in the order of 13 ~ 30 nm. Substitution of 5-hydroxyl group resulted in a 5 ~ 15 nm shift in Band II, and glucuronidation of 4'-hydroxyl group produced a 5 ~ 10 nm shift in Band I. In contrast, substitution of the hydroxyl group at position C7 had minimal or no effect on the λ_{max} of the UV spectrum.

3.3.6. Data analysis

Kinetic parameters (V_{max} , K_m and K_{si} (substrate inhibition constant)) were estimated by fitting the Michaelis-Menten and/or substrate inhibition equations to the substrate concentrations and initial rates. Similar to glucuronidation rates, V_{max} values were also determined as nmol glucuronide formed/mg Supersomes protein/min (or nmol/mg protein/min). Eadie-Hofstee plots were used as diagnostics for model selection. Data analysis was performed by GraphPad Prism V5 for Windows (GraphPad Software, San Diego, CA). The goodness of fit was evaluated on the basis of R^2 values, RSS (residual sum of squares), RMS (root mean square) and residual plots.

For a better inter-enzyme comparisons, catalytic efficiencies (or CL_{int} values) of various UGT isoforms-mediated glucuronidation were normalized to UGT1A1 using the relative UGT protein expression level. Then, relative catalytic efficiencies were determined by arbitrarily assigning the calibrated CL_{int} as 1 for the 3-O-glucuronidation of 3,7DHF by UGT1A1.

3.3.7. Statistical analysis

Significance of mean comparison was examined base on student's t-test using GraphPad Prism V5 for Windows (GraphPad Software, San Diego, CA). Statistical significance was demonstrated with $p < 0.05$.

3.4. Results

3.4.1. Relative expression level between the UGT1A enzymes

Relative expression level between the six UGT1A isoform was estimated by Western blot analysis using anti-UGT1A antibody (UGT1A proteins). Each of the isoforms expressed as a protein of apparent molecular mass of approximately 55 kDa (Figure 13). Expression of UGT1A1, 1A3, 1A7, 1A8, 1A9, and 1A10 relative to UGT1A1 was 1:0.82:0.94:1.15:0.87:0.93.

3.4.2. Regioselective glucuronidation of flavonols by UGT1A1

The model flavonols (3,7DHF, 3,5,7THF, 3,7,4'THF and 3,5,7,4'QHF) present four possible glucuronidation sites (i.e., 3-OH, 5-OH, 7-OH and 4'-OH). Only 3-O- and 7-O-glucuronides were observed at all studied concentrations for all four compounds. This is consistent with the fact that 4'-OH and 5-OH are typically inactive positions for UGT1As, when they are co-present with 3-OH or 7-OH (Tang *et al.*, 2010). The kinetics parameters of 3,7,4'THF glucuronidation by UGT1A3, 1A7, 1A8 and 1A10 were not determined, because the compound was not found to be metabolized by these UGT isoforms.

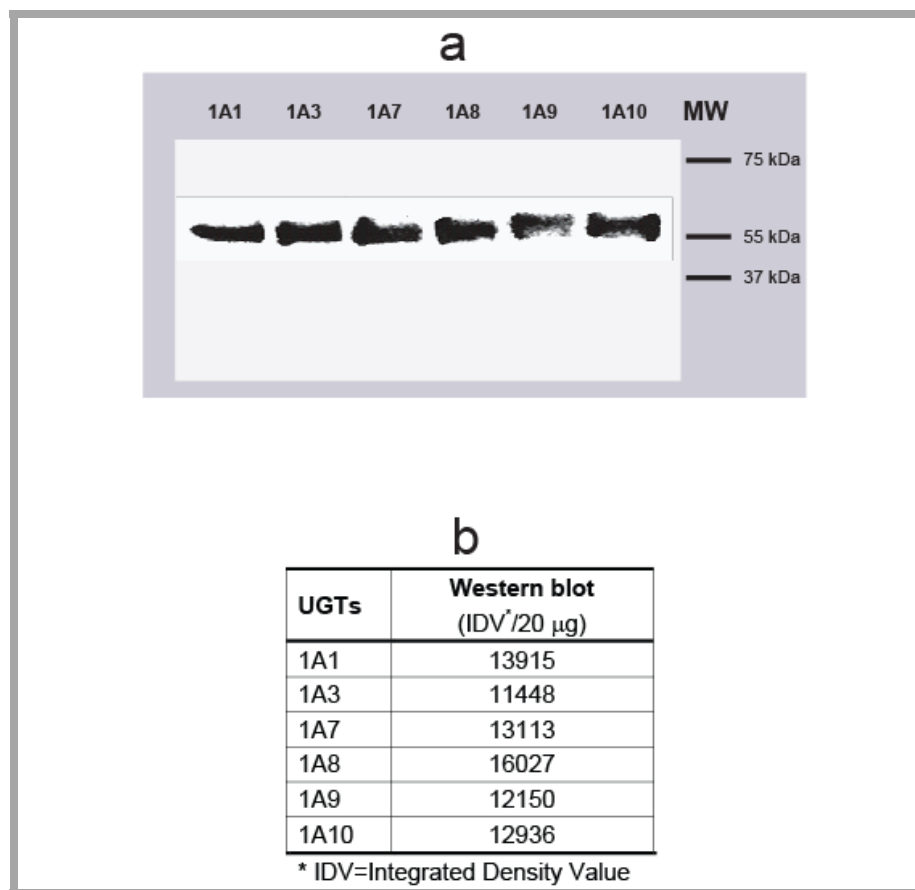


Figure 13. Relative protein quantification of UGT isoforms

Panel a: Western blot analysis of UGT expression levels in recombinant human UGT SupersomesTM. **Panel b:** UGT band intensities for the six UGT isoforms.

UGT1A1 consistently generated much more flavonol-7-O-glucuronides than 3-O-glucuronides over the tested concentration range for 3,7DHF, 3,5,7THF and 3,5,7,4'QHF (Figure 14). The formation ratios of 7-O-glucuronides/3-O-glucuronides fell into the narrow ranges of 3.0~4.2 and 2.3~4.1 for 3,7DHF and 3,5,7THF, respectively. In the cases of 3,7DHF and 3,5,7THF, K_m values were similar between the formation of 3-O- and 7-O-glucuronides, but the differences of V_{max} values were more than 3 folds in favor of 7-O-glucuronidation. Therefore, UGT1A1 had much higher catalytic efficiency (as reflected by $CL_{int} = V_{max}/K_m$) for 7-OH than that for 3-OH group (greater than 3.4 folds). Together with the fact that the enzyme had the highest binding affinity with 3,5,7,4'QHF but showed medium V_{max} , the results suggested that higher binding affinity was not as necessarily associated with higher catalytic capacity. For 3,7,4'THF, the formation rates of 7-O-glucuronide were slightly higher than those of 3-O-glucuronide (Figure 14), and the derived kinetics parameters for the positional glucuronidation were similar to each other.

Surprisingly, strong substrate inhibition pattern characterized by K_{si} values in the range of 0.60 ~ 5.41 μM was observed for both 3-O-glucuronidation and 7-O-glucuronidation. The K_m values were in the range of 0.13~1.57 μM , which were much smaller than reported K_m value (49.8 μM) for ethinylestradiol (Luukkanen *et al.*, 2005). UGT1A1 kinetics towards ethinylestradiol also presented substrate inhibition profile at high concentrations of UDPGA, which gave the K_{si}/K_m ratio of 1.61. By contrast, K_{si}/K_m ratio for 3,7DHF was much less than this number, at 0.38 and 1.16 for 3-O- and 7-O-glucuronidation, respectively.

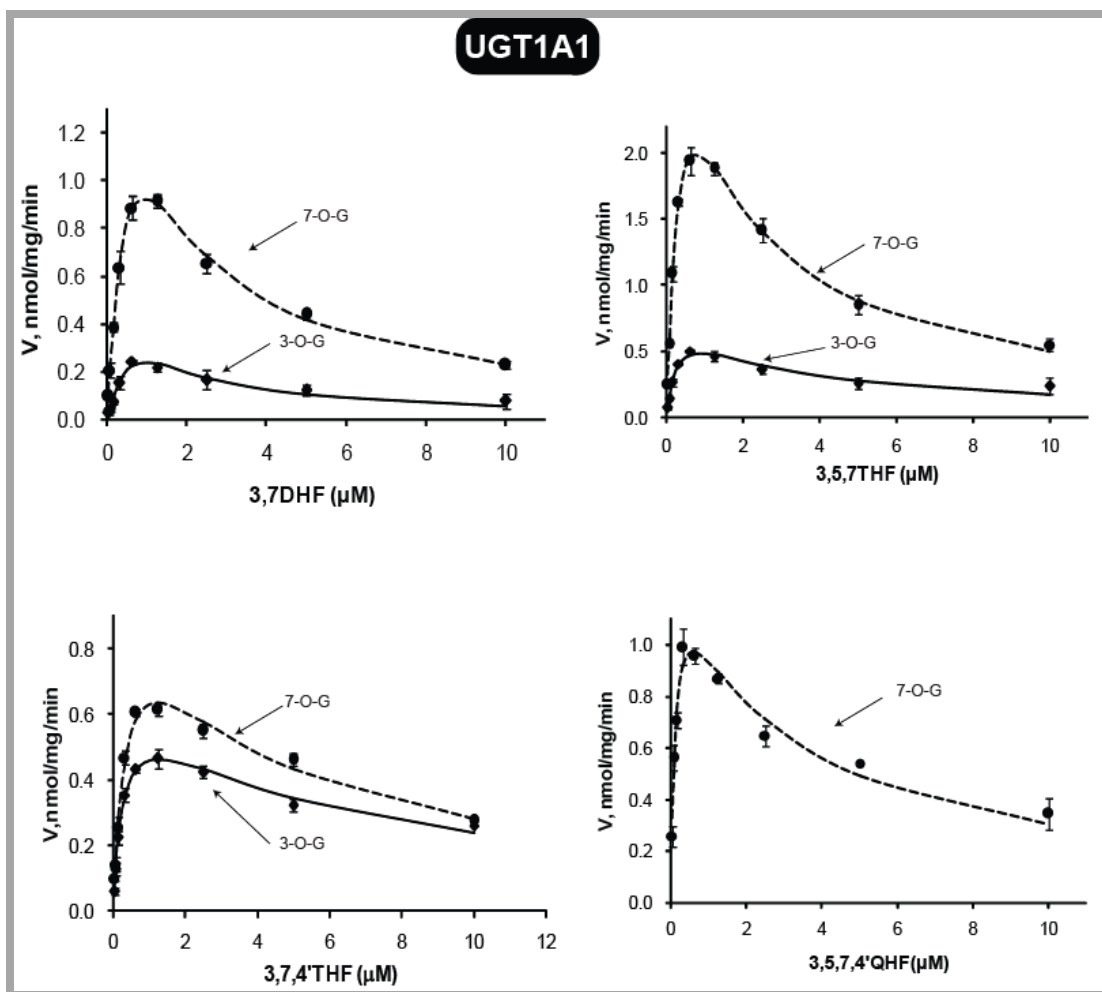


Figure 14. Kinetic profiles for UGT1A1-mediated glucuronidation of four flavonols (3,7DHF, 3,5,7THF, 3,7,4'THF and 3,5,7,4'QHF)

For figures 14~19, solid and dashed lines denote formation rates of flavonol 3-O-glucuronides and 7-O-glucuronide respectively. Each data point represents the average of three replicates. Experimental details are presented under Materials and Methods.

3.4.3. Regioselective glucuronidation of flavonols by UGT1A3

Similar to UGT1A1, UGT1A3 also produced much more flavonol 7-O-glucuronides than 3-O-glucuronides (Figure 15). The formation ratios of 7-O-glucuronides/3-O-glucuronides ranged from 8.6~11.9 for 3,7DHF, whereas they spanned from 7.2 to 17 for 3,5,7THF. Likewise, UGT1A3 displayed substrate inhibition kinetics with the regiospecific metabolism (Figure 15). The substrate inhibition constants (K_{si}) lied within 7.52~100.05 μM that are significantly larger than those of UGT1A1 ($p < 0.05$). K_m values of the UGT1A3-flavonols interaction ranged from 0.84 to 8.81 μM . Comparing to UGT1A1, UGT1A3 seemed to have even higher preference for 7-OH metabolism, since the catalytic efficiency ratios (i.e., 7-OH over 3-OH) were up to 13.5 and 8.1 for 3,7DHF and 3,5,7THF, respectively. However, UGT1A3 was generally less efficient than UGT1A1 in glucuronidating flavonols, as evidenced by lower relative catalytic efficiencies for each flavonol (Table 1). It is also noted that, for 3,5,7,4'QHF, UGT1A1 and 1A3 only generated 7-O-glucuronide. These two enzymes were also shown to very efficiently metabolize flavones that contain 7-OH (data not shown).

3.4.4. Regioselective glucuronidation of flavonols by UGT1A7

In contrast to UGT1A1 and 1A3, UGT1A7 more specifically catalyzed formation of flavonol 3-O-glucuronide (Figure 16). The rate differences between 3-O- and 7-O-glucuronidation decreased markedly with increasing concentration of flavonols. The formation ratios of 3-O-glucuronide over 7-O-glucuronide at 1.25 μM were 24.7, 11.0 and 5.6 for 3,7DHF, 3,5,7THF and 3,5,7,4'QHF respectively, whereas those corresponding

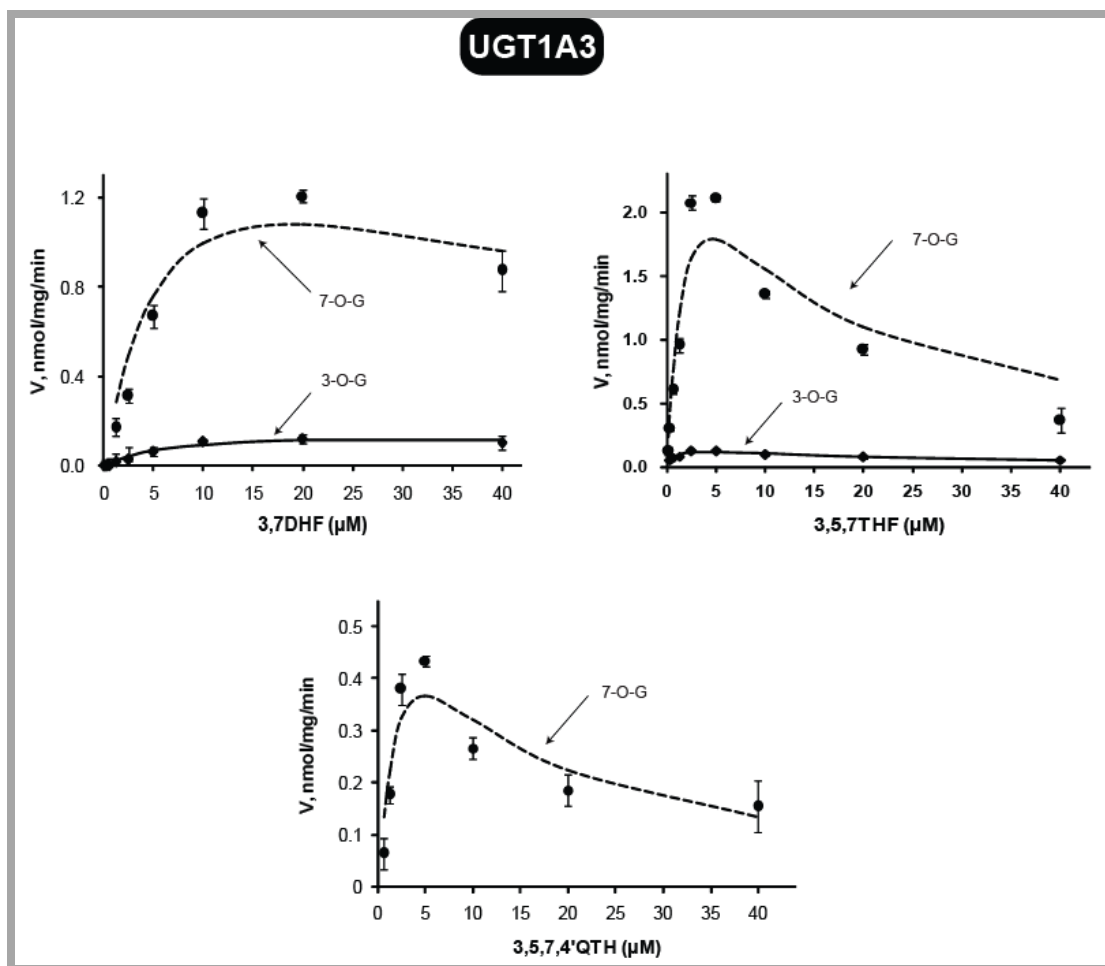


Figure 15. Kinetic profiles for UGT1A3-mediated glucuronidation of three flavonols (3,7DHF, 3,5,7THF and 3,5,7,4'QHF)

Table 1. Normalized catalytic efficiencies (based on the relative UGT1A expression levels) of six recombinant human UGT1As in glucuronidation of flavonoids. Relative catalytic efficiency ($V_{\max}/K_m = 1.0$) was arbitrarily assigned for the 3-O-glucuronidation of 3,7DHF by UGT1A1.

UGT1A	3,7DHF		3,5,7THF		3,7,4'THF		3,5,7,4'QHF	
	3-O-G*	7-O-G*	3-O-G*	7-O-G*	3-O-G*	7-O-G*	3-O-G*	7-O-G*
1A1	1.0	4.5	4.1	13.8	3.5	3.9	0.0	16.3
1A3	0.0	0.5	0.4	3.0	0	0	0.0	0.5
1A7	2.1	0.0	6.7	0.2	0	0	0.9	0.2
1A8	0.1	0.0	0.8	0.2	0	0	0.4	0.3
1A9	36.8	2.4	19.2	8.4	12.8	0.8	10.6	0.4
1A10	0.0	0.0	0.7	0.3	0	0	1.0	0.5

*3-O-G: 3-O-glucuronidation; 7-O-G: 7-O-glucuronidation

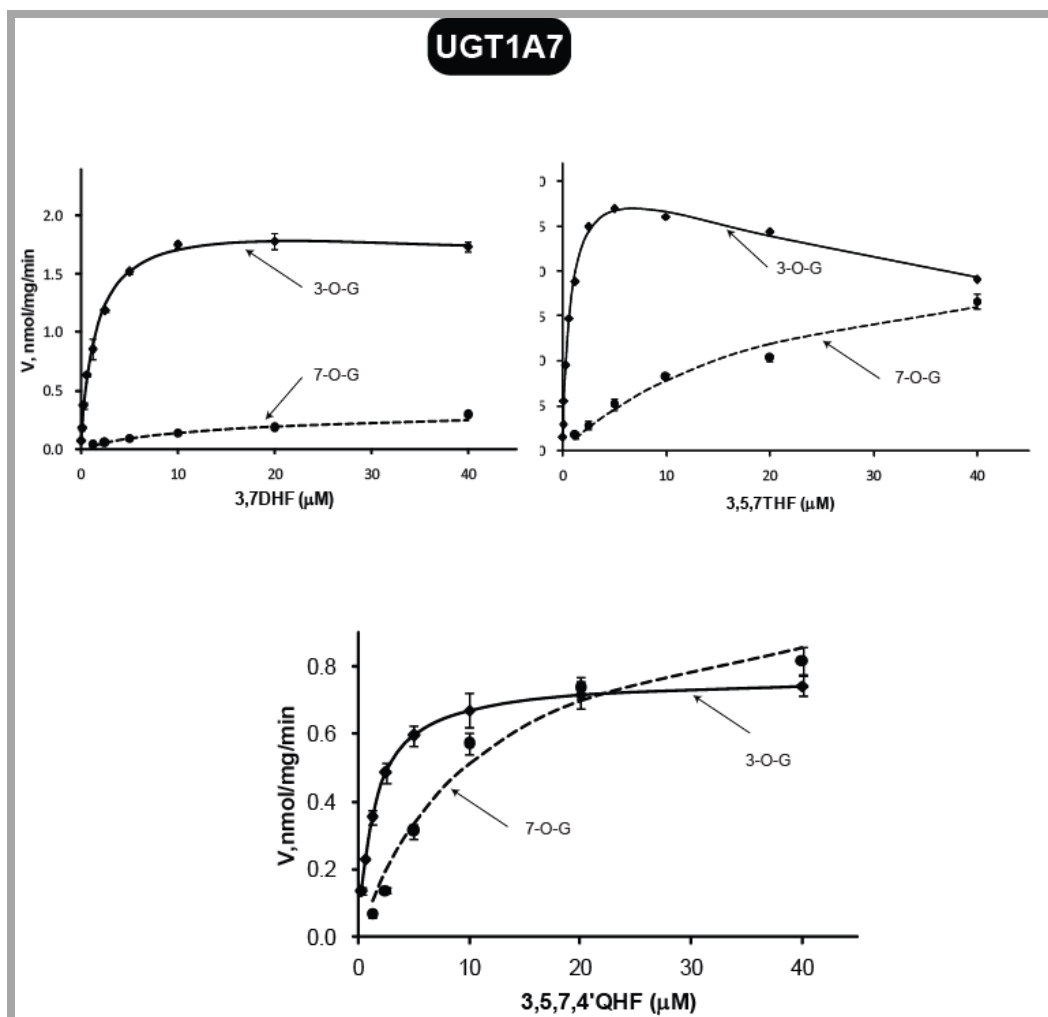


Figure 16. Kinetic profiles for UGT1A7-mediated glucuronidation of three flavonols (3,7DHF, 3,5,7THF and 3,5,7,4'QHF).

values were 5.9, 1.1 and 1.0 at 40 μM . CL_{int} differences between 3-O- and 7-O-glucuronidation hit 63.5-, 37.2- and 5.3-folds for 3,7DHF, 3,5,7THF and 3,5,7,4'QHF, respectively. K_m values for 7-O-glucuronidation (11.56~23.17 μM) were much higher than that for 3-O-glucuronidation (0.82~1.61 μM), which suggested that UGT1A7 binding pocket might favor more the binding mode of flavonols for producing 3-O-glucuronides than that for generating 7-O-glucuronides.

3.4.5. Regioselective glucuronidation of flavonols by UGT1A8

The comparisons between formation of flavonol 3-O- and 7-O-glucuronides revealed that UGT1A8 recognized 3-OH better than 7-OH (Figure 17). The degree of regioselectivity between 3-OH and 7-OH varied with the concentration of flavonols. The ranges of the glucuronidation ratios of 3-OH over 7-OH were 1.5~3.8, 2.6~4.4 and 0.81~2.59 for 3,7DHF, 3,5,7THF and 3,5,7,4'QHF, respectively. The differences in catalytic efficiency of 3-OH and 7-OH were >4-fold for 3,7DHF and 3,5,7THF, >2-fold for 3,5,7,4'QHF.

3-O-/7-O-glucuronidation were enhanced more than 5.7 times in the presence of 5-OH (3,7DHF vs. 3,5,7THF), however, additional 4'-OH decreased the catalytic efficiency of 3-O-glucuronidation from 0.60 to 0.31 ml/min/mg protein. The catalytic capacities (V_{max}) for 3,7DHF and 3,5,7,4'QHF were as low as 0.74~0.76 nmol/mg protein/min, whereas for the analog 3,5,7THF, the enzyme showed a much higher V_{max} value of 3.89 nmol/mg protein/min (3-O-glucuronidation alone).

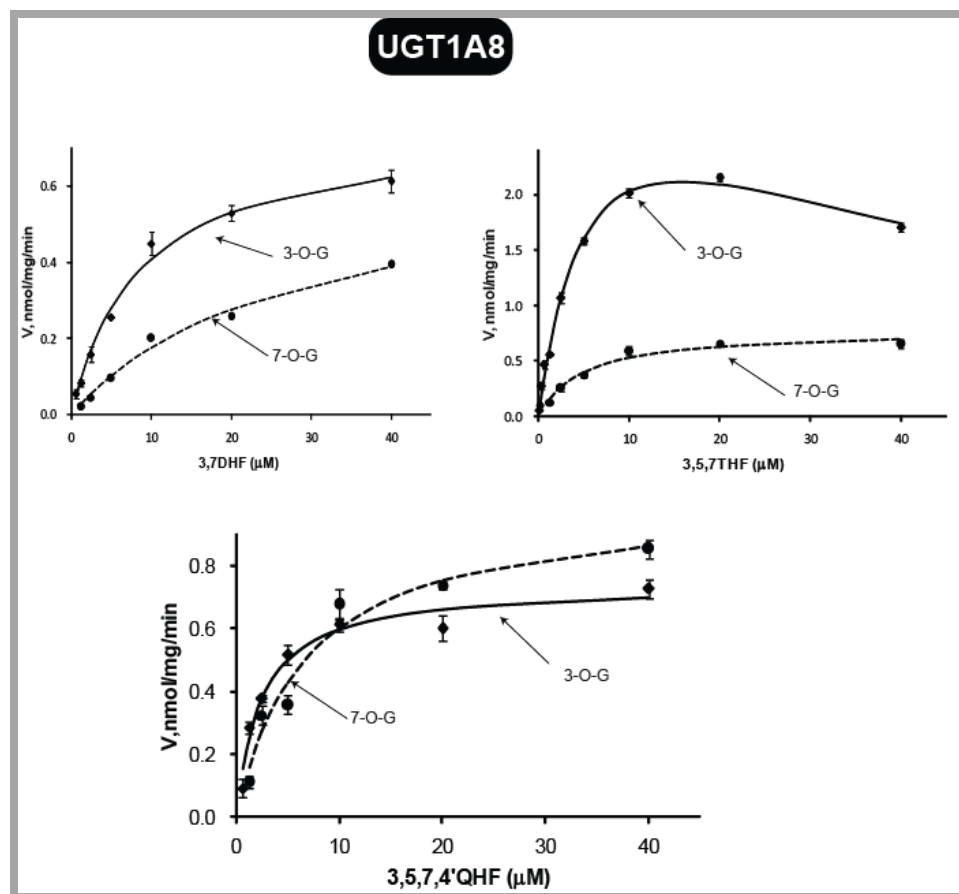


Figure 17. Kinetic profiles for UGT1A8-mediated glucuronidation of three flavonols (3,7DHF, 3,5,7THF and 3,5,7,4'QHF).

3.4.6. Regioselective glucuronidation of flavonols by UGT1A9

UGT1A9 also preferentially glucuronidated 3-OH of flavonols (Figure 18). The 3-OH preference was more obvious at lower concentration. The formation ratio of 3-O- over 7-O-glucuronide was typically larger than 2 at concentrations of $< 2 \mu\text{M}$. The catalytic efficiencies of UGT1A9 for 3-OH were more than 14.4-folds higher than that for 7-OH (except 3,5,7THF which showed a smaller difference at 2.3-fold). The K_m values of 7-O-glucuronidation were generally significantly ($p < 0.05$) larger than those of 3-O-glucuronidation (except 3,5,7THF that had similar K_m values). UGT1A9 showed the highest catalytic efficiency among the tested UGT1A isoforms (Table 1), and the CL_{int} values were no less than 6 ml/min/mg protein (3-O-glucuronidation alone). Interestingly, the V_{max} values appeared negatively correlated with the K_m values, the K_m values that were less than $1 \mu\text{M}$ coincided with V_{max} values of higher than 1.9 nmol/mg protein/min (except 7-O-glucuronidation of 3,7DHF). Additionally, 3,7,4'THF was a good substrate for UGT1A9, a fair substrate for UGT1A1, but a non-substrate for 1A3, 1A7, 1A8 or 1A10.

3.4.7. Regioselective glucuronidation of flavonols by UGT1A10

UGT1A10 was another 3-OH preferred enzyme (Figure 19). This was observed in the regioselective glucuronidation of 3,5,7THF and 3,5,7,4'QHF. The ratio of 3-O- over 7-O-glucuronidation rate were ~ 2.3 and $1.1\sim 1.9$ for 3,5,7THF and 3,5,7,4'QHF, respectively. The CL_{int} values for 3-O-/7-O-glucuronidation were 0.45/0.19 ml/min/mg protein for 3,5,7THF, 0.60/0.33 ml/min/mg protein for 3,5,7,4'QHF. In the absence of 5-OH, 3,7DHF was a very poor substrate of UGT1A10 having V_{max} value of $0.19\sim 0.26$ nmol/mg

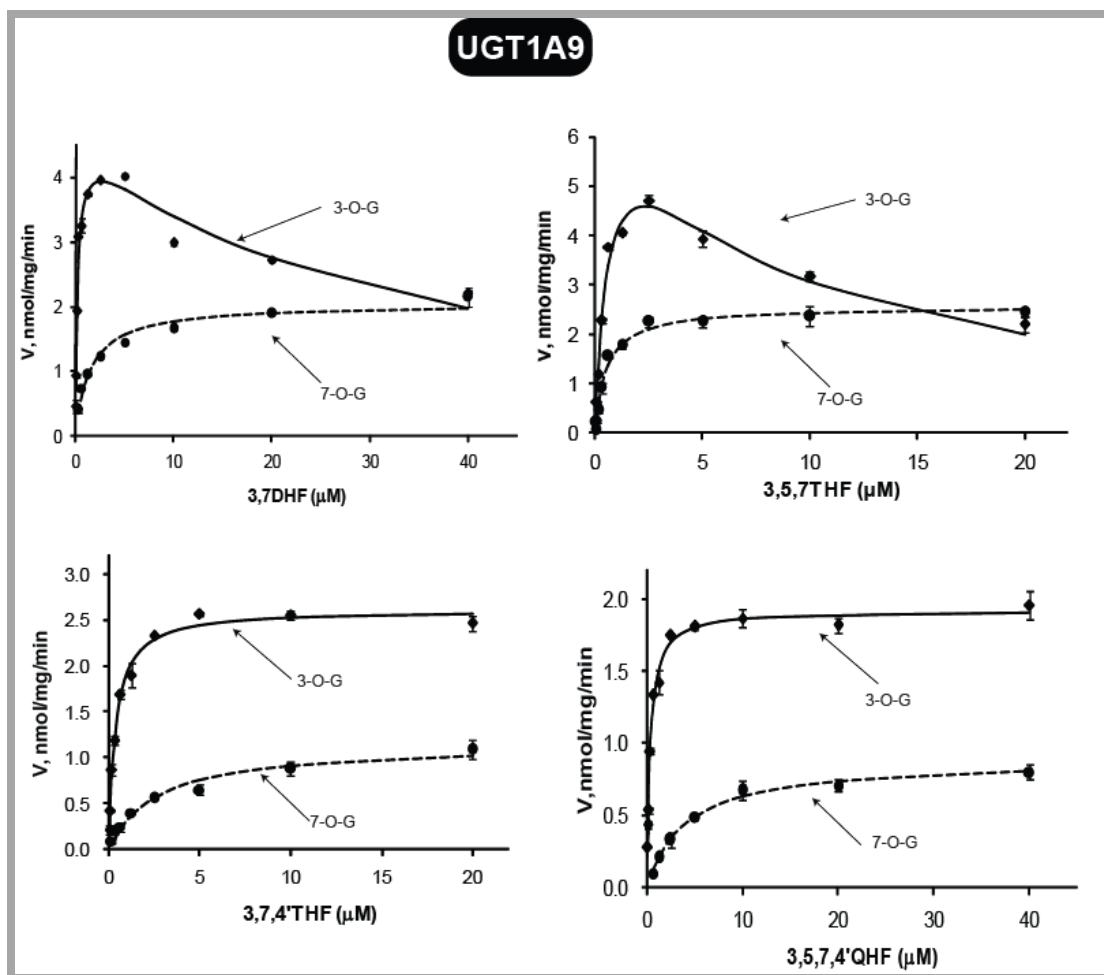


Figure 18. Kinetic profiles for UGT1A9-mediated glucuronidation of four flavonols (3,7DHF, 3,5,7THF, 3,7,4'THF and 3,5,7,4'QHF).

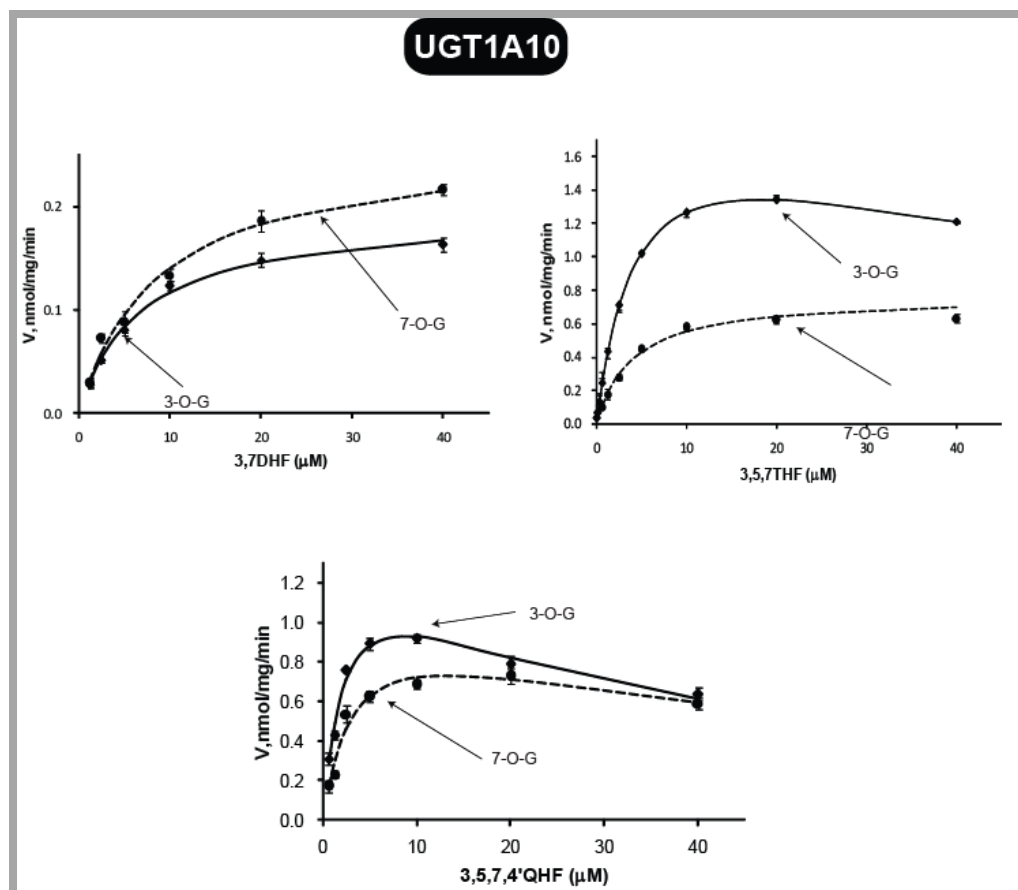


Figure 19. Kinetic profiles of UGT1A10-mediated glucuronidation of three flavonols (3,7DHF, 3,5,7THF and 3,5,7,4'QHF).

protein/min and CL_{int} value of 0.03 ml/min/mg protein, and 3,7,4'THF was a non-substrate of the enzyme. This indicated that 5-OH was essential for the interaction between UGT1A10 and flavonols, although this group itself was not glucuronidated. It is also reflected that the model compounds bind much weaker to UGT1A10 than to UGT1A9. UGT1A10 exhibited similar K_m values for 3-O-/7-O-glucuronidation, which ranges from 3.96 to 8.74 μ M and were significantly larger than the K_m values of UGT1A9 ($p < 0.05$) (0.22~0.68 μ M for 3-O-glucuronidation alone).

3.4.8. Relative catalytic efficiencies between UGT1A enzymes

Relative catalytic efficiencies of the six UGT1As are summarized in Table 1. Based on protein sequence identity counting the substrate binding domain, UGT1A1 and 1A3, on average, are only approximately 50% identical to each other and to the polypeptides of UGT1A7–1A10 cluster. By contrast, the polypeptides within UGT1A7–1A10 cluster are 75–92% identical ([Mackenzie et al., 2005](#)). Interestingly, with less shared amino acids, UGT1A1 and 1A3 showed great similarity in regioselective glucuronidation of flavonols (7-OH preference), despite of the existing gaps in relative catalytic efficiency (CL_{int}) (Table 1). On the other hand, UGT1A7–1A10 cluster which share □much higher sequence identities commonly preferred to metabolize 3-OH of flavonols. Nevertheless, these isoforms exhibited divergent catalytic efficiency towards the aglycones (Table 1). UGT1A9 showed relative CL_{int} ratio of >11, whereas the rest of enzymes generally glucuronidated flavonols at relative CL_{int} ratio of < 2.1 with the exception of 3-O-glucuronidation of 3,5,7THF by UGT1A7.

3.5. Discussion

In this paper, we for the first time elucidated regioselective glucuronidation of four multi-hydroxyl flavonols by six human UGT1A isoforms via kinetics determination utilizing a normalized expressed level. The “hallmarks” (i.e., distinct regioselectivity and/or substrate selectivity) as presented by the glucuronidation patterns (Table 1), helped uncover the fact that these UGT1A isoforms do not always have overlapping substrate specificities with respect to regiospecific glucuronidation. The findings are novel in contrast to previous reports that showed extensive overlapping of UGT1A substrate specificity towards flavonoids (Tang *et al.*, 2009, 2010; Miners *et al.*, 2010). For example, 3-hydroxyflavone at 2.5 μ M was similarly metabolized by UGT1A1, 1A7, 1A8, 1A9 and 1A10 (Tang *et al.*, 2010). The current approach holds great promises on identifying those substrates (probes) that are exclusively metabolized by a particular UGT isoform. Because of the prevalence of UGT generic variants, understanding of regiospecificity of UGT isoform-mediated glucuronidation is also very important to anticipate metabolism in vivo, and modeling/prediction of glucuronidation in silico. Moreover, results here would greatly assist in enzymatically synthesizing flavonoid glucuronides conjugated at desired position(s) for pharmaceutical and/or analytical purposes, as accumulating in vitro and in vivo evidences point to the ability of various (regiospecific) flavonoid glucuronides to retain biological activities (Williamson *et al.*, 2005).

The above observations were made using kinetics profiling (specificity and/or regioselectivity) over a wide concentration range. This approach appears to be superior

to the more commonly used method of measuring the enzyme activities at a single high substrate concentration ($>100\ \mu\text{M}$) (Boersma *et al.*, 2002; Davis and Brodbelt, 2008). Although the latter approach has the advantages of less cost and labor, this practice might generate an erroneous conclusion, if the concentration was not properly chosen. For example, the formation of 3-O-glucuronide by UGT1A9 was much faster than that of 7-O-glucuronide for 3,7DHF at concentrations of less than $20\ \mu\text{M}$ (Figure 18). However, no significant regioselectivity between 3-OH and 7-OH was visible, if glucuronidation rates were only determined at a concentration of over $40\ \mu\text{M}$. The similar observations were made with UGT1A7 metabolism of 3,5,7THF, as well as glucuronidation of 3,5,7,4'QHF by UGT1A7, 1A8 and 1A10. In addition, the kinetics profiling included substrate concentrations less than $1\ \mu\text{M}$, which is close to the in vivo plasma concentration of flavonoids after they are taken orally (Setchell *et al.*, 2001). Therefore, the data might have greater potential to correlate with in vivo especially hepatic metabolism.

The kinetics profiling studies indicate that all UGT1A isoforms have more than one binding site for flavonoids, since their glucuronidation of flavonols displayed strong substrate inhibition patterns. To explain this pattern, one model was proposed by Hutzler and Tracy, who advocate a hypothetical two-site binding model, in which one binding site is productive, whereas the other site is inhibitory and operable only at high substrate concentrations (Hutzler and Tracy, 2002). Another group of investigators proposed a compulsory ordered bi bi (two substrates and two products) kinetic model to explain substrate inhibition of UGT1As (Luukkanen *et al.*, 2005). We used a similar approach

and showed that UGT1A9 catalyzed glucuronidation of 3,7,4'-trihydroxyflavone indeed followed the identical kinetic model (data not shown). Therefore, one reasonable explanation of the substrate inhibition was that binding of the aglycone substrate to the enzyme-UDP complex led to a nonproductive dead-end complex that slows the completion of the catalytic cycle (Segel, 1993).

The hypothesis that there are at least two distinct binding modes present in UGT1As is also strongly supported by the fact that positional (3-O- or 7-O-) glucuronidation always has different kinetic parameters (Miners *et al.*, 2004). The differentiated K_m (binding affinity) or V_{max} (reflecting turnover K_{cat}) values in production of the regiospecific glucuronides indicate that the enzymes provide two divergent interacting environments within which a single flavonol may orient differently. This most likely resulted from one very large active site, instead of two separate small active sites, as supported by the use of UGT1A1 homology models (Li and Wu, 2007; Laakkonen and Finel, 2010). Taken together, this body of evidences is in strong support of the theorem that there are at least two binding modes for UGT1A-mediated glucuronidation of flavonols, which can be used as the “expert knowledge” for in silico modeling of UGT1A-mediated glucuronidation.

Structure of flavonols could significantly impact the regioselective glucuronidation rates, regardless of how many modes of bindings are present in UGT1As. In general, the preference order was 3-OH or 7-OH > 4'-OH > 5-OH among the model flavonols, where the 5-OH and 4'-OH groups were relatively inactive for glucuronidation. These two positions remain poorly active even in the absence of more active -OH groups, as

reaction rates of eight flavones with only 5 or 4'-OH available for conjugation was much slower than those shown in this study (data not shown). Even though 5-OH or 4'-OH was not glucuronidated itself, the presence of a -OH group at the C4' or C5 had major but opposite effects on glucuronidation at the 3 or 7-OH position. The addition of 5-OH generally enhanced the UGT1A-mediated conjugation (excluding UGT1A9), as evidenced by the comparisons between 3,7DHF and 3,5,7THF, or between 3,7,4'THF and 3,5,7,4'QHF in catalytic efficiency (Table 1). The enhancement was largely ascribed to more efficient formation of the regioselective conjugates (7-O-glucuronide for UGT1A1 and 1A3; 3-O-glucuronide for UGT1A7, 1A8 and 1A10). The significance of 5-OH in isoform-specific glucuronidation at the 3-OH or 7-OH positions were also observed for compounds such as chrysin, wogonin, oroxylin A, and 3,5-dihydroxyflavone (Zhou *et al.*, 2010; Tang *et al.*, 2010). On the contrary, the addition of 4'-OH compromised UGT1A3-, 1A7-, 1A8-, and 1A9-mediated glucuronidation by substantially reducing their respective positional glucuronidation (Table 1). The fact that 3-O- or 7-O-glucuronidation was reduced in the presence of 4'-OH was also supported by the observation that 3-O-glucuronidation of 3,4'-dihydroxyflavone was slower than 3-hydroxyflavone at three different concentrations (Tang *et al.*, 2010).

In conclusion, among the six UGT1As (UGT1A1, 1A3, 1A7, 1A8, 1A9 and 1A10), UGT1A1 and UGT1A9 were the most efficient conjugating enzymes with the smallest K_m values ($\leq 1\mu\text{M}$) and highest intrinsic clearance values. Regardless of their distinctive substrate specificities towards the flavonols, UGT1A1 and 1A3 favored 7-O-glucuronidation, whereas UGT1A7, 1A8, 1A9 and 1A10 preferred 3-O-glucuronidation.

The highly different kinetic parameters between 3-O- and 7-O- glucuronidation suggested that the (at least) two distinct binding modes within the catalytic domain were responsible for the formation of these two glucuronide isomers, which should be considered as useful “expert knowledge” for modeling and predicting UGT1A-mediated glucuronidation. Studies are ongoing to explore these binding modes using homology-based approaches and plant UGT crystal structures.

Chapter 4 Evaluation of 3,3',4'-trihydroxyflavone and 3,6,4'-trihydroxyflavone as the in vitro functional markers for hepatic UGT1A1 (Study II)

4.1. Abstract

Identifying UDP-glucuronosyltransferase (UGT)-selective probes (substrates that are primarily glucuronidated by a single isoform) is complicated by the enzymes' large overlapping substrate specificity. In this study, regioselective glucuronidation of two flavonoids 3,3',4'-trihydroxyflavone (33'4'THF) and 3,6,4'-trihydroxyflavone (364'THF) is used to probe the activity of hepatic UGT1A1. The glucuronidation kinetics of 33'4'THF and 364'THF was determined using 12 recombinant human UGT isoforms and pooled human liver microsomes (pHLM). The individual contribution of main UGT isoforms to the metabolism of the two flavonoids in pHLM was estimated using the relative activity factor approach. UGT1A1 activity correlation analyses using flavonoids-4'-O-glucuronidation vs. β -estradiol-3-glucuronidation (a well-recognized marker for UGT1A1) or vs. SN-38 glucuronidation were performed using a bank of HLMS (n=12) including three UGT1A1-genotyped HLMS (i.e., UGT1A1*1*1, UGT1A1*1*28 and UGT1A1*28*28). The results showed that UGT1A1 and 1A9, followed by 1A7, were the main isoforms for glucuronidating the two flavonoids, where UGT1A1 accounted for $92 \pm 7\%$ and $91 \pm 10\%$ of 4'-O-glucuronidation of 33'4'THF and 364'THF, respectively, and UGT1A9 accounted for most of the 3-O-glucuronidation. Highly significant correlations ($R^2 > 0.944$, $p < 0.0001$) between the rates of flavonoids 4'-O-glucuronidation and that of estradiol-3-glucuronidation or SN-38 glucuronidation were observed across 12 HLMS. In conclusion, UGT1A1-mediated 4'-O-glucuronidation of 33'4'THF and 364'THF were

highly correlated with glucuronidation of estradiol (3-OH) and SN-38. This study demonstrated for the first time that regioselective glucuronidation of flavonoids can be applied to probe hepatic UGT1A1 activity in vitro.

4.2. Introduction

UDP-glucuronosyltransferases (UGTs)-mediated glucuronidation is a major phase II metabolic pathway that facilitates efficient elimination and detoxification of structurally diverse groups of xenobiotics (e.g., SN-38 and nitrosamines) and endogenous compounds (e.g., bilirubin and estradiol). UGT genetic deficiency and polymorphisms are associated with inherited physiological disorders, whereas inhibition of glucuronidation by the concomitant use of certain drugs is related to drug induced toxicities (Tukey and Strassburg, 2000; Kiang *et al.*, 2005; Wu *et al.*, 2011). On the other hand, extensive glucuronidation can be a barrier to oral bioavailability as rapid and extensive first-pass glucuronidation (or premature clearance by UGTs) of orally administered agents usually results in the poor oral bioavailability and/or lack of efficacies (Gao and Hu, 2010; Wu *et al.*, 2011).

Human UGTs are classified into four families: UGT1, UGT2, UGT3, and UGT8 (Mackenzie *et al.*, 2005). The most important drug-conjugating UGTs belong to UGT1 and UGT2 families. At present, 16 human UGT isoforms from UGT1A (9 members) and UGT2B (7 members) subfamilies are identified: namely, UGT1A1, 1A3, 1A4, 1A5, 1A6, 1A7, 1A8, 1A9, 1A10, 2B4, 2B7, 2B10, 2B11, 2B15, 2B17 and 2B28 (Mackenzie *et al.*, 2005). Their distribution (probed by mRNA level) in major metabolizing organs, as well

as other organs/tissues were well studied (Ohno and Nakajin, 2009; Izukawa *et al.*, 2009). Compared to UGT1As, UGT2Bs are much more abundantly expressed in human liver. UGT2B4 has the highest expression, followed by UGT2B15. Among the UGT1A isoforms, UGT1A1, 1A4, 1A6 and 1A9 have moderate expression in the liver (Ohno and Nakajin, 2009).

Within the 9 UGT1A isoforms, UGT1A1 is perhaps the most significant one for maintaining human health. Its genetic deficiency may impair the metabolism of bilirubin, resulting in severe hyperbilirubinemia disorders such as Crigler-Najjar Syndrome and Gilbert's syndrome (Radomska-Pandya *et al.*, 1999; Emoto *et al.*, 2010). Moreover, UGT1A1 is mainly responsible for SN-38 clearance (Fujita and Sparreboom, 2010). SN-38 is the active metabolite of irinotecan (CPT-11), a widely used anticancer drug, especially for the treatment of colorectal cancer. Generic polymorphisms in UGT1A1 (e.g., UGT1A1*28 variant with low UGT1A1 expression) has been linked to irinotecan toxicity (O'Dwyer and Catalano, 2006). The frequency of UGT1A1*28 allele (promoter (TA)_{6/7}TAA mutation) varies by ethnic and racial origin, and is ~10% in a white population (Beutler *et al.*, 1998). This high penetration rate necessitates the UGT1A1 genotyping of patients prior to the irinotecan treatment, a protocol recommended by the FDA (O'Dwyer and Catalano, 2006).

Flavonoids are a class of natural polyphenols, consumption of which is linked to numerous health benefits such as antioxidant and anticancer (Crozier *et al.*, 2009). It is well-known that flavonoids are subjected to extensive glucuronidation, resulting in poor oral bioavailabilities (Jeong *et al.*, 2005b; Hu, 2007). Although UGT1A isoforms showed

vast overlapping substrate specificities (as evaluated by counting all metabolites) (Joseph *et al.*, 2007; Tang *et al.*, 2009, 2010; Zhou *et al.*, 2010), regioselective glucuronidation of multi-hydroxyl flavonoids has been demonstrated to be highly isoform-dependent for many flavonoids (Wu *et al.*, 2011). In the study of quercetin glucuronidation, UGT1A3's highest glucuronidation preferred 3'-O-glucuronide, whereas UGT1A9 favored 3-O-glucuronidation (Chen *et al.*, 2005b).

Regioselectivity refers to the preference for formation of one glucuronide isomer over another, when a substrate possesses more than one possible glucuronidation site. Regioselectivity of various UGTs has been examined for a number of compounds such as estradiol, estrone, morphine and resveratrol (Lépine *et al.*, 2004; Brill *et al.*, 2006; Ohno, *et al.*, 2008). In particular, typical generation of a particular glucuronide isomer from a substrate was used to probe UGT activity in human tissues *in vitro*. For example, β -estradiol 3-glucuronidation is considered an excellent marker of UGT1A1 activity (Court, 2005; Donato *et al.*, 2010), and morphine 6-glucuronidation may be used as a selective probe for UGT2B7 activity (Stone *et al.*, 2003).

As stated by Court (2005) and Miners *et al* (2010), UGT-selective probes have many significant applications in the study of drug glucuronidation. For example, they can be used to (1) identify a specific functional UGT in human tissues; (2) predict possible UGT-mediated drug-drug interactions; and (3) elucidate the functional significance of genetic polymorphisms. In this study, we characterized two flavonoids (3,3',4'-trihydroxyflavone and 3,6,4'-trihydroxyflavone) as the UGT1A1 probes based on initial screening (i.e., selectivity evaluation by phenotyping each compound with a panel of recombinant UGT

isoforms) of ~ 67 flavonoid compounds derived from 5 subclasses (flavones, isoflavones, flavonones, chalcones and flavonols) (published and unpublished data) (Joseph *et al.*, 2007; Tang *et al.*, 2009, 2010; Zhou *et al.*, 2010; Singh *et al.*, 2011). The individual contributions of UGT1A1 and/or 1A9 to metabolism of the two flavonoids and SN38 in pooled human liver microsomes were estimated using enzyme kinetic experiments combined with the relative activity factor (RAF). The selectivity of UGT1A1 towards the flavonoids, estradiol and SN-38 were further evaluated in a bank of 12 HLMs based on activity correlation analysis.

4.3. Materials and methods

4.3.1. Materials

Twelve recombinant human UGT isoforms (SupersomesTM, i.e., UGT1A1, 1A3, 1A4, 1A6, 1A7, 1A8, 1A9, 1A10, 2B4, 2B7, 2B15 and 2B17), pooled human liver microsomes (from 50 donors), three UGT1A1 genotyped human liver microsomes (i.e., UGT1A1*1*1 (Wild-type), UGT1A1*1*28 (allelic variant) and UGT1A1*28*28 (allelic variant), and rabbit anti-human UGT1A1 polyclonal antibody were purchased from BD Biosciences (Woburn, MA). A bank of individual human liver microsomes with diverse UGTs activities (n=8, designated as HLM-1, HLM-2, ..., HLM-8) was purchased from Xenotech (Lenexa, KS). Rabbit anti-goat IgG-HRP was purchased from Santa Cruz Biotechnology (Santa Cruz, CA). Two flavonoids (see Figure 20 for chemical structures) (i.e., 3,3',4'-trihydroxyflavone (33'4'THF), and 3,6,4'-trihydroxyflavone (364'THF)) were purchased from Indofine Chemicals (Somerville, NJ). 17 β -estradiol (also referred as estradiol in this paper, see Figure 24 for chemical structure), β -estradiol-3-glucuronide, 7-ethyl-10-

hydroxycamptothecin (SN-38, see Figure 24 for chemical structure), SN-38-glucuronide, propofol, and propofol-glucuronide were obtained from Toronto Research Chemicals (North York, Ontario, Canada). Uridine diphosphoglucuronic acid (UDPGA), alamethicin, D-saccharic-1,4-lactone monohydrate, and magnesium chloride were purchased from Sigma-Aldrich (St Louis, MO). Ammonium acetate was purchased from J.T. Baker (Phillipsburg, NT). All other materials (typically analytical grade or better) were used as received.

4.3.2. Immunoblotting

The recombinant UGT1A1 and human liver microsomes were analyzed by SDS-polyacrylamide gel electrophoresis (10% acrylamide gels) and transferred onto PVDF membranes (Millipore, Bedford, MA). Blots were probed with anti-UGT1A1 antibody (BD Biosciences, Woburn, MA), followed by horseradish peroxidase-conjugated rabbit anti-goat IgG (Santa Cruz Biotechnology, Santa Cruz, CA). Membranes were analyzed on a FluorChem FC Imaging System (Alpha Innotech), and intensities of UGT bands were measured by densitometry using the AlphaEase software.

4.3.3. Glucuronidation assay and kinetics

The experimental procedures of glucuronidation assays were exactly the same as our previous publications ([Singh *et al.*, 2010](#)). Glucuronide(s) formation was verified to be linear with respect to incubation time (5-60 min) and protein concentration (13-53 µg/ml). Glucuronidation rates were calculated as nmol glucuronide(s) formed per reaction time per protein amount (or nmol/min/mg protein), as the actual enzyme concentration is unknown. Enzyme kinetics parameters for glucuronidation were determined by

measuring initial reaction rates at a series of substrate concentrations. All experiments were performed in triplicates.

4.3.4. UPLC analysis:

The Waters ACQUITY™ UPLC (Ultra performance liquid chromatography) system was used to analyze parent compounds (or aglycones) and their respective glucuronides (see Appendix B/C)

4.3.5. Identification of the structure of flavonoid glucuronide

Glucuronide structures were identified using 3 independent methods in a sequential process as summarized in our earlier publication (Singh *et al.*, 2010). First, the glucuronides were hydrolyzed by β -D-glucuronidase to the aglycones. Second, the glucuronides were identified as mono-glucuronides which showed mass of (aglycone's mass+176) Da using UPLC/MS/MS. 176 Da is the mass of a single attached glucuronic acid.

Finally, the sites of glucuronidation were confirmed by the "UV spectrum maxima (λ_{max}) shift method".²⁹⁻³¹ Substitution of 3-hydroxyl group led to a hypsochromic shift (i.e. to shorter wavelength) in band I (300~380nm), the shift was in the order of 13 ~ 30 nm, whereas glucuronidation of 4'-hydroxyl group produced a 5 ~ 10 nm shift. In contrast, substitution of the hydroxyl group at position C6 or C3' had minimal or no effect on the λ_{max} of the UV spectrum.

4.3.6. Data analysis

Kinetic parameters were estimated by fitting the proper models (Michaelis-Menten, substrate inhibition or Hill equations) to the substrate concentrations and initial rates with a weighting of $1/y$. Similar to glucuronidation rates, V_{\max} values were also determined as nmol glucuronide formed /min/mg Supersomes protein (or nmol/mg protein/min). Eadie-Hofstee plots were used as diagnostics for model selection. Data analysis was performed by GraphPad Prism V5 for Windows (GraphPad Software, San Diego, CA). The goodness of fit was evaluated on the basis of R^2 values, RSS (residual sum of squares), RMS (root mean square) and residual plots.

Maximal clearances (CL_{\max}) were estimated using eq. I (Houston and Kenworthy, 2000; Uchaipichat *et al.*, 2004), where V_{\max} is the maximal velocity rate, S_{50} is the substrate concentration resulting in 50% of V_{\max} , and n is the Hill coefficient:

$$CL_{\max} = \frac{V_{\max}}{S_{50}} \times \frac{n-1}{n(n-1)^{1/n}} \quad (\text{eq. I})$$

Correlation (Pearson) analysis was performed by GraphPad Prism V5 for Windows (GraphPad Software, San Diego, CA).

4.3.7. UGT1A1 and 1A9 relative activity factor determination

The relative activity factor (RAF) approach was used for scaling UGT activities obtained using cDNA-expressed enzymes to HLM (Rouguieg *et al.*, 2010). RAFs (eq. II) here were defined as the HLM/recombinant enzyme activity (e.g., CL_{int} , the intrinsic clearance) ratio of a particular isoform toward a probe substrate (Rouguieg *et al.*, 2010).

$$RAF = \frac{CL_{int}\{probe, HLM\}}{CL_{int}\{probe, Supersomes\}} \quad (\text{eq. II})$$

The relative amount of specific substrate metabolism attributed to an individual UGT enzyme was estimated by multiplying glucuronidation parameters (i.e., CL_{int}) observed with this enzyme by the corresponding RAF. In this study, we calculated RAFs for UGT1A1 and UGT1A9 using selective probe substrates for UGT1A1 and 1A9 (1A1: estradiol, 3-glucuronide; 1A9: propofol). Estradiol 3-glucuronidation is an excellent marker for UGT1A1, showing a good correlation with bilirubin glucuronidation ([Zhou *et al.*, 2011](#)). Propofol is considered as an appropriate probe substrate for UGT1A9 in human liver, insomuch as a concentration of below 100 μM (lower than K_m value) is used for activity measurement, because of the potential to be glucuronidated by other UGT isoforms ([Court, 2005](#)).

4.4. Results

4.4.1. UGTs involved in 33'4'THF and 364'THF glucuronidation.

As shown in Figure 20, UGT1A1, 1A7 and 1A9 were the main isoforms glucuronidating both flavonoids. UGT1A9 showed the highest activities, followed by UGT1A1 and 1A7. In terms of the number of glucuronides formed, UGT1A7 and 1A9 only generated a single 3-O-glucuronide, demonstrating a strict 3-OH regioselectivity. By contrast, multiple glucuronide isomers were formed by UGT1A1 (two for 33'4'THF: 3'-O- and 4'-O-glucuronide; three for 364'THF: 3-O-, 6-O-, and 4'-O-glucuronide). UGT1A7 was not considered in further studies, because it expresses only in extrahepatic tissues (i.e., stomach or esophagus) ([Ohno and Nakajin, 2009](#)). We also determined the relative

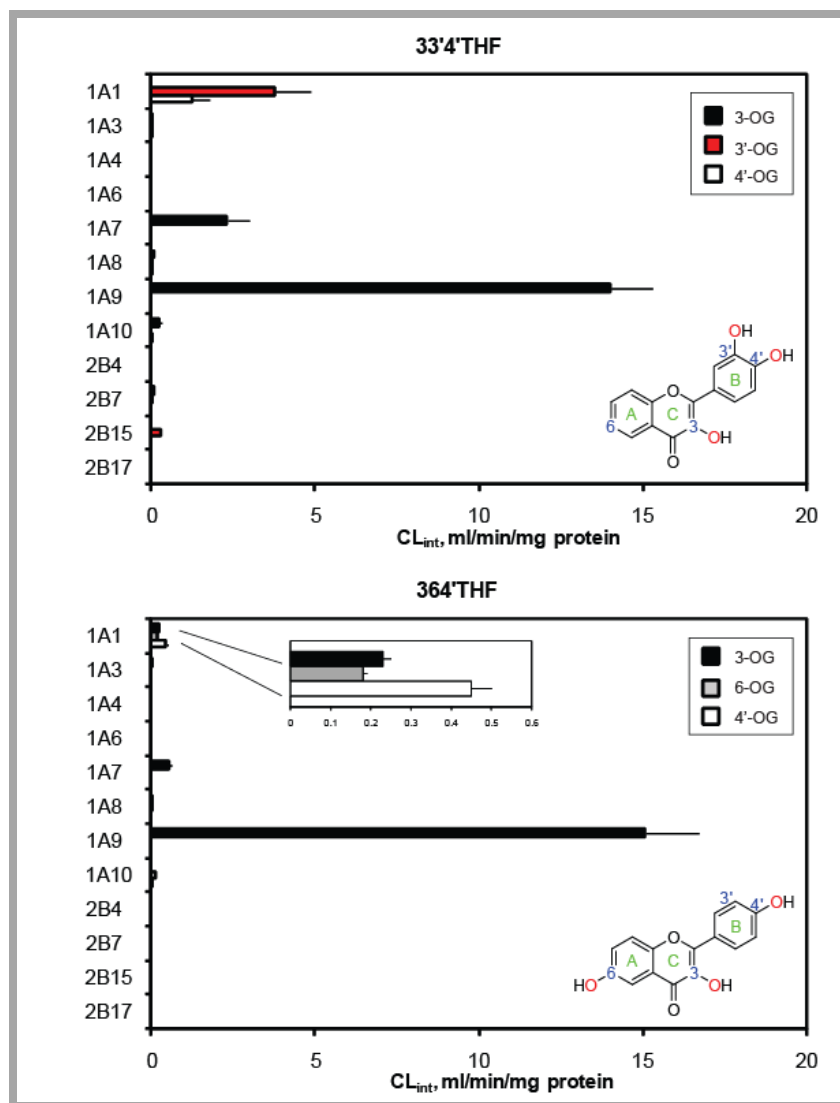


Figure 20. Phenotyping of 33'4'THF (top) and 364'THF (bottom) using 12 recombinant UGTs

UGT1A1, 1A7 and 1A9 were the main isoforms glucuronidating both flavonoids. Intrinsic clearances ($CL_{int} = V_{max}/K_m$) were obtained from kinetic determination. OG: O-glucuronide. Insets show corresponding chemical structures for each flavonoid probe.

expression level between the 8 UGT1A isoforms by Western blot analysis using anti-UGT1A antibody (Santa Cruz Biotechnology, Santa Cruz, CA), as described previously (Uchaipichat *et al.*, 2004). There was only <1.3-fold variability in the apparent expression of the UGT1A isoforms. Thus the UGT1A activity was not normalized using the relative expression. It is acknowledged though that the inter-enzyme activity comparison between UGT1As and UGT2Bs might be affected by the actual enzyme levels which could not be determined due to the lack of a specific antibody for the majority of human UGT isoforms.

4.4.2. Contribution of UGT1A1 and 1A9 to metabolism of 33'4'THF in pHLM

Glucuronidation kinetic profiles and constants derived from incubation of 33'4'THF with pHLM, UGT1A1 and UGT1A9 were shown in Figure 21. The intrinsic clearance (CL_{int}) obtained with recombinant UGT1A1 and UGT1A9 were scaled to pHLM using the RAFs calculated from the UGT1A1-mediated 3-glucuronidation of estradiol (RAF = 0.83, Figure 22a) and UGT1A9-mediated glucuronidation of propofol (RAF = 0.14, Figure 22b). As can be seen in Figure 21, the scaled CL_{int} of UGT1A1 and UGT1A9 represented $92 \pm 7\%$ (4'-O-glucuronidation) and $95 \pm 9\%$ (3-O-glucuronidation) of the CL_{int} values in pHLM, respectively. In addition, UGT1A1 contributed a less percentage (77%) of 3'-O-glucuronidation in pHLM. The residual (approximately 23%) 3'-O-glucuronide production in pHLM might be attributable to UGT2B15, which is second most abundant in human liver 6 and showed some 3'-O-glucuronidation activity (Figure 20).

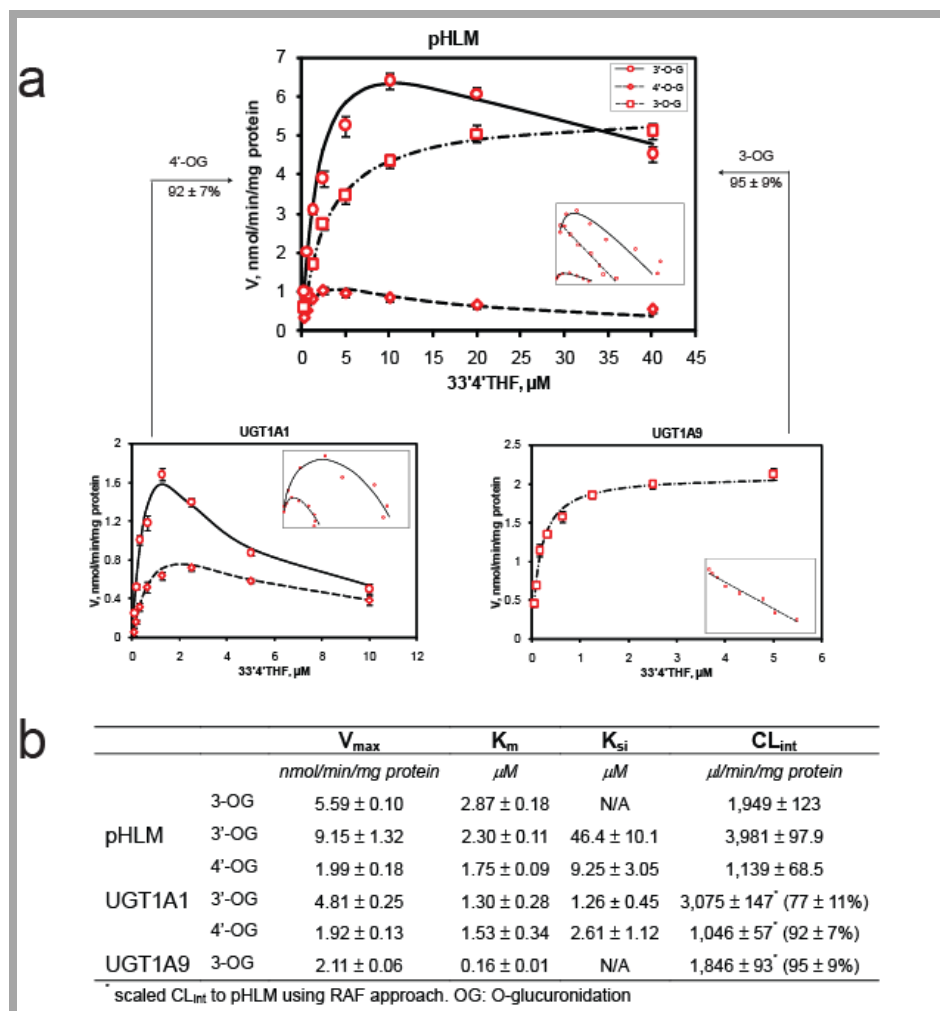


Figure 21. Kinetic profiles (panel a) and parameters (panel b) of glucuronidation derived from incubation of 3,3',4'-trihydroxyflavone (33'4'THF) with pooled human liver microsomes (pHLM), recombinant UGT1A1 and UGT1A9

Insets show corresponding Eadie-Hofstee plots for each kinetic profile. Circles and solid lines denote observed and predicted formation rates of flavonoid 3'-O-glucuronides, respectively; diamonds and dashed lines denote observed and predicted formation rates of flavonoid 4'-O-glucuronides, respectively; squares and dash-dotted lines denote observed and predicted formation rates of flavonoid 3-O-glucuronides, respectively. Predicted rates were from Michaelis-Menten or substrate inhibition models. Each data point represents the average of three replicates.

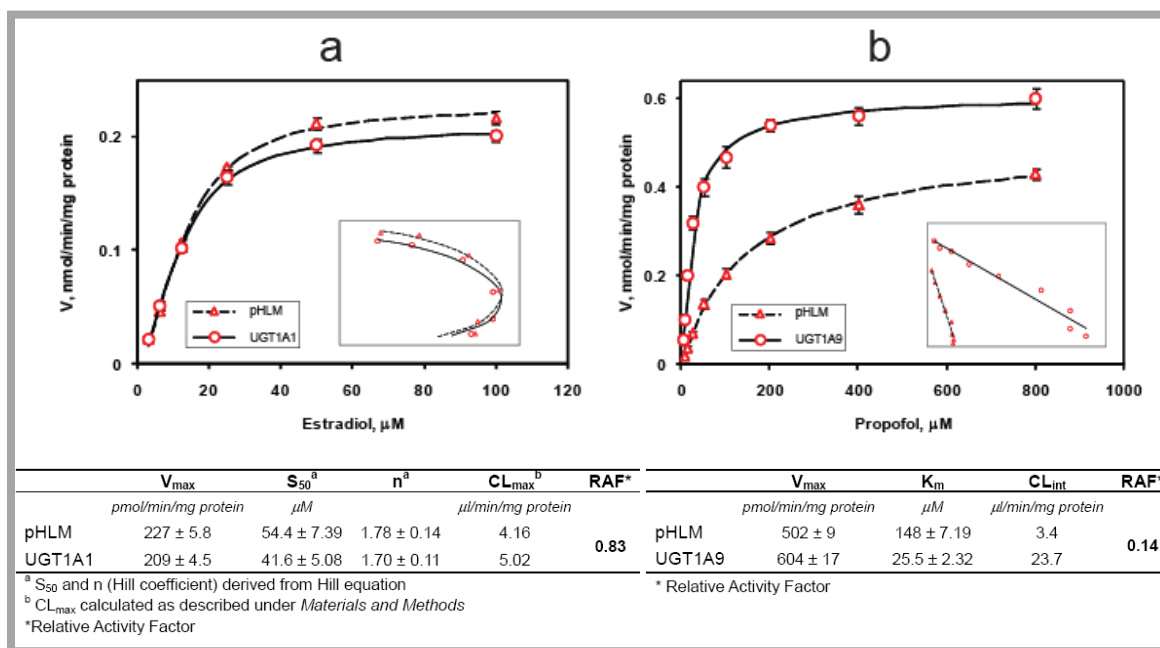


Figure 22. Kinetic profiles (top) and parameters (bottom) of glucuronidation of estradiol (a) and propofol (b) using recombinant UGTs and pooled human liver microsomes,

Relative activity factors (RAFs) of UGT1A1 (= 0.83) and UGT1A9 (= 0.14) were derived. Insets show corresponding Eadie-Hofstee plots for each kinetic profile.

4.4.3. Contribution of UGT1A1 and 1A9 to metabolism of 364'THF in pHLM

Glucuronidation kinetic profiles and constants derived from incubation of 364'THF with pHLM, UGT1A1 and UGT1A9 were shown in Figure 23. The scaled CL_{int} values of UGT1A1 and UGT1A9 accounted for $91 \pm 10\%$ (4'-O-glucuronidation) and $94 \pm 7\%$ (3-O-glucuronidation) of the CL_{int} values in pHLM, respectively. Although 3-O-glucuronide was primarily generated by UGT1A9, a minor contribution (9%) from UGT1A1 was also observed. For 6-O-glucuronide formation, a large portion (68%) was attributed to UGT1A1. However, it remains to be identified as to the other contributor(s) responsible for the remaining 32% of 6-O-glucuronide formation.

4.4.4. Expression-activity correlation for UGT1A1 in human livers

The expression levels of UGT1A1 in 12 human liver microsomes were determined by Western blot analysis (Figure 24a). In the product datasheet, it is described that the UGT1A1 antibody does not cross-react with UGT1A4, UGT1A6, UGT1A9, UGT1A10, and UGT2B15, which was also confirmed by Izukawa *et al* (2009). We verified that the UGT1A1 antibody did not have co-reactivity with UGT1A9 (data not shown). The variability of UGT1A1 protein in HLMs was 8.2-fold (Figure 24). The UGT1A1 protein levels were significantly correlated with the UGT1A1 activities probed with 4'-O-glucuronidation of 33'4'THF and 364'THF ($R^2 > 0.811$; $p < 0.0001$) (Figure 24b). Substantial correlations between the UGT1A1 protein and UGT1A1-mediated estradiol (3-OH) glucuronidation and SN-38 glucuronidation were also observed ($R^2 > 0.811$; $p < 0.0001$) (Figure 24c).

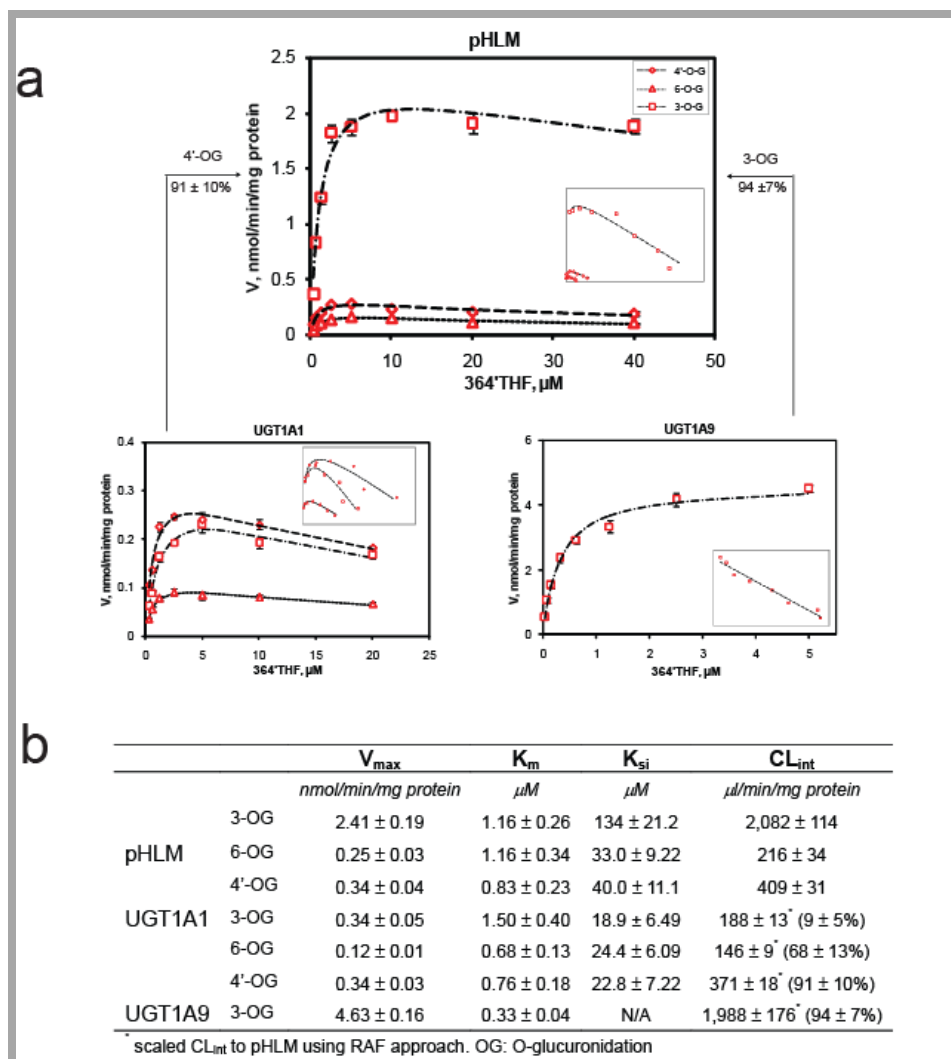


Figure 23. Kinetic profiles (panel a) and parameters (panel b) of glucuronidation derived from incubation of 3,6,4'-trihydroxyflavone (364'THF) with pooled human liver microsomes (pHLM), recombinant UGT1A1 and UGT1A9.

Insets show corresponding Eadie-Hofstee plots for each kinetic profile. Diamonds and dashed lines denote observed and predicted formation rates of flavonoid 4'-O-glucuronides, respectively; triangle and dotted lines denote observed and predicted formation rates of flavonoid 6-O-glucuronides, respectively; squares and dash-dotted lines denote observed and predicted formation rates of flavonoid 3-O-glucuronides, respectively. Predicted rates were from Michaelis-Menten or substrate inhibition models. Each data point represents the average of three replicates.

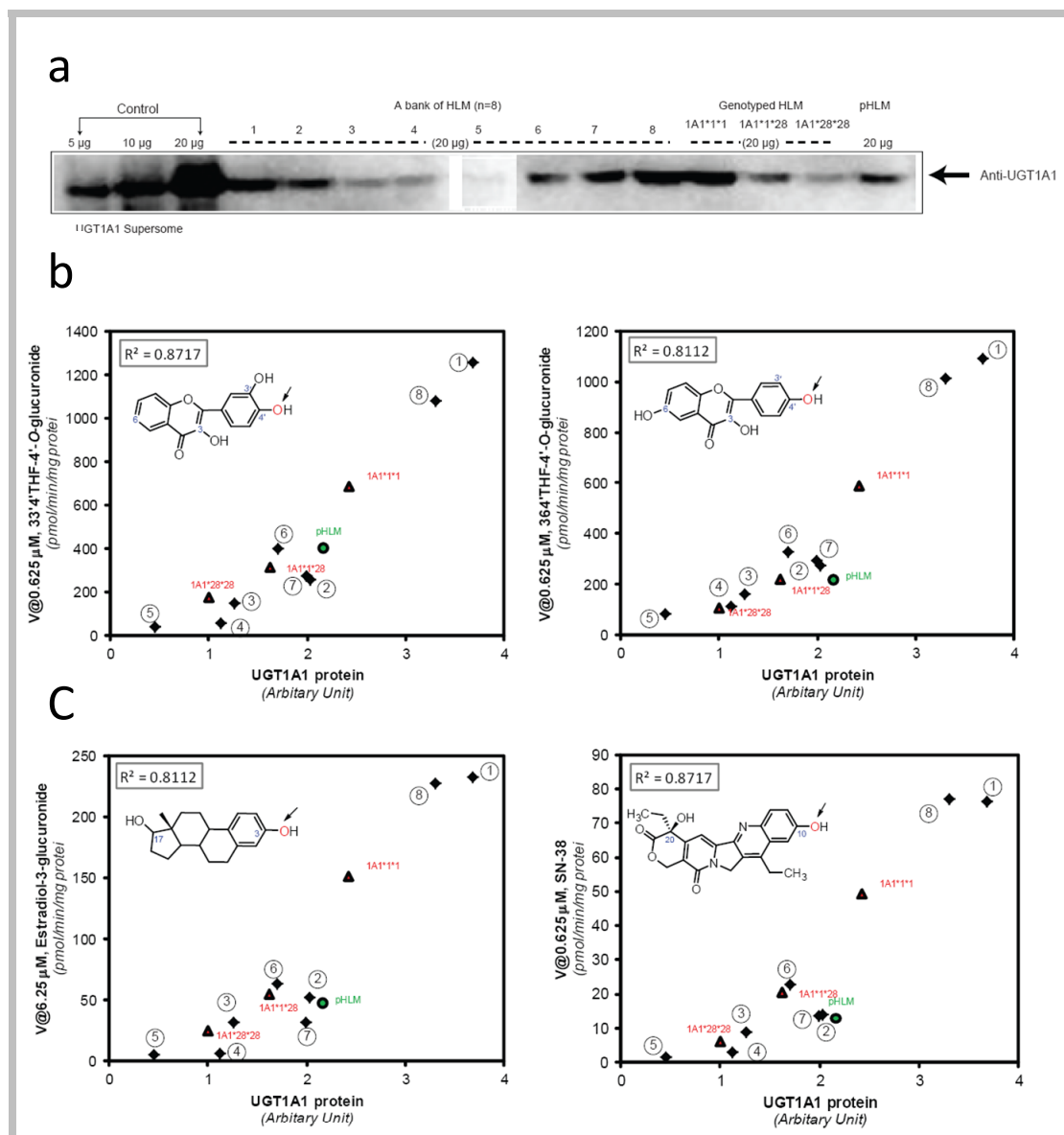


Figure 24. Expression-activity correlation for UGT1A1 in human livers

Panel a: Western blots of recombinant UGT1A1 and HLMs. **Panels B-C:** the correlation analyses ($n=12$) were performed between the UGT1A1 protein and 33'4'THF glucuronidation (4'-OH) (b, left), 364'THF glucuronidation (4'-OH) (b, right), estradiol glucuronidation (3-OH) (c, left), and SN-38 glucuronidation (c, right). The 8 individual HLMs from XenoTech were indicated in numbers. R^2 : Pearson correlation coefficient. In panel b-c, insets show corresponding chemical structures for each UGT1A1 substrate. The arrows indicate the sites of glucuronidation.

4.4.5. UGT1A1 activity correlation analysis

We chose estradiol and SN-38 glucuronidation rates for correlation analysis because estradiol is the most important female hormone, and also a prototypical substrate of human UGT1A1. In contrast, SN-38 is the active moiety for the widely used anticancer drug irinotecan, and UGT1A1 activities are inversely correlated to its intestinal toxicities ([O'Dwyer and Catalano, 2006](#)).

Highly significant correlations ($R^2 \geq 0.970$, $p < 0.0001$) were observed between rates of estradiol-3-O-glucuronidation and rates of 4'-O-glucuronidation of 33'4'THF or 364'THF measured in a panel of HLMs ($n=12$) (Figure 25). Please note that the activity correlation here was made between reaction rates measured at substrate concentrations that were lower than or near K_m (S_{50} for estradiol) values (for pHLM-mediated glucuronidation), which best approximate the intrinsic activity of a specific UGT isoform in HLMs ([Zhang *et al.*, 2007](#)).

Glucuronidation of SN-38 in pHLM appeared to be fully ($103 \pm 8\%$) correlated with UGT1A1 activities (Figure 26a), based on the RAF approach. As expected, rates of SN-38 glucuronidation was highly correlated ($R^2 > 0.965$, $p < 0.0001$) with rates of 4'-O-glucuronidation of 33'4'THF or 364'THF in the same 12 HLMs bank (Figure 26c/d). Additionally, similar pattern of kinetic profile (substrate inhibition) was observed between 4'-O-glucuronidation of 33'4'THF or 364'THF and SN-38 glucuronidation (Figure 26b). To rule out the possibility that the observed correlations between the flavonoids and known UGT1A1 probes were due to the differences in the quality of the liver microsomes, we demonstrated that there was a lack of correlation ($p > 0.5$) between

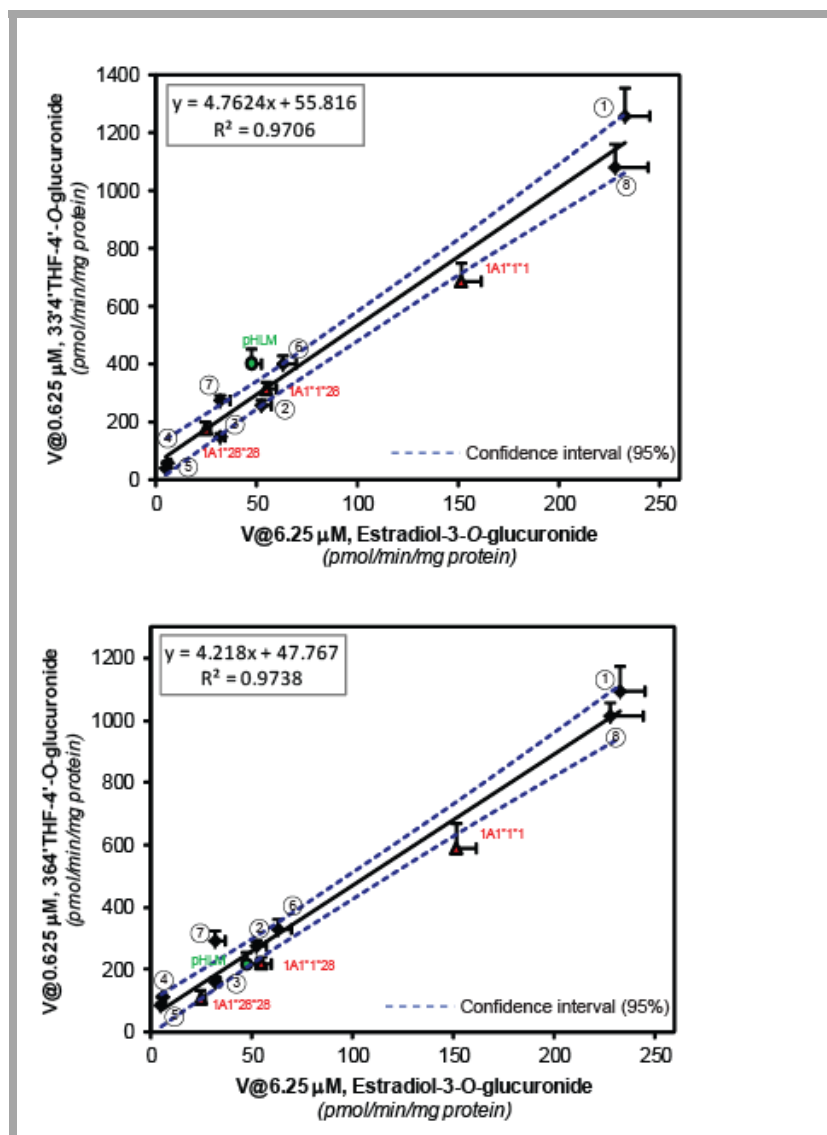


Figure 25. UGT1A1 activity correlation between flavonoid-4'-O-glucuronidation (top: 33'4'THF; bottom: 364'THF) and estradiol-3-glucuronidation in a bank of HLMs (n=12).

The 8 individual HLMs from XenoTech were indicated in numbers. The borders of the 95% confidence intervals were plotted as dashed lines. R^2 : Pearson correlation coefficient

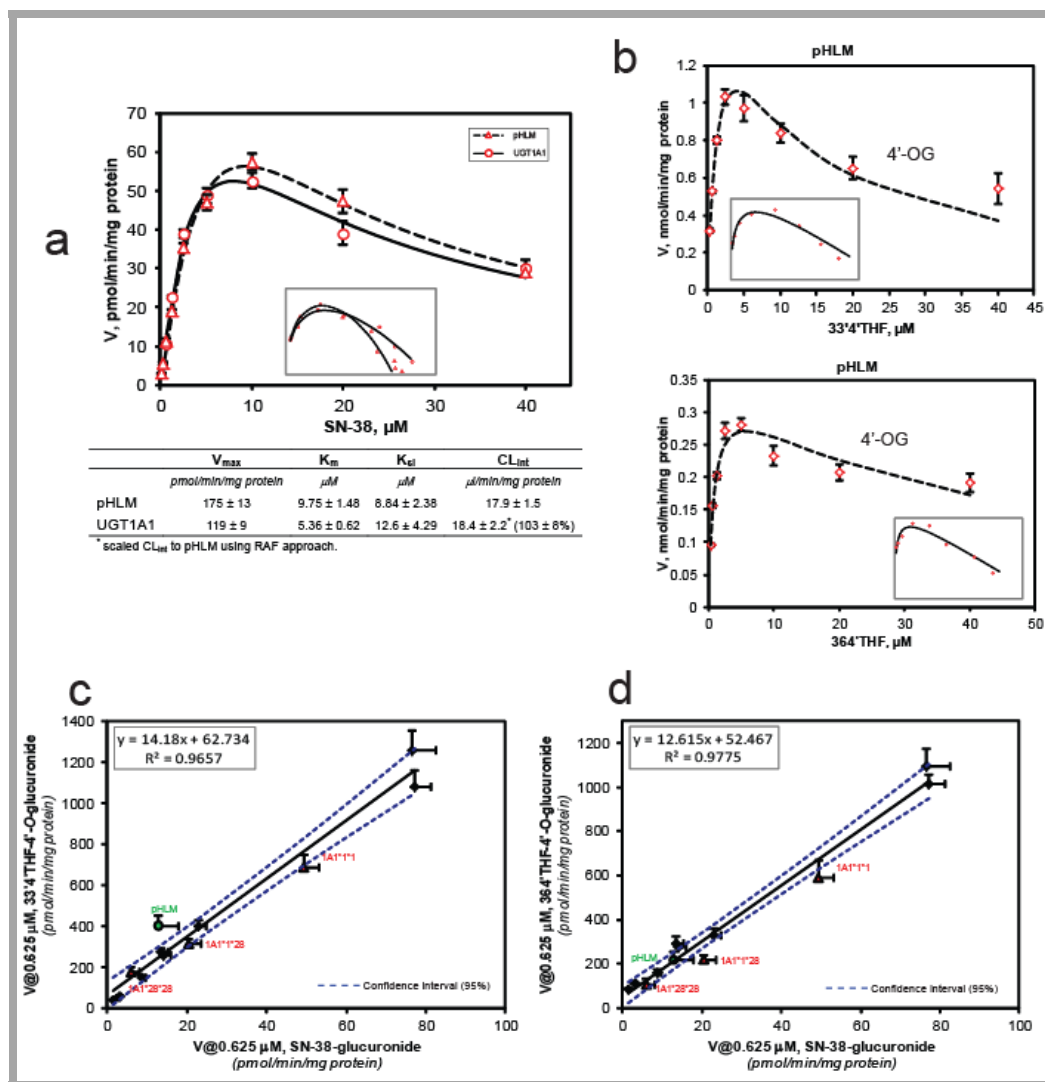


Figure 26. Rate correlations between SN-38 glucuronidation and flavonoid glucuronidation (4'-OH)

Panel a: Kinetic profiles (top) and parameters (bottom) of glucuronidation derived from incubation of SN-38 with pHLM and recombinant UGT1A1. **Panel b:** Kinetic profile of 33'4'THF-4'-O-glucuronidation (top) and 364'THF-4'-O-glucuronidation (bottom) mediated by pHLM. **Panels c/d:** UGT1A1 activity correlation between flavonoid-4'-O-glucuronidation (c: 33'4'THF; d: 364'THF) and SN-38 glucuronidation in a bank of HLMS ($n=12$). The borders of the 95% confidence intervals were plotted as dashed lines. In Panels a-b, insets show corresponding Eadie-Hofstee plots for each kinetic profile.

the flavonoid-4'-O-glucuronidation and testosterone-O-glucuronidation (a UGT2Bs probe (Sten *et al.*, 2009) in the same set of 12 HLMs. Lastly, we confirmed that recombinant UGT1A9 had no measurable activity towards SN-38 at lower concentrations (0.625-5 μ M), and limited activity (10 ± 0.8 pmol/min/mg protein, ~5-folds less than that of UGT1A1) at a higher concentration of 10 μ M, somewhat similar to the early observation (Hanioka *et al.*, 2001). Considering the fact that the in vivo concentration of SN-38 is quite low (< 0.1 μ M) after a standard therapy (Mathijssen *et al.*, 2001), we believe that UGT1A9's contribution to SN-38 glucuronidation is likely to be quite limited.

4.5. Discussion

We have shown that 33'4'THF and 364'THF may be used as probe substrates for UGT1A1 because UGT1A1 displayed high degree of selectivity toward their 4'-O-glucuronidation, and rates of their 4'-O-glucuronidation are highly correlated with UGT1A1 expression and activities in human liver microsomes. The evidence is strong and includes four sets of independent results: (1) the probes were predominantly glucuronidated (at 4'-OH) by UGT1A1 based on phenotyping of commercially available recombinant UGTs; (2) metabolism (at 4'-OH) of the probes in human liver microsomes was mainly contributed by the targeted UGT isoform; (3) the selectivity of UGT1A1 towards the flavonoid probes (4'-O-glucuronidation) were comparable to the known selective substrates (estradiol and SN-38) derived from activity correlation analysis; and (4) The polymorphic variants (UGT1A1*28) with decreased UGT1A1 protein expression showed markedly lower UGT1A1 activity towards the probes. Therefore, the interference

of other untested hepatic isoforms (e.g., UGT2B10) on the use of the two probes was presumed to be negligible, which was supported in part by the poor correlation between 4'-O-glucuronidation of these 2 flavonoids and that of testosterone, an important substrate of UGT2Bs.

Utilities of UGT-selective probes are multifaceted in the area of glucuronidation during the drug development process (Court, 2005; Miner *et al.*, 2010). Firstly, they can be used to substantiate the identification of specific UGTs involved in glucuronidation of drug candidates in human tissues via activity correlation analysis. Secondly, UGT-selective probes can be used to evaluate and predict the role of particular UGTs in drug-drug interactions through enzyme induction or inhibition (Donato *et al.*, 2010). Thirdly, glucuronidation measured using UGT-selective probe in tissues from different individuals can be used as a phenotype measure to elucidate the functional significance of genetic polymorphisms (Court, 2005). Fourthly, UGT probes can be used to screen the potential inhibitors of individual UGT enzymes (Miner *et al.*, 2010). Finally, they can be used to establish selective functional assays to assess functionality of individual UGT isoforms (can be reflective of metabolic status) in vitro (e.g., hepatocytes), and provide guidance for clinical dosing regimen (Donato *et al.*, 2010; Bonora-Centelles *et al.*, 2010).

Current available UGT1A1 probes are limited to three compounds: bilirubin, estradiol and etoposide (Miners *et al.*, 2010). Bilirubin and estradiol are endogenous compounds, whereas etoposide is cytotoxic, precluding their use in *in vivo* glucuronidation studies. In this regard, the flavonoid probes here hold greater potential for *in vivo* prediction of UGT1A1 activity, because they are exogenous and non-toxic (Hu, 2007). As a proof of

principle, UGT1A1-selective probes (in vivo) would be of clinical value for predicting SN-38 glucuronidation and determining the proper dose and dosing regimen (O'Dwyer and Catalano, 2006). SN-38 glucuronidation has been shown repeatedly to be an important factor for its gastrointestinal side effects; deficiency in UGT1A1 activity is correlated with more severe side effects in humans (O'Dwyer and Catalano, 2006). It is acknowledged whether these 2 flavonoid probes can be used as a UGT1A1 selective probe in human remains uncertain until appropriate demonstration in vivo.

Interestingly, 3-O-glucuronidation rates of 33'4'THF and 364'THF are also well correlated with hepatic UGT1A9 activities as measured by the glucuronidation rates of propofol at 25 μ M using the same set of HLMs (n=12). High significant correlation ($R^2 \geq 0.944$, $p < 0.0001$) were observed between the glucuronidation of these two flavonoid probes at the 3-OH position and that of propofol (Figure 27). Attempt to quantify UGT1A9 using antibody against UGT1A9 obtained from Abnova (Taipei City, Taiwan) was unsuccessful, as the antibody cross-reacted with UGT1A1 (data not shown) and other UGT1A isoforms (Izukawa *et al.*, 2009). Therefore, we could not determine the UGT1A9 levels in human liver microsomes. This technical difficulty means that we cannot determine unequivocally if 3-O-glucuronidation rates of 33'4'THF and 364'THF could be used as activity indicators for human UGT1A9, although it could be used as an indicator for glucuronidation rates of propofol, a clinically useful drug.

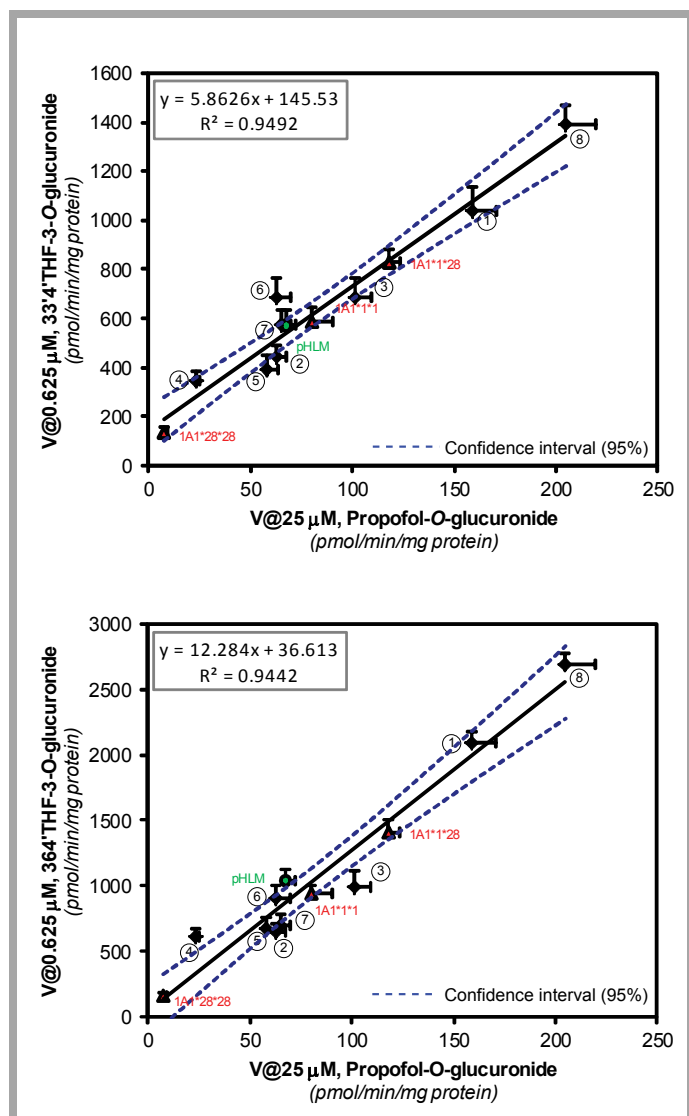


Figure 27. UGT1A9 activity correlation between flavonoid-3-O-glucuronidation (top: 33'4'THF; bottom: 364'THF) and propofol glucuronidation in a bank of HLMs (n=12).

The 8 individual HLMs from XenoTech were indicated in numbers. R^2 : Pearson correlation coefficient

In addition to correlation analysis, we also used the K_m values to determine if regiospecific glucuronidation was similar in expressed UGTs and HLMs. We found that K_m values for recombinant UGT1A1 (4'-O-glucuronidation of 33'4'THF and 364'THF) were essentially identical to those for pooled HLM, which indicated UGT1A1 was likely the predominant enzyme that catalyzed the 4'-O-glucuronidation. With this additional criterion, 4'-O-glucuronide of two flavonoids were considered the excellent markers for UGT1A1. By contrast, The K_m values for recombinant UGT1A9 (3-O-glucuronidation of 33'4'THF and 364'THF) were, respectively, ~ 17 (33'4'THF) and ~ 2.5 (364'THF) times lower than those for pooled HLM. The strikingly higher K_m value of HLM than the target recombinant UGT, as also had been found for propofol (Soars *et al.*, 2003; Shimizu *et al.*, 2007), could arise from the “membrane effect” (or “albumin effect”) proposed by Miners *et al* (2010). It might also suggest that other UGT isoforms could contribute to the metabolism (Court, 2005). These isoforms most likely are UGT2B7 (for 33'4'THF) and UGT1A1 (for 364'THF), inferred from the reaction-phenotyping data (Figure 20). Hence, it is necessary to reduce the low background glucuronidation activities resulted from the off-target UGTs, and to use these flavonoid probes at lower concentrations (e.g., 0.625 μ M for the flavonoid probes, much lower than their reported K_m values in HLMs).

It is noteworthy that UGT1A1 expression-activity correlation did not hold between recombinant UGT1A1 and HLMs. Compared to pHLM, recombinant UGT1A1 had notably higher UGT1A1 expression in Western blot, but similar activities towards estradiol (3-glucuronide), 33'4'THF and 364'THF (4'-O-glucuronides). The catalytic differences might be contributed by UGT protein-protein interactions (hetero-dimerization

or hetero-oligomers) in HLMs (Fujiwara *et al.*, 2007, 2010). There are another two possibilities that cannot be ruled out: 1) protein separation and/or binding to the membrane during Western blotting were affected by the differences in the sample matrices; 2) over-expression of UGT1A1 in insect cells may lead to the accumulation of inactive enzyme. Further studies are warranted to address this discrepancy.

In conclusion, this study presented two flavonoids (4'-O-glucuronidation), whose regioselective glucuronidation can be used as *in vitro* selective probes for hepatic UGT1A1, and hold great promise for use as *in vivo* probes as well. The selectivity of UGT1A1 towards the proposed probes was systematically evaluated via studies including recombinant UGT phenotyping, individual UGT contribution estimation, and activity correlation analysis. UGT1A1 and 1A9 are the main isoforms responsible for glucuronidating 33'4'THF and 364'THF, but at different positions (1A1, 4'-OH; 1A9, 3-OH). Glucuronidation of these 2 flavonoid probes at 4'-OH position by UGT1A1 were well correlated with estradiol-3-glucuronidation (a well-recognized and widely used UGT1A1 probe) and SN-38 glucuronidation (drug's toxicity is associated with UGT1A1 function). The results indicated that 4'-O-glucuronidation of 33'4'THF and 364'THF is excellent markers for UGT1A1, and for UGT1A1-mediated glucuronidation of SN-38. Future work should assess the selectivity of these probes in *in vivo* glucuronidation studies.

Chapter 5 3D-QSAR studies on UGT1A9-mediated 3-O-glucuronidation of flavonols using a pharmacophore-based CoMFA model (Study III)

5.1. Abstract

Glucuronidation is often recognized as one of the rate-determining factors that limit the bioavailability of flavonols. Hence, design and synthesis of more bioavailable flavonol(s) would benefit from the establishment of predictive models of glucuronidation using kinetic parameters (e.g., K_m , V_{max} , $CL_{int}=V_{max}/K_m$) derived for flavonols. This study aims to construct position (3-OH) specific CoMFA models to describe UGT1A9-mediated glucuronidation of flavonols, which can be used to design poor UGT1A9 substrates. The kinetics of UGT1A9-mediated 3-O-glucuronidation of 30 flavonols was characterized and kinetic parameters (K_m , V_{max} , and CL_{int}) were obtained. The observed K_m , V_{max} and CL_{int} values of 3-O-glucuronidation ranged 0.04~0.68 μM , 0.04~12.95 nmol/mg/min and 0.06~109.60 ml/mg/min, respectively. To model the UGT1A9-mediated glucuronidation, 30 flavonols were splitted into the training (23 compounds) and test (7 compounds) sets. These flavonols were then aligned by mapping the flavonols to a specific common feature pharmacophore, which were used to construct CoMFA models of V_{max} and CL_{int} , respectively. The derived CoMFA models possessed good internal and external consistency and showed statistical significance and substantive predictive abilities (V_{max} model: $q^2 = 0.738$, $r^2 = 0.976$, $r^2_{pred} = 0.735$; CL_{int} model: $q^2 = 0.561$, $r^2 = 0.938$, $r^2_{pred} = 0.630$). The contour maps derived from CoMFA modeling clearly indicated structural characteristics associated with rapid or slow 3-O-glucuronidation. In conclusion, the approach of coupling CoMFA analysis with a pharmacophore-based structural alignment

is viable for constructing a predictive model for regiospecific glucuronidation rates of flavonols by UGT1A9.

5.2. Introduction

Flavonols are widely distributed in regular human diets (D'Archivio *et al.*, 2007). There are nearly 400 natural flavonols reported, and majority of them have flavonol structural scaffold with hydroxyl (-OH) and/or methoxy (-OMe) substitutions (Andersen and Markham, 2006). It is well-known that this class of natural-occurring compounds is linked to a variety of health-promoting activities such as antioxidant and anticancer (Birt *et al.*, 2001; Ross and Kasum, 2002). However, the undesired biopharmaceutical properties of flavonols (e.g., quercetin and kaempferol), which undergo particularly rapid and extensive phase II metabolism, produced low levels of the parent compounds but high levels of the conjugated forms (e.g., glucuronides or sulfates to a lesser extent) being found in the blood (Erlund *et al.*, 2006; Barve *et al.*, 2009).

UDP-glucuronosyltransferases (UGTs) is a family of enzymes that mediate the glucuronidation of endogenous or exogenous compounds. The substrates need to contain one or more nucleophilic groups (e.g., hydroxyl, alcohol, amine, thiol or carboxylic acid groups) to which the cofactor UDP-glucuronic acid (UDPGA) is covalently linked (Jancova *et al.*, 2010). This pattern of structural recognition explains the broad substrate specificity of UGTs, and underpins its wide detoxification functionality by turning the substrates to hydrophilic metabolite, which can be readily eliminated (Iyanagi, 2007). In the UGTs superfamily, the enzymes of the UGT1A and

UGT2B subfamilies contribute significantly to phase II metabolism (Wong *et al.*, 2009). To date, a total of 16 functional isoforms were identified (9 for UGT1A and 7 for 2B family): UGT1A1, 1A3, 1A4, 1A5, 1A6, 1A7, 1A8, 1A9, 1A10, 2B4, 2B7, 2B10, 2B11, 2B15, 2B17 and 2B28 (Mackenzie *et al.*, 2005). Liver, as the major first-pass metabolizing organ, expresses a variety of UGT isoforms including UGT1A1, 1A3, 1A4, 1A5, 1A6, 1A9, 2B7 and 2B15. In contrast, UGT1A7, 1A8 and 1A10 are primarily present in gastrointestinal tract or esophagus (Fisher *et al.*, 2001; Ohno and Nakajin, 2009).

UGT1A9 is a unique enzyme among the 9 UGT1A isoforms. UGT1A9 is resistant to detergent and is stable in response to heat treatment at 57°C for 15 min (Fujiwara *et al.*, 2009). Consistent with this observation, our earlier study showed that UGT1A9 was thermostable in metabolizing prunetin (an isoflavone) at 37°C for more than 8 hours (Joseph *et al.*, 2007). Moreover, UGT1A9 demonstrated greater proficiency in glucuronidating flavonoids. In the study of Chen *et al.* (2008), the catalyzing efficiency (V_{\max}/K_m) of UGT1A9 was higher than that of UGT1A3. It is also observed that UGT1A9 ranks within the top three isoforms that most effectively metabolize isoflavones, flavones and flavonols (Tang *et al.*, 2009, 2010). The good correlation between glucuronidation rates derived from UGT isoforms (UGT1A9 plus 1A1) and those from human liver microsomes highlighted the fact that UGT1A9 contribute significantly to the glucuronidation activity of liver microsomes in metabolizing flavonoids (Tang *et al.*, 2010).

It is therefore hypothesized that a poor flavonol substrate of UGT1A9 will have less efficient glucuronidation in vivo and higher bioavailability. One approach to find the poor substrate (with potential for high bioavailability) is to test every compound experimentally, which is labor and cost extensive. Alternatively, quantitative structure activity relationship (QSAR) can be established. Approaches to predict biological activities by building QSAR models are usually from two directions: structure-based or ligand-based. Due to lack of mammalian UGTs crystal structures, ligand-based approaches (e.g., 2D/3D-QSAR, pharmacophore modeling and CoMFA) had been applied to establish quantitative or qualitative structure-glucuronidation relationships (Sorich *et al.*, 2008). Predictive regression and pharmacophore models were generated with UGT1A1 and UGT1A4 using structurally diverse compounds (Sorich *et al.*, 2002; Smith *et al.*, 2003). However, attempts to develop predictive QSAR for substrates of UGT1A9 were unsuccessful (Miners *et al.*, 2004). On the other hand, the comparative molecular field analysis (CoMFA) was used to examine a series of 18 compounds (triphenylalkyl carboxylic acid analogue) that inhibited glucuronidation of bilirubin by UGT1A1, the resulting model allowed good prediction of inhibitory potency (Said *et al.*, 1996).

CoMFA is a 3D QSAR technique (Cramer *et al.*, 1988) which aims to derive a correlation between the biological activity of ligands and their structural characteristics (i.e., steric and electrostatic properties). The final validated CoMFA model can be used for the design of novel ligands and to predict the biological activities thereof. CoMFA methodology had been widely and successfully utilized to model interactions between

proteins and many types of biological ligands such as enzyme inhibitors ([Barreca et al., 1999](#); [Holder et al., 2007](#)), CYP2D6 substrates ([Haji-Momenian et al., 2003](#)), and antifungal agents ([Wei et al., 2005](#)).

It is still not fully understood what characteristics make flavonol a good or poor UGT1A9 substrate. UGT1A9 often generated multiple mono-glucuronide isomers from single flavonoid that bears more than one conjugation site. For example, 2 glucuronides were generated from 3,7-dihydroxyflavone ([Tang et al., 2010](#)), 3 glucuronides from galangin and luteolin ([Chen et al., 2008](#); [Otake et al., 2002](#)), and 4 glucuronides from quercetin ([Chen et al., 2008](#)). Currently, there is no method that can be used to predict kinetic parameters of glucuronidation for polyphenolic compounds such as flavonols. It is assumed that the difficulties arose from the approach that seeks to build a single model that will predict the rates of glucuronidation at multiple sites. We hypothesize that a new predictive algorithm is needed to account for glucuronidation at all phenolic groups (-OH) in flavonols. This algorithm must consist of multiple regiospecific (position-specific) models, which can separately predict the glucuronidation rates on a particular position (e.g., 3-O-glucuronidation in flavonols), and the addition of glucuronidation rates from the multiple positions will represent the total glucuronidation rates or overall metabolic susceptibility. Therefore, the objective of this study is to construct a position (3-OH) specific CoMFA model to predict 3-O-glucuronidation. 3-O-glucuronidation is chosen because it is the most active position in UGT1A9-mediated glucuronidation ([Otake et al., 2002](#); [Tang et al., 2010](#)), Kinetics parameters (K_m , V_{max} , CL_{int}) of UGT1A9-mediated 3-O-glucuronidation with 30 flavonols were determined. The V_{max} and CL_{int} datasets were

used to construct their respective position specific (3-OH) CoMFA models, based on molecular alignments generated from a defined pharmacophore search. Contour maps from CoMFA provided insightful structural characteristics associated with rapidly or slowly metabolized flavonol substrates for 3-O-glucuronidation.

5.3. Materials and methods

5.3.1. Materials

Expressed human UGT1A9 isoform (Supersomes™) were purchased from BD Biosciences (Woburn, MA). The recombinant UGT1A9 is characterized using the probe substrate propofol with K_m value of $25.8 \pm 4.47 \mu\text{M}$ and V_{max} value of $148 \pm 7.03 \text{ pmol/mg/min}$. Uridine diphosphoglucuronic acid (UDPGA), alamethicin, D-saccharic-1,4-lactone monohydrate, and magnesium chloride were purchased from Sigma-Aldrich (St Louis, MO). Ammonium acetate was purchased from J.T. Baker (Phillipsburg, NT). Thirty (30) flavonols (Figure 28 & Table 2) were purchased from Indofine Chemicals (Somerville, NJ). The flavonols structurally differ in numbers and position of substituents (hydroxyl (-OH) or methoxy (-OMe)) on the A-ring or B-ring. Particularly, compound 16 and 27 have methyl groups at C6. C3' and C4' of compound 16 are co-substituted by methylenedioxy group. The All other materials (typically analytical grade or better) were used as received.

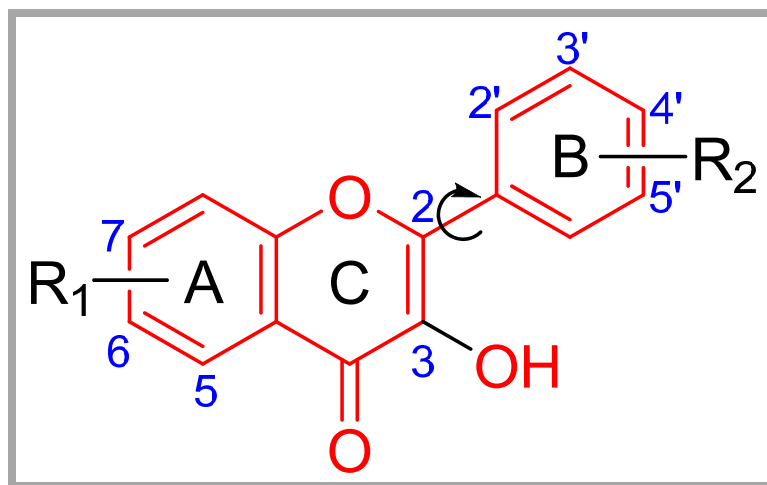


Figure 28. Backbone of flavonol structures (See Table 2 for the definitions of the substituents)

Comparing with flavonols, flavones lack 3-OH on the 2-phenylbenzopyran scaffold.

Table 2. Flavonols used in the work (see Figure.28 for chemical structures)

No.	Flavonols	Abbrev.	R_1	R_2
1	3,2'-dihydroxyflavone	32'DHF		2'-OH
2	3,3',4'-trihydroxyflavone	33'4'THF		3'-OH;4'-OH
3	3,4'-dihydroxyflavone	34'DHF		4'-OH
4	3,6,4'-trihydroxyflavone	364'THF	6-OH	4'-OH
5	3,6-dihydroxyflavone	36DHF	6-OH	
6	3,7-dihydroxyflavone	37DHF	7-OH	
7	3-hydroxy-2'-methoxyflavone	3H2'MF		2'-OMe
8	3-hydroxy-3'-methoxyflavone	3H3'MF		3'-OMe
9	3-hydroxy-4'-methoxyflavone	3H4'MF		4'-OMe
10	3-hydroxy-5,7-dimethoxyflavone	3H57DMF	5-OMe; 7-OMe	
11	3-hydroxy-5-methoxyflavone	3H5MF	5-OMe	
12	3-hydroxy-6,4'-dimethoxyflavone	3H64'DMF	6-OMe	4'-OMe
13	3-hydroxy-6-methoxyflavone	3H6MF	6-OMe	
14	3-hydroxy-7-methoxyflavone	3H7MF	7-OMe	
15	3-hydroxyflavone	3HF		
16	3-hydroxy-6-methyl-3',4'-methylenedioxyflavone	Dioxy	6-Me	3',4'-methylenedioxy
17	Isorhamnetin	Iso	5-OH; 7-OH	4'-OH; 3'-OMe
18	Kaempferol	3574'QHF	5-OH; 7-OH	4'-OH
19	Morin	/	5-OH; 7-OH	2'-OH; 4'-OH
20	Myricetin	Myr	5-OH; 7-OH	3'-OH; 4'-OH; 5'-OH
21	Quercetin	3573'4'PHF	5-OH; 7-OH	3'-OH; 4'-OH
22	Resokaempferol	374'THF	7-OH	4'-OH
23	Rhamnetin	Rha	5-OH; 7-OMe	4'-OH; 3'-OH
24	3,3'-dihydroxyflavone	33'DHF		3'-OH
25	3,5-dihydroxyflavone	35DHF	5-OH	
26	3-hydroxy-2',3'-dimethoxyflavone	3H2'3'DMF		2'-OMe;3'-OMe
27	3-hydroxy-6-methylflavone	3H6MeF	6-Me	
28	3-hydroxy-7,4'-dimethoxyflavone	3H74'DMF	7-OMe	4'-OMe
29	Fisetin	/	7-OH	3'-OH; 4'-OH
30	Galangin	357THF	5-OH; 7-OH	

-OH: hydroxyl group; -Me: methyl group; -OMe: methoxyl group.

5.3.2. UGT1A9 enzyme kinetics

Enzyme kinetics parameters of glucuronidation by UGT1A9 were determined by measuring initial glucuronidation rates of flavonols at a series of concentrations. The experimental procedures of UGT assays were exactly the same as our previous publications (Joseph *et al.*, 2007; Tang *et al.*, 2009 & 2010; Singh *et al.*, 2010). Glucuronidation rates were calculated as the amount of glucuronide(s) formed per enzyme quantity per reaction time (or nmol/mg/min). The aglycone substrate concentrations in the range of 0.039-40 μ M were used unless method sensitivity or substrate solubility necessitated otherwise. All experiments were performed in triplicates.

5.3.3. UPLC analysis of flavonols and their glucuronides:

The Waters ACQUITY UPLC (Ultra performance liquid chromatography) system was used to analyze the parent compounds and their corresponding glucuronides (see Appendix B/C).

5.3.4. Glucuronide structure confirmation

Glucuronide structures were confirmed via a 3-step process as summarized in our early publication (Singh *et al.*, 2010). First, the glucuronides were hydrolyzed by α -D-glucuronidase to the aglycones. Second, the glucuronides were identified as mono-glucuronides which showed mass of [(aglycone's mass)+176] Da using UPLC/MS/MS. 176 Da is the mass of single glucuronic acid. The same UPLC/MS/MS instruments and methods in earlier publication (Singh *et al.*, 2010) were applied in this paper. Finally, the 3-O-glucuronides were confirmed by the "UV spectrum maxima (λ_{max}) shift method" (Singh *et al.*, 2010). This method is based on the characteristic UV shifts caused by

glucuronic acid substitution on a particular hydroxyl group. Briefly, if 3-hydroxyl group on the flavonol nucleus was glucuronidated, disappearance of UV maxima or hypsochromic shifts (i.e., to shorter wavelength) were observed in Band I (300~400nm). The shift in Band I associated with the substitution was in the order of 13 ~ 30 nm.

5.3.5. Kinetics analysis

Kinetic parameters (V_{\max} , K_m or K_{si} (substrate inhibition constant)) were estimated by fitting the initial rate data to Michaelis-Menten and substrate inhibition rate equations by nonlinear least-squares regression. Data analysis was performed by GraphPad Prism V5 for Windows (GraphPad Software, San Diego, CA). The goodness-of-fit was evaluated on the basis of R^2 values, RSS (residual sum of squares), RMS (root mean square) and residual plots.

5.3.6. Pharmacophore generation and conformation search

Pharmacophore modeling was performed using Molecular Operating Environment (MOE) software, version 2008.10 (Chemical Computing Group, Canada). All the compounds were drawn on the builder module of MOE and subjected to energy minimization at RMS gradient of 0.00001. The conformational database was created by “conformation import” using MMFF94x forcefield for every compound. The forcefield parameters were kept at their default values of the strain limit of 4 Kcal/mol and the conformations limit of 250 conformations/molecule. Compound 15 (3-hydroxyflavone) was used as a reference molecule to develop the pharmacophore query with the “pharmacophore query editor”. Pharmacophore search using the created query was run against the conformational database of flavonols. The best matched conformer for each

flavonol (lowest RMSD) was selected and the alignments were used for CoMFA analysis.

5.3.7. Comparative molecular field analysis (CoMFA)

The 30 flavonol molecules were divided into training (23 compounds) and test (7 compounds) sets, as shown in Table 3. The test set compounds were arbitrarily assigned by considering the fact that test set compounds reflect the variations in glucuronidation activity similar to that of the training set, and indicate a moderate diversity in their chemical structures. The training set (compounds 1-23, Table 3) was used for CoMFA modeling. The molecular alignments generated from the pharmacophore model were used in CoMFA studies utilizing Sybyl8.0 software (Tripos, US). Partial charges were re-calculated using the MNDO (modified neglect of diatomic overlap) method. The molecules were placed in a three-dimensional grid (2.0 Å spacing). At each grid point, steric energy (Lennard-Jones potential) and electrostatic energy were calculated. Cross-validated partial least squares (PLS) analysis was performed to determine the optimal number of components. Maximal number of components was limited to 8 to avoid over-fitting. The definitive CoMFA model, which was used for prediction of activity, was built by non-cross-validated PLS analysis using the optimal number of components. The q^2 (cross-validated r^2), SEP (cross-validated standard error of prediction), r^2 (non-cross-validated r^2), F values, and standard error of estimate (SE) values were computed and shown in Table 4. P_{r2} denotes the probability of obtaining the observed F ratio value by chance alone.

5.4. Results

5.4.1. Kinetic parameters for UGT1A9-mediated 3-O-glucuronidation

The derived kinetics parameters were listed in Table 3. The K_m values of 3-O-glucuronidation ranged from 0.042 to 0.68 μM (~ 1 log unit difference). The unanimous low K_m values ($< 0.7 \mu\text{M}$) suggested that the flavonol analogs bind strongly to the UGT1A9 for 3-OH catalysis. The structural elements contributing to lower K_m values (or higher binding affinity) were identified as: substitutions of -OH at positions of C3' or C4'; -OMe groups at C3', C4', C5 or C6; and -Me group at C6 (Figure 29a). 3H64'DMF (compound 12) had the lowest K_m value of 0.04 in the presence of two K_m contributing elements (i.e., -OMe at both C4' and C6). In contrast, -OH substitution at 2'- or 6 position increased the K_m values by >1 -fold (Figure 29b).

The V_{\max} and CL_{int} values of 3-O-glucuronidation ranged 0.04~12.95 nmol/mg/min and 0.06~109.60 ml/mg/min, respectively (Table 3). The turnover of the enzyme (reflected by V_{\max}) varied more towards the flavonols (~ 2.5 log folds) than the K_m values. Poor correlation between K_m and V_{\max} was observed ($r^2 = 0.000$). Moreover, the ratio of V_{\max} over K_m , CL_{int} displayed greater divergence (~ 3.3 log folds). Because V_{\max} best describes the measured susceptibility of chemicals to be glucuronidated, while CL_{int} defines the catalytic efficiency of the enzyme towards its substrates at low concentrations. Both V_{\max} and CL_{int} were used to construct CoMFA models.

Table 3. Kinetics parameters of UGT1A9 mediated 3-O-glucuronidation with flavonols, together with the predicted V_{\max} and CL_{int} values from their respective CoMFA models.

No.	Flavonols	K_m	V_{\max}	$CL_{\text{int}}(V_{\max}/K_m)$	Log(V_{\max})		Log(CL_{int})	
		μM	$nmol/mg/min$	$ml/mg/min$	Obs ^a	Calcd ^b	Obs ^a	Calcd ^b
1	32'DHF	0.67	0.052	0.078	1.72	1.68	1.89	2.31
2	33'4'THF	0.10	2.2	22	3.34	3.41	4.34	4.37
3	34'DHF	0.13	1.8	14	3.25	3.30	4.14	4.06
4	364'THF	0.31	6.8	22	3.84	3.94	4.34	4.29
5	36DHF	0.62	13	21	4.11	4.08	4.32	4.31
6	37DHF	0.22	4.6	21	3.66	3.51	4.32	4.07
7	3H2'MF	0.21	3.8	18	3.58	3.59	4.25	4.08
8	3H3'MF	0.063	2.9	46	3.47	3.44	4.66	4.47
9	3H4'MF	0.059	1.9	32	3.28	3.33	4.51	4.59
10	3H57DMF	0.13	3.3	26	3.52	3.70	4.40	4.52
11	3H5MF	0.082	1.9	24	3.29	3.24	4.36	4.11
12	3H64'DMF	0.043	2.2	51	3.34	3.33	4.71	4.73
13	3H6MF	0.074	5.4	73	3.73	3.66	4.86	4.84
14	3H7MF	0.27	10	37	4.01	4.00	4.57	4.62
15	3HF	0.30	2.1	7.0	3.32	3.45	3.84	4.16
16	Dioxy	0.066	6.0	91	3.78	3.69	4.96	5.20
17	Iso	0.32	12	38	4.09	4.17	4.59	4.81
18	3574'QHF	0.32	1.9	6.0	3.28	3.24	3.78	3.51
19	Morin	0.68	0.040	0.060	1.60	1.62	1.77	1.86
20	Myr	0.61	0.49	0.80	2.69	2.88	2.90	3.24
21	3573'4'PHF	0.36	3.3	9.2	3.52	3.32	3.97	3.77
22	374'THF	0.36	2.6	7.3	3.42	3.35	3.86	3.98
23	Rha	0.23	10	45	4.01	3.92	4.65	4.38
24 ^c	33'DHF	0.11	3.1	29	3.50	3.47	4.44	4.27
25 ^c	35DHF	0.25	1.9	7.4	3.27	3.48	3.87	3.74
26 ^c	3H2'3'DMF	0.52	4.4	16	3.91	3.15	3.92	3.84
27 ^c	3H6MeF	0.0616	6.75	110	3.83	3.61	5.04	4.76
28 ^c	3H74'DMF	0.19	8.7	46	4.25	3.80	4.66	5.02
29 ^c	Fisetin	0.63	1.5	2.3	3.16	3.34	3.38	4.01
30 ^c	357THF	0.68	7.4	11	3.87	3.95	4.04	3.83

^a Experimental determined activities. ^b Calculated activities using the CoMFA models. ^c These compounds were used as a test set and not included in the derivation of equations.

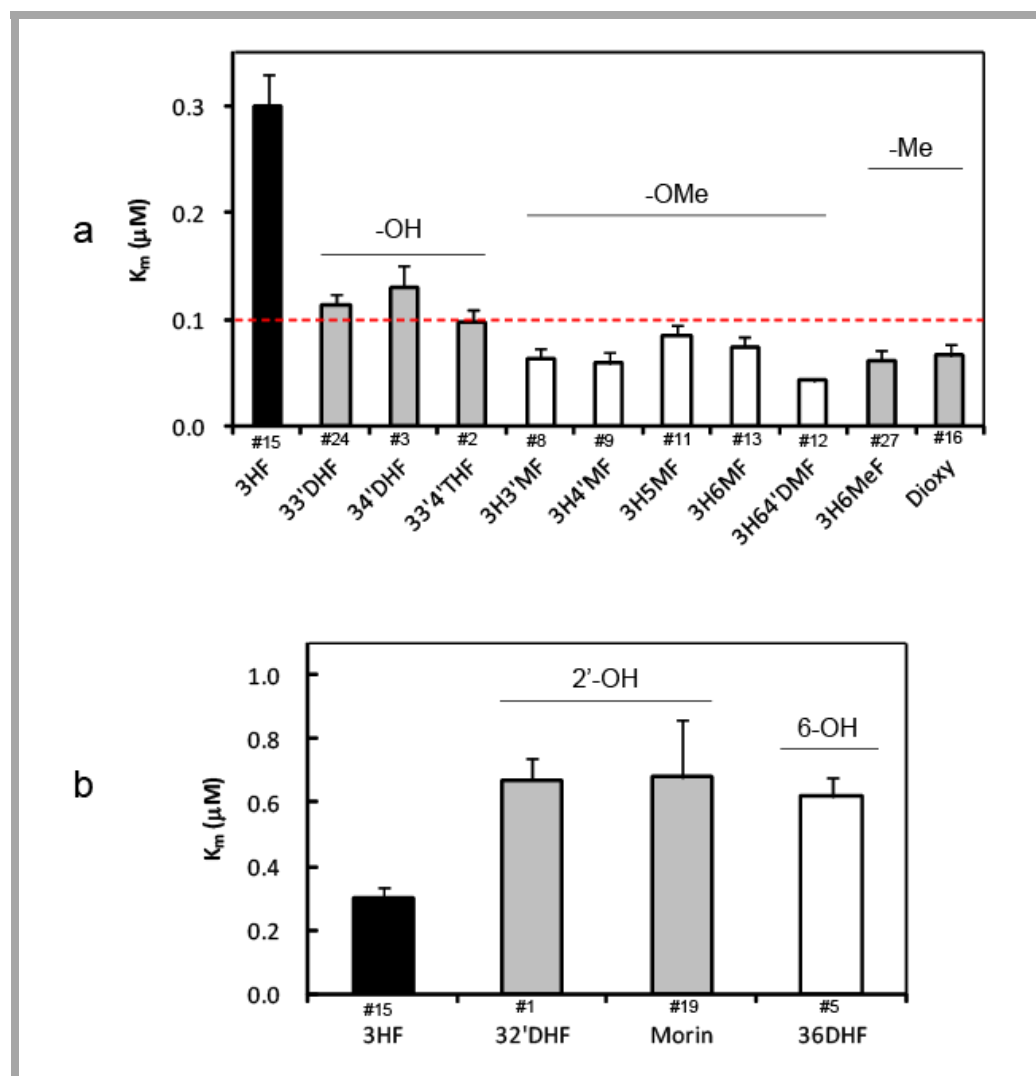


Figure 29. Structural modifications affect the K_m values of UGT1A9-mediated 3-O-glucuronidation.

Panel a: K_m values were decreased in the presence of (1). substitutions of -OH at positions of C3' or C4'; (2). -OMe groups at C3', C4', C5 or C6; or (3). -Me group at C6. **Panel b:** K_m values were increased by > 1 folds with the additions of 2'-OH or 6-OH. The compound numbers (#) are labeled above the abbreviated chemical names.

Table 4. Summary of modeling parameters from CoMFA analysis

	V_{max} model	CL_{int} model
q ^{2a}	0.738	0.561
SEP ^b	0.383	0.561
r ^{2c}	0.976	0.938
r _{pred} ^d	0.735	0.630
S.E. ^e	0.116	0.229
Components ^f	6	4
F ^g	108.836	68.436
P _{r2=0} ^h	0.000	0.000
Fraction		
Steric	0.395	0.450
Electrostatic	0.605	0.550

^a Cross-validated correlation coefficient after the leave-one-out procedure.

^b Cross-validated standard error of prediction.

^c Non-cross-validated correlation coefficient.

^d Correlation coefficient for test set predictions.

^e Standard error of estimate

^f Optimum number of components.

^g F-test value.

^h Probability of obtaining the observed F ratio value by chance alone.

5.4.2. Pharmacophore modeling

Aside from glucuronidation site (i.e. hydroxyl group), hydrophobic features were considered in developing UGT isoform-specific pharmacophore, since they had been demonstrated to be critical for interactions between UGTs and its substrates (Sorich *et al.*, 2002, 2008). In the flavonol structures, the prominent hydrophobic feature is the aromatic rings: B ring and A/C bicyclic ring. Conformation analysis revealed that two distinct orientation modes of flavonol were required to generate 3-O-glucuronide or 7-O-glucuronide, respectively (Figure 30). In this study, the pharmacophore model was built based on 3-hydroxyflavone to capture the common interaction poses for 3-O-glucuronidation. The final pharmacophore query consisted of three features: one glucuronidation site (i.e. hydroxyl group) which is represented by “Don & Acc” (F1) and two neighboring aromatic regions (F2 & F3), as illustrated graphically (Figure 31). The “Don & Acc” feature was able to distinguish hydroxyl oxygen from other types of oxygen(s) in the flavonol structures. The distances from the glucuronidation feature to the aromatic regions are 3.9 Å and 4.2 Å respectively, and the angle between the glucuronidation feature and the two aromatic regions is 84.2°. The pharmacophore query was used to search against conformation database of 67 flavonoids including those from flavonoid subclasses of flavones, isoflavones, flavanone, chalcone and flavonols. All the flavonols were hit to match the three defined pharmacophoric features, whereas other flavonoids did not conform to this pharmacophore model.

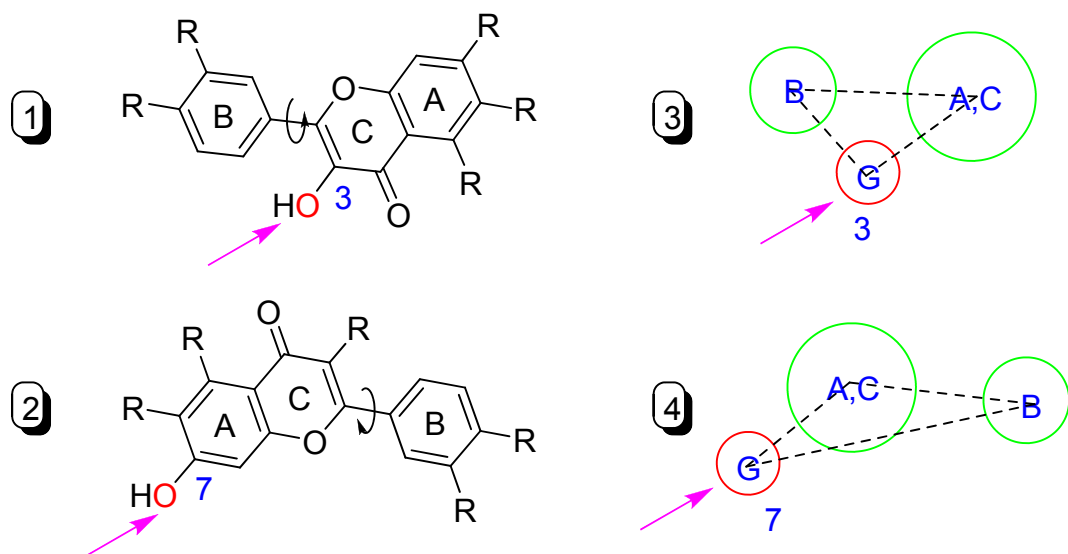


Figure 30. Two hypothetically distinct flavonol orientations that are required to generate 3-O-glucuronide (panel 1 or 3) and 7-O-glucuronide (panel 2 or 4).

*Arrows indicate the site of glucuronidation. In **panels 3 & 4**, G stands for site of glucuronidation. A, B and C are short for A-ring, B-ring, and C-ring, respectively.*

5.4.3. CoMFA models

CoMFA modeling was performed using flavonol alignments based on a 3-OH specific pharmacophore (Figure 32). The flavonol conformers were presumed to be in the bioactive poses which interact with UGT1A9 to produce 3-O-glucuronides. CoMFA analysis resulted in high quality models for UGT1A9 (V_{\max} : $q^2 = 0.738$, $r^2 = 0.976$; CL_{int} : $q^2=0.561$, $r^2=0.938$) (Table 4). For V_{\max} model, the steric field descriptors explained 39.5% of the variance, while the electrostatic descriptors explained 60.5%. For CL_{int} model, the contributing proportions of steric and electrostatic fields to the variance were 45% and 55%, respectively. These models were validated by an external test set of 7 compounds not included in the model construction. The predicted r^2 values from the V_{\max} and CL_{int} CoMFA models were found to be 0.735 and 0.630, respectively (Table 4). The predicted activity and experimental activity are listed in Table 3, and the correlations between them are depicted in Figure 33.

The steric (in green and yellow) and electrostatic (in blue and red) contours of CoMFA were generated. The green contour defines an area where the presence of steric bulky groups would facilitate the UGT reaction. In contrast, the yellow contour indicates a region where bulky groups would diminish glucuronidation (not shown because it is unimportant). The blue contour denotes a space where UGT1A9 metabolism would benefit from electropositive atoms. On the opposite, the red contour is a space where the presence of electronegative atoms would favor glucuronidation. Apparently, no sterically disfavored regions (i.e. yellow areas) surrounding the indicated that the cavities of possible active site of UGT1A9 was very large. This was not

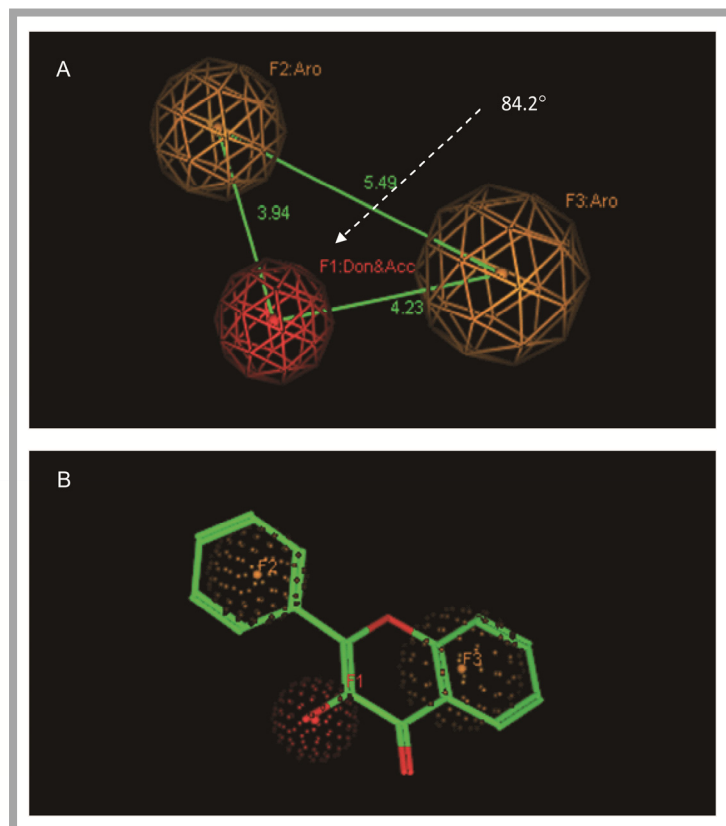


Figure 31. 3-OH specific pharmacophore model

Panel A, 3-OH specific pharmacophore model, it is composed of one glucuronidation site (red sphere with radius of 1 Å) and two aromatic regions (yellow spheres with radius of 1.2 Å and 1.5 Å respectively); **Panel B**, 3-OH specific pharmacophore model superimposed with 3HF (compound 15).

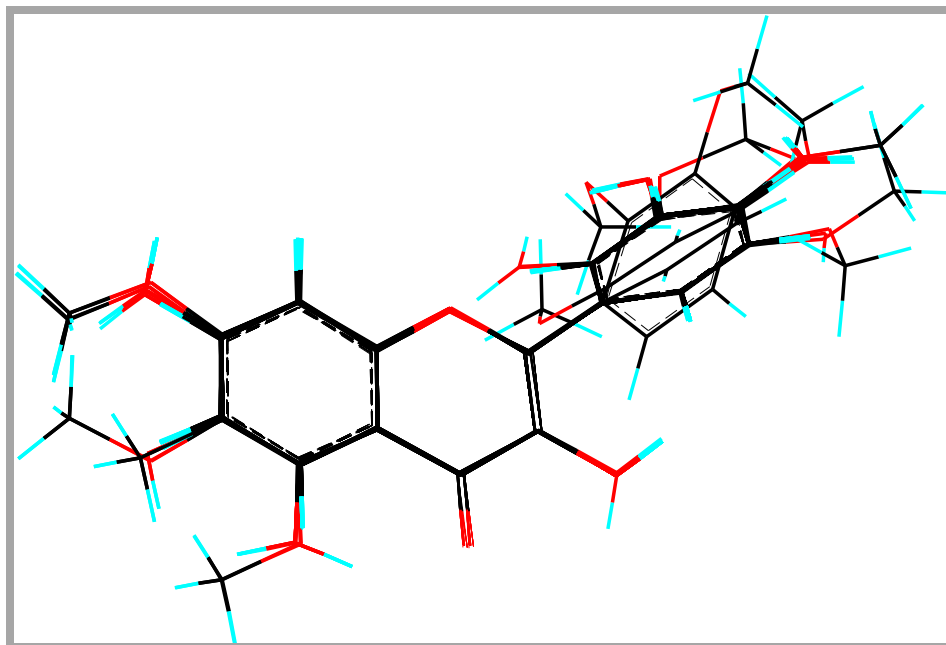


Figure 32. Structural alignment for constructing 3D-QSAR CoMFA model generated from the 3-OH specific pharmacophore.

surprising, because UGT1A9 also efficiently catalyzed compounds which were structurally much larger than flavonols (Luukkanen *et al.*, 2005).

5.4.4. V_{\max} CoMFA model of UGT1A9

The contour map obtained from the V_{\max} CoMFA model are illustrated together with the compound 19 (poor substrate, left panel) and compound 17 (good substrate, right panel) (Figure 34a). In the CoMFA contour map, the green (sterically favorable) and yellow (sterically unfavorable) contours represent 80% and 20% contributions, respectively. Similarly, the blue (electropositive atom favorable) and red (electronegative atom favorable) contours in the CoMFA electrostatic field make 80% and 20% contributions, respectively. Four regions (designated as region I, II, III and IV) that contain the contours, indicating the relations between the properties of the substrates and V_{\max} values, were elucidated as follows.

In region I, the steric favorable green contour near the C6 indicates that bulky group in the contour is important for glucuronidation. This can explain why the V_{\max} values of 36DHF (6-OH), 3H6MF (6-OMe) and 3H6MeF (6-Me) are generally higher than that of 3HF (6-H) (Figure 34.b.I). There is also a red contour positioned (near the green proportion) a bit further from the C6. This contour can be reached and occupied by the hydrogen(s) (electropositive atom) of methoxy group substituted at C6. The placement of electropositive atom(s) in this red area would disfavor the glucuronidation, which is consistent with the fact that 3H6MF (6-OMe) had lower V_{\max} than those of 36DHF (6-OH) and 3H6MeF (6-Me) (Figure 34.b.I).

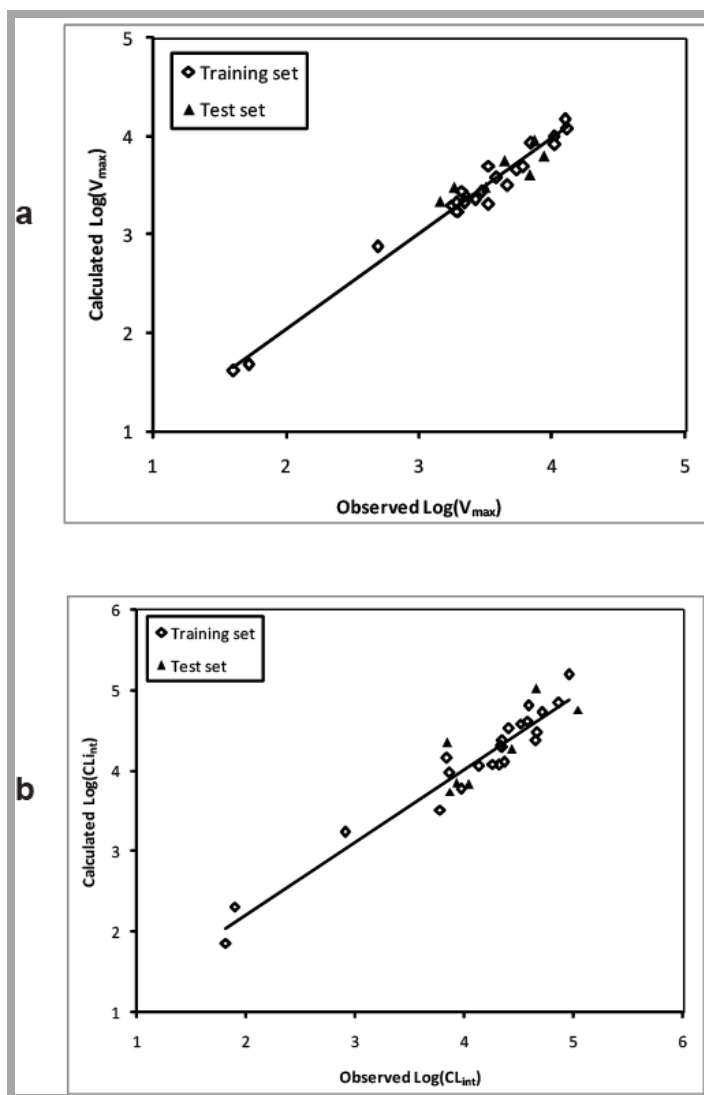


Figure 33. Correlation between the experimental glucuronidation parameters and the predicted ones from the CoMFA models for the training and test sets (a, V_{max} ; b, CL_{int}).

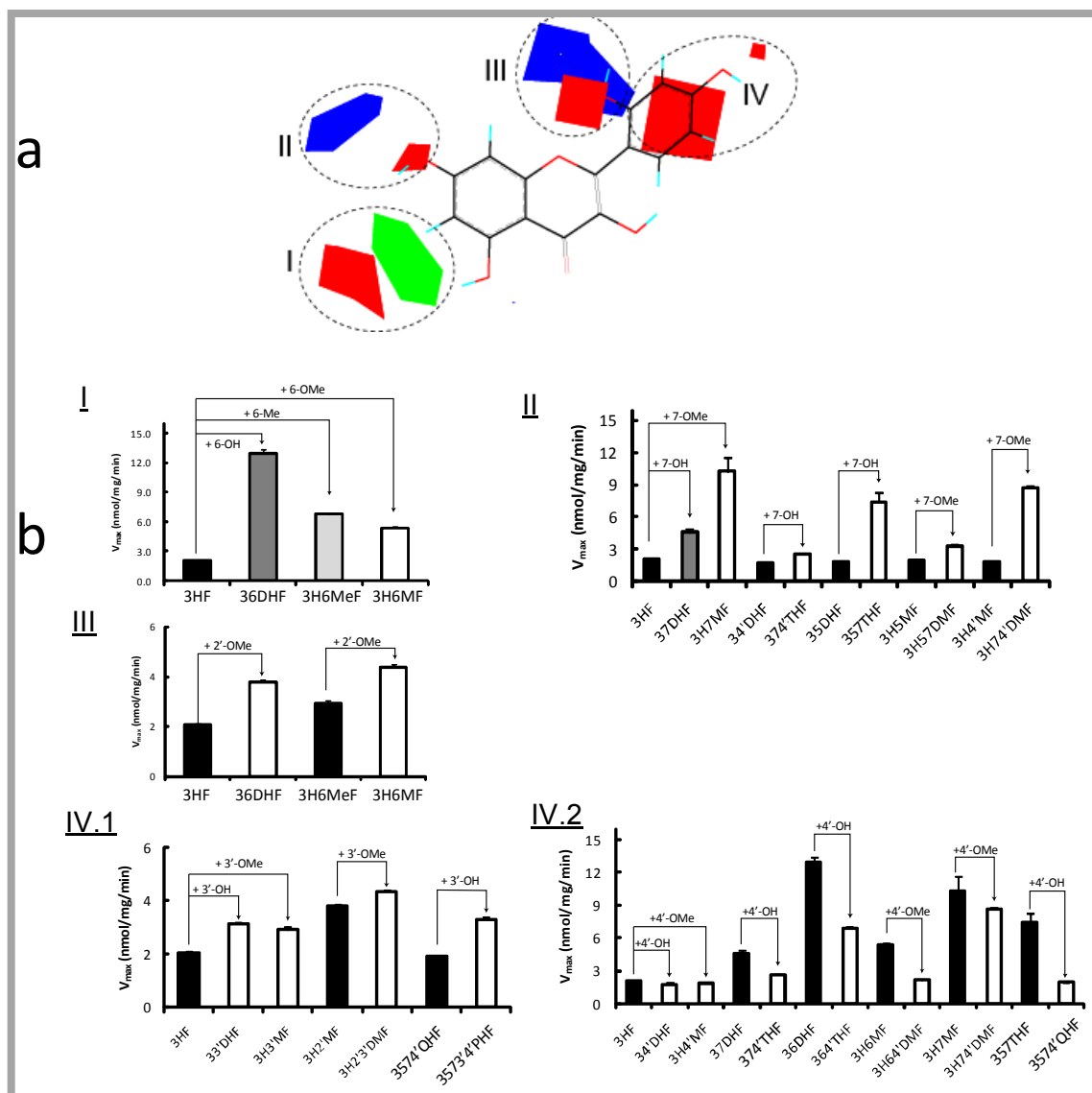


Figure 34. Steric and electrostatic maps from the UGT1A9 CoMFA model of V_{max} .

Panel a: Morin is shown inside the molecular fields for reference. Green: Areas in which bulky groups are sterically favorable for glucuronidation; Blue: Areas in which electropositive atoms are favorable for glucuronidation; Red: Areas in which electronegative atoms are favorable for glucuronidation. **Panel b:** Matching of the CoMFA to experimental data: I, bulky groups at C6 increased V_{max} values; II, 7-OH or 7-OMe increased V_{max} values; III, 2'-OMe increased V_{max} values; IV.1, 3-OH or 3-OMe increased V_{max} values; IV.2, 4-OH or 4-OMe decreased V_{max} values.

In region II, a small red polyhedron (occupied by electronegative oxygen of 7-OH or 7-OMe) and a blue contour (occupied by hydrogen(s) of 7-OMe) aligned diagonally along the C7. It suggests that an electronegative atom(s) in the red polyhedron, and/or electropositive atom(s) in the blue contour are favorable for UGT1A9 glucuronidation. Therefore, the presence of 7-OH or 7-OMe would contribute to higher V_{\max} values. This is supported by the comparisons between the structures and V_{\max} values: 3HF (7-H) < 37DHF (7-OH) < 3H7MF (7-OMe); 34'DHF (7-H) < 374'THF (7-OH); 35DHF (7-H) < 357THF(7-OH); 3H5MF(7-H) < 3H57DMF (7-OMe) and 3H4'MF (7-H)< 3H74'DMF (7-OMe) (Figure 34.b.II).

In region III, The red contour slightly further away from the C2' suggested an electropositive atom (or hydrogen attached to -OH) substitution would compromise the glucuronidation, as seen from the data that compound 1, 32'DHF and compound 19, morin (with 2'-OH) had the smallest V_{\max} values (Table 3). A nearby large blue area which is occupied by multiple electropositive hydrogen atoms of 2'-OMe, indicated that 2'-OMe contribute significantly to the glucuronidation. For this reason, 3H2'MF (2'-OMe) and 3H2'3'DMF (2'-OMe) had bigger V_{\max} values than those of 3HF (2'-H) and 3H3'MF (2'-H), respectively (Figure 34.b.III).

For region IV, the big red contour is in the close vicinity of C3', suggesting that glucuronidation would benefit from electronegative atoms such as oxygen in hydroxyl or methoxy group placed in this area. This is consistent with the fact that V_{\max} values are increased in the presence of 3'-OH or 3'-OMe: 3HF (3'-H) < 33'DHF (3'-OH) or 3H3'MF (3'-OMe); 3H2'MF (3'-H) < 3H2'3'DMF (3'-OMe); and 3574'QHF (3'-H) < 3573'4'PHF (3'-

OH) (Figure 34.b.IV.1). There is a small red contour (close to the hydrogen of 4'-OH) that can be occupied by electropositive hydrogen(s) of 4'-OMe. It is suggested that electropositive atoms in or near this contour will be detrimental to the glucuronidation. Therefore, 4'-OH or 4'-OMe most likely would reduce the value of V_{max} , which is evidenced from the observations: 3HF (4'-H) > 34'DHF (4'-OH) or 3H4'MF(4'-OMe); 37DHF (4'-H) > 374'THF (4'-OH); 36DHF (4'-H) > 364'THF (4'-OH); 3H6MF(4'-H) > 3H64'DMF(4'-OMe); 3H7MF (4'-H) > 3H74'DMF (4'-OMe); and 357THF (4'-H) > 3574'QHF (4'-OH) (Figure 34.b.IV.2).

5.4.5. CL_{int} CoMFA model of UGT1A9

The contour map obtained from the CL_{int} CoMFA model are shown together with the compound 19 (poor substrate, left panel) and compound 16 (good substrate, right panel) (Figure 35.a). It is observed that five regions (designated as region I, II, III, IV and V) contain the contours, indicating the relationships between the properties of the substituents and CL_{int} values. In region I, the blue contour near C5 suggested that electropositive entities placed in this area would result in higher CL_{int} value. This can be demonstrated by the fact that 3H5MF (5-OMe) is more efficiently metabolized than 3HF (5-H) or 35DHF (5-OH) (Figure 35.b.I). However, 3H57DMF (5-OMe) had a smaller CL_{int} than that of 3H7MF (5-H), indicating some uncertainties at this position.

In region II, a green contour presents around C6. It was reasoned that steric bulks substituted at C6 would enhance conjugation activity with higher CL_{int} . This is supported by the fact that 36DHF (6-OH), 3H6MF (6-OMe) and 3H6MeF (6-Me) showed much

higher catalytic efficiency than that of 3HF (6-H), and 364'THF (6-OH) had higher CL_{int} value than that of 34'THF (6-H) (Figure 35.b.II).

In region III, the blue polyhedron near C7 suggested that placement of electropositive atoms (e.g., hydrogen(s) of 7-OMe) would increase the metabolism. This is in agreement with the observations (ordered in term of CL_{int} values): 3H7Me (7-OMe) > 3HF (7-H); 3H74'DMF (7-OMe) > 3H4'MF (7-H); and 3H57DMF (7-OMe) > 3H5MF (7-H) (minor difference) (Figure 35.b.III).

In region IV, a red contour appears in the vicinity of C2', which indicated electropositive atoms placed in this volume would be metabolism unfavorable. This might explain why 32'DHF (2'-OH) and morin (2'-OH) showed poorest glucuronidation with the smallest CL_{int} values (Table 1Table 3). A nearby large blue area is shown to cover the electropositive hydrogen(s) of 2'-OMe. The presence of 2'-OMe therefore is predicted to enhance the glucuronidation, which is experimentally interpreted by the fact that 3H2'MF (2'-OMe) was more efficiently glucuronidated than 3HF (2'-H). Unexpectedly, the 3H2'3'MF (2'-OMe) had a CL_{int} value smaller than that of 3H3'MF (2'-H) (Figure 35.b.IV).

In region V, a big red contour shows around C3'/C4'. There is also a small red contour that is occupied by oxygen of 3'-OH. This can be translated to that glucuronidation would benefit from the electronegative atoms (e.g., oxygen of -OH) in the area, as evidenced by that 3HF (3'-H), 34'DHF (3'-H) and 3574'QHF (3'-H) were less

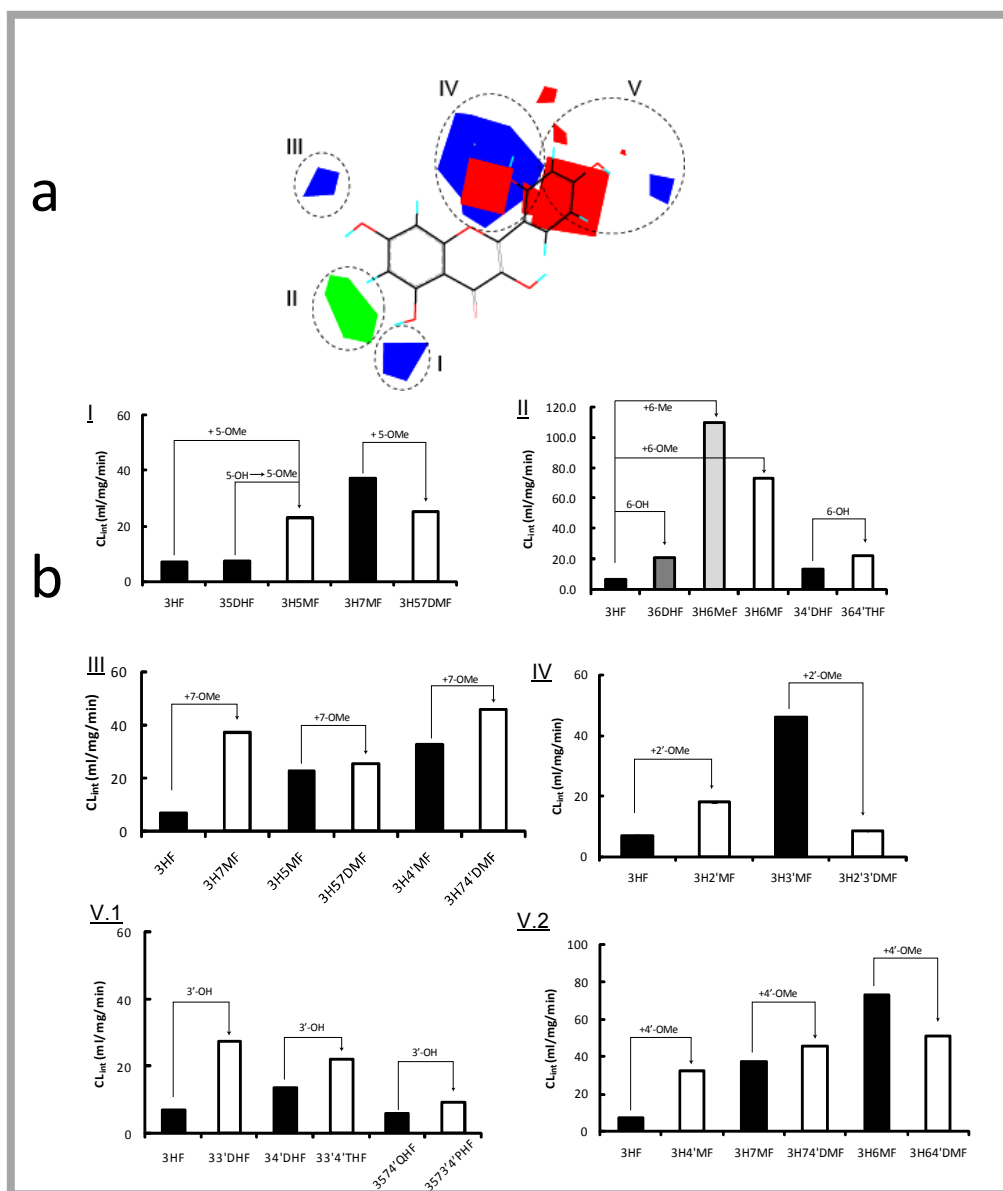


Figure 35. Steric and electrostatic maps from the UGT1A9 CoMFA model of CL_{int}

Panel a: Green: Areas in which bulky groups are sterically favorable; Blue: Areas in which electropositive atoms are favorable for glucuronidation; Red: Areas in which electronegative atoms are favorable for glucuronidation. **Panel b:** Matching of the CoMFA to experimental data: I, effect of 5-OMe on CL_{int} was not well defined; II, bulky groups at C6 increased CL_{int} values; III, 7-OMe increased CL_{int} values; IV, effect of 2'-OMe on CL_{int} was not well defined; V.1, 3-OH increased CL_{int} values; V.2, effect of 4'-OMe on CL_{int} was not well defined.

metabolized (smaller CL_{int} values) than 33'DHF (3'-OH), 33'4'THF (3'-OH) and 3573'4'PHF (3'-OH), respectively (Figure 35.b.V.1). A blue contour situates in the vicinity of C4', which can be occupied by electropositive hydrogen(s) of 4'-OMe group. It is suggested that CL_{int} will be increased in presence of 4'-OMe, as supported by the fact that 3HF (4'-H) and 3H7MF (4'-H) were less efficiently glucuronidated by 3H4'MF (4'-OMe) and 3H74'DMF (4'-OMe), respectively. However, addition of 4'-OMe in 3H64'MF did not result in higher CL_{int} value, comparing to 3H6MF (4'-H) (Figure 35.b.V.2).

5.5. Discussion

We have constructed successfully for the first time in silico models for glucuronidation of flavonols by human UGT1A9 that focused on predicting V_{max} and CL_{int} of 3-O-glucuronidation. 2D/3D-QSAR models developed for UGTs in literatures ([Sorich *et al.*, 2002, 2008](#); [Smith *et al.*, 2004](#)) predicted the substrate selectivity and/or binding affinity of inhibitors (as reflected by low apparent inhibitor constant ($K_{i,app}$)). However, V_{max} or CL_{int} is more relevant to define the susceptibility of chemicals to be metabolized and reflect the in vivo biotransformation efficiency by individual human UGT isoforms (at low physiological concentrations at or below 1 μ M), because higher substrate affinity towards UGTs does not always translate to faster glucuronidation rates. For example, 3-hydroxyflavone ($K_{i,app}$ = 3.5 μ M) binds much strongly to UGT1A9 than naringenin ($K_{i,app}$ = 219 μ M) (Smith *et al.*, 2004), but 3-hydroxyflavone (1.99 ± 0.09 nmol/mg/min) was glucuronidated slower than naringenin (3.26 ± 0.07 nmol/mg/min) at 10 μ M by UGT1A9.

This study validates our approach of quantitatively describe the position (3-OH) specific (or regiospecific) glucuronidation using in silico models. It directly tackles the challenges of predicting UGT metabolism of flavonols in silico that potentially generate multiple conjugates. Successful implementation of this approach to other hydroxyl groups will allow the estimation of overall glucuronidation of multi-hydroxyl flavonols (by summation of predicted values from the separate position specific models). It is consistent with the hypothesis of Miners et al., who stated that “multiple binding modes within the aglycone-binding domain are required to generate multiple metabolites from single substrate that bears more than one nucleophilic group” (Miners *et al.*, 2004). Since available 3D QSAR algorithms are based on only one presumed bioactive conformation corresponding to each ligand (i.e. one binding mode), it hinders one-step prediction of formation of multiple mono-glucuronides from a single substrate with more than one nucleophilic site. This limitation can be readily observed in the pharmacophore models. Mapping of quercetin into UGT1A9 pharmacophore generated by using the substrates with great structural diversity (Miners *et al.*, 2004) indicates 3'-OH is the only site of glucuronidation, which is in conflict with the fact that UGT1A9 generates multiple glucuronides from quercetin (Chen *et al.*, 2005; Singh *et al.*, 2010).

We chose to model 3-O-glucuronidation of flavonols using CoMFA, a widely recognized 3D-QSAR technique for modeling biological properties. Main advantages of CoMFA include (1) the ability to display the model graphically and (2) it allows inference regarding binding pocket geometry. Up to 3155 hits were generated by PubMed search (conducted on August 20, 2010) using “Comparative molecular field analysis or CoMFA”

as keywords. In contrast, linear or non-linear regression models based on 2D/3D descriptors showed good predictability, but the interpretation of important features and descriptors is difficult (Sorich *et al.*, 2008). As stated by Chohan *et al.* (2006), QSAR model is more like a “black box”, with only computers able to interpret which molecular properties modulate the metabolism.

The predictive CoMFA models of UGT1A9 can be used to guide the design of novel flavonol with desired UGTs metabolism or predict 3-O-glucuronidation of untested analogs. From the perspective of reducing metabolism, introduction of multiple electropositive atoms or groups (e.g., hydrogen(s) of –OH) to B-ring would result in poor 3-O-glucuronidation by UGT1A9. On the contrary, fast conjugation of 3-OH may be resulted from substrates with bulky substituents at C6 or electronegative atoms or groups (e.g., –Cl, –F and –O of methoxy group) around B ring. As advancement is made of quantitation technologies of specific UGT isoforms, it is envisioned that successful prediction of glucuronidation by major metabolizing isoforms would enable the precise estimation of the UGT metabolism at tissue/organ level (e.g., liver, intestine and kidney) (Tang *et al.*, 2010). In addition, the CoMFA model highlighted the significant role of electrostatic potential (i.e., electronegative vs. electropositive entity) in determining UGT1A9-mediated glucuronidation. This structural property was also shown to be the key descriptor in the successfully modeling of UGT1A9 catalyzed glucuronidation of phenols (Ethell *et al.*, 2002). This important information will be used to guide future descriptors selection or model refinement in 2D/3D-QSAR modeling of UGT1A9 using

more diverse dataset, as UGT1A9 was shown to present more challenges for in silico modeling (Smith *et al.*, 2004).

The success of CoMFA modeling in turn corroborated the underlying assumption about the alignment of bioactive poses, suggesting the aglycones interact with UGT1A9 protein using similar mode to generate 3-O-glucuronide. Hence, it lends strong support to the hypothesis that multiple distinct binding modes are required to generate different glucuronide isomers by 1A9, if not all UGT1A isoforms. Interesting, plant UGTs (e.g., UGT71G1, VvGT1 and UGT78G1) with crystal structures do possess the big catalytic cavities in aglycone-binding domain. The binding pocket with sufficient space permits the distinct orientations from single flavonoids that rendering the respective hydroxyl groups for conjugation (Osmani *et al.*, 2009). Due to the marked similarity of catalytic mechanism between human and plant UGTs (Patana *et al.*, 2008), UGT1A9 may also have large aglycone-binding domain that serves as the molecular basis for the generating multiple metabolites. This assumed large binding pocket is also supported by the CoMFA contours that did not show any steric disfavoring areas. Therefore, only an algorithm which considers all the active conjugation sites will allow acceptable prediction of the overall glucuronidation rates of flavonols with multiple hydroxyl groups. Because different hydroxyl group of a flavonol or other flavone may be predominantly metabolized by a particular isoform, this type of modeling must be extended to multiple UGT isoforms if we were able to successfully extend this approach to predict the metabolism of flavonols at all sites.

An interesting discovery is that the linkage between K_m and the enzyme turnover is weak if they are present at all (Figure 33). Our data clearly showed that comparing with V_{max} or CL_{int} , K_m is less susceptible to minor structural changes. Also, kinetics profiling of positional (3-O- and 7-O-) glucuronidation in our lab showed identical K_m but divergent V_{max} (data not shown). This might indicate that the UGT1A9 protein adopt distinct conformations for aglycone binding and product expelling/releasing, since the turnover is determined in a large part by the departure of product (3-O-glucuronides). This hypothesis is supported by the fact that UGTs undergo dramatic conformation changes during the catalysis (Laakkonen and Finel, 2010). Therefore, as mentioned earlier, conventional use of K_m or K_i as an indicator of substrate selectivity might lead to erroneous interpretation of interaction between substrates and UGT1As. Although being independent from V_{max} , K_m influenced the modeling results between V_{max} and CL_{int} . For example, 4'-OMe is unfavorable for V_{max} , but favorable for CL_{int} (Figure 34.b.IV.2 & Figure 35.b.V.2).

The predictability of current model might be compromised by the unevenly distributed activity (e.g., existing gap of 1.8-2.8 for Log (V_{max})), especially when those compounds that are to be predicted have activities fall into the gaps. Refinement of the model appears to be essential by adding those flavonols whose activity can fill in those gaps. However, considering the remarkable similarity of the chemical structures between the modeled compounds, but divergent activity spanning ~ 3 log orders, the model seemed to be able to sufficiently capture the key chemical characteristics associated with the modeled parameters. This is evidenced by the establishment of a predictive model with

strong statistical significance, as well as the consistency between experimental results and the contour maps. Therefore, the current CoMFA models are insightful with acceptable predictability.

In conclusion, 3D-QSAR study of UGT1A9-flavonols was carried out using pharmacophore-based CoMFA. The constructed CoMFA models possessed good internal and external consistency and showed statistical significance and predictive abilities (V_{\max} model: $q^2 = 0.738$, $r^2 = 0.976$, $r^2_{\text{pred}} = 0.735$; CL_{int} model: $q^2 = 0.561$, $r^2 = 0.938$, $r^2_{\text{pred}} = 0.630$). The contour maps from CoMFA clearly indicated key structural characteristics (e.g., electropositive entities at C2' or C3') that were associated with poor 3-O-glucuronidation. The results suggested that the approach of coupling CoMFA analysis with pharmacophoric alignments is viable for constructing predictive models regarding regiospecific or 3-O- glucuronidation of flavonols by UGT1A9.

Chapter 6 Accurate prediction of glucuronidation of structurally diverse phenolics by human UGT1A9 using combined experimental and in silico approaches (Study IV)

6.1. Abstract

UDP-glucuronosyltransferase 1A9 (UGT1A9) is an important membrane protein that catalyzes glucuronidation of xenobiotics including many drugs. However, the molecular mechanism of drug recognition by UGT1A9 has remained elusive. The purpose of this study is to elucidate the catalytic selectivity of UGT1A9 by experimentally determining the activities of a large number of phenolics and applying three-dimensional quantitative structure-activity relationship (3D-QSAR) methods (i.e., Comparative Molecular Field Analysis (CoMFA) and Comparative Molecular Similarity Indices Analysis (CoMSIA)). The catalytic efficiency of UGT1A9 (expressed as $\log(V_{\max}/K_m)$) was carefully determined by kinetic profiling for structurally diverse phenolics ($n = 145$). Molecular alignment of the substrate structures was made to superimpose the glucuronidation site and its adjacent aromatic ring. In the case of a substrate with multiple active glucuronidation sites, more than one structural pose was aligned corresponding to the glucuronidation at each site. The 3D-QSAR analyses produced statistically reliable models with good predictive power (CoMFA: $q^2 = 0.548$, $r^2 = 0.949$, $r^2_{\text{pred}} = 0.775$; CoMSIA: $q^2 = 0.579$, $r^2 = 0.876$, $r^2_{\text{pred}} = 0.700$). The contour coefficient maps generated from CoMFA/CoMSIA were applied to elucidate structural features among substrates that are responsible for the selectivity differences. Furthermore, the contour coefficient maps were overlaid in the catalytic pocket of a homology model of UGT1A9; this enabled us to identify the UGT1A9

catalytic pocket with a high degree of confidence. In conclusion, based on a large set of structurally diverse molecules (including those with multiple glucuronidation sites) we have experimentally investigated, the 3D-QSAR techniques CoMFA/CoMSIA are used to predict the substrate selectivity of UGT1A9. Our findings also provide a possible molecular basis for understanding UGT1A9 functions and its substrate selectivity.

6.2. Introduction

The high rate of attrition in drug development has become a conundrum in pharmaceutical industry. One root cause for attrition is the unfavorable absorption, distribution, metabolism, and elimination (ADME) characteristics ([Kola and Landis, 2004](#)). Accordingly, there are considerable interests in developing either computational (in silico) or in vitro ADME methods to aid the lead compound selection ([Wishart, 2007](#); [Emoto *et al.*, 2010](#)). A main advantage of a computational model is that it allows the ADME properties predicted for a new structure without experimental determination. This merit is rather tempting when thousands of (even more) drug candidates need to be screened. In fact, the use of ADME modeling/prediction has become an effective approach for industry to reduce late-stage attrition in drug discovery ([Wishart, 2007](#)).

Predicting the metabolic fate of a drug candidate is an indispensable component of ADME evaluation. Extensive metabolism may result in poor bioavailability and/or drug inefficacy, whereas poor metabolism can be associated with drug toxicity. Significant advances have been made to predict cytochrome p450 (CYPs)-mediated metabolism using molecular modeling techniques such as two dimensional/three dimensional

(2D/3D) quantitative structure-activity relationships (QSAR), pharmacophore, and homology modeling ([Wang and Chou, 2010](#); [Mendieta-Wejebe *et al.*, 2011](#)). And a number of software packages to predict CYP metabolism have been commercialized (e.g., MetaSite, Simcyp). However, relatively fewer efforts are directed to develop such models and to characterize structural features of substrates for other important drug metabolizing enzymes such as UDP-glucuronosyltransferases (UGTs) ([Smith *et al.*, 2003](#)).

UGTs catalyze the glucuronidation reaction which has been recognized as a prevailing metabolic and detoxification pathway for many drugs, sometimes targeting the products (hydroxylated phenols) of CYP-mediated metabolism ([Emoto *et al.*, 2010](#)). Human UGTs constitute a large family of enzymes, and are systematically classified into four subfamilies, UGT1, UGT2, UGT3, and UGT8 ([Mackenzie *et al.*, 2005](#)). One unique feature about human UGTs is that these enzymes show remarkably broad substrate specificity. A UGT substrate usually contains one nucleophilic group (i.e., hydroxyl (-OH) group, carboxylic acid (-COOH), and amines) to which the glucuronic acid derived from the cofactor UDP-glucuronic acid (UDPGA) is transferred. Although it is rare, the acidic carbons and thiol group can also be glucuronidated ([Radomska-Pandya *et al.*, 1999](#)). Another important feature of human UGTs is that they exhibit vast overlapping substrate specificity; this has challenged the identification of specific probe substrates (and possibly inhibitors) for a particular UGT enzyme ([Court, 2005](#)). Lacking of an in vivo selective UGT probe is a significant barrier to in vivo glucuronidation studies with respect to evaluation of the role of a UGT enzyme ([Miners *et al.*, 2010](#)).

A complete three dimensional structure of human UGTs is not yet available. Only a partial crystal structure of UGT2B7 (C-terminal domain) was resolved in 2007 (Miley *et al.*, 2007). This structure, combined with molecular modeling studies, provides substantial insights into the UDPGA binding and possible catalytic mechanism (Radomska-Pandya *et al.*, 2010). Due to the lack of structural information of the N-terminus (for substrate binding), relatively little is known about the specific molecular interactions that govern UGT selectivity for its substrates. Nonetheless, Miners and colleagues demonstrate that substrate hydrophobicity and the spatial arrangement of two hydrophobic regions (close to the glucuronidation site) are important for substrate recognition by several human UGT isoforms based on (2D/3D) regression models and a pharmacophore model (Smith *et al.*, 2003; Sorich *et al.*, 2002, 2004).

UGT1A9 is a major UGT1A isoform in human liver. Its role in clearance of both chemotherapeutic and non-chemotherapeutic drugs (e.g., SN-38, tamoxifen and acetaminophen) and in detoxification of carcinogens (e.g., NNAL and benzo[a]pyrene) has been widely recognized (Fang *et al.*, 2002; Olson *et al.*, 2009; Lazarus *et al.*, 2010). Moreover, UGT1A9 polymorphisms (e.g., M33T, C183G and V167A) are being identified; those genetic variants have impaired glucuronidation activity that might have clinical implications (Villeneuve *et al.*, 2003; Olson *et al.*, 2009). Given its importance in clearance of many xenobiotics/drugs, UGT1A9 has received considerable studies in recent years (Kurkela *et al.*, 2003; Patana *et al.*, 2008; Fujiwara *et al.*, 2009; Itäaho *et al.*, 2010). The aim of this work is to enhance our understanding of molecular interactions of UGT1A9 with its substrates, and to develop a more generalized model

that can be used to predict UGT1A9-mediated glucuronidation of novel drug candidates. To this end, ligand-based three-dimensional quantitative structure-activity relationship (3D-QSAR) methods (i.e., Comparative Molecular Field Analysis (CoMFA) and Comparative Molecular Similarity Indices Analysis (CoMSIA)) were applied to yield statistically reliable models with good predictive power. The correlation results obtained by CoMFA/CoMSIA were graphically interpreted in terms of field contribution maps. The catalytic pocket (or binding pocket) geometry and its physiochemical properties indicated from the CoMFA/CoMSIA analyses were compared with that from a homology model of UGT1A9.

6.3. Materials and methods

6.3.1. Materials

Expressed human UGT1A9 isoform (Supersomes™) was purchased from BD Biosciences (Woburn, MA). 4-Methylumbelliferone-glucuronide, baicalin (baicalein-7-O-glucuronide), uridine diphosphoglucuronic acid (UDPGA), alamethicin, D-saccharic-1,4-lactone monohydrate, and magnesium chloride were purchased from Sigma-Aldrich (St Louis, MO). Ammonium acetate was purchased from J.T. Baker (Phillipsburg, NT). SN-38-glucuronide, and propofol-glucuronide were obtained from Toronto Research Chemicals (North York, Ontario, Canada). Wogonoside (wogonin-7-O-glucuronide) was purchased from Chengdu Mansite Pharmaceutical Co. Ltd. (Chengdu, China). All (145) UGT1A9 substrates (Table 5) were obtained from commercial sources. The chemical structures of these UGT1A9 substrates are shown in appendix A.

6.3.2. Enzyme Assays

Enzyme assays using expressed UGT1A9 were conducted following a standard protocol as described in our earlier publications (Tang *et al.*, 2009, 2010; Singh *et al.*, 2010). Briefly, the incubation procedures were as follows: [1] UGT1A9 (13-53 µg/ml as optimum for the reaction), magnesium chloride (0.88 mM), saccharolactone (4.4 mM), alamethicin (0.022 mg/ml), different concentrations of substrates in a 50 mM potassium phosphate buffer (pH 7.4), and UDPGA (3.5 mM, added last) were mixed; [2] the mixture (final volume, 200 µl) was incubated at 37°C for a predetermined period of time (15-120 min); and [3] the reaction was stopped by the addition of 50 µl of 94% acetonitrile/6% glacial acetic acid. Great effort was made to ensure that the rates of metabolite formation were linear with respect to time (15-120 min) and protein concentration (13-53 µg/ml), so we can obtain accurate and reliable initial metabolism rates. Apparent glucuronidation rates were calculated as the amount of glucuronide(s) formed per protein concentration per reaction time (or pmol/mg/min). All experiments were performed in triplicates.

6.3.3. UPLC analysis

The Waters ACQUITY UPLC (Ultra performance liquid chromatography) system was used to analyze the UGT1A9 substrates and their glucuronides (Appendix B/C).

6.3.4. Identification of glucuronide and glucuronidation site

Glucuronide formation by UGT1A9 was confirmed via the hydrolysis (by β -D-glucuronidase) experiment and the molecular weight detection by UPLC/MS/MS, a standard procedure in our lab (Singh *et al.*, 2010). The site (-OH group) of glucuronidation is an important information that was incorporated into CoMFA/CoMSIA

analyses (see later section). However, regular MS/MS is unable to probe the site of glucuronidation (or deduce the exact structure of a glucuronide); because the glucuronic acid moiety is readily detached from a glucuronide once collision energy is applied. For a substrate with a single -OH group, the site of glucuronidation has to be this -OH group and no addition effort is needed. By contrast, for a substrate containing multiple -OH groups, three methods were used to elucidate a glucuronidation site. That is (1) for flavones and flavonols, the site of glucuronidation was assigned by the “UV spectrum maxima (λ_{max}) shift method” (Singh *et al.*, 2010). This method is based on the characteristic UV shifts caused by glucuronic acid substitution on a particular -OH group; (2) the information regarding site of glucuronidation was collated from the literature; (3) the site of glucuronidation was arbitrary assigned for **7** phloretin and **23** tyrphostin B42 (each forms two glucuronides); these assignments are uncertain, even though they demonstrate a good consistency in later 3D-QSAR analyses.

6.3.5. Kinetics analysis

Kinetic data points were model-fitted using a nonlinear least-squares regression method performed by GraphPad Prism V5 for Windows (GraphPad Software, San Diego, CA). The model used to fit a kinetic profile was carefully selected based on a diagnostic plot (i.e., Eadie-hofstee plot). Overall, Michaelis-Menten equation (eq.1), the substrate inhibition equation (eq.2), and a biphasic kinetic model (eq.3) were used. The intrinsic clearance CL_{int} representing the catalytic efficiency was calculated as V_{max}/K_m for eq.1 and eq.2 fitting and V_{max1}/K_{m1} for eq.3 fitting. Representative fitting of the equations to kinetic data was demonstrated in Figure 36.

$$V = \frac{V_{\max} [S]}{K_m + [S]} \quad \text{Eq.1}$$

$$V = \frac{V_{\max} [S]}{K_m + [S] + \frac{[S]^2}{K_{si}}} \quad \text{Eq.2}$$

$$V = \frac{V_{\max 1} [S] + CL_{\text{int} 2} [S]^2}{K_{m1} + [S]} \quad \text{Eq.3}$$

6.3.6. Molecular Alignment

All substrate structures were prepared using SYBYL 8.0 (Tripos, US). Carboxylate groups were considered to be deprotonated. Energy minimizations were performed using the Tripos force field with partial atomic charges (assigned by Gasteiger-Hückel method). One of the most important factors affecting the quality of a model is the alignment of the individual molecules. The frequently used alignment methods (i.e., substructure overlap, pharmacophore overlap, and docking) are not suitable for this study, because a common core of atoms or a common feature pharmacophore cannot be defined for the 145 structurally diverse substrates (Table 5) and the protein structure is not available. To achieve our goals, we performed a flexible alignment of three most active substrates (**66**: 3-hydroxy-6-methylflavone, **140**: entacapone; **52**: chrysin) with a constraint that the glucuronidation site must be overlaid. The important common features of the most active substrates were found to be the glucuronidation site and its adjacent

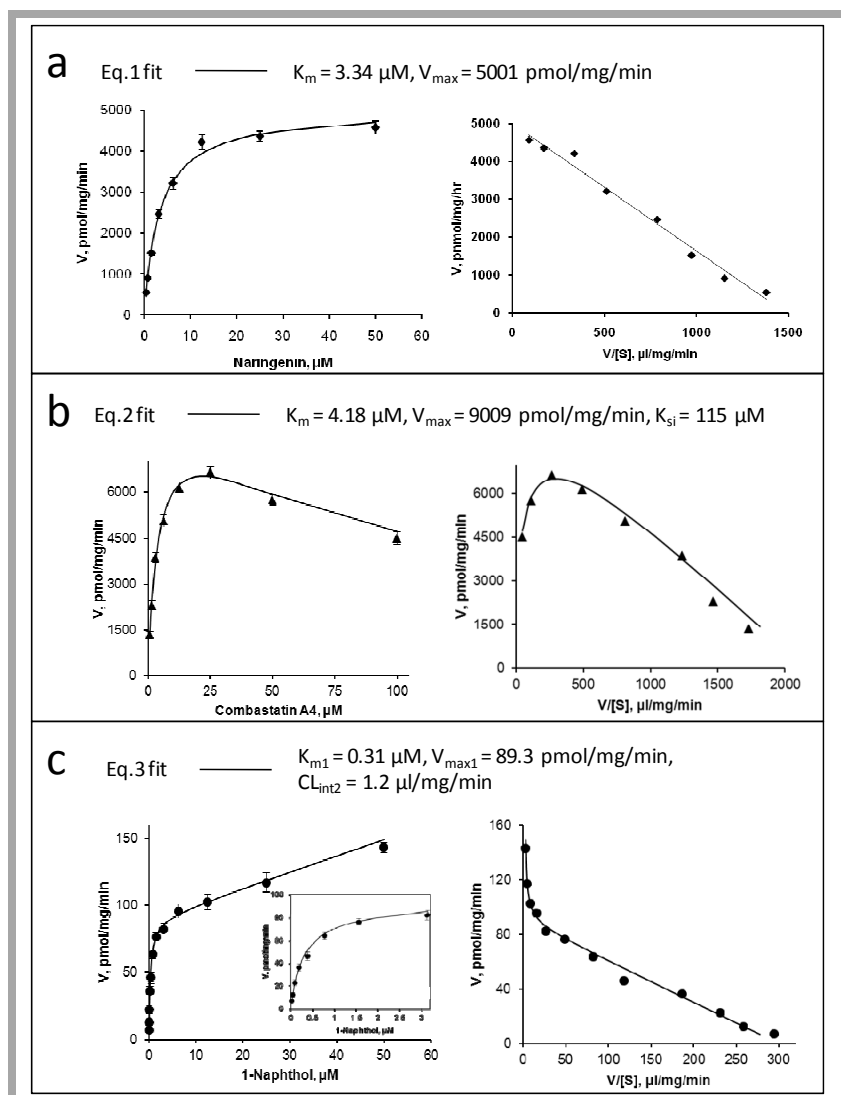


Figure 36. Representative fitting of the model equations (eqs.1-3) to kinetic data of UGT1A9 with its substrates

Both rate plot (left) and Eadie-Hofstee plot (right) are given. **Panel a:** Eq.1 (Michaelis-Menten model) is used to describe glucuronidation of **27** naringenin by UGT1A9. **Panel b:** Eq.2 (a substrate inhibition model) is used to describe glucuronidation of **136** combrestatin A4 by UGT1A9. **Panel c:** Eq.3 (a biphasic model) is used to describe glucuronidation of **21** 1-naphthol by UGT1A9. Points are experimentally determined values, while the solid lines show the computer-derived curves of best fit.

aromatic ring (Figure 37). All other substrates were then aligned to superimpose these two features. In the case of a substrate with multiple active glucuronidation sites, more than one structural pose was aligned corresponding to the glucuronidation at each site. This treatment rendered a final total 166 aligned structure conformations (Table 5). The structural diversity of the aligned ligands is shown in Figure 38.a.

6.3.7. CoMFA and CoMSIA analyses

The whole data set was arbitrarily divided into two parts, the training set ($n = 141$) and the test set ($n = 25$) (Table 5). Selection of the training set and test set molecules was done by considering the fact that the test set could reflect the variations in glucuronidation activity of the training set, and both data sets covered similar diversity in their chemical space. The training set was used for model building and the test set for an external validation of the model. All comparative molecular field evaluations were performed using SYBL 8.0 (Tripos, US). The CoMFA steric energy (Lennard-Jones) and electrostatic (Coulomb) energy were calculated with SYBYL standard parameters (TRIPOS standard field, 2 Å grid spacing, dielectric distance $1/r^2$, cutoff 30 kcal/mol) using a sp^3 carbon probe atom with a charge of +1. In CoMSIA, three different similarity fields (steric, electrostatic, and hydrophobic) were evaluated with SYBYL standard parameters (2 Å grid spacing, attenuation factor $\alpha = 0.3$) using a probe atom with 1 Å radius, charge +1, and hydrophobicity +1. Hydrogen bond donor and acceptor fields were not considered because CoMSIA analyses with these two extra features did not result in significant improvement of model quality. Partial least squares (PLS) analyses were performed following the CoMFA standard implementation in SYBYL. To check

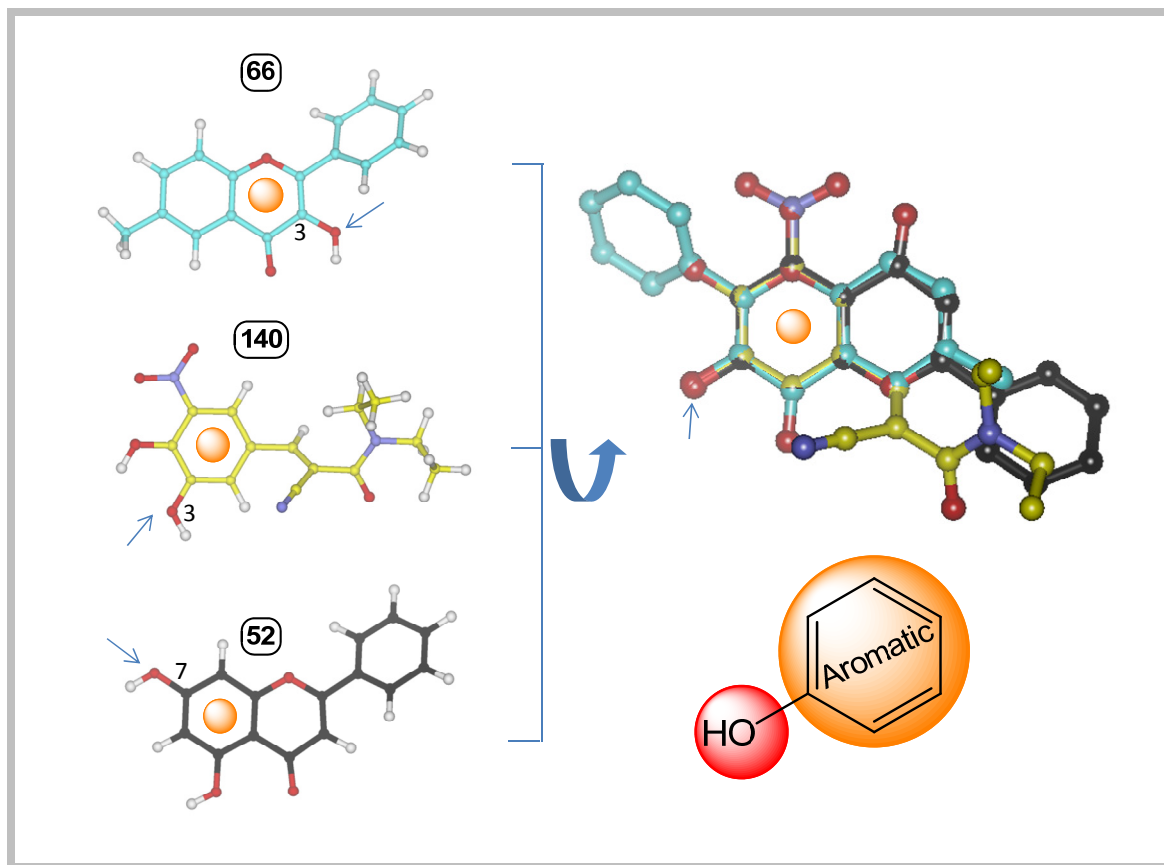


Figure 37. A flexible alignment of three most active substrates (66: 3-hydroxy-6-methylflavone, 140: entacapone; 52: chrysin)

A flexible alignment of three most active substrates (66: 3-hydroxy-6-methylflavone, 140: entacapone; 52: chrysin) to identify their common structural features. The flexible alignment was performed with a constraint that the glucuronidation site must be overlaid. The important commonalities of the most active substrates are found to be the glucuronidation site and its adjacent aromatic ring. Arrows indicate the site of glucuronidation.

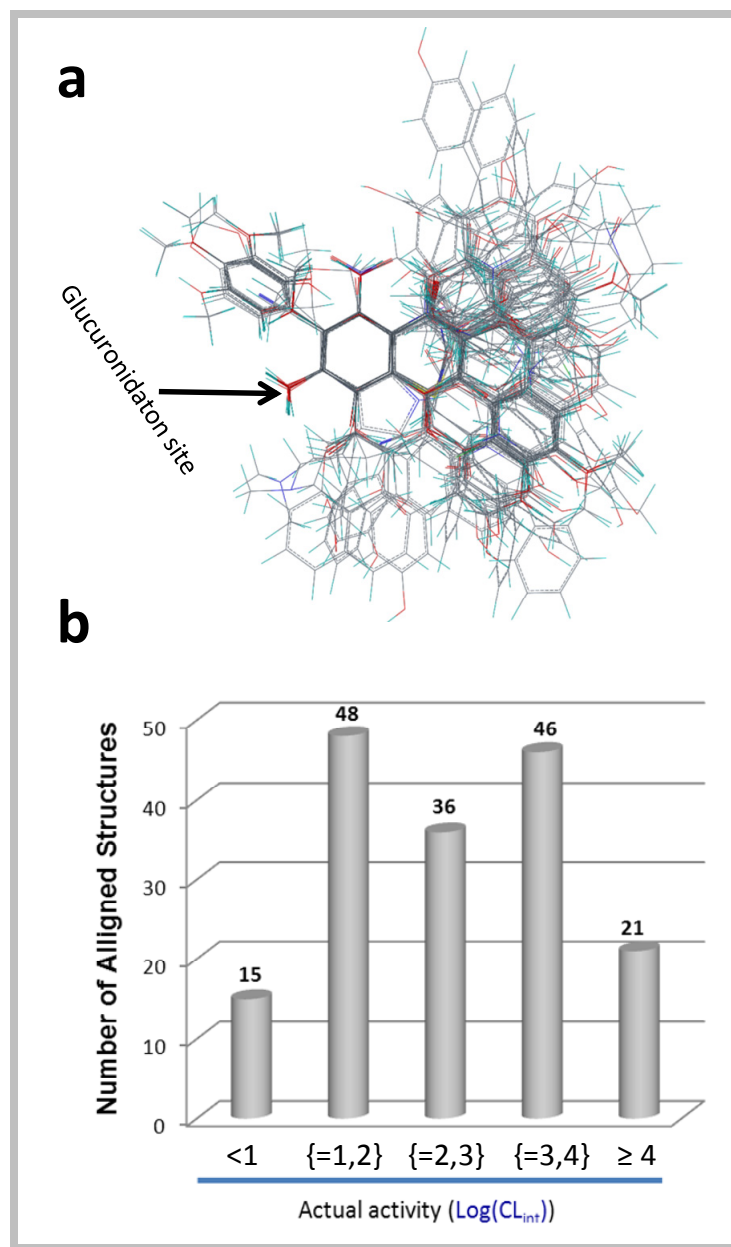


Figure 38. A wide diversity in both chemical structure (a) and activity (b) for UGT1A9 substrates in this study.

Panel a: Overview of all aligned structures in training set and test set ($n=166$). **Panel b:** UGT1A9 activity distribution (expressed as $\text{log}(\text{CL}_{\text{int}})$) of the training and test set.

statistical significance of the models, cross-validations were performed by means of the “leave-one-out” procedure using enhanced version of PLS, the SAMPLS method. The optimal number of components was determined by selecting the smallest S_{press} (corresponds to the highest q^2 value). The same number of components was subsequently used to derive the final QSAR models with no validation (column filtering was set to 2.0 kcal/mol); these models were used for prediction of activity. The statistical results are summarized in Table 6. The q^2 (cross-validated r^2), S_{press} (cross-validated standard error of prediction), r^2 (non-cross-validated r^2), and standard error of estimate (SEE) values were computed as defined in SYBYL. Predictive power of the obtained CoMFA and CoMSIA models was further validated with the test set which was not included in the model derivation. The predictive correlation coefficient, r^2_{pred} , of the CoMFA and CoMSIA models were calculated according to the definition of Cramer et al and are also shown in Table 6.

6.3.8. Homology modeling and molecular docking

A homology model for human UGT1A9 was constructed using Modeler 9v6 with a standard protocol (Sali and Blundell, 1993). The best model with the lowest objective function values (DOPE) was selected for loop refinement and followed by energy minimization in GROMACS 3.3 program package (Van Der Spoel *et al.*, 2005). Energy minimization was done by steepest gradient descent, with an initial step size of 0.01 nm and a maximum of 1000 step. The VvGT1 (PDB code: 2c1z) from red grape was used as the template for two reasons (Offen *et al.*, 2006): First, both UGT1A9 and VvGT1 belong to the glycosyltransferase 1 family (GT1) according to the CAZY database

(<http://www.cazy.org/>). Although sharing a low sequence identity, GT1 members adopt a similar $\alpha/\beta/\alpha$ folding (so called “GT-B” fold) and their 3D structures are predicted to be highly conserved. Second, UGT1A9 and VvGT1 surprisingly share an overlapping substrate specificity (including regioselectivity), for example, they both preferentially metabolize flavonols at the 3-OH position ([Offen *et al.*, 2006](#)).

Due to a low sequence identity between the target and template proteins (~15 %), sequence alignment was aided with secondary structure predictions, a strategy used earlier ([Laakkonen and Finel, 2010](#)). The co-crystallized cofactor (UDP-2-fluoro glucose) was copied to the homology model as a block residue. Molecular docking of kaempferol (**88.a**) for 3-O-glucuronidation to the UGT1A9 model with the program GOLD (CCDC, Cambridge, UK) was performed using a distant constraint, a procedure similar to earlier publications ([Shao *et al.*, 2005](#); [Li *et al.*, 2007a](#)). A distance constraint (2.5~4 Å) was set between 3-OH and His37 (the catalytic residue). GOLDScore was used to identify the lowest energy docking results. The UGT1A9 model (with kaempferol docked) coordinates are available upon request.

6.4. Results

6.4.1. Experimental dataset

A large database of kinetic parameters was experimentally determined by kinetic profiling for UGT1A9-mediated glucuronidation of 145 phenolics (structures in Appendix A), which are from 12 different classes (see Table 5 for compound names, their classification and kinetic parameters). The $\log(\text{CL}_{\text{int}})$ values for glucuronidation of

selected substrates range from -0.56 (**141**) to 5.04 (**66**), demonstrating a wide diversity in the catalytic activity (Figure 38.b). To our knowledge, this is the largest dataset of kinetic data obtained using expressed UGT1A9 in current literature. Among all UGT substrates here, 17 compounds form more than one glucuronide; in particular, there are 4 compounds (i.e., **41**, **84**, **90**, **91**) from which three glucuronides at different positions (-OH groups) are generated. Differentiated kinetic properties for glucuronidation at each position suggest that distinct (productive) binding modes within the catalytic domain are possible (Chapters 2 & 3). The existence of multiple binding modes provide the "expert" knowledge for our modeling strategy. Based on this knowledge, multiple active poses (for each of the aforementioned 17 substrates) were incorporated to the molecular alignment for QSAR analyses (please also see Discussion section).

6.4.2. Predictive power of the analyses

A training dataset of UGT1A9 substrates allows the derivation of two separate QSAR models with statistical significance (Table 6). The predictive power of the two models was validated by predicting the catalytic efficiency of 25 additional substrates not included in the training set (Figure 39). For almost all substrates, the predicted values fall close to the observed $\log(\text{CL}_{\text{int}})$ values, deviating by no more than 1 logarithmic unit (Table 5 & Figure 39). However, in CoMSIA prediction, the activities of **47** (7-hydroxy-3'-methoxyflavone) and **70** (3,7,3'-trihydroxyflavone) are significantly over-estimated more than 1 logarithmic unit, even though CoMSIA analysis reveals significantly better correlation in terms of a higher q^2 .

Table 5. Experimentally determined kinetic parameters for UGT1A9-mediated glucuronidation of 145 compounds, including 2 catechins (No.1-2), 5 chalcones (No.3-7), 1 chromone (No.8), 6 coumarins (No.9-14), 3 curcumins (No.15-17), 6 aromatic hydrocarbons (No.18-23), 4 flavanones (No.24-27), 31 flavones (No.28-58), 36 flavonols (No.59-94), 3 hydroxycinnamic acids (No.95-97), 11 isoflavones (No.98-108), 27 phenols (No.109-135), and 7 other compounds (No.136-145). The chemical structures of all compounds are shown in Appendix A. The site of glucuronidation is indicated in the parenthesis. For a compound with multiple glucuronides generated, a lower-case letter is appended for a distinction.

No.	Name	K _m	V _{max}	CL _{int} (V _{max} /K _m)	Log (CL _{int})	Log (CL _{int})	Log (CL _{int})
		μM	pmol/mg/min	μl/mg/min	(Actual)	(CoMFA)	(CoMSIA)
1.a	(-)-Epigallocatechingallate (3'-OH)	18.7	2955	158	2.20	2.32	2.42
1.b	(-)-Epigallocatechingallate (4''-OH)	15.3	9984	646	2.81	2.72	3.36
2	(-)-Epigallocatechin(3'-OH)	135	5130	38	1.58	1.40	1.90
3	2-Hydroxychalcone [§]	0.23	552	2400	3.38	3.83	3.36
4	4-Hydroxychalcone [§]	1.62	54.8	34	1.53	1.68	1.32
5	2'-Hydroxychalcone [§]	0.77	1008	1309	3.12	2.80	2.40
6	4'-Hydroxychalcone [§]	1.72	339	197	2.29	1.95	1.97
7.a	Phloretin (2'-OH) [§]	0.63	467	741	2.87	2.88	2.64
7.b	Phloretin (4'-OH) [§]	0.43	636	1479	3.17	3.21	3.14
8	7-Hydroxychromone	82.8	668	8	0.91	1.37	1.62
9	3,4-Diphenyl-7-hydroxycoumarin	3.37	137	41	1.61	1.53	1.46
10	4-Methylumbelliferone	12	3653	304	2.48	2.43	2.06
11	4-Hydroxy-6-methylcoumarin	57.8	225	4	0.59	1.06	0.84
12	6-Hydroxy-7-methoxyl-4-phenylcoumarin	312	3744	12	1.07	1.04	1.69
13	8-Hydroxywarfarin	369	9229	25	1.40	1.69	1.67

No.	Name	K _m	V _{max}	CL _{int} (V _{max} /K _m)	Log (CL _{int})	Log (CL _{int})	Log (CL _{int})
		μM	pmol/mg/min	μl/mg/min	(Actual)	(CoMFA)	(CoMSIA)
14	Scopoletin	5.53	1064	192	2.28	2.60	2.56
15	Curcumin	35.4	1958	55	1.74	1.59	1.60
16	Demethoxycurcumin	18.6	258	14	1.14	1.37	1.16
17	Bisdemethoxycurcumin *	257	2070	8	0.90	1.04	0.68
18	Emodin	2.87	2928	1020	3.01	3.10	3.05
19	Endoxifen *	316	2086	6.6	0.82	1.97	1.01
20	Enterolactone (3-OH)	57.4	5292	92	1.96	1.95	2.04
21	Naphthol [§]	0.25	72.1	288	2.46	1.89	1.55
22	Raloxifene (6-OH)	1.93	39.3	20	1.31	1.15	1.06
23.a	Tyrphostin B42 (3-OH)	3.60	3677	1020	3.01	3.02	3.16
23.b	Tyrphostin B42 (4-OH) *	14.5	2008	138	2.14	2.27	2.63
24	7-Hydroxyflavanone *	3.34	5001	1497	3.18	2.88	2.58
25	4'-Hydroxy-3-methoxyflavanone	83.4	1687	20	1.31	1.29	1.39
26.a	Hesperetin (3'-OH)	4.29	4192	977	2.99	2.99	3.31
26.b	Hesperetin (7-OH)	6.00	2444	407	2.61	2.45	2.49
27	Narigenin (7-OH)	3.34	5001	1497	3.18	3.35	2.98
28	2'-Hydroxyflavone	0.40	74.4	186	2.27	2.44	2.26
29	3,4'-Dimethoxy-5,7,3'-trihydroxyflavone (7-OH)	1.64	7494	4570	3.66	3.43	3.43
30	3'-Benzyloxy-5,7-dihydroxy-3,4'-dimethoxyflavone (7-OH)	1.25	2079	1663	3.22	3.25	3.22
31	3'-Hydroxyflavone	2.02	926	458	2.66	2.66	2.63
32	4'-Hydroxyflavone	1.46	98.7	67.6	1.83	1.83	2.11
33	5,7-Dihydroxy-3',4',5'-trimethoxyflavone (7-OH)	0.45	382	849	2.93	3.25	2.84
34	5-Hydroxyflavone	0.96	118	123	2.09	2.09	2.77
35	6,3',4'-Trihydroxyflavone (3'-OH)*	1.87	6470	3450	3.54	2.93	2.86

No.	Name	K _m	V _{max}	CL _{int} (V _{max} /K _m)	Log (CL _{int})	Log (CL _{int})	Log (CL _{int})
		μM	pmol/mg/min	μl/mg/min	(Actual)	(CoMFA)	(CoMSIA)
36	6,7,3'-Trihydroxyflavone (7-OH)	3.01	2333	775	2.89	3.05	3.14
37	6,7-Dihydroxyflavone (7-OH)	4.49	4090	910	2.96	3.07	3.18
38	6-Hydroxyflavone	2.27	76.1	34	1.53	1.30	1.64
39	6-Methoxyluteolin (7-OH)	1.15	1902	1654	3.22	3.28	3.18
40	5,7,2'-Trihydroxyflavone (7-OH) *	0.23	862	3748	3.57	3.44	3.39
41.a	7,3',4'-Trihydroxyflavone (3'-OH)	2.45	2921	1192	3.08	3.23	2.92
41.b	7,3',4'-Trihydroxyflavone (4'-OH)	2.44	744	305	2.48	2.38	2.74
41.c	7,3',4'-Trihydroxyflavone (7-OH)	6.38	820	128	2.11	2.70	2.75
42	7,2'-Dihydroxyflavone (7-OH) *	0.65	381	586	2.77	2.74	2.94
43	7,3'-Dihydroxyflavone (7-OH)	29.6	16166	546	2.74	2.85	2.86
44	7-Hydroxy-2'-methoxyflavone	2.21	2228	1008	3.00	3.04	2.82
45	7-Hydroxy-3-methylflavone	1.46	2929	2006	3.30	3.19	2.83
46	7-Hydroxy-3'-methoxyflavone *	25.3	132	5	1.02	2.81	2.80
47	7-Hydroxy-4'-methoxyflavone	3.37	764	227	2.36	3.00	3.24
48	7-Hydroxy-5-methylflavone	0.94	5369	5712	3.76	3.34	3.03
49	7-Hydroxyflavone	3.59	4895	1364	3.13	2.88	2.90
50	Apigenin (7-OH)	1.93	3289	1704	3.23	2.96	3.24
51	Baicalein (OH) [#]	0.70	5310	7586	3.88	3.37	3.64
52	Chrysin (7-OH)	0.25	4537	18148	3.96	3.56	3.34
53	Chrysoeriol (7-OH)	0.91	2765	3038	3.48	3.16	3.09
54	Diosmetin (7-OH)	0.56	5361	9573	3.41	2.63	2.99
55	Flavopiridol (7-OH)	37.5	219	5.8	0.77	0.57	1.02
56.a	Luteolin (3'-OH)	0.17	660	3870	3.58	3.56	3.08
56.b	Luteolin (7-OH)	0.33	700	2100	3.32	3.38	3.20
57	OroxylinA (7-OH)	2.38	2060	866	2.94	3.46	3.32

No.	Name	K _m	V _{max}	CL _{int} (V _{max} /K _m)	Log (CL _{int})	Log (CL _{int})	Log (CL _{int})
		μM	pmol/mg/min	μl/mg/min	(Actual)	(CoMFA)	(CoMSIA)
58	Wogonin (7-OH)	1.27	5070	3992	3.60	3.98	3.63
59	3,2'-Dihydroxyflavone (3-OH)	0.67	52	78	1.89	2.68	3.34
60	3,3'-Dihydroxyflavone (3-OH) *	0.11	3100	29000	4.44	4.31	4.30
61	3,5-Dihydroxyflavone (3-OH) *	0.25	1900	7400	3.87	4.05	3.88
62	3,6,4'-Trihydroxyflavone (3-OH) *	0.31	6800	22000	4.34	4.31	3.97
63	3,3',4'-Trihydroxyflavone (3-OH)	0.10	2200	22000	4.34	4.21	3.92
64	3,4'-Dihydroxyflavone (3-OH)	0.13	1800	14000	4.14	3.89	3.77
65	3,6-Dihydroxyflavone (3-OH)	0.62	13000	21000	4.32	4.42	4.34
66	3-Hydroxy-6-methylflavone *	0.062	6750	110000	5.04	4.34	4.29
67.a	3,7-Dihydroxy-3',4',5'-trimethoxyflavone (3-OH)	0.63	2872	4551	3.66	3.67	3.70
67.b	3,7-Dihydroxy-3',4',5'-trimethoxyflavone (7-OH) *	1.61	289	180	1.00	1.15	2.17
68.a	3,7-Dihydroxyflavone (3-OH) [#]	0.22	4600	21000	4.32	3.69	4.18
68.b	3,7-Dihydroxyflavone (7-OH)	1.50	2040	1360	3.13	3.09	3.05
69.a	3,7-Dihydroxy-3',4'-dimethoxyflavone (3-OH)	1.03	753	731	3.16	3.48	3.79
69.b	3,7-Dihydroxy-3',4'-dimethoxyflavone (7-OH)	1.16	11.6	10	1.00	1.22	2.37
70	3,7,3'-Trihydroxyflavone (3-OH) *	3.37	764	227	2.86	4.00	4.33
71	3-Hydroxy-2',3'-dimethoxyflavone	0.52	4400	16000	3.92	3.60	3.91
72	3-Hydroxy-2'-methoxyflavone	0.21	3800	18000	4.25	4.10	3.47
73	3-Hydroxy-3'-methoxyflavone	0.063	2900	46000	4.66	4.56	4.58
74	3-Hydroxy-4'-methoxyflavone	0.059	1900	32000	4.51	4.24	4.47
75	3-Hydroxy-5,7-dimethoxyflavone	0.13	3300	26000	4.40	4.35	4.59
76	3-Hydroxy-5-methoxyflavone	0.082	1900	24000	4.36	4.56	4.46
77	3-Hydroxy-6,4'-dimethoxyflavone	0.043	2200	51000	4.71	4.97	5.05
78	3-Hydroxy-6-methoxyflavone	0.074	5400	73000	4.86	4.97	4.79

No.	Name	K _m	V _{max}	CL _{int} (V _{max} /K _m)	Log (CL _{int})	Log (CL _{int})	Log (CL _{int})
		μM	pmol/mg/min	μl/mg/min	(Actual)	(CoMFA)	(CoMSIA)
79	3-Hydroxy-7,4'-dimethoxyflavone	0.19	8700	46000	4.66	4.47	4.60
80	3-Hydroxy-7-methoxyflavone	0.27	10000	37000	4.57	4.36	4.28
81	3-Hydroxyflavone	0.30	2100	7000	3.84	4.01	4.15
82	3-Hydroxy-6-methyl-3',4'-methylenedioxyflavone	0.066	6000	91000	4.96	4.82	4.63
83	Datiscetin (3-OH) *	2.46	246	100	2.00	2.42	3.10
84.a	Fisetin (3-OH)	0.63	1500	2300	3.38	3.90	3.95
84.b	Fisetin (3'-OH)	0.74	2620	3520	3.55	3.37	3.33
84.c	Fisetin (4'-OH)	0.52	1620	3090	3.49	3.63	3.54
85.a	Galangin (3-OH) [#]	0.68	7400	11000	4.04	3.71	3.91
85.b	Galangin (7-OH)	0.54	2560	4740	3.68	3.77	3.50
86	Geraldol (3-OH)	1.47	5885	4003	3.60	3.89	3.76
87	Isorhamnetin (3-OH)	0.32	12000	38000	4.59	4.13	3.49
88.a	Kaempferol (3-OH)	0.32	1900	6000	3.78	3.60	3.54
88.b	Kaempferol (7-OH) *	3.87	870	220	2.34	3.36	3.41
89	Morin (3-OH)	0.68	40	60	1.77	2.33	2.73
90.a	Myricetin (3-OH)	0.61	490	800	2.90	3.33	3.39
90.b	Myricetin (3'-OH) [#]	0.67	1530	2290	3.36	3.25	3.73
90.c	Myricetin (4'-OH)	0.64	3170	4930	3.69	3.69	3.30
91.a	Quercetin (3-OH) *	0.36	3300	9200	3.97	3.91	3.68
91.b	Quercetin (3'-OH)	0.90	1880	2100	3.32	3.49	3.44
91.c	Quercetin (7-OH)	0.85	3820	4490	3.65	3.52	3.24
92.a	Resokaempferol (3-OH)	0.36	2600	7300	3.86	3.59	3.80
92.b	Resokaempferol (7-OH) *	2.67	1150	430	2.63	2.67	2.94
93	Rhamnetin (3-OH)	0.23	10000	45000	4.65	4.34	3.84

No.	Name	K _m	V _{max}	CL _{int} (V _{max} /K _m)	Log (CL _{int})	Log (CL _{int})	Log (CL _{int})
		μM	pmol/mg/min	μl/mg/min	(Actual)	(CoMFA)	(CoMSIA)
94.a	Syringetin (3OH)	0.98	7810	7333	3.87	4.11	3.46
94.b	Syringetin (7OH)	1.61	289	178	2.26	2.05	2.88
95	Ferulic Acid *	884	372	0.4	0.30	1.50	0.09
96	Isoferulic Acid	237	15640	66	1.82	1.62	1.16
97.a	Caffeic Acid (3-OH)	564	6204	11	1.04	1.50	0.86
97.b	Caffeic Acid (4-OH)	1012	2024	2	0.30	0.51	0.50
98	7-Hydroxy-6-methoxyisoflavone	3.08	1143	371	2.57	2.44	2.21
99	8-Hydroxy-7-methoxyisoflavone	1.42	5299	3732	3.57	3.76	3.34
100	Biochanin A (7-OH) *	1.13	379	335	2.53	2.17	1.93
101	Daidzein (7-OH)	14.3	1107	77	1.89	2.17	1.78
102	Dihydrodaidzein (7-OH)	77.7	628	8.1	0.91	0.89	0.74
103	Equol (7-OH)	213	794	3.7	0.57	0.44	0.68
104	Formononetin (7-OH)	4.59	139	30	1.48	1.48	1.48
105	Genistein (7-OH)	2.09	1290	617	2.79	2.96	2.23
106	Glycitein (7-OH)	1.47	403	274	2.44	2.56	2.33
107	Maackiain	3.12	234	75	1.87	1.57	1.29
108	Prunetin (5-OH)	1.29	230	178	2.25	2.20	2.42
109	4-Bromophenol *#	30.9	3057	99	2.00	1.53	1.49
110	4-n-Butylphenol	43.1	647	15	1.18	1.45	1.53
111	4-Chlorophenol	34.0	3230	95	1.98	1.44	1.60
112	4-Cyclopentylphenol [#]	18.2	1083	60	1.78	1.40	1.11
113	4-Ethoxyphenol	454	3761	8.3	0.92	1.25	1.57
114	4-Ethylphenol *#	15.8	1179	75	1.87	1.45	1.39
115	4-Fluorophenol *	112	1680	15	1.18	1.56	1.79

No.	Name	K_m	V_{max}	$CL_{int} (V_{max}/K_m)$	$\text{Log} (CL_{int})$	$\text{Log} (CL_{int})$	$\text{Log} (CL_{int})$
		μM	$\mu mol/mg/min$	$\mu l/mg/min$	(Actual)	(CoMFA)	(CoMSIA)
116	4-Iodophenol	20.5	3034	148	1.87	1.40	1.35
117	4-Isopropylphenol	36.4	2184	60	1.78	1.62	1.17
118	4-Methoxyphenol	154	2310	15	1.18	1.01	1.41
119	4-Methylphenol	57.3	1433	25	1.39	1.30	1.41
120	4-Nitrophenol [#]	80.6	2902	36	1.56	1.50	1.92
121	4-Hydroxyacetophenone	317	4438	14	1.15	1.40	1.61
122	4-Hydroxybenzophenone	35.9	2441	68	1.83	1.90	1.38
123	4-Phenylphenol	56.2	1236	22	1.34	1.50	1.33
124	4-Phenylzophenol	82.5	1155	14	1.15	1.29	1.48
125	4-Propoxyphenol	156	1560	10	1.00	1.06	1.55
126	4-n-Propylphenol	47.6	1999	42	1.62	1.49	1.39
127	4-sec-Butylphenol *	87.5	3237	37	1.57	1.66	1.19
128	4-tert-Butylphenol *	78.4	5253	67	1.83	1.90	1.47
129	Butyl-4-hydroxybenzoate	84.1	2691	32	1.51	1.51	1.91
130	Ethyl-4-hydroxybenzoate	74.5	3055	41	1.61	1.43	1.97
131	Eugenol	25	1004	40	1.60	1.80	1.95
132	Methyl-4-hydroxybenzoate	101	5454	54	1.73	1.61	1.98
133	Propofol	26	148	6	0.76	0.86	1.32
134	Propyl-4-hydroxybenzoate	152	4560	30	1.48	1.54	2.08
135	Bisphenol A	91.8	4420	48	1.68	1.85	1.02
136	Combretastatin A4 [#]	4.18	9009	2155	3.33	3.34	2.88
137	Pterostilbene	35.9	40.4	1.1	0.05	-0.09	0.52
138	Resveratrol (3-OH)	3.09	196	63	1.8	2.23	2.14
139	A-769662 (6-OH)	0.78	10.8	14	1.14	0.89	0.62
140	Entacapone (3-OH)	8.64	88400	10233	4.01	4.10	4.43

No.	Name	K_m	V_{max}	$CL_{int} (V_{max}/K_m)$	Log (CL_{int})	Log (CL_{int})	Log (CL_{int})
		μM	$pmol/mg/min$	$\mu l/mg/min$	(Actual)	(CoMFA)	(CoMSIA)
141	Ezetimibe	268	73.6	0.30	-0.56	-0.68	-0.50
142	Mycophenolic Acid	71.5	6538	91	1.96	1.99	1.92
143	Psilocin	748	5984	8	0.90	0.90	0.66
144	SN-38	26.4	73.1	3	0.44	0.68	0.41
145	Tolcapone (3-OH) *	43.4	18100	417	2.62	2.79	2.08

* These 25 compounds were used as a test set and not included in the derivation of model equations. # Described using the substrate inhibition equation (eq.2). K_{si} value is not shown because it is unimportant in calculation of CL_{int} (please see *Materials and Methods*).[§] Described using a biphasic kinetics model (eq.3). K_{m1} and V_{max1} values are shown in the columns K_m and V_{max} , respectively. CL_{int2} value is not shown because it is unimportant in calculation of CL_{int} (please see *Materials and Methods*).

6.4.3. CoMFA model

The usual way of understanding CoMFA is by graphing the associated fields. In Figure 40.a, the steric maps derived from CoMFA are displayed. Areas indicated by green contours (numbered 1 and 2) correspond to regions where steric occupancy with bulky groups will increase catalytic activity. The yellow contours (numbered 3 and 4) mean bulky groups should be avoided; otherwise reduced activity can be expected. **74** is more active than **81**, which is possibly explained by the fact that the former orients its 4'-methoxy group into the favored region (contour 1) (Figure 40). Similarly, compared to the less active **8**, the more active **49** fills the favorable region (contour 2) by the 2-benzene moiety (Figure 40). **9** is less active than **10**, this is most likely because it orients the 3,4-diphenyl group into the disfavored region (contour 3) (Figure 40). Likewise, due to the occupancy of the disfavored region (contour 4) by a piperidinyl group, **55** has a lower activity than **52** (Figure 40).

The maps of electrostatic properties are shown in Figure 40b. The areas contoured in blue (numbered 5 and 6) correspond to regions where electropositive groups will enhance the catalytic activity, as will electronegative groups placed into areas indicated in red (number 7 and 8). Contour 5 is close to the glucuronidation site and in parallel with the bicyclic ring of **52** chrysin (shown in Figure 40b); its contribution to the activity-structure correlation however is uncertain because no chemical groups/atoms are aligned into this region. Although being isomers, **95** and **96** possess distinct catalytic activity. Due to a substitution difference of the acrylic acid group on the benzene skeleton, the less active **95** orients its carboxylate group into an area (contour 6)

Table 6. Summary of modeling parameters from CoMFA and CoMSIA analyses

Statistics	CoMFA	CoMSIA
q^2 ^a	0.548	0.579
S_{press} ^b	0.885	0.799
r^2 ^c	0.949	0.876
r_{pred} ^d	0.775	0.700
SEE ^e	0.282	0.435
Components ^f	8	5
F^g	271.8	190.0
$P_{r^2=0}$ ^h	0.000	0.000
Fraction		
Steric	0.465	0.185
Electrostatic	0.535	0.435
Hydrophobic	/	0.380

^a Cross-validated correlation coefficient after the leave-one-out procedure.

^b Cross-validated standard error of prediction.

^c Non-cross-validated correlation coefficient.

^d Correlation coefficient for test set predictions.

^e Standard error of estimate

^f Optimum number of components.

^g F-test value.

^h Probability of obtaining the observed F ratio value by chance alone.

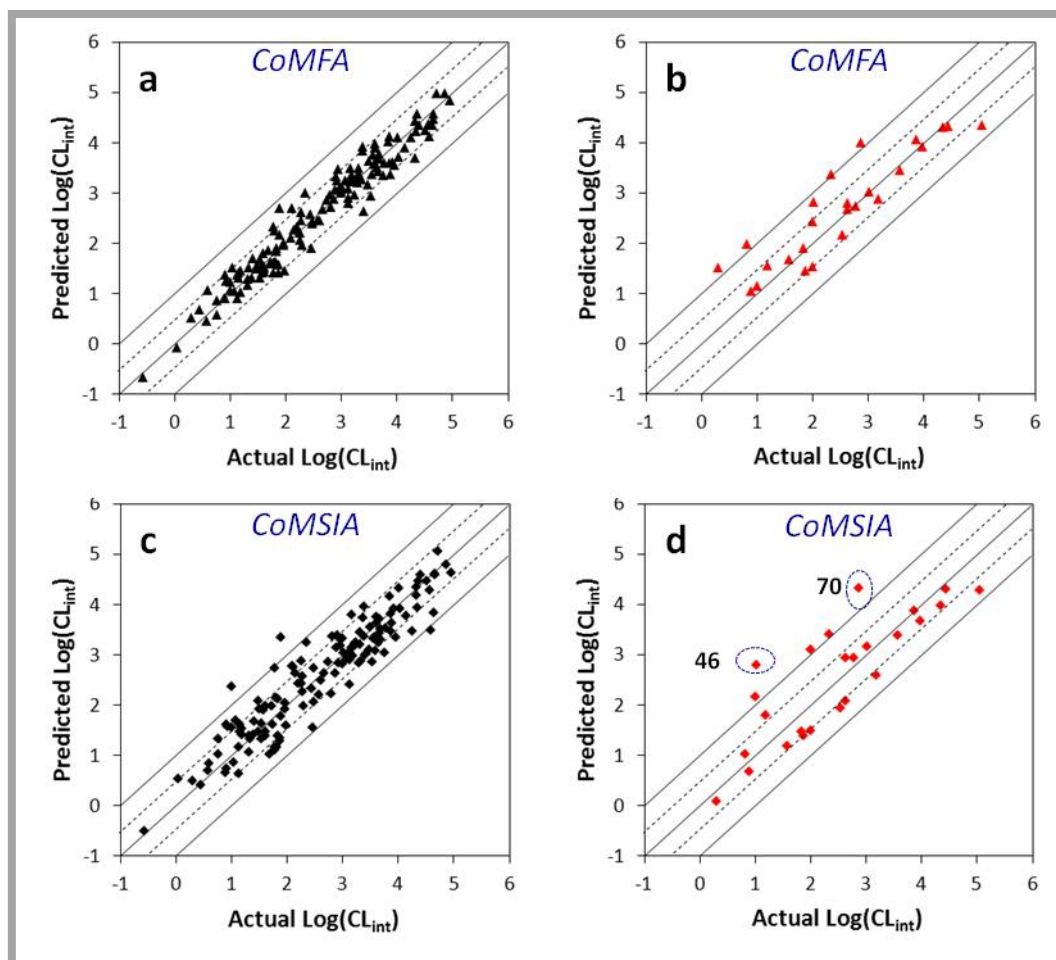


Figure 39. Correlations between the experimental glucuronidation parameters and the predicted ones from the 3D-QSAR models

Panel a: Fitted predictions versus actual catalytic efficiencies for the training set. The predicted values were obtained using the CoMFA method. **Panel b:** Predicted versus actual catalytic efficiencies for the test set not included in model derivation. The predicted values were obtained using the CoMFA method. **Panel c:** Fitted predictions versus actual catalytic efficiencies for the training set. The predicted values were obtained using the CoMSIA method. **Panel d:** Predicted versus actual catalytic efficiencies for the test set not included in model derivation. The predicted values were obtained using the CoMSIA method. Dashed lines represent the observed prediction bias of 3.0-fold deviation from unity. Solid lines represent the observed prediction bias of 10.0-fold deviation from unity.

indicated to be unfavorable for negatively charged groups (Figure 40). **55** occupies the contour 7 (unfavorable for electropositive groups) by the 3-hydroxyl group of the piperidinyll moiety; this is consistent with the fact that **55** is less active compared to **52** (Figure 40). **32** orients a carbonyl group with an electronegative oxygen into a site highlighted to be favorable for negatively charged residues, thus it possesses a higher activity than **123** (Figure 40).

6.4.4. CoMSIA model

The CoMSIA method also provides field contribution contours that allow the correlation results to be mapped back onto the molecular structures. These contours are given in Figure 41 together with some exemplary substrates. For consistency, coloring scheme of the contoured areas (to indicate a property contribution) for steric and electrostatic fields is the same as used in CoMFA maps. In Figure 41a, the steric property is displayed. Interestingly, the contours (numbered 1, 2, and 3) are largely consistent with those derived from CoMFA. The more active **49** orients its 2-benzene ring into the favorable region (contour 1), whereas the less active **101** orients its 3-benzene ring into the unfavorable region (contour 3) (Figure 41). For a similar reason, **133** partially occupies the unfavorable region (contour 2) by a isopropyl group and shows a lower activity compared to **115**. As an additional example pair (molecules 14 and 38) is given, **14** avoids the unfavorable steric groups and are more active than **38**, whose 2-benzene ring is positioned into contour 3 highlighted to be unfavorable for bulky groups.

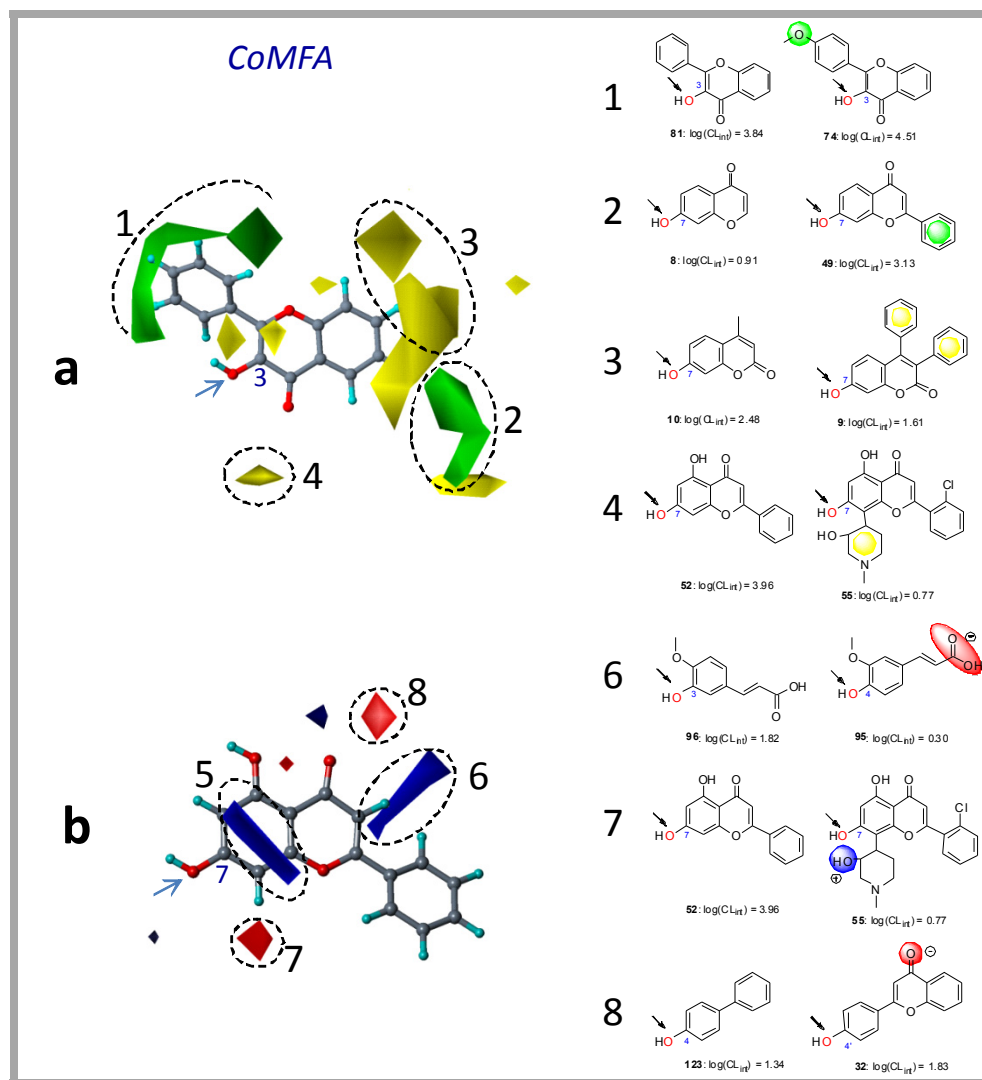


Figure 40. Field contribution maps from the CoMFA analysis.

Panel a presents the steric maps. 3-Hydroxyflavone (**81**) is shown inside the field for reference. Green: Areas in which bulky groups are sterically favorable for glucuronidation; Yellow: Areas in which bulky groups are unfavorable for glucuronidation. **Panel b** presents the electrostatic maps. Chrysin (**52**) is shown inside the field for reference. Blue: Areas in which electropositive atoms/groups are favorable for glucuronidation; Red: Areas in which electronegative atoms/groups are favorable for glucuronidation. Examples are given to on the right side matching the CoMFA results to experimental data. Favored and disfavored contour levels for CoMFA were fixed at 85% and 15%, respectively.

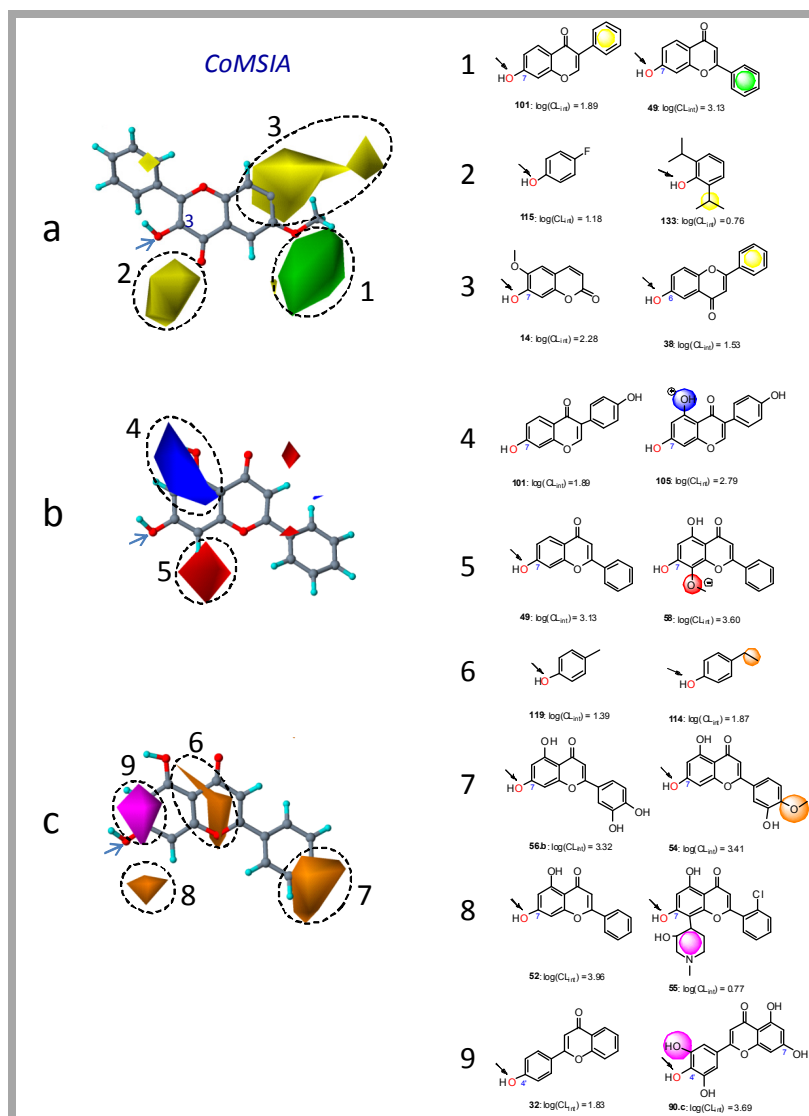


Figure 41. Field contribution maps from the CoMSIA analysis

Panel a presents the steric maps with 3-hydroxy-6-methylflavone (**66**). Green: Areas in which bulky groups are sterically favorable; Yellow: Areas in which bulky groups are unfavorable. **Panel b** presents the electrostatic maps with Chrysin (**52**) Blue: Areas in which electropositive groups are favorable; Red: Areas in which electronegative groups are favorable. **Panel c** presents the hydrophobic maps. Orange: Areas where hydrophobic groups enhance glucuronidation; Magenta: Areas where hydrophilic groups decrease glucuronidation. Examples are given on the right side matching the CoMFA results to experimental data.

The maps of electrostatic properties (numbered 4 and 5) show fewer features in space (Figure 41b), compared to those from CoMFA. **105** is more active than **101**, largely because it has a hydroxyl group (with an electropositive hydrogen) overlaid with the favorable region (contour 4). By contrast, **58** is more active than **49** for the reason that an ether group (with an electronegative oxygen) occupied in contour 5 indicated to be favorable for electronegative groups.

The maps for hydrophobic properties are shown in Figure 41c. Substrates orienting groups with increasing hydrophobicity into areas contoured in orange (numbered 6, 7, and 8) will enhance activity, as will groups with increasingly hydrophilicity placed in areas indicated in purple (numbered 9). **114** is more active than **119**; this is probably because both ethyl and methyl groups substituted on the phenol backbone are adjacent to the hydrophobic favorable region (contour 6), but the former is more hydrophobic than the latter (Figure 41). An increased hydrophobicity (from a hydroxyl group to a methoxy group) in contour 7 (hydrophobicity favorable) leads to an enhanced activity, as is seen from a comparison between **54** and **56.b** (Figure 41). **55** possesses an activity significantly lower than **32**, which is in complete agreement with the indication that the presence of a hydrophilic piperidinyll group in the unfavorable region (contour 8) would result in a diminished activity compared to its absence (Figure 41). Contour 9 highlights an area where occupancy of a hydrophilic (polar) group would enhance the activity, which exemplified by a comparison of **32** and **90.c**. **90.c** orients a 3'-hydroxyl group into the favorable region contour 9, thus is more active than **32**.

6.4.5. Exploring UGT1A9 catalytic pocket using a homology model and CoMFA/CoMSIA maps

To explore the molecular mechanisms of UGT1A9-substrate interaction, a homology model of UGT1A9 was constructed. This structural model incorporates a simulated binding of **88.a** kaempferol (in an active 3-O-glucuronidation mode) where 3-OH group of kaempferol is reasonably hydrogen-bonded with the catalytic residue His37. The protein residues forming the pocket wall were identified and presented in Figure 42. The binding pocket is divided into four sub-pockets designated as S1, S2, S3 and S4 (Figure 42b), among which pocket S3 is relatively small in size due to the steric hindrance by residues from helix N α 3 and its preceding loop. Interestingly, pocket S4 appears to be open to solvent, and potentially contributes to accommodation of a long-chain substrate such as **15** curcumin. The three most active substrates (**66**: 3-hydroxy-6-methylflavone, **140**: entacapone; **52**: chrysin) were mapped into the pocket by an alignment with kaempferol. The B-ring of **66** is fitted to S1, and the common aromatic ring to S2. S4 accommodates the B-ring of **52** or the N,N-dimethylamide group of **140**.

The CoMFA/CoMSIA maps were superimposed on the binding site of this structural model based on the binding mode of kaempferol. The contour maps are largely consistent with the 3D shape of the UGT1A9 catalytic site (Figure 43). The green regions where bulky groups favor activity correspond to the regions of the active site where unfilled spaces exist. This indicates that a bulky group in these regions increases the van de Waals interaction between a substrate and UGT1A9, thus increasing the activity (Figure 43a/b). Also, the yellow regions (e.g., α and β in Figure 43b) where bulky groups disfavor activity correspond to the regions of the active site where steric

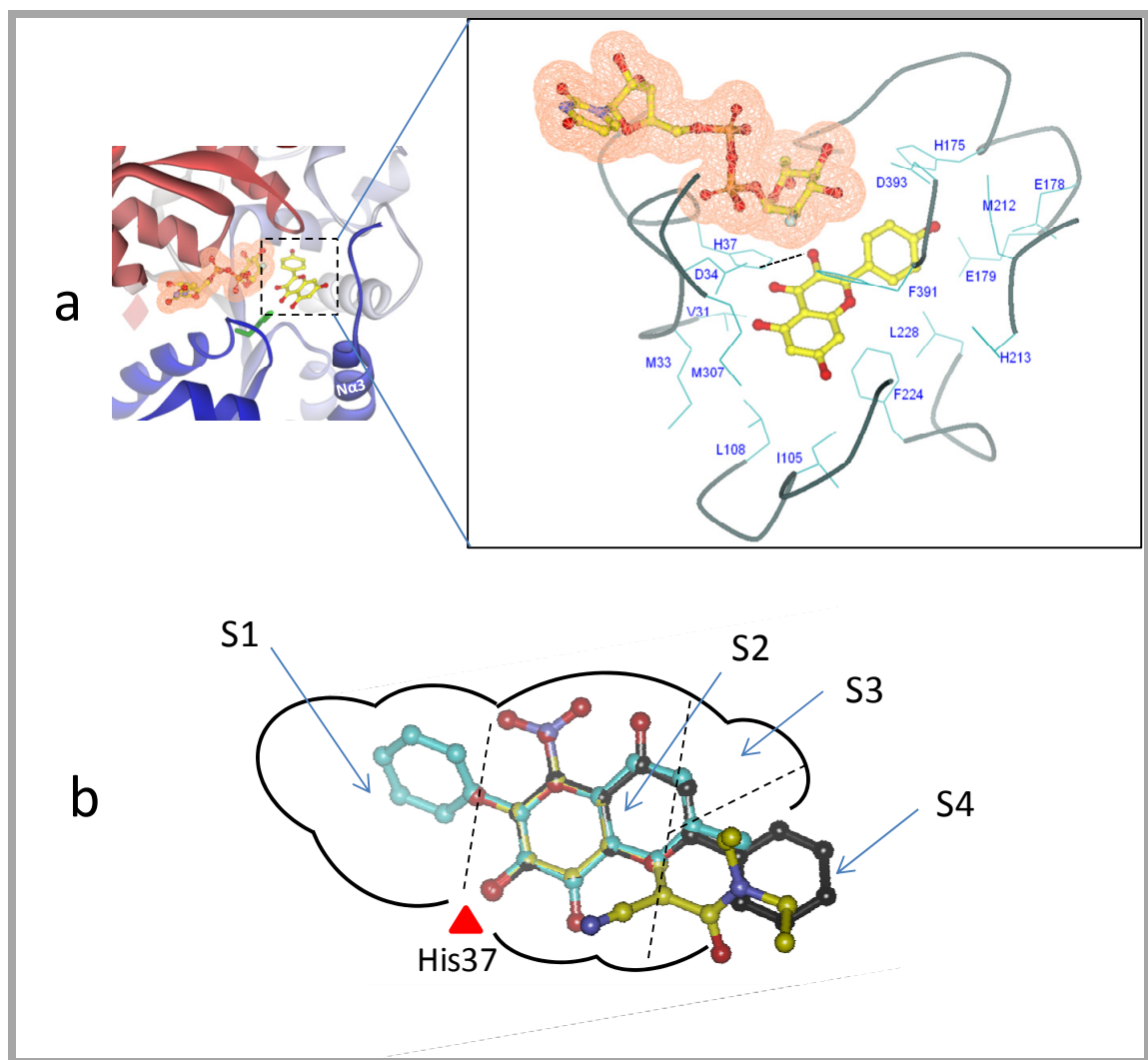


Figure 42. Three-dimensional model of the UGT1A9-kaempferol (88.a) complex.

Panel a, a side view of the three-dimensional model of UGT1A9-kaempferol complex. Kaempferol is indicated in a ball-and-stick model. The cofactor is indicated in a ball-and-stick model with a molecular surface. An expanded view of residues potentially involved in the interactions with kaempferol (3-O-glucuronidation) in the model is presented. Dashed black line indicates the potential hydrogen bond. **Panel b**, A two-dimensional schematic representation of UGT1A9 catalytic pocket. The three most active substrates (66: 3-hydroxy-6-methylflavone, 140: entacapone; 52: chrysin) are mapped into the pocket. The binding pocket is divided into four sub-pockets designated as S1, S2, S3 and S4.

hindrance is noted.

Unexpectedly, electrostatic maps between CoMFA and CoMSIA are not consistent with each other; this might indicate an uncertainty in correlating the electrostatic property of substrates with their activity (Figure 43a/c). In contrast to the fact that CoMFA electrostatic maps appear in the regions where no polar residues can be identified, CoMSIA electrostatic maps show a good compatibility with the surrounding residues. An electronegative group in its favorable region (contour γ or previously named contour 5 in Figure 41) presumably interacts with UGT1A9 by forming a hydrogen bond or through electrostatic interactions. As only polar residues Asp34 (with an electronegative side chain) and His37 (with an electropositive side chain) appear in the neighborhood of contour γ , His37 is proposed to contribute to the interaction of UGT1A9 with an electronegative group (of a substrate) positioned in this region (Figure 43). The residues that are around region δ (Figure 43c) favoring an electropositive group on a substrate are Glu178, Glu179 and Asp393 (all are electronegative). In addition, the hydrophobic regions (ϵ and η) are lined with the hydrophobic residues Val31, Met33, Leu108, Phe224, Leu228, Met307, and Phe391 (Figure 43d).

6.5. Discussion

In this study, a ligand-based 3D-QSAR approach (CoMFA/CoMSIA) is employed to elucidate UGT1A9 substrate selectivity, and the yielded models are useful for prediction of the catalytic efficiencies of UGT1A9. Such model is challenged by the fact that many substrates form more than one glucuronide at different sites (so called “glucuronide

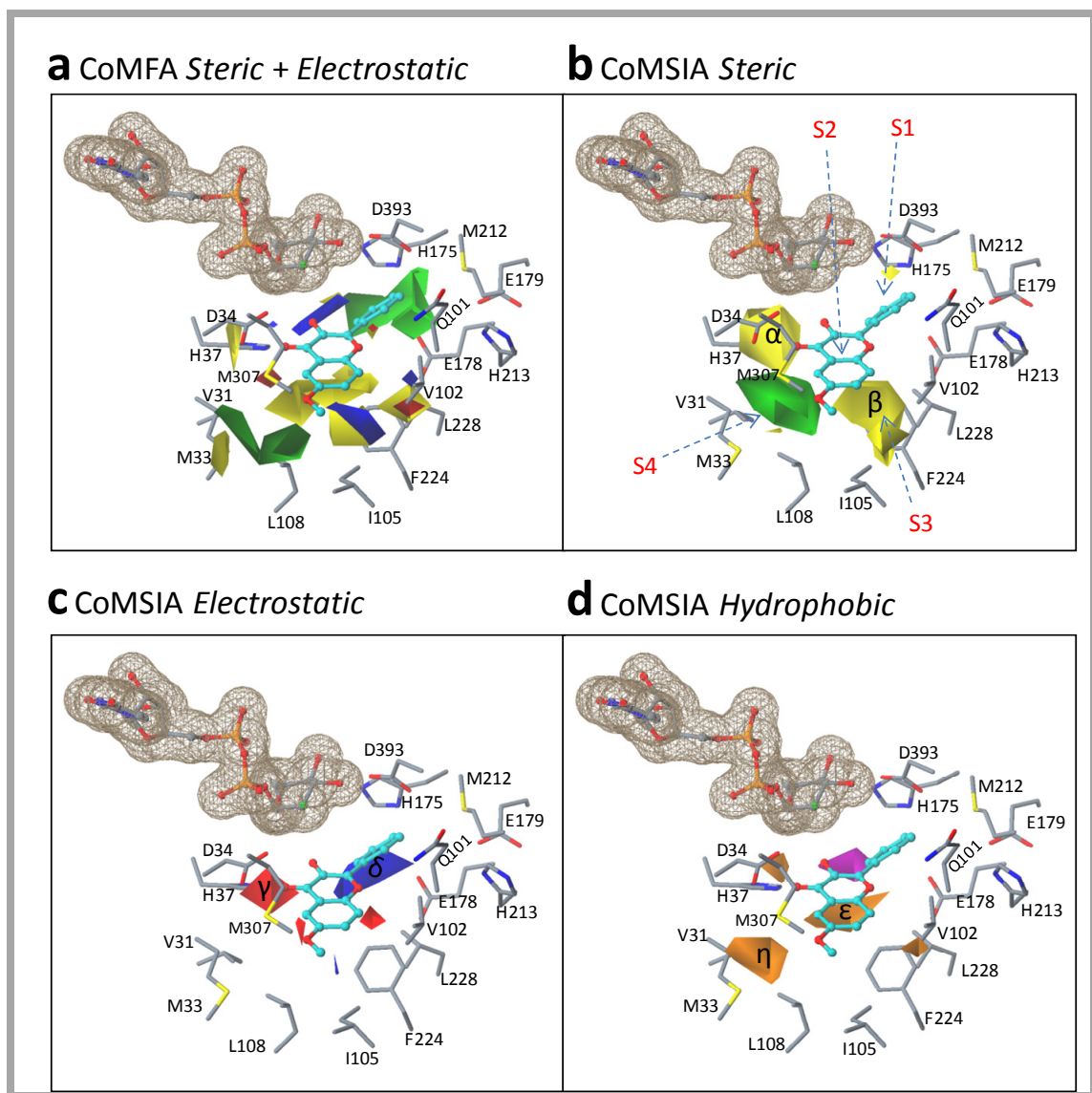


Figure 43. Superposition of the CoMFA/CoMSIA contour maps over the binding site of a homology-modeled UGT1A9 structure based on a simulated binding model of kaempferol (3-OH).

The UGT1A9 protein is shown in a stick model. Kaempferol is indicated in a ball-and-stick model and the cofactor is shown in a ball-and-stick model with a molecular surface. **Panel a:** Overlay of the CoMFA steric and electrostatic maps with the UGT1A9 binding site. **Panel b-d:** Overlay of the CoMSIA steric (b), electrostatic (c), and hydrophobic (d) fields with the UGT1A9 binding site.

isomers”). Our studies (Chapters 2 & 3) indicate that generation of glucuronide isomers is resulted from distinct binding modes of the same substrate in the catalytic domain of UGT protein. Each binding mode orients a glucuronidation site (-OH) towards the catalytic residue (usually a histidine) for reaction, and to generate a corresponding glucuronide isomer. Therefore, multiple binding modes should be considered in a predictive algorithm for a UGT substrate with multiple active glucuronidation sites. Accordingly, we treat such a UGT substrate as multiple “substrates” that adopt distinct spatial conformations; each of which corresponds to a binding mode to form a regiospecific glucuronide isomer. Our derived models with statistical significance and high predictive capability suggest that this treatment is reasonable and useful in terms of in silico modeling of UGT substrates. It is also highlighted that our model can be used to predict regiospecific glucuronidation mediated by UGT1A9, which was unlikely accomplished earlier on.

Another challenge to our model is that it incorporates a large diversity of (n=145) substrate structures. As a result, difficulty is raised with respect to the molecular alignment of those structures. We proposed a unique alignment method that is to superimpose the glucuronidation site and its adjacent aromatic ring, the two important features identified by a flexible alignment of three most active substrates (Figure 37). Glucuronidation sites should be aligned to improve model quality as suggested from previous modeling experiences (Sorich *et al.*, 2002; Smith *et al.*, 2003). The importance of positioning of a glucuronidation site into an area close to both cofactor and the catalytic histidine residue for glucuronidation is also demonstrated in a recent study

(Takaoka *et al.*, 2010). Early studies identify a common feature pharmacophore for several UGT isoforms, which unanimously include two separate hydrophobic regions (adjacent to the glucuronidation site) (Sorich *et al.*, 2002; Smith *et al.*, 2003, 2004). However, we believe two hydrophobic regions spatially isolated might not be universal features for all UGT1A9 substrates. For example, such features cannot be found in **109** (a simple phenol) structure. Therefore, the alignment rule here is straightforward and conforms to the catalytic mechanism, and is proven to be successful in terms of the quality of resulting models.

The use of $\log (CL_{int})$, a measure of catalytic efficiency, as the parameter for correlation analyses is more reliable and meaningful, compared to other kinetic parameters such as K_m and V_{max} . As stated by Sharma and Duffel (2002, 2005), in the case of enzymes that may exhibit nonproductive binding interactions with some substrates, a highly relevant kinetic parameter for a CoMFA correlation of the structure to its ability to serve as a substrate for such enzymes is the CL_{int} value, or $\log (CL_{int})$. This is because CL_{int} is independent of nonproductive binding contributions. Although there is no direct evidence (e.g., crystal structure) of nonproductive binding of a substrate to a UGT protein, kinetic characterization has indicated that nonproductive binding of substrates to a UGT isoform can be a major reason why the enzymes frequently exhibit substrate inhibition kinetics (Luukkanen *et al.*, 2005). Therefore, the use of CL_{int} value for our CoMFA/CoMSIA analyses of UGT1A9 is justified. Moreover, in vitro intrinsic clearance (CL_{int}) is frequently used to predict in vivo clearance such as hepatic clearance with a reasonable success rate (Kilford *et al.*, 2009; Cubitt *et al.*,

2009). Hence, this parameter is a more appropriate indicator as the susceptibility of a substrate to glucuronidation in vivo.

The recognition of glucuronidation as an important metabolic pathway has lent increasing efforts towards better understanding of the molecular mechanisms of UGT functions and of the substrate structural features associated with UGT selectivity. Inevitably, a molecular-level structural elucidation of the protein is necessary for such pursuits. Here, a homology model of UGT1A9 was constructed aiming to enhance our understanding of interactions between UGT1A9 and substrates, in addition to the CoMFA/CoMSIA results. The structural information of our UGT1A9 model was imported from the template protein VvGT1 (a plant UGT). At present, the use of a plant UGT for homology modeling of human UGTs is preferred and justifiable, because (1) plant and human UGTs are classified into the same superfamily GT1; GT1 members adopt a GT-B fold and their tertiary structures are predicted to be highly conserved; (2) plant and human UGTs share a similar catalytic mechanism (i.e., serine hydrolase-like mechanism); (3) a determined partial crystal structure (for C-terminal or UDPGA binding domain portion only) of human UGT2B7 agrees well with its counterparts in plant UGT crystal structures (Miley *et al.*, 2007; Radomska-Pandya *et al.*, 2010). Such modeling effort appears to be useful here and has also been utilized to elucidate the amino acids that are responsible for the large activity differences between UGT1A9 and 1A10 (Itäaho *et al.*, 2010).

A good consistency between the CoMFA/CoMSIA maps and a homology model of UGT1A9 is highlighted in terms of the steric and hydrophobic interactions (Figure 43).

The results provide a highly possible 3D structure of UGT1A9 binding pocket as well as substantial insights into the molecular mechanisms regarding the recognition of a substrate by UGT1A9. The models can be used to guide de novo design of compounds with desired UGT1A9 activity. For example, a more active compound should have its -OH group towards the catalytic residue, and the rest of its structure occupies those green regions (cavities in the binding site), and avoids those yellow regions where steric hindrance exists. We anticipate that this approach of CoMFA/CoMSIA coupled with a protein homology model may be applicable to other UGT isoforms. A more exhaustive elucidation of molecular interactions of other UGT isoforms and a more complete comparison of substrate selectivity across UGT isoforms might be necessary in order to ultimately predict overall glucuronidation and uncover the fine substrate selectivity difference. This is important as the knowledge can be used to accelerate drug development and to promote human health.

Although model construction is based on the active poses of UGT1A9 substrates, it is of interest to see if the model can be used to distinguish a non-substrate from a substrate. We experimentally identified three UGT1A9 non-substrates, namely, estradiol (a selective probe for UGT1A1), salicylic acid, and aminosalicic acid (no metabolite can be detected when incubating these compounds with UGT1A9). The predicted log (CL_{int}) values from the CoMFA model are 1.41, 1.11, and 1.42, respectively, indicating these compounds are very poor substrates of UGT1A9. Therefore, the model is fairly accurate; though its capability to predict an absolute non-substrate is somewhat limited.

In conclusion, we have performed 3D-QSAR analyses using the powerful techniques Comparative Molecular Field Analysis (CoMFA) and Comparative Molecular Similarity Indices Analysis (CoMSIA) based on a large training dataset with a 10^6 -fold range of relative catalytic activity. The derived models show statistical significance and substantive predictability (CoMFA: $q^2 = 0.548$, $r^2 = 0.949$, $r^2_{\text{pred}} = 0.775$; CoMSIA: $q^2 = 0.579$, $r^2 = 0.876$, $r^2_{\text{pred}} = 0.700$). The real-world use of these models is fully expected to predict the catalytic activity of structural diverse chemicals (including drug candidates) towards UGT1A9. Moreover, the field contribution maps from CoMFA/CoMSIA were applied to elucidate the catalytic pocket of UGT1A9 with the aid of a homology model of UGT1A9. The results consistently depict a plausible catalytic pocket with a set of geometry configuration and a hydrophobic interacting environment, even though the electrostatic interactions are less defined. Our findings for the first time provide a possible molecular basis for understanding UGT1A9 functions and its substrate selectivity.

Chapter 7 Summary

The key role of UDP-glucuronosyltransferases (UGTs) in metabolism and detoxification of xenobiotics including drugs has been recognized. Understanding of the enzymes' function (including substrate selectivity) assumes great importance with respect to prediction of pharmacokinetics of drugs undergoing glucuronidation. In this thesis work, we aim to elucidate the molecular mechanisms of UGTs that determine the substrate selectivity. In the absence of a crystallographic structure for any mammalian UGTs, a ligand-based approach fortified with experimentally derived "expert" knowledge has been used for this purpose.

We first used the approach of kinetic profiling to determine the regioselectivity of six UGT1A isoforms (the major isoforms glucuronidating phenolics based on the literature) towards flavonols (i.e., 37DHF, 357THF, 374'THF, and 3574'QHF) (**Aim 1**). The results show that UGT1A1 and 1A3 regioselectively metabolized 7-OH of flavonols, whereas UGT1A7, 1A8, 1A9 and 1A10 preferred to glucuronidate 3-OH group. Further, the differentiated kinetics properties (i.e., binding affinity and turnover rate) between 3-O- and 7-O- glucuronidation indicated that the at least two distinct binding modes (from a same substrate molecule) within the catalytic domain were responsible for the formation of these two glucuronide isomers. This "expert" knowledge was used in the *in silico* modeling of UGT1A9 substrates (**Aims 2 and 3**). In addition, we also show that UGT1A1 and 1A9 were the most efficient conjugating enzymes with K_m values of ≤ 1 μM . This information has helped us select UGT1A9 for further studies.

A general notion in current literature is that UGT isoform (especially isoforms within a subfamily e.g., UGT1A) displays a vast overlapping substrate specificity. Our findings in **study I** (or aim 1a) indicate UGT1A isoforms might have large differences in substrate regioselectivity towards a flavonol. This hypothesis is further validated in **study II** (or Aim 1b), where two flavonoids 3,3',4'-trihydroxyflavone (33'4'THF) and 3,6,4'-trihydroxyflavone (364'THF) is used to probe the activities of hepatic UGT1A1. Four sets of independent experiments were performed to provide strong evidence: (1) the probes were predominantly glucuronidated (at 4'-OH) by UGT1A1 based on phenotyping of commercially available recombinant UGTs; (2) metabolism (at 4'-OH) of the probes in human liver microsomes was mainly contributed by the targeted UGT isoform; (3) the selectivity of UGT1A1 towards the flavonoid probes (4'-O-glucuronidation) were comparable to the known selective substrates (estradiol and SN-38) derived from activity correlation analysis; and (4) The polymorphic variants (UGT1A1*28) with decreased UGT1A1 protein expression showed markedly lower UGT1A1 activity towards the probes.

Next, a dataset of UGT1A9-mediated glucuronidation of 30 flavonols (at 3-OH) was experimentally derived (**study III**). We used the CoMFA technique to analyze the structure-activity relationships. The alignment of all flavonols molecular was performed using a 3-OH specific pharmacophore, a hypothetical (unique) pose for 3-O-glucuronidation that might differ from those for glucuronidation at other positions (e.g., 7-OH). The derived CoMFA models for possessed good internal and external consistency and showed statistical significance and substantive predictive abilities (V_{\max} model: $q^2 =$

0.738, $r^2 = 0.976$, $r^2_{\text{pred}} = 0.735$; CL_{int} model: $q^2 = 0.561$, $r^2 = 0.938$, $r^2_{\text{pred}} = 0.630$). The contour maps derived from CoMFA modeling clearly indicated structural characteristics associated with rapid or slow 3-O-glucuronidation. This successful modeling lends a strong support to the hypothesis that multiple distinct binding modes within the catalytic domain were possible for single substrate molecule.

At last, our proposed modeling strategy was vigorously validated against a large number ($n = 145$) of structurally diverse phenolics (**study IV**). The “multiple binding modes” hypothesis was used to guide the molecular alignment. Thus for a substrate with multiple active glucuronidation sites, more than one structural pose was aligned corresponding to the glucuronidation at each site. The 3D-QSAR analyses produced statistically reliable models with good predictive power (CoMFA: $q^2 = 0.548$, $r^2 = 0.949$, $r^2_{\text{pred}} = 0.775$; CoMSIA: $q^2 = 0.579$, $r^2 = 0.876$, $r^2_{\text{pred}} = 0.700$). The contour coefficient maps generated from CoMFA/CoMSIA were applied to elucidate structural features among substrates that are responsible for the selectivity differences. Furthermore, the contour coefficient maps were overlaid in the catalytic pocket from a homology model of UGT1A9; this enabled us to identify the UGT1A9 catalytic pocket with a high degree of confidence.

The experimental scientists have been confused by the complex behaviors of UGTs in substrate selection. This thesis reveals that *in silico* approaches can be used to analyze glucuronidation data and provide possible underlying basis for the intricate data pattern. The work therefore opens the door to the computer-aided data analyses of glucuronidation, and related reactions. It is noteworthy that our current studies are not

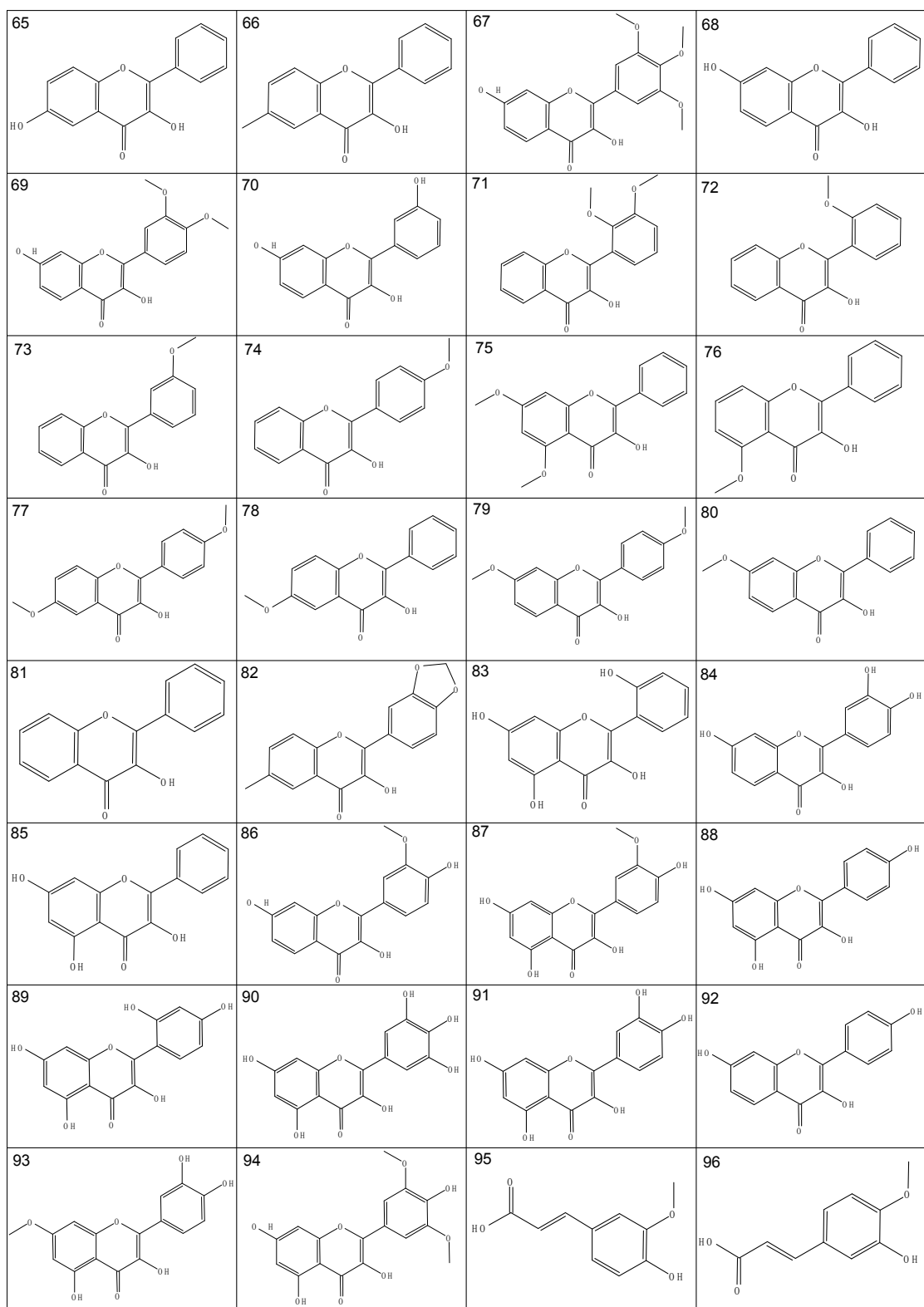
without limitations. First, this work focuses only on O-glucuronidation, the primary type of reaction catalyzed by UGTs. We believe that a predictive model incorporating N-aglycones will be of greater value in drug development as many drugs contain amines. Second, our models are based on microsomal metabolism data. Their ability to predict glucuronidation *in vivo* might be compromised by the lack of consideration of glucuronide efflux, a step that could influence the glucuronidation reaction *in vivo*. Modeling of the two-step process (glucuronide formation and excretion) appears to be necessary in an attempt to predicting *in vivo* disposition of drugs undergoing glucuronidation.

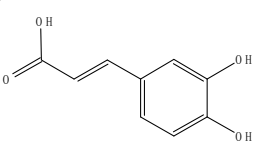
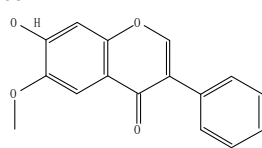
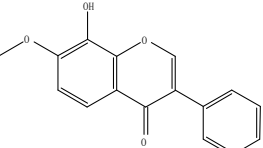
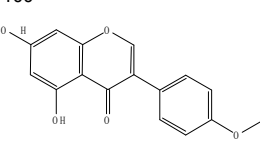
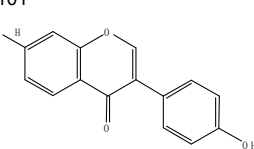
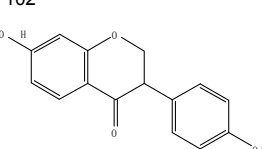
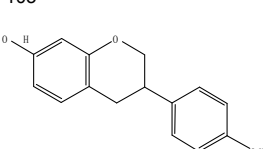
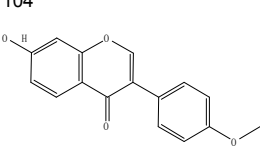
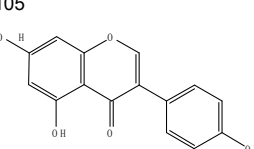
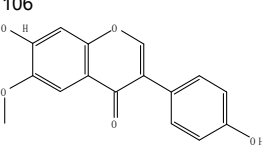
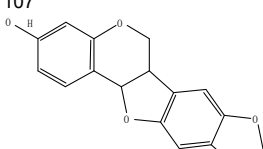
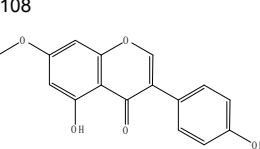
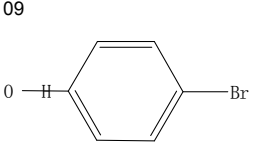
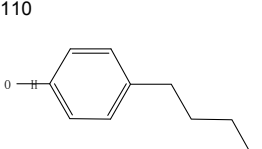
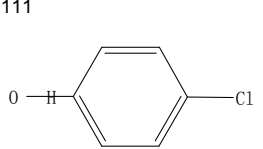
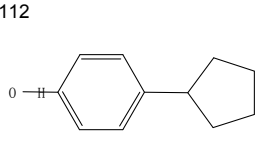
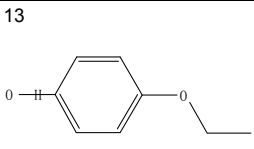
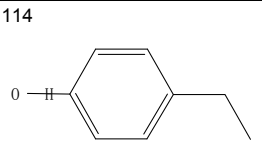
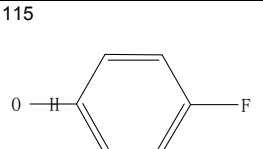
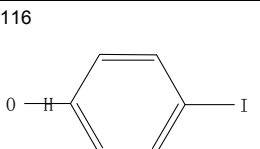
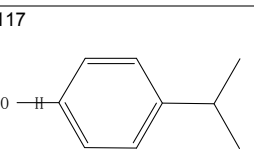
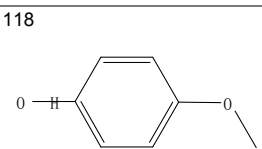
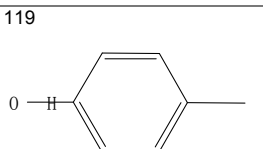
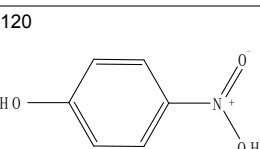
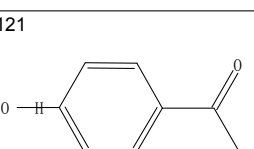
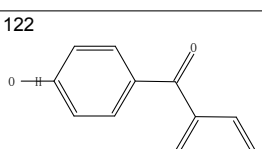
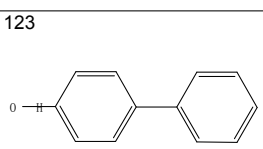
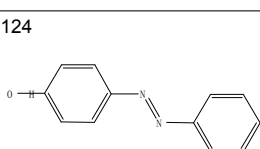
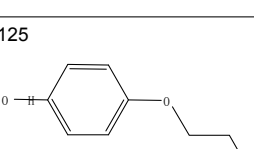
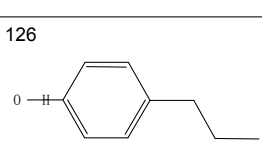
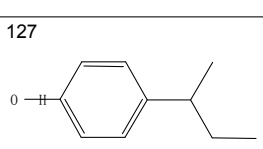
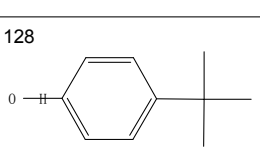
Take together, this thesis represents great efforts towards a better understanding of how UGTs function, and provides unique knowledge about substrate recognition by UGTs. We anticipate that our original approach, CoMFA analysis coupled with “expert” knowledge might be applied to other UGT isoforms and other drug-metabolizing enzymes with a similar catalytic mechanism such as sulfotransferases.

Appendix A: Chemical structures of 145 UGT1A9 substrates in this thesis.

1		2		3		4	
5		6		7		8	
9		10		11		12	
13		14		15		16	
17		18		19		20	
21		22		23		24	
25		26		27		28	
29		30		31		32	

33		34		35		36	
37		38		39		40	
41		42		43		44	
45		46		47		48	
49		50		51		52	
53		54		55		56	
57		58		59		60	
61		62		63		64	



97 	98 	99 	100 
101 	102 	103 	104 
105 	106 	107 	108 
109 	110 	111 	112 
113 	114 	115 	116 
117 	118 	119 	120 
121 	122 	123 	124 
125 	126 	127 	128 

129 	130 	131 	132
133 	134 	135 	136
137 	138 	139 	140
141 	142 	143 	144
145 			

Appendix B: UPLC conditions used for glucuronidation assay and kinetic analysis

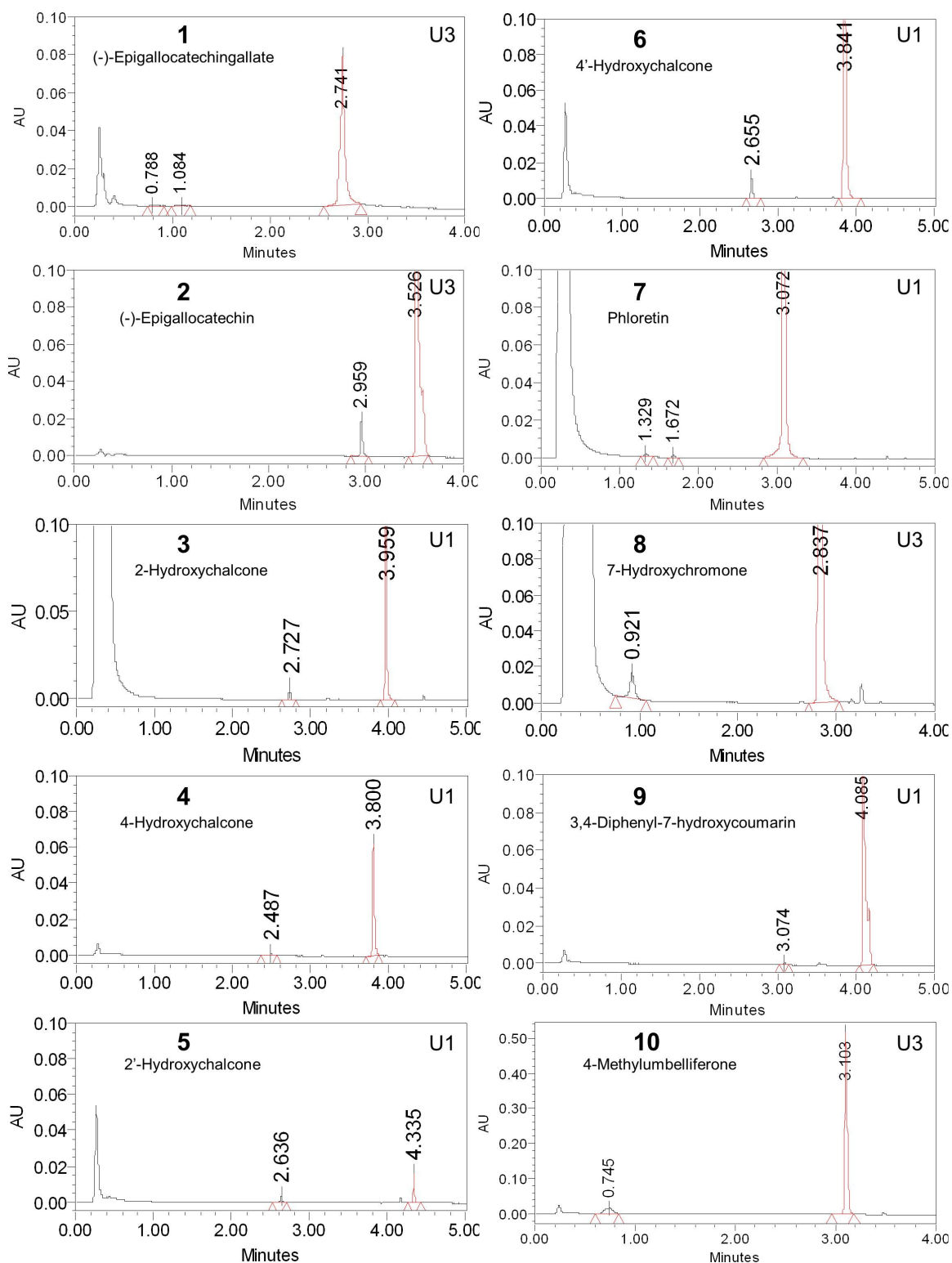
In this thesis work, all (145) UGT substrates (aglycones) and their glucuronide were quantified using Waters ACQUITY UPLC. Five different UPLC methods (designated as U1, U2, U3, U4, and U5) were used and are shown below. The exact UPLC method for a UGT substrate is listed in Appendix C (on the right corner of a chromatogram).

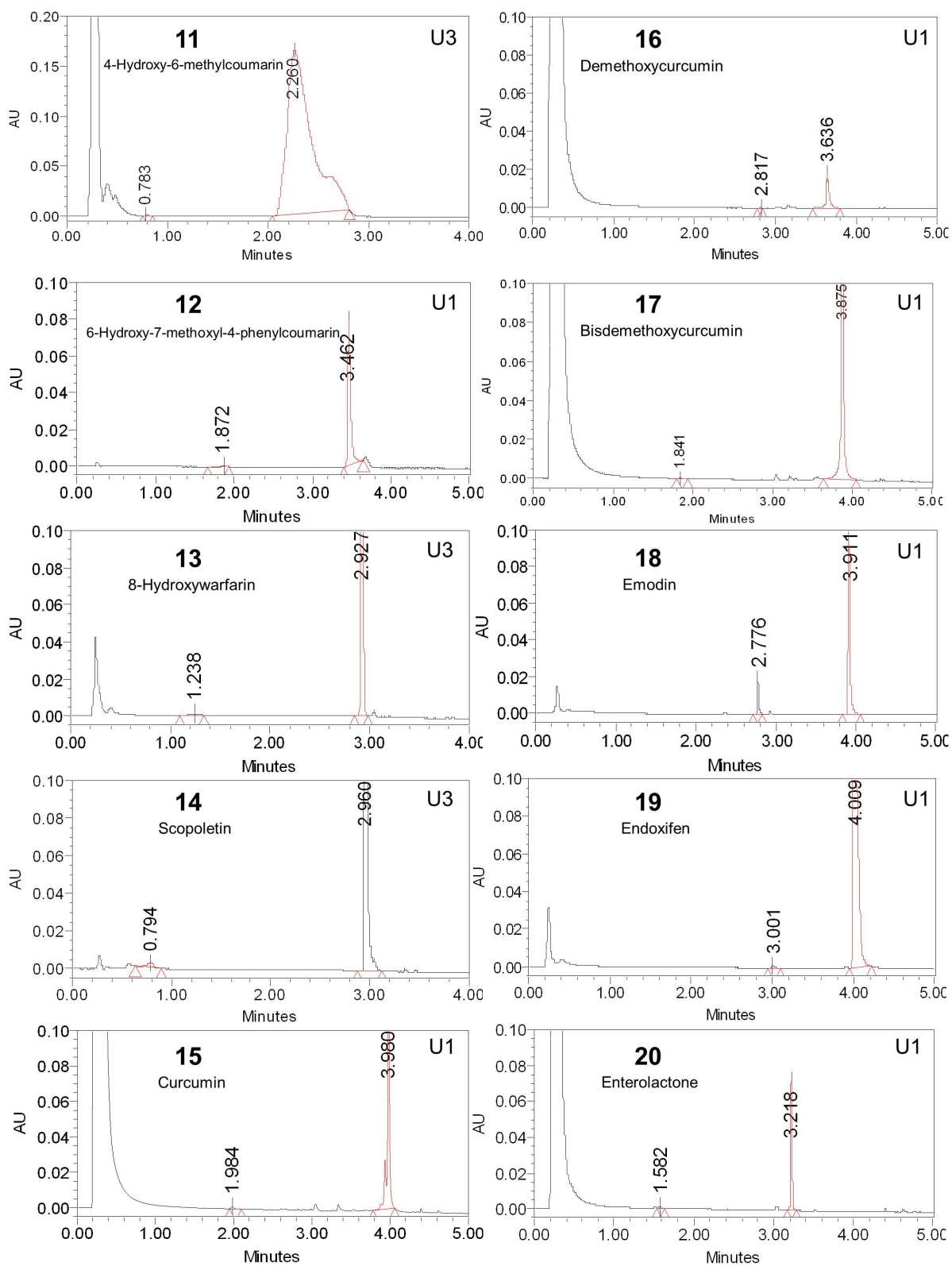
UPLC method*	Gradient	Mobile phase A [#]	Mobile phase B
U1	0–2 min (10–20%B), 2–3 min (20–40%B), 3–3.5 min (40–50%B), 3.5–4 min (50–90%B), 4–4.5 min (90%B), 4.5–5 min (90–10%B)	A1	100% Acetonitrile
U2	0–3 min (10–90%B), 3–4 min (90–10%B)	A1	100% Acetonitrile
U3	0–2 min (5%B), 2–3 min (5–40%B), 3–3.5 min (40–70%B), 3.5–4 min (70–5%B)	A1	100% Acetonitrile
U4	0–1 min (0%B), 1–2 min (0–5%B), 2–3 min (5–40%B), 3–3.5 min (40–50%B), 3.5–4 min (50–70%B), 4–4.5 min (70%B), 4.5–5 min (70–0%B)	A2	100% Acetonitrile
U5	0–2 min (10–20%B), 2–3 min (20–40%B), 3–3.5 min (40–50%B), 3.5–4 min (50–70%B), 4–5 min (70–90%B), 5–5.5 min (90%), 5.5–6 min (90–10%B)	A1	100% Methanol

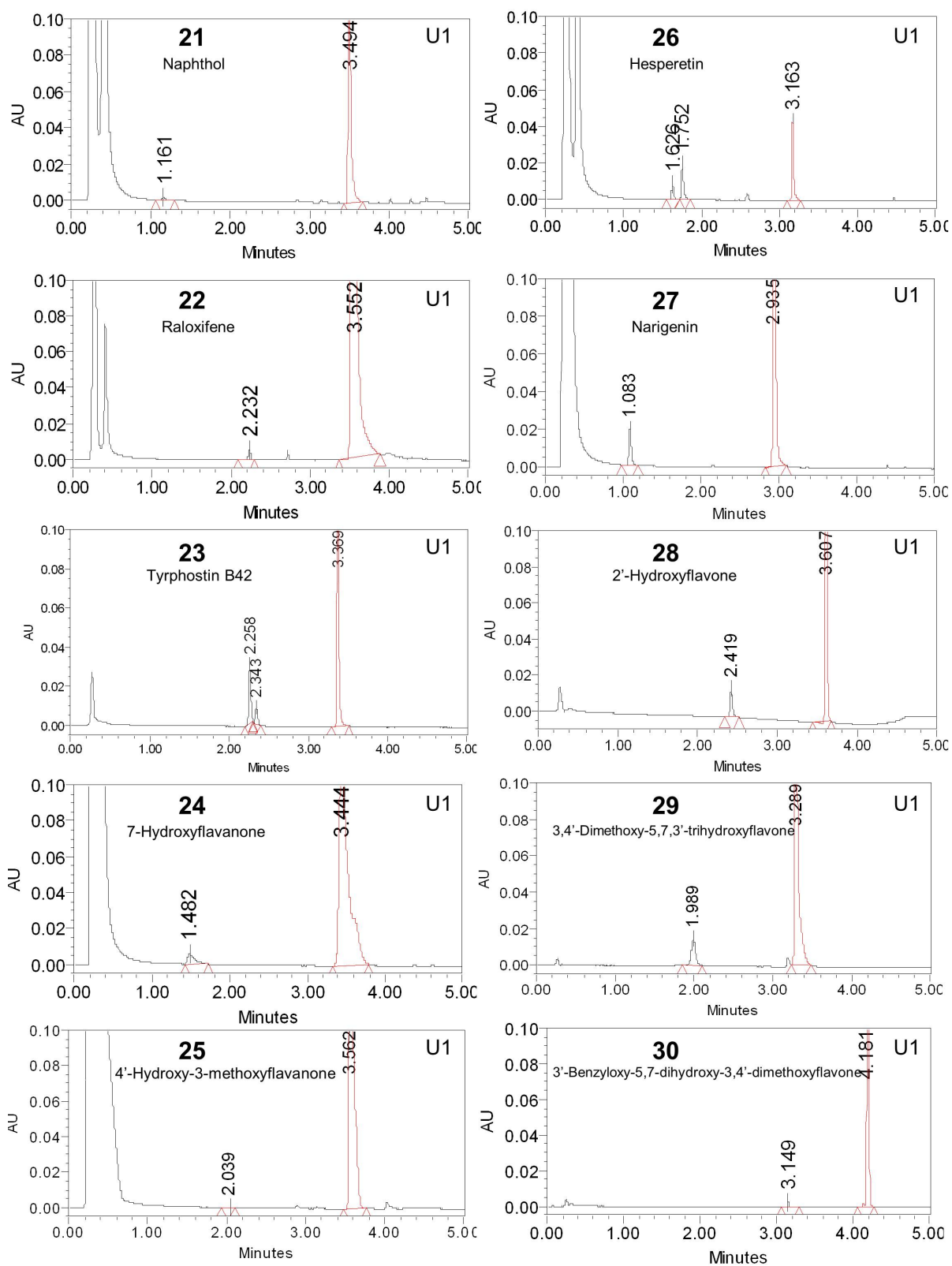
*Flow rate is 0.45 ml/min, injection volume is 10 µL, column is 2.1×50 mm BEH C18 (1.7 µm, Waters).

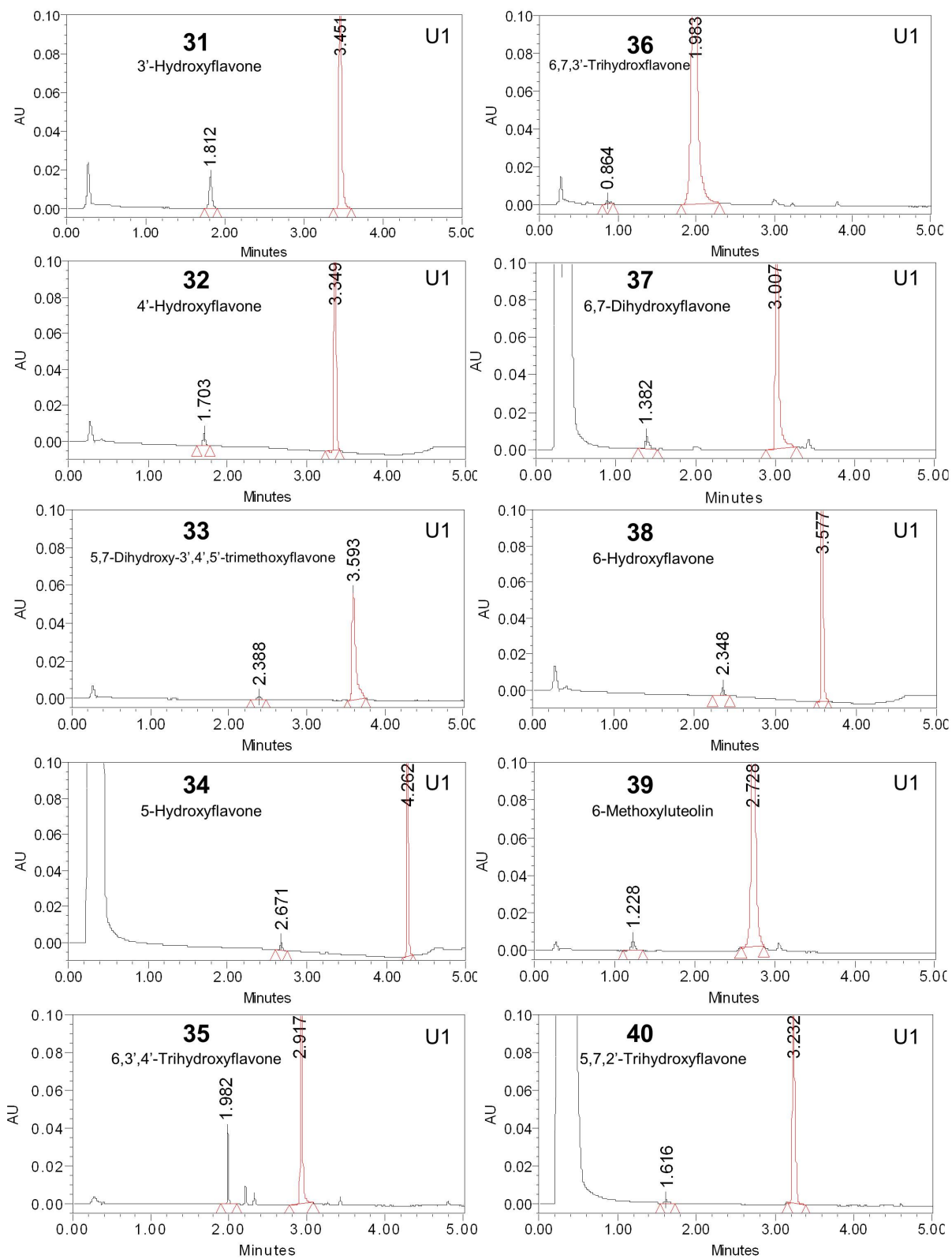
[#]Mobile phase A1: 2.5 mM ammonium acetate in water (pH=6.5); mobile phase A2: 0.1% Formic acid

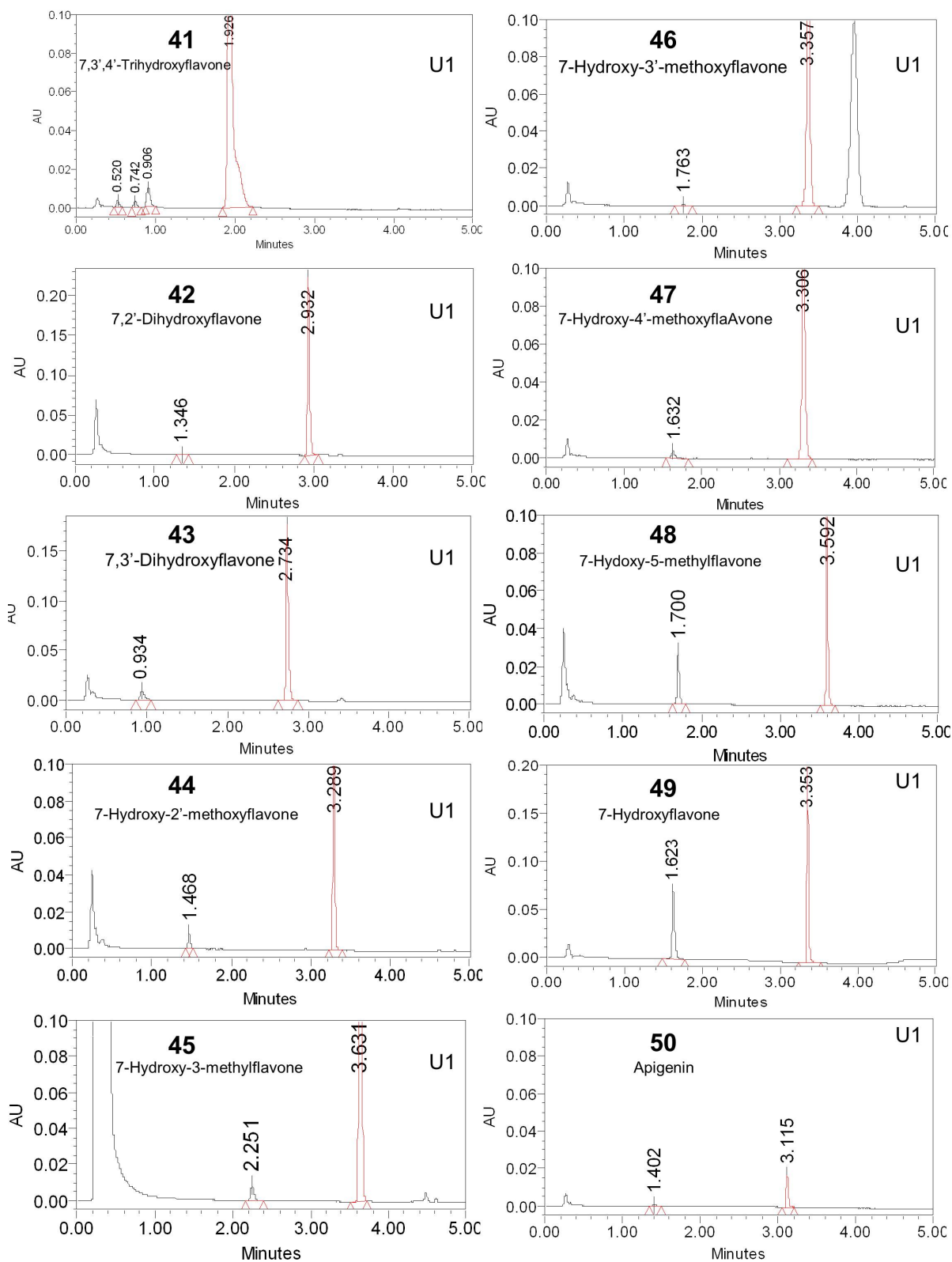
Appendix C Representative chromatograms

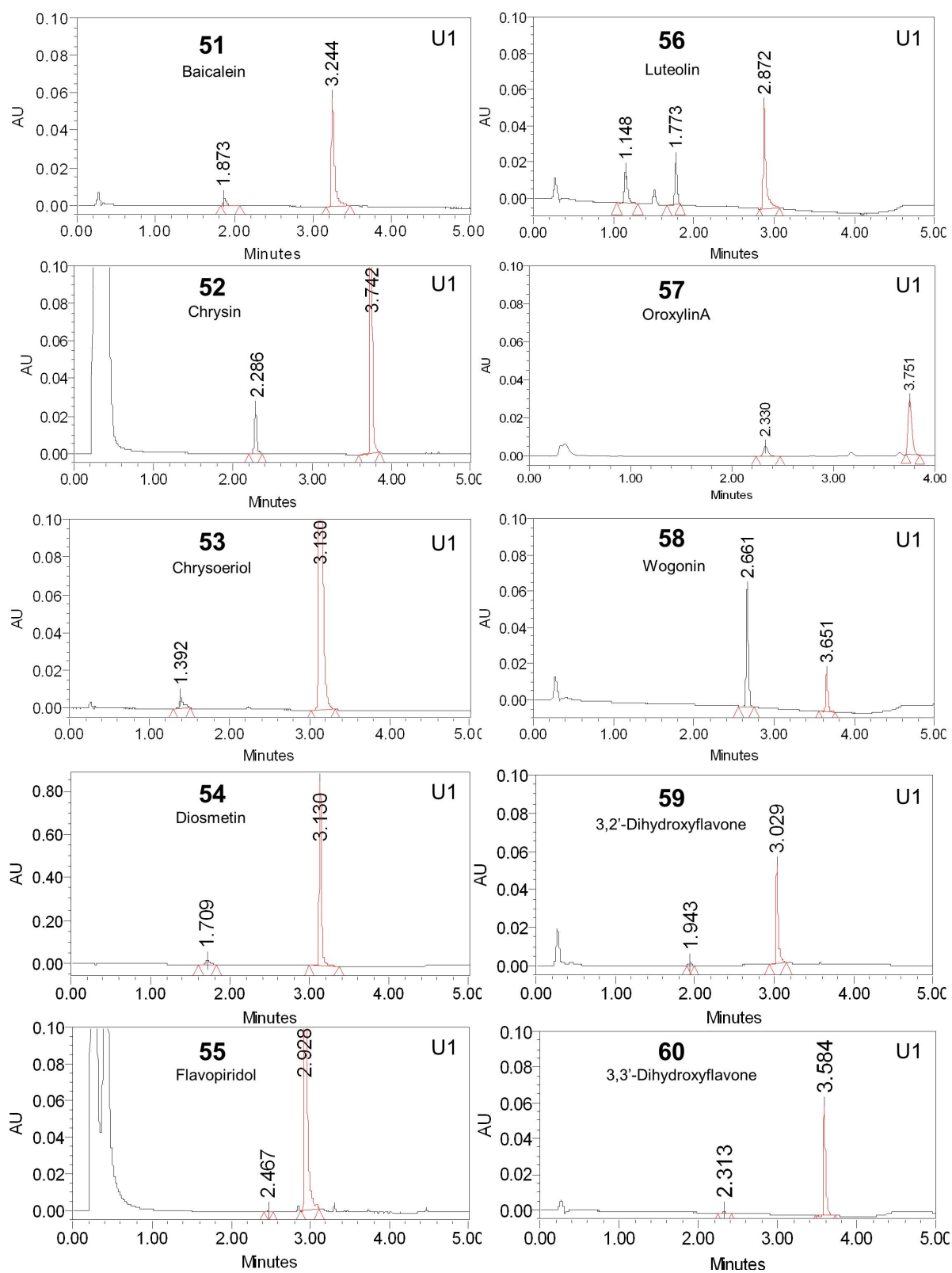


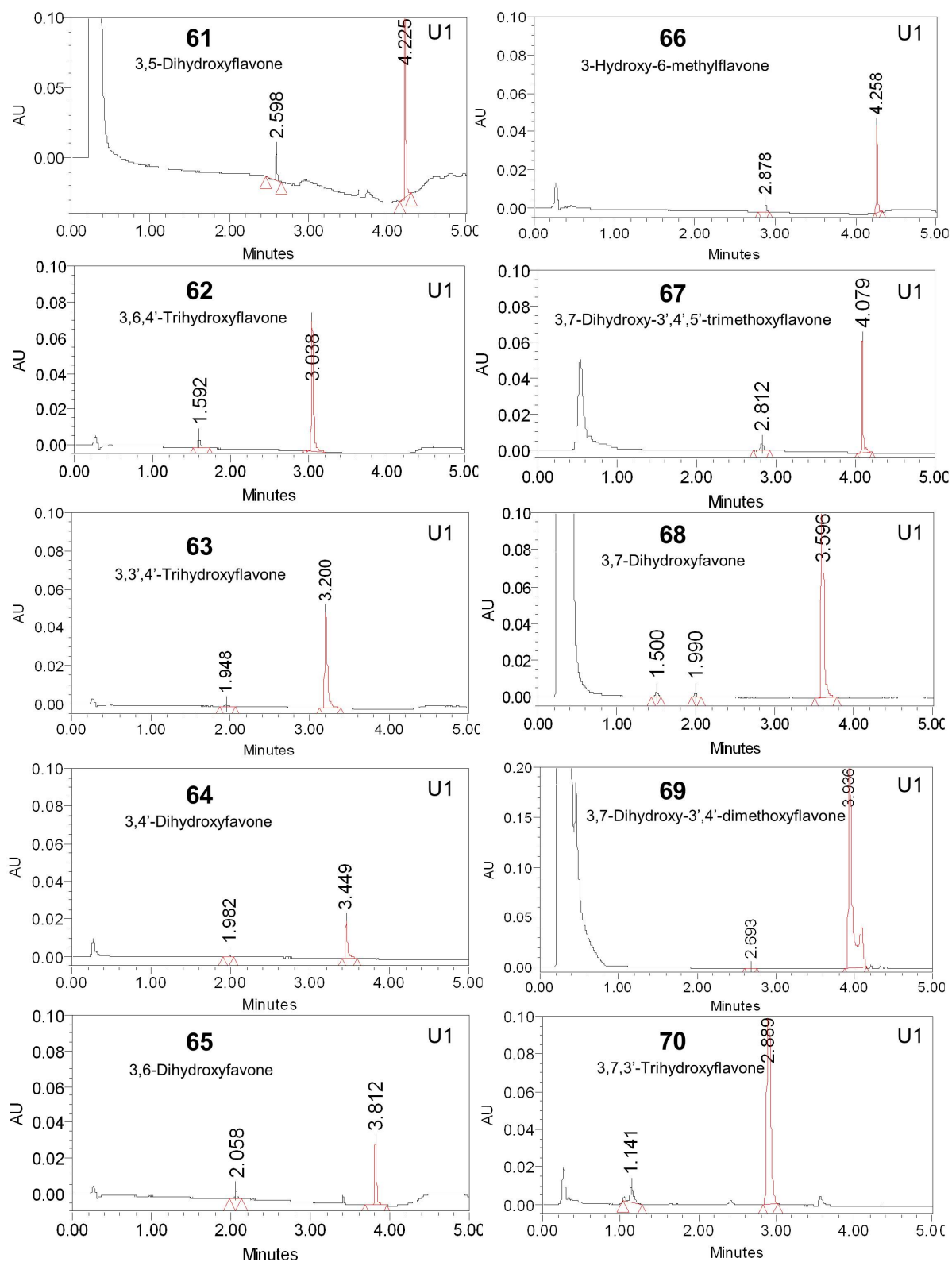


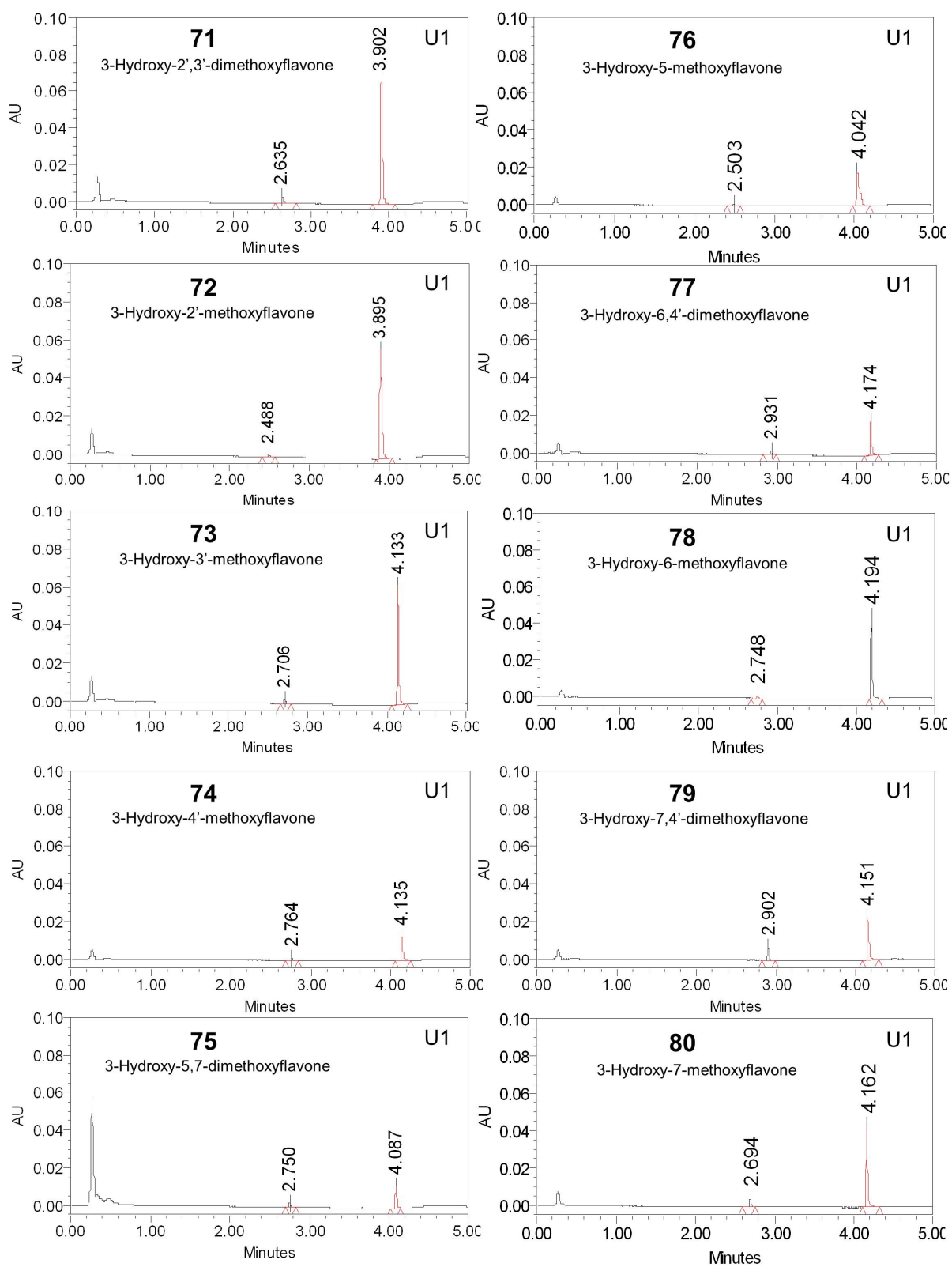


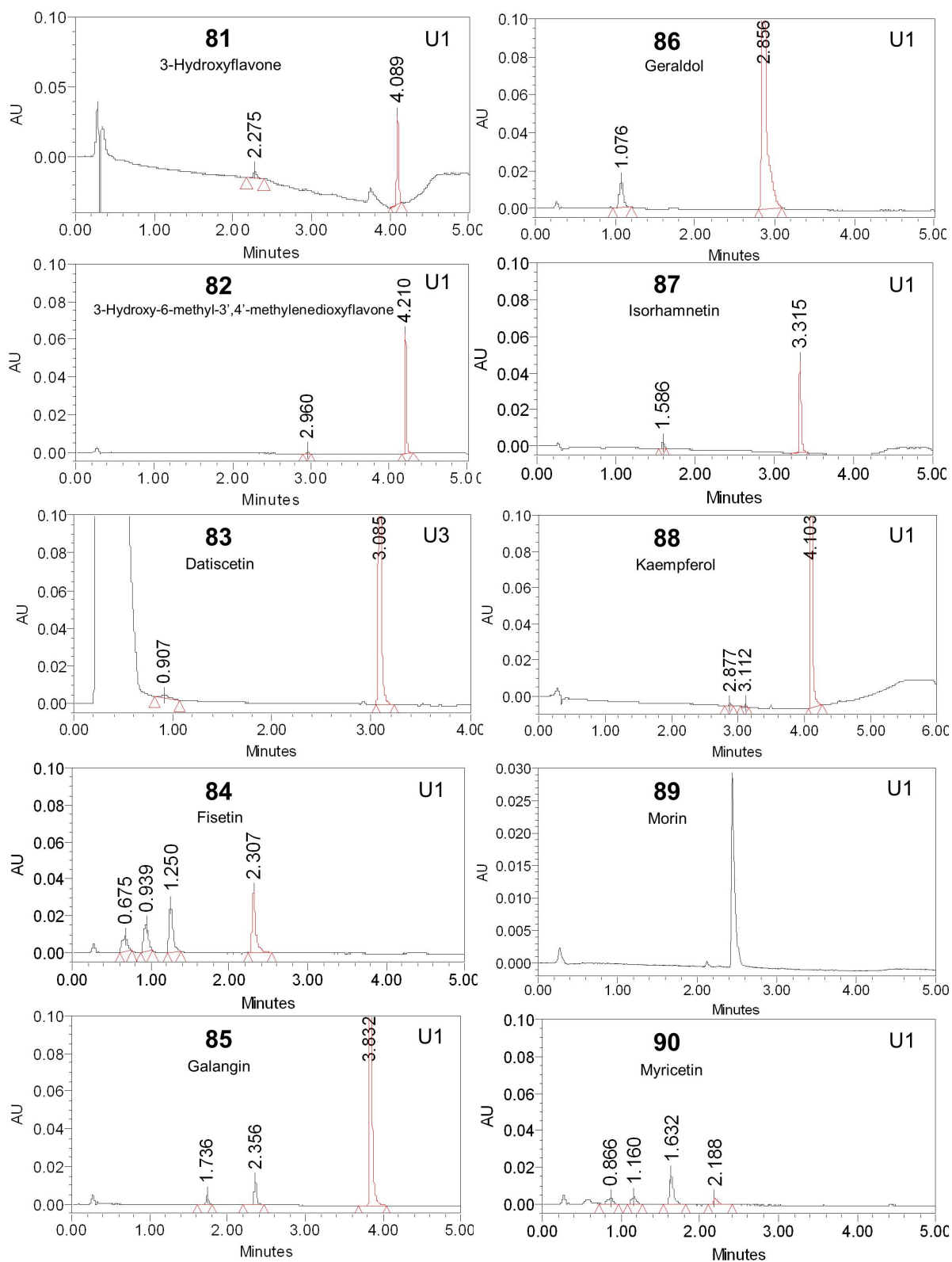


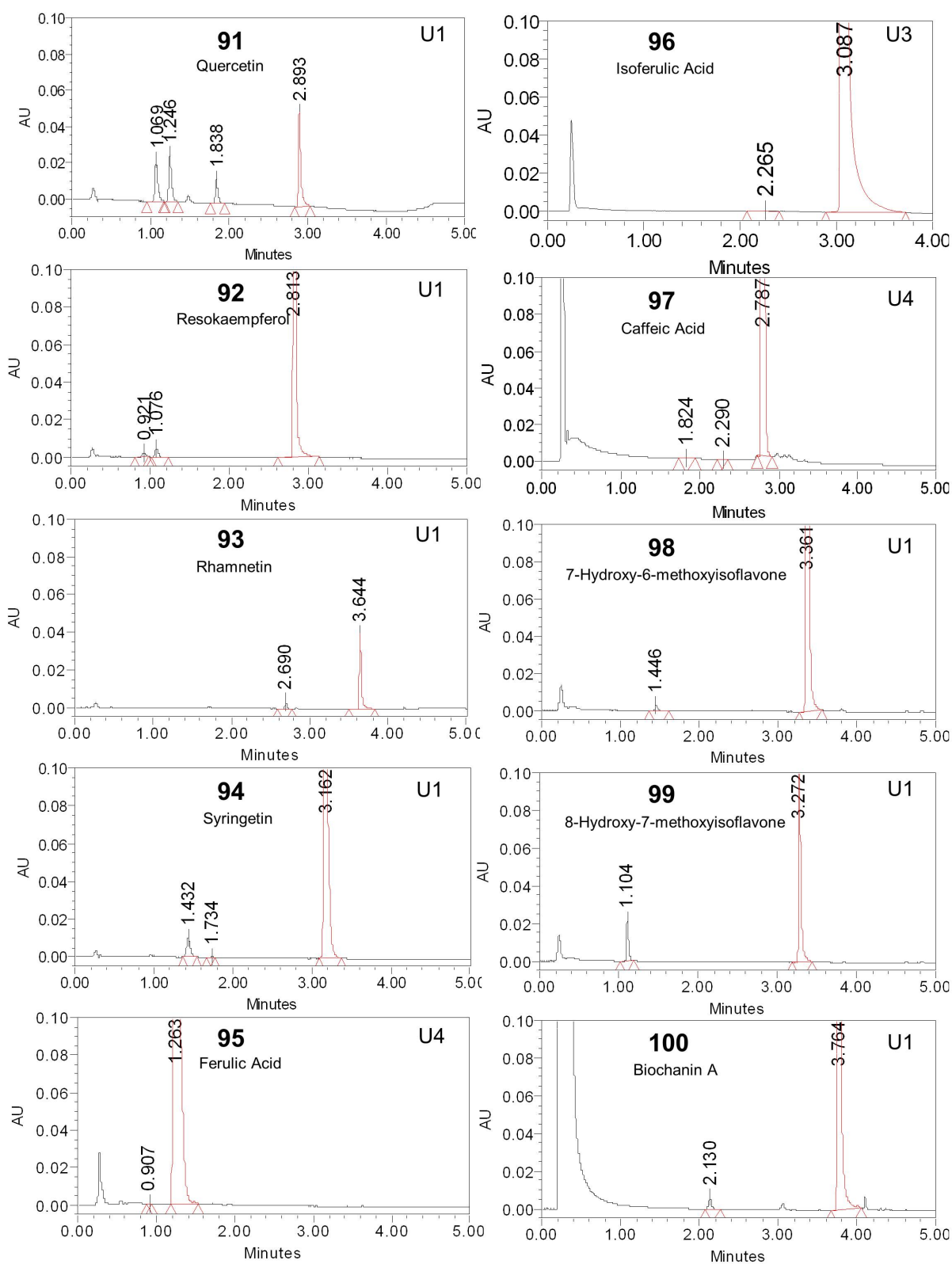


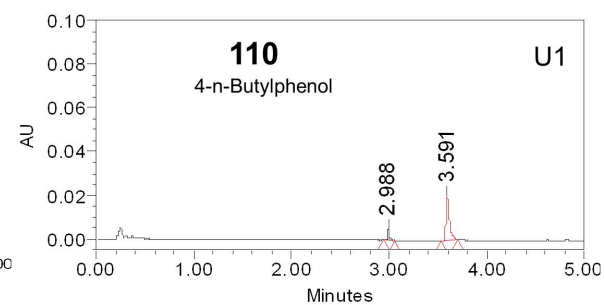
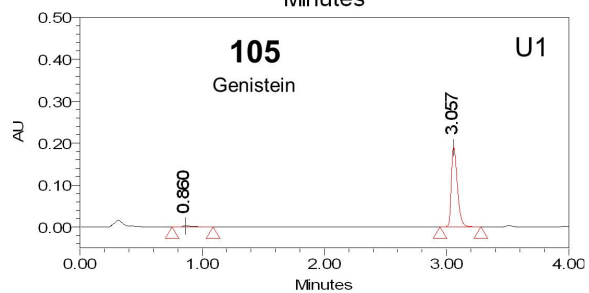
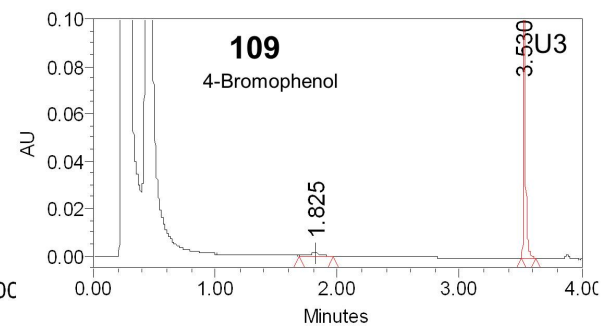
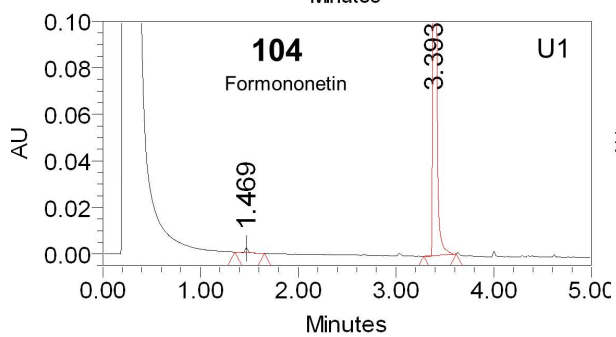
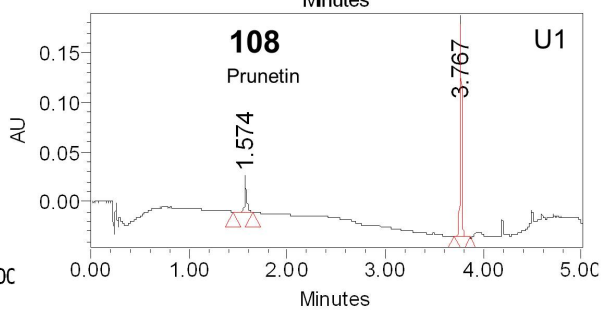
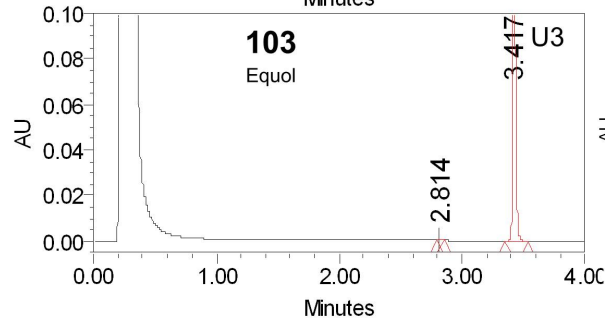
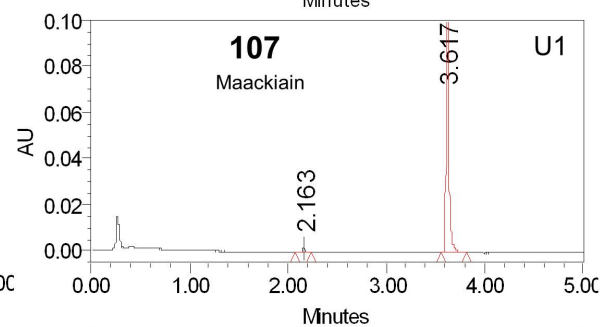
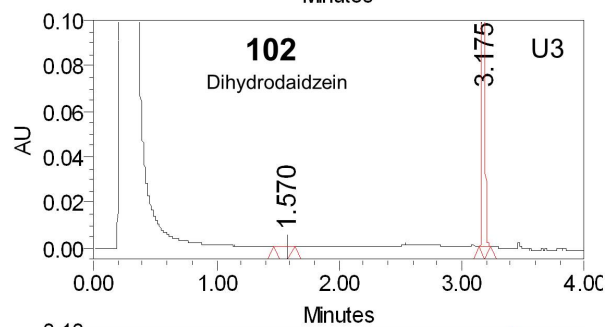
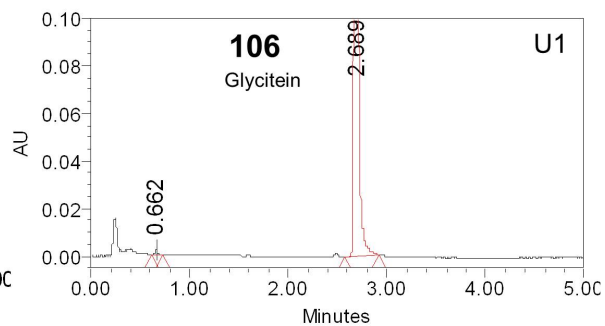
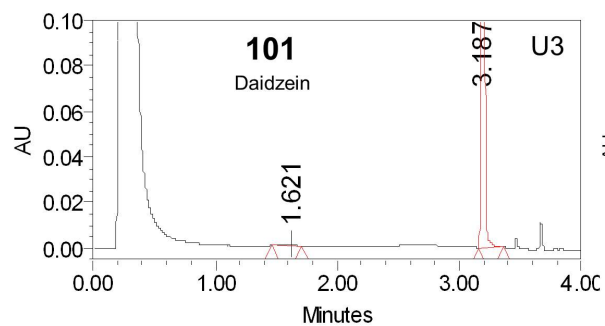


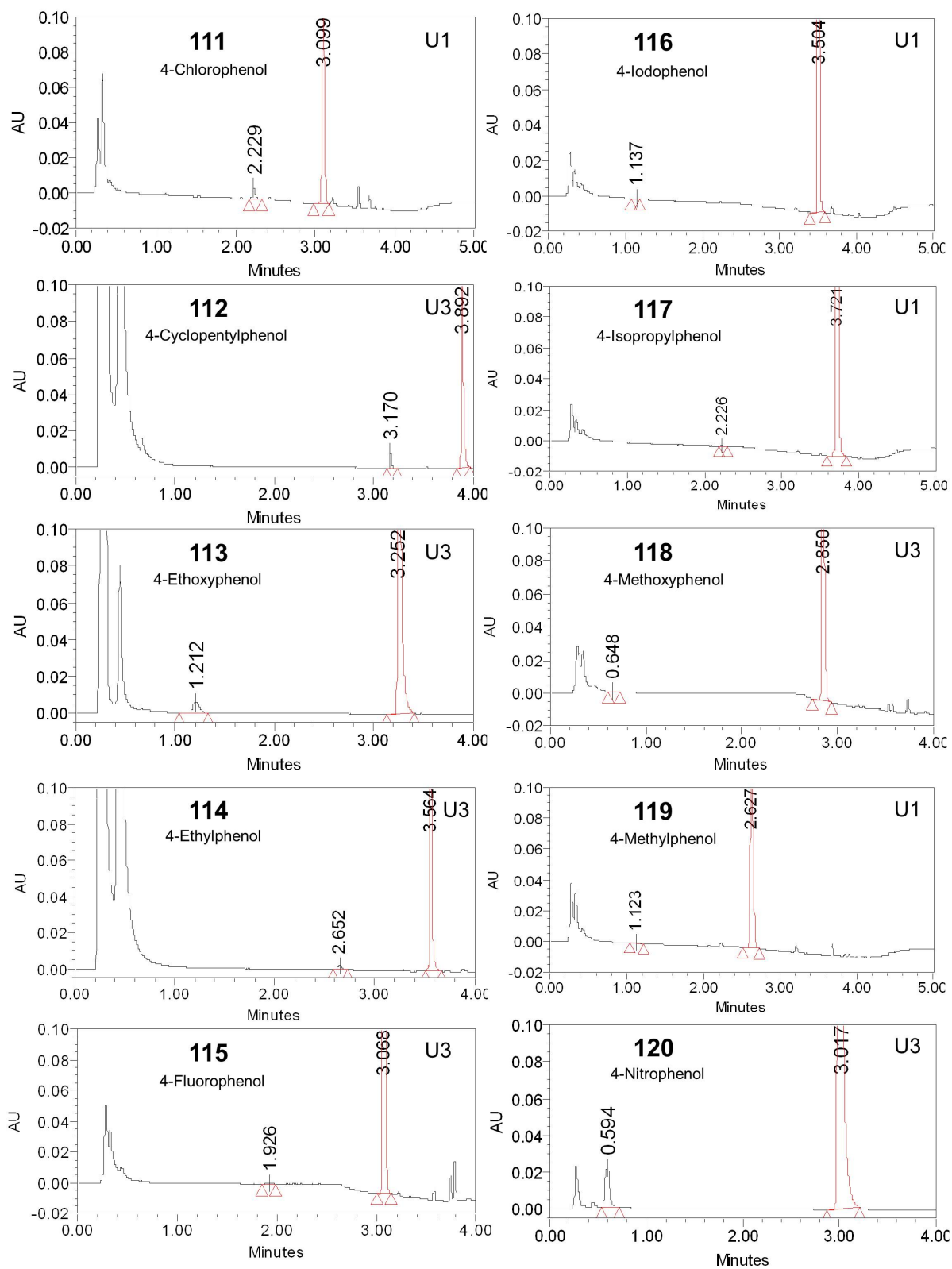


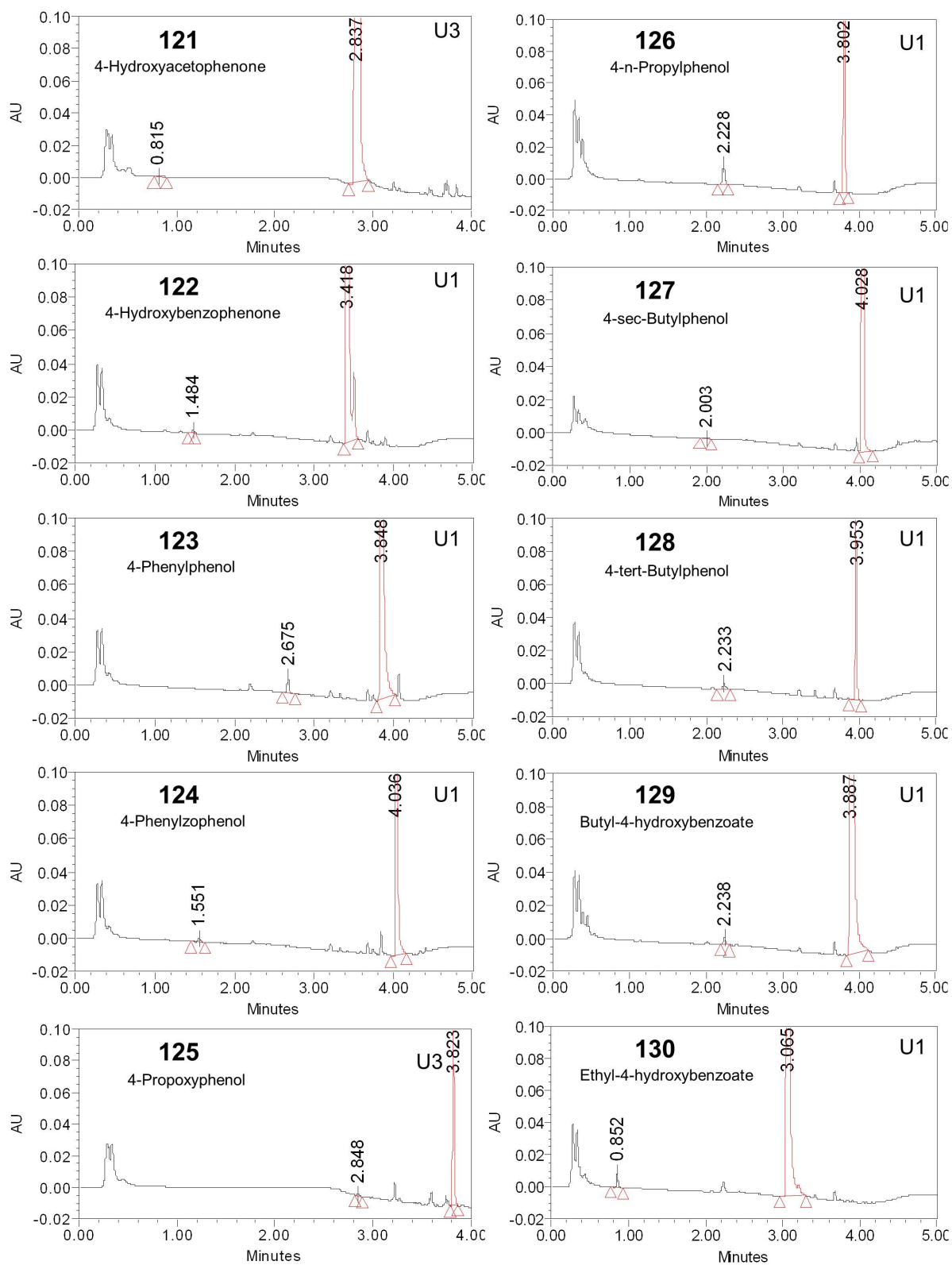


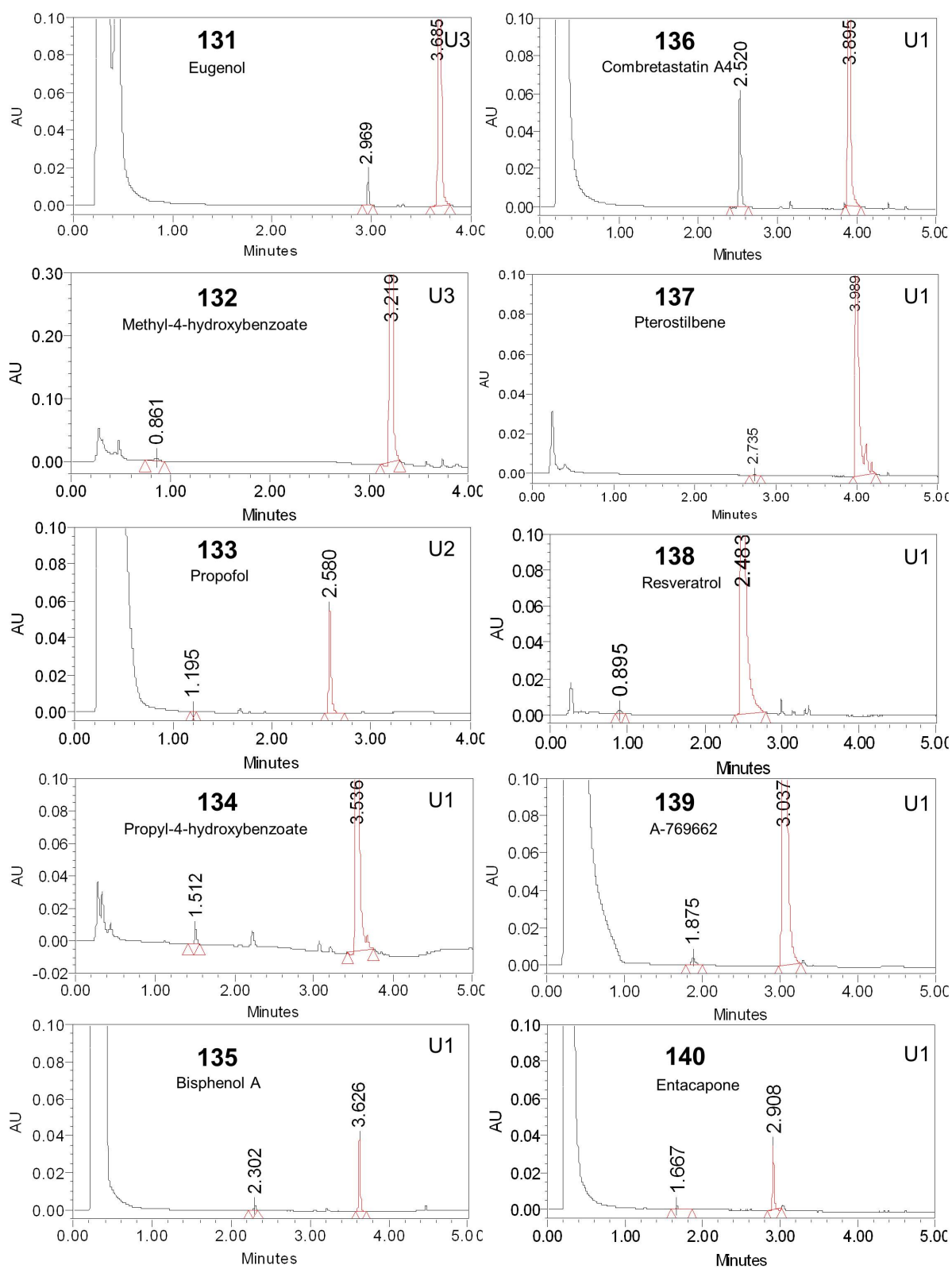


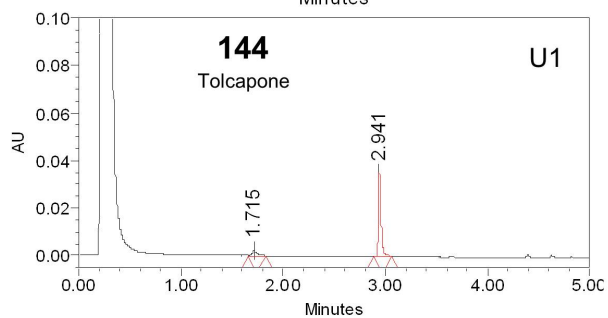
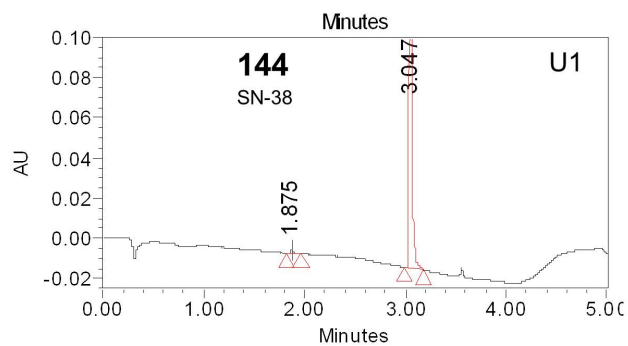
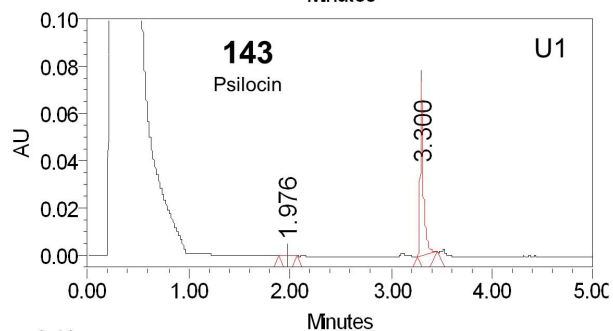
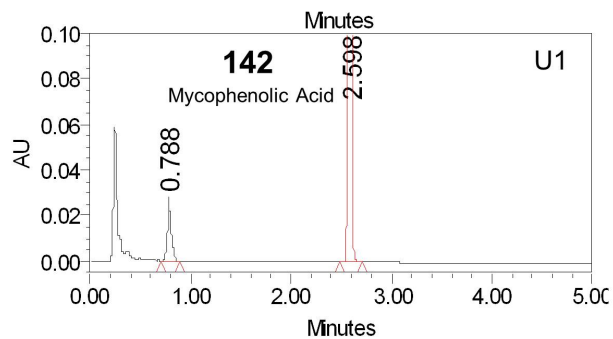
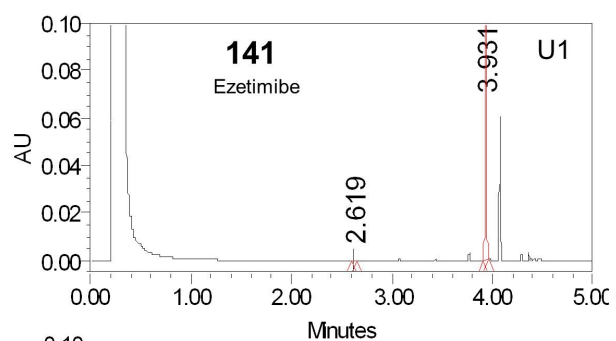












References

- Andersen OM and Markham KR (2006) *Flavonoids – Chemistry, Biochemistry and Applications*. CRC Taylor & Francis, Boca Raton.
- Aprile S, Del Grosso E, Grosa G (2010) Identification of the human UDP-glucuronosyltransferases involved in the glucuronidation of combretastatin A-4. *Drug Metab Dispos* 38(7):1141-6.
- Aumont V, Krisa S, Battaglia E, Netter P, Richard T, Mérillon JM, Magdalou J, Sabolovic N (2001) Regioselective and stereospecific glucuronidation of trans- and cis-resveratrol in human. *Arch Biochem Biophys* 393(2):281-9.
- Barre L, Fournel-Gigleux S, Finel M, Netter P, Magdalou J, Ouzzine M (2007) Substrate specificity of the human UDP-glucuronosyltransferase UGT2B4 and UGT2B7: Identification of a critical aromatic amino acid residue at position 33. *FEBS J* 274(5):1256-64.
- Barreca ML, Carotti A, Carrieri A, Chimirri A, Monforte AM, Calace MP and Rao A (1999) Comparative molecular field analysis (CoMFA) and docking studies of non-nucleoside HIV-1 RT inhibitors (NNIs). *Bioorg Med Chem* 7(11):2283-2292.
- Barve A, Chen C, Hebbar V, Desiderio J, Saw CL and Kong AN (2009) Metabolism, oral bioavailability and pharmacokinetics of chemopreventive kaempferol in rats. *Biopharm Drug Dispos* 30(7):356-65.
- Basu NK, Kole L, Basu M, Chakraborty K, Mitra PS, Owens IS (2008) The major chemical-detoxifying system of UDP-glucuronosyltransferases requires regulated phosphorylation supported by protein kinase C. *J Biol Chem* 283(34):23048-61.
- Basu NK, Kole L, Basu M, McDonagh AF, Owens IS (2007) Targeted inhibition of glucuronidation markedly improves drug efficacy in mice - a model. *Biochem Biophys Res Commun* 360(1):7-13.
- Basu NK, Kole L, Owens IS (2003) Evidence for phosphorylation requirement for human bilirubin UDP-glucuronosyltransferase (UGT1A1) activity. *Biochem Biophys Res Commun* 303(1):98-104.
- Basu NK, Korava M, Garza A, Kubota S, Saha T, Mitra PS, Banerjee R, Rivera J, Owens IS (2005) Phosphorylation of UDP-glucuronosyltransferase regulates substrate specificity. *Proc Natl Acad Sci USA* 102:6285-6290.
- Basu NK, Kubota S, Meselhy MR, Ciotti M, Chowdhury B, Hartori M, Owens IS (2004) Gastrointestinally distributed UDP-glucuronosyltransferase 1A10, which metabolizes estrogens and non-steroidal anti-inflammatory drugs, depends upon phosphorylation. *J Biol Chem* 279:28320-28329.
- Beutler E, Gelbart T, Demina A (1998) Racial variability in the UDP-glucuronosyltransferase 1 (UGT1A1) promoter: a balanced polymorphism for regulation of bilirubin metabolism? *Proc Natl Acad Sci USA* 95:8170-8174.
- Birt DF, Hendrich S, Wang W (2001) Dietary agents in cancer prevention: flavonoids and isoflavonoids. *Pharmacol Ther* 90(2-3):157-177.
- Bock KW (2010) Functions and transcriptional regulation of adult human hepatic UDP-glucuronosyl-transferases (UGTs): mechanisms responsible for interindividual variation of UGT levels. *Biochem Pharmacol* 80(6):771-7.

- Bock KW, Köhle C (2009) Topological aspects of oligomeric UDP-glucuronosyltransferases in endoplasmic reticulum membranes: advances and open questions. *Biochem Pharmacol* 77(9):1458-65.
- Boersma MG, van der Woude H, Bogaards J, Boeren S, Vervoort J, Cnubben NH, van Iersel ML, van Bladeren PJ, Rietjens IM (2002) Regioselectivity of phase II metabolism of luteolin and quercetin by UDP-glucuronosyl transferases. *Chem Res Toxicol* 15(5):662-670.
- Bohnenstengel F, Kroemer HK, Sperker B (1999) In vitro cleavage of paracetamol glucuronide by human liver and kidney beta-glucuronidase: determination of paracetamol by capillary electrophoresis. *J Chromatogr B Biomed Sci Appl* 721(2):295-9.
- Bolam DN, Roberts S, Proctor MR, Turkenburg JP, Dodson EJ, Martinez-Fleites C, Yang M, Davis BG, Davies GJ and Gilbert HJ (2007) The crystal structure of two macrolide glycosyltransferases provides a blueprint for host cell antibiotic immunity. *Proc Natl Acad Sci U S A* 104:5336-5341.
- Bonora-Centelles A, Donato MT, Lahoz A, Pareja E, Mir J, Castell JV, Gómez-Lechón MJ (2010) Functional characterization of hepatocytes for cell transplantation: customized cell preparation for each receptor. *Cell. Transplant* 19,21-8.
- Bosma PJ (2003) Inherited disorders of bilirubin metabolism. *J Hepatol* 38:107-117.
- Strassburg CP (2008) Pharmacogenetics of Gilbert's syndrome. *Pharmacogenomics* 9:703-715.
- Bossuyt X, Blanckaert N (1995) Mechanism of stimulation of microsomal UDP-glucosyltransferase by UDP-N-acetylglucosamine. *Biochem J* 305: 321–328.
- Bowles D, Lim EK, Poppenberger B, Vaistij FE (2006) Glycosyltransferases of lipophilic small molecules. *Annu Rev Plant Biol* 57:567-597
- Brazier-Hicks M, Offen WA, Gershater, MC, Revett TJ, Lim EK, Bowles DJ, Davies GJ, Edwards R (2007) Characterization and engineering of the bifunctional N- and O-glucosyltransferase involved in xenobiotic metabolism in plants. *Proc Natl Acad Sci* 104:20238–20243.
- Brill SS, Furimsky AM, Ho MN, Furniss MJ, Li Y, Green AG, Bradford WW, Green CE, Kapetanovic IM, Iyer LV (2006) Glucuronidation of trans-resveratrol by human liver and intestinal microsomes and UGT isoforms. *J Pharm Pharmacol* 58(4):469-79.
- Buckley DB, Klaassen CD (2007) Tissue- and gender-specific mRNA expression of UDP-glucuronosyltransferases (UGTs) in mice. *Drug Metab Dispos* 35(1):121-7.
- Busby MG, Jeffcoat AR, Bloedon LT, Koch MA, Black T, Dix KJ, Heizer WD, Thomas BF, Hill JM, Crowell JA, Zeisel SH (2002) Clinical characteristics and pharmacokinetics of purified soy isoflavones: single-dose administration to healthy men. *Am J Clin Nutr* 75(1):126-136.
- Chen J, Lin H, Hu M (2003) Metabolism of flavonoids via enteric recycling: role of intestinal disposition. *J Pharmacol Exp Ther* 304(3):1228-35.
- Chen J, Lin H, Hu M (2005) Absorption and metabolism of genistein and its five isoflavone analogs in the human intestinal Caco-2 model. *Cancer Chemother Pharmacol* 55(2):159-69
- Chen Y, Xie S, Chen S, Zeng S (2008). Glucuronidation of flavonoids by recombinant UGT1A3 and UGT1A9. *Biochem Pharmacol* 76(3):416-25.
- Chen YK, Chen SQ, Li X, Zeng S (2005) Quantitative regioselectivity of glucuronidation of quercetin by recombinant UDP-glucuronosyltransferases 1A9 and 1A3 using enzymatic kinetic parameters. *Xenobiotica* 35(10-11):943-954.

- Chohan KK, Paine SW, Waters NJ (2006) Quantitative structure activity relationships in drug metabolism. *Curr Top Med Chem* 6(15):1569-1578.
- Court MH (2001) Acetaminophen UDP-glucuronosyltransferase in ferrets: species and gender differences, and sequence analysis of ferret UGT1A6. *J Vet Pharmacol Ther* 24(6):415-22.
- Court MH (2005) Isoform-selective probe substrates for in vitro studies of human UDP-glucuronosyltransferases. *Methods Enzymol* 400,104-16.
- Cramer III RD; Patterson DE and Bunce J D (1988) Comparative Molecular Field Analysis (CoMFA) 1. Effect of Shape on Binding of Steroids to Carrier Proteins. *J Am Chem Soc* 110:5959-5967.
- Crozier A, Jaganath IB, Clifford MN (2009) Dietary phenolics: chemistry, bioavailability and effects on health. *Nat Prod Rep* 26:1001-43.
- Csala M, Staines AG, Banhegyi G, Mandl J, Coughtrie MWH, Burchell B (2004) Evidence for multiple glucuronide transporters in rat liver microsomes. *Biochem Pharmacol* 68:1353–1362.
- Cubitt HE, Houston JB, Galetin A (2009) Relative importance of intestinal and hepatic glucuronidation-impact on the prediction of drug clearance. *Pharm Res* 26(5):1073-83.
- Dalvie D, Kang P, Zientek M, Xiang C, Zhou S, Obach RS (2008) Effect of intestinal glucuronidation in limiting hepatic exposure and bioactivation of raloxifene in humans and rats. *Chem Res Toxicol* 21(12):2260-71.
- D'Archivio M, Filesi C, Di Benedetto R, Gargiulo R, Giovannini C and Masella R (2007) Polyphenols, dietary sources and bioavailability. *Ann Ist Super Sanita* 43(4):348-61.
- Davis BD, Brodbelt JS (2008) Regioselectivity of human UDP-glucuronosyl-transferase 1A1 in the synthesis of flavonoid glucuronides determined by metal complexation and tandem mass spectrometry. *J Am Soc Mass Spectrom* 19(2):246-256.
- Donato MT, Montero S, Castell JV, Gómez-Lechón MJ, Lahoz A (2010) Validated assay for studying activity profiles of human liver UGTs after drug exposure: inhibition and induction studies. *Anal Bioanal Chem* 396,2251-63.
- Emoto C, Murayama N, Rostami-Hodjegan A, Yamazaki H (2010) Methodologies for investigating drug metabolism at the early drug discovery stage: prediction of hepatic drug clearance and P450 contribution. *Curr Drug Metab* 11(8):678-85.
- Erlund I, Freese R, Marniemi J, Hakala P and Alfthan G (2006) Bioavailability of quercetin from berries and the diet. *Nutr Cancer* 54(1):13-7.
- Ethell BT, Ekins S, Wang J and Burchell B (2002) Quantitative structure activity relationships for the glucuronidation of simple phenols by expressed human UGT1A6 and UGT1A9. *Drug Metab Dispos* 30(6):734-8.
- Fang JL, Beland FA, Doerge DR, Wiener D, Guillemette C, Marques MM, Lazarus P (2002) Characterization of benzo(a)pyrene-trans-7,8-dihydrodiol glucuronidation by human tissue microsomes and overexpressed UDP-glucuronosyltransferase enzymes. *Cancer Res* 62(7):1978-86.
- Finel M, Kurkela M (2008) The UDP-glucuronosyltransferases as oligomeric enzymes. *Curr Drug Metab* 9:70–76.
- Fisher MB, Paine MF, Strelevitz TJ, Wrighton SA (2001) The role of hepatic and extrahepatic UDP-glucuronosyltransferases in human drug metabolism. *Drug Metab Rev* 33(3-4):273-297.
- Fujita K, Sparreboom A (2010) Pharmacogenetics of irinotecan disposition and toxicity: a review. *Curr Clin Pharmacol* 5,209-17.

- Fujiwara R, Nakajima M, Oda S, Yamanaka H, Ikushiro S, Sakaki T, Yokoi T (2010) Interactions between human UDP-glucuronosyltransferase (UGT) 2B7 and UGT1A enzymes. *J Pharm Sci* 99:442-54.
- Fujiwara R, Nakajima M, Yamamoto T, Nagao H, Yokoi T (2009) In silico and in vitro approaches to elucidate the thermal stability of human UDP-glucuronosyltransferase (UGT) 1A9. *Drug Metab Pharmacokinet* 24(3):235-244.
- Fujiwara R, Nakajima M, Yamanaka H, Katoh M, Yokoi T (2007) Interactions between human UGT1A1, UGT1A4, and UGT1A6 affect their enzymatic activities. *Drug Metab Dispos* 35:1781-7.
- Gao S, Hu M (2010) Bioavailability challenges associated with development of anti-cancer phenolics. *Mini Rev Med Chem* 10(6):550-67.
- Ghosal A, Hapangama N, Yuan Y, Achanfuo-Yeboah J, Iannucci R, Chowdhury S, Alton K, Patrick JE, Zbaida S (2004) Identification of human UDP-glucuronosyltransferase enzyme(s) responsible for the glucuronidation of ezetimibe (Zetia). *Drug Metab Dispos* 32(3):314-20.
- Haji-Momenian S, Rieger JM, Macdonald TL and Brown ML (2003) Comparative molecular field analysis and QSAR on substrates binding to cytochrome p450 2D6. *Bioorg Med Chem* 11(24):5545-5554.
- Hanioka N, Ozawa S, Jinno H, Ando M, Saito Y, Sawada J (2001) Human liver UDP-glucuronosyltransferase isoforms involved in the glucuronidation of 7-ethyl-10-hydroxycamptothecin. *Xenobiotica* 31(10):687-99.
- Holder S, Lilly M and Brown ML (2007) Comparative molecular field analysis of flavonoid inhibitors of the PIM-1 kinase. *Bioorg Med Chem* 15(19):6463-6473.
- Houston JB, Kenworthy KE (2000) In vitro-in vivo scaling of CYP kinetic data not consistent with the classical Michaelis-Menten model. *Drug Metab Dispos* 28:246-54.
- Hu M (2007) Commentary: bioavailability of flavonoids and polyphenols: call to arms. *Mol Pharm* 4(6):803-6.
- Hutzler JM, Tracy TS (2002) Atypical kinetic profiles in drug metabolism reactions. *Drug Metab Dispos* 30(4):355-62.
- Innis CA, Shi J and Blundell TL (2000) Evolutionary trace analysis of TGF- β and related growth factors: implications for site-directed mutagenesis. *Protein Eng* 13:839-847.
- Itäaho K, Laakkonen L, Finel M (2010) How many and which amino acids are responsible for the large activity differences between the highly homologous UDP-glucuronosyltransferases (UGT) 1A9 and UGT1A10? *Drug Metab Dispos* 38(4):687-696.
- Iyanagi T (2007) Molecular mechanism of phase I and phase II drug-metabolizing enzymes: implications for detoxification. *Int Rev Cytol* 260:35-112.
- Izukawa T, Nakajima M, Fujiwara R, Yamanaka H, Fukami T, Takamiya M, Aoki Y, Ikushiro S, Sakaki T, Yokoi T (2009) Quantitative analysis of UDP-glucuronosyltransferase (UGT) 1A and UGT2B expression levels in human livers. *Drug Metab Dispos* 37(8):1759-68.
- Jancova P, Anzenbacher P and Anzenbacherova E (2010) Phase II drug metabolizing enzymes. *Biomed Pap Med Fac Univ Palacky Olomouc Czech Repub.* 154(2):103-16.
- Jeong EJ, Liu X, Jia X, Chen J, Hu M (2005b) Coupling of conjugating enzymes and efflux transporters: impact on bioavailability and drug interactions. *Curr Drug Metab* 6(5):455-68.
- Jeong EJ, Liu Y, Lin H, Hu M (2005a) Species- and disposition model-dependent metabolism of raloxifene in gut and liver: role of UGT1A10. *Drug Metab Dispos* 33(6):785-94.

- Joseph TB, Wang SW, Liu X, Kulkarni KH, Wang J, Xu H, Hu M (2007) Disposition of flavonoids via enteric recycling: enzyme stability affects characterization of prunetin glucuronidation across species, organs, and UGT isoforms. *Mol Pharm* 4(6):883-94.
- Kaivosaaari S, Finel M, Koskinen M (2011) N-glucuronidation of drugs and other xenobiotics by human and animal UDP-glucuronosyltransferases. *Xenobiotica* 41(8):652-69
- Kerdpin O, Elliot DJ, Mackenzie PI, Miners JO (2006) Sulfapyrazone C-glucuronidation is catalyzed selectively by human UDP-glucuronosyltransferase 1A9. *Drug Metab Dispos* 34:1950-1953.
- Kerdpin O, Mackenzie PI, Bowalgaha K, Finel M, Miners JO (2009) Influence of N-terminal domain histidine and proline residues on the substrate selectivities of human UDP-glucuronosyltransferase (UGT) 1A1, 1A6, 1A9, 2B7 and 2B10. *Drug Metab Dispos* 37(9):1948-1955.
- Kiang TK, Ensom MH, Chang TK (2005) UDP-glucuronosyltransferases and clinical drug-drug interactions. *Pharmacol Ther* 106(1):97-132.
- Kilford PJ, Stringer R, Sohal B, Houston JB, Galetin A (2009) Prediction of drug clearance by glucuronidation from in vitro data: use of combined cytochrome P450 and UDP-glucuronosyltransferase cofactors in alamethicin-activated human liver microsomes. *Drug Metab Dispos* 37(1):82-9.
- Kobayashi T, Sleeman JE, Coughtrie MWH, Burchell B (2005) Molecular and functional characterization of microsomal UDP-glucuronic acid uptake by members of the nucleotide sugar transporter (NST) family. *Biochem J* 400:281–289.
- Kola I, Landis J (2004) Can the pharmaceutical industry reduce attrition rates? *Nat Rev Drug Discov* 3(8):711-5.
- Kuntz E, Kuntz H-D (2008) *Hepatology: Textbook and Atlas: History, Morphology, Biochemistry, Diagnostics, Clinic, Therapy*. 3rd ed. Berlin, Heidelberg : Springer
- Kurkela M, García-Horsman JA, Luukkanen L, Mörsky S, Taskinen J, Baumann M, Kostainen R, Hirvonen J, Finel M (2003) Expression and characterization of recombinant human UDP-glucuronosyltransferases (UGTs). UGT1A9 is more resistant to detergent inhibition than other UGTs and was purified as an active dimeric enzyme. *J Biol Chem* 278(6):3536-44.
- Laakkonen L, Finel M (2010) A molecular model of the human UGT1A1, its membrane orientation and the interactions between different parts of the enzyme. *Mol Pharmacol* 77(6):931-939
- Larkin MA, Blackshields G, Brown NP, Chenna R, McGettigan PA, McWilliam H, Valentin F, Wallace IM, Wilm A, Lopez R, Thompson JD, Gibson TJ and Higgins DG (2007) Clustal W and Clustal X version 2.0. *Bioinformatics* 23:2947-2948.
- Lazarus P, Sun D (2010) Potential role of UGT pharmacogenetics in cancer treatment and prevention: focus on tamoxifen and aromatase inhibitors. *Drug Metab Rev* 42(1):182-94.
- Lee JK, Abe K, Bridges AS, Patel NJ, Raub TJ, Pollack GM, Brouwer KL (2009) Sex-dependent disposition of acetaminophen sulfate and glucuronide in the in situ perfused mouse liver. *Drug Metab Dispos* 37(9):1916-21.
- Lee-Hilz YY, Stolaki M, van Berkel WJ, Aarts JM, Rietjens IM (2008) Activation of EpRE-mediated gene transcription by quercetin glucuronides depends on their deconjugation. *Food Chem Toxicol* 46(6):2128-34.
- Lépine J, Bernard O, Plante M, Têtu B, Pelletier G, Labrie F, Bélanger A, Guillemette C (2004) Specificity and regioselectivity of the conjugation of estradiol, estrone, and their catecholestrogen and methoxyestrogen metabolites by human uridine diphospho-glucuronosyltransferases expressed in endometrium. *J Clin Endocrinol Metab* 89:5222-32.

- Li C, Wu Q (2007a) Adaptive evolution of multiple-variable exons and structural diversity of drug metabolizing enzymes. *BMC Evol Biol* 7:69.
- Li D, Fournel-Gigleux S, Barré L, Mulliert G, Netter P, Magdalou J, Ouzzine M (2007b) Identification of aspartic acid and histidine residues mediating the reaction mechanism and the substrate specificity of the human UDP-glucuronosyltransferases 1A. *J Biol Chem* 282(50):36514-24.
- Li L, Modolo LV, Escamilla-Trevino, LL, Achnine L, Dixon RA, Wang X (2007) Crystal Structure of *Medicago truncatula* UGT85H2 - Insights into the Structural Basis of a Multifunctional (Iso)flavonoid Glycosyltransferase. *J Mol Biol* 370:951-963
- Li X, Shang L, Wu Y, Abbas S, Li D, Netter P, Ouzzine M, Wang H, Magdalou J (2011) Identification of the human UDP-glucuronosyltransferase isoforms involved in the glucuronidation of the phytochemical ferulic acid. *Drug Metab Pharmacokinet* 26(4):341-50
- Liang SC, Ge GB, Liu HX, Zhang YY, Wang LM, Zhang JW, Yin L, Li W, Fang ZZ, Wu JJ, Li GH, Yang L (2010) Identification and characterization of human UDP-glucuronosyltransferases responsible for the in vitro glucuronidation of daphnetin. *Drug Metab Dispos* 38(6):973-80.
- Liu W, Tang L, Ye L, Cai Z, Xia B, Zhang J, Hu M, Liu Z (2010) Species and gender differences affect the metabolism of emodin via glucuronidation. *AAPS J* 12(3):424-36.
- Liu Y, Hu M (2002) Absorption and metabolism of flavonoids in the caco-2 cell culture model and a perused rat intestinal model. *Drug Metab Dispos* 30(4):370-7.
- Liu Z, Hu M (2007) Natural polyphenol disposition via coupled metabolic pathways. *Expert Opin Drug Metab Toxicol* 3(3):389-406.
- Locuson CW, Tracy TS (2007) Comparative modelling of the human UDPglucuronosyltransferases: insights into structure and mechanism. *Xenobiotica* 37(2):155-68.
- Lu H, Meng X, Li C, Sang S, Patten C, Sheng S, Hong J, Bai N, Winnik B, Ho CT, Yang CS (2003) Glucuronides of tea catechins: enzymology of biosynthesis and biological activities. *Drug Metab Dispos* 31(4):452-61.
- Luukkanen L, Taskinen J, Kurkela M, Kostiaainen R, Hirvonen J, Finel M (2005) Kinetic characterization of the 1A subfamily of recombinant human UDP-glucuronosyltransferases. *Drug Metab Dispos* 33(7):1017-1026.
- Mackenzie PI (1990) Expression of chimeric cDNAs in cell culture defines a region of UDP glucuronosyltransferase involved in substrate selection. *J Biol Chem* 265:3432-3435.
- Mackenzie PI, Bock KW, Burchell B, Guillemette C, Ikushiro S, Iyanagi T, Miners JO, Owens IS, Nebert DW (2005) Nomenclature update for the mammalian UDP glycosyltransferase (UGT) gene superfamily. *Pharmacogenetics Genomics* 15: 677–685.
- Mackenzie PI, Gregory PA, Gardner-Stephen DA, Lewinsky RH, Jorgensen BR, Nishiyama T, Xie W, Radomska-Pandya A (2003) Regulation of UDP glucuronosyltransferase genes. *Curr Drug Metab* 4(3):249-57.
- Magdalou J, Fournel-Gigleux S, Ouzzine M (2010) Insights on membrane topology and structure/function of UDP-glucuronosyltransferases. *Drug Metab Rev* 42(1):154-61.
- Mathijssen RH, van Alphen RJ, Verweij J, Loos WJ, Nooter K, Stoter G, Sparreboom A (2001) Clinical pharmacokinetics and metabolism of irinotecan (CPT-11). *Clin Cancer Res* 7:2182-94.
- Mazur A, Lichti CF, Prather PL, Zielinska AK, Bratton SM, Gallus-Zawada A, Finel M, Miller GP, Radomińska-Pandya A, Moran JH (2009) Characterization of human hepatic and extrahepatic UDP-

- glucuronosyltransferase enzymes involved in the metabolism of classic cannabinoids. *Drug Metab Dispos* 37(7):1496-504.
- Mendieta-Wejebe JE, Correa-Basurto J, García-Segovia EM, Ceballos-Cancino G, Rosales-Hernández MC (2011). Molecular Modeling Used to Evaluate CYP2C9-Dependent Metabolism: Homology Modeling, Molecular Dynamics and Docking Simulations. *Curr Drug Metab* (in press)
- Miley MJ, Zielinska AK, Keenan JE, Bratton SM, Radomska-Pandya A, Redinbo MR (2007) Crystal structure of the cofactor-binding domain of the human phase II drug-metabolism enzyme UDP-glucuronosyltransferase 2B7. *J Mol Biol* 369(2):498-511.
- Miners JO, Knights KM, Houston JB, Mackenzie PI (2006) In vitro-in vivo correlation for drugs and other compounds eliminated by glucuronidation in humans: pitfalls and promises. *Biochem Pharmacol* 71(11):1531-9.
- Miners JO, Mackenzie PI, Knights KM (2010) The prediction of drug-glucuronidation parameters in humans: UDP-glucuronosyltransferase enzyme-selective substrate and inhibitor probes for reaction phenotyping and in vitro-in vivo extrapolation of drug clearance and drug-drug interaction potential. *Drug Metab Rev* 42(1):189-201.
- Miners JO, Smith PA, Sorich MJ, McKinnon RA, Mackenzie PI (2004) Predicting human drug glucuronidation parameters: application of in vitro and in silico modeling approaches. *Annu Rev Pharmacol Toxicol* 44:1-25.
- Mitra PS, Basu NK, Basu M, Chakraborty S, Saha T, Owens IS (2010) Regulated phosphorylation of a major UDP-glucuronosyltransferase isozyme by tyrosine kinases dictates endogenous substrate-selection for detoxification. *J Biol Chem* 286(2):1639-48
- Mitra PS, Basu NK, Owens IS (2009) Src supports UDP-glucuronosyltransferase-2B7 detoxification of catechol estrogens associated with breast cancer. *Biochem Biophys Res Commun* 382(4):651-6.
- Mittler M, Bechthold A and Schulz GE (2007) Structure and action of the C-C bond-forming glycosyltransferase UrdGT2 involved in the biosynthesis of the antibiotic urdamycin. *J Mol Biol* 372:67-76.
- Mizuma T (2009) Intestinal glucuronidation metabolism may have a greater impact on oral bioavailability than hepatic glucuronidation metabolism in humans: a study with raloxifene, substrate for UGT1A1, 1A8, 1A9, and 1A10. *Int J Pharm* 378(1-2):140-1.
- Mochizuki M, Kajiya K, Terao J, Kaji K, Kumazawa S, Nakayama T, Shimoi K (2004) Effect of quercetin conjugates on vascular permeability and expression of adhesion molecules. *Biofactors* 22(1-4):201-4.
- Modolo LV, Li L, Pan H, Blount JW, Dixon RA, Wang X (2009) Crystal structures of glycosyltransferase UGT78G1 reveal the molecular basis for glycosylation and deglycosylation of (iso) flavonoids. *J Mol Biol* 392(5):1292-302.
- Mulichak AM, Losey HC, Lu W, Wawrzak Z, Walsh CT and Garavito RM (2003) Structure of the TDP-epi-vancosaminyltransferase GtfA from the chloroeremomycin biosynthetic pathway. *Proc Natl Acad Sci U S A* 100:9238-9243.
- Mulichak AM, Losey HC, Walsh CT and Garavito RM (2001) Structure of the UDPglucosyltransferase GtfB that modifies the heptapeptide aglycone in the biosynthesis of vancomycin group antibiotics. *Structure* 9:547-557.
- Mulichak AM, Lu W, Losey HC, Walsh CT and Garavito RM (2004) Crystal structure of vancosaminyltransferase GtfD from the vancomycin biosynthetic pathway: interactions with acceptor and nucleotide ligands. *Biochemistry* 43:5170-5180.

- Nishiyama T, Fujishima M, Masuda Y, Izawa T, Ohnuma T, Ogura K and Hiratsuka A (2008) Amino acid positions 69-132 of UGT1A9 are involved in the C-glucuronidation of phenylbutazone. *Arch Biochem Biophys* 478:75-80.
- O'Dwyer PJ, Catalano RB (2006) Uridine diphosphate glucuronosyltransferase (UGT) 1A1 and irinotecan: practical pharmacogenomics arrives in cancer therapy. *J Clin Oncol* 24:4534-8.
- Offen W, Martinez-Fleites C, Yang M, Kiat-Lim E, Davis BG, Tarling CA, Ford CM, Bowles DJ, Davies GJ (2006) Structure of a flavonoid glucosyltransferase reveals the basis for plant natural product modification. *EMBO J* 25:1396-1405.
- Ohno S, Kawana K, Nakajin S (2008) Contribution of UDP-glucuronosyltransferase 1A1 and 1A8 to morphine-6-glucuronidation and its kinetic properties. *Drug Metab Dispos* 36:688-94.
- Ohno S, Nakajin S (2009) Determination of mRNA expression of human UDP-glucuronosyltransferases and application for localization in various human tissues by real-time reverse transcriptase-polymerase chain reaction. *Drug Metab Dispos* 37(1):32-40.
- O'Leary KA, Day AJ, Needs PW, Mellon FA, O'Brien NM, Williamson G (2003) Metabolism of quercetin-7- and quercetin-3-glucuronides by an in vitro hepatic model: the role of human beta-glucuronidase, sulfotransferase, catechol-O-methyltransferase and multi-resistant protein 2 (MRP2) in flavonoid metabolism. *Biochem Pharmacol* 65(3):479-91.
- Olson KC, Dellinger RW, Zhong Q, Sun D, Amin S, Spratt TE, Lazarus P (2009) Functional characterization of low-prevalence missense polymorphisms in the UDP-glucuronosyltransferase 1A9 gene. *Drug Metab Dispos* 37(10):1999-2007.
- Osmani SA, Bak S, Møller BL (2009) Substrate specificity of plant UDP-dependent glycosyltransferases predicted from crystal structures and homology modeling. *Phytochemistry* 70(3):325-347
- Otake Y, Hsieh F and Walle T (2002) Glucuronidation versus oxidation of the flavonoid galangin by human liver microsomes and hepatocytes. *Drug Metab Dispos* 30(5):576-581.
- Owens IS, Basu NK, Banerjee R (2005) UDP-glucuronosyltransferases: gene structures of UGT1 and UGT2 families. *Methods Enzymol* 400:1-22.
- Paquette S, Moller BL, Bak S (2003) On the origin of family 1 plant glycosyltransferases. *Phytochemistry* 62:399-413.
- Patana A-S, Kurkela M, Finel M, Goldman A (2008) Mutation analysis in UGT1A9 suggests a relationship between substrate and catalytic residues in UDP-glucuronosyltransferases. *Protein Eng Des Sel* 21:537-543.
- Radominska-Pandya A, Bratton SM, Redinbo MR, Miley MJ (2010) The crystal structure of human UDP-glucuronosyltransferase 2B7 C-terminal end is the first mammalian UGT target to be revealed: the significance for human UGTs from both the 1A and 2B families. *Drug Metab Rev* 42(1):128-39.
- Radominska-Pandya A, Czernik PJ, Little JM, Battaglia E, Mackenzie PI (1999) Structural and functional studies of UDP-glucuronosyltransferases. *Drug Metab Rev* 31: 817-899
- Radominska-Pandya A, Ouzzine M, Fournel-Gigleux S, Magdalou J (2005) Structure of UDP-glucuronosyltransferases in membranes. *Methods Enzymol* 400:116-47.
- Ross J, Li Y, Lim E, Bowles DJ (2001) Higher plant glycosyltransferases. *Genome Biol* 2(2):REVIEWS3004.
- Ross JA, Kasum CM (2002) Dietary flavonoids: bioavailability, metabolic effects, and safety. *Annu Rev Nutr* 22:19-34.

- Rouguieg K, Picard N, Sauvage FL, Gaulier JM, Marquet P (2010) Contribution of the different UDP-glucuronosyltransferase (UGT) isoforms to buprenorphine and norbuprenorphine metabolism and relationship with the main UGT polymorphisms in a bank of human liver microsomes. *Drug Metab Dispos* 38:40-5.
- Said M, Ziegler JC, Magdalou J, Ellass A and Vergoten G (1996) Inhibition of bilirubin Udp-glucuronosyltransferase: A comparative molecular field analysis (COMFA). *Quant Struct-Act Relat* 15:382-388.
- Sali A, Blundell TL (1993) Comparative protein modelling by satisfaction of spatial restraints. *J Mol Biol* 234(3):779-815.
- Segel IH (1993) *Enzyme kinetics: behavior and analysis of rapid equilibrium and steady state enzyme systems*, New ed. Wiley, New York
- Setchell KD, Brown NM, Desai P, Zimmer-Nechemias L, Wolfe BE, Brashear WT, Kirschner AS, Cassidy A, Heubi JE (2001) Bioavailability of pure isoflavones in healthy humans and analysis of commercial soy isoflavone supplements. *J Nutr* 131(4 Suppl):1362S-1375S.
- Shao H, He X, Achnine L, Blount JW, Dixon RA, Wang X (2005) Crystal structures of a multifunctional triterpene/flavonoid glycosyltransferase from *Medicago truncatula*. *Plant Cell* 17:3141-3154.
- Sharma V, Duffel MW (2002) Comparative molecular field analysis of substrates for an aryl sulfotransferase based on catalytic mechanism and protein homology modeling. *J Med Chem* 45(25):5514-22.
- Sharma V, Duffel MW (2005) A comparative molecular field analysis-based approach to prediction of sulfotransferase catalytic specificity. *Methods Enzymol* 400:249-63.
- Shelby MK, Cherrington NJ, Vansell NR, Klaassen CD (2003) Tissue mRNA expression of the rat UDP-glucuronosyltransferase gene family. *Drug Metab Dispos* 31(3):326-33.
- Shimizu M, Matsumoto Y, Yamazaki H (2007) Effects of propofol analogs on glucuronidation of propofol, an anesthetic drug, by human liver microsomes. *Drug Metab Lett* 1:77-9.
- Shimoi K, Nakayama T (2005) Glucuronidase deconjugation in inflammation. *Methods Enzymol* 400:263-72.
- Shimoi K, Saka N, Kaji K, Nozawa R, Kinae N. (2000) Metabolic fate of luteolin and its functional activity at focal site. *Biofactors* 12(1-4):181-6.
- Shimoi K, Saka N, Nozawa R, Sato M, Amano I, Nakayama T, Kinae N (2001) Deglucuronidation of a flavonoid, luteolin monoglucuronide, during inflammation. *Drug Metab Dispos* 29(12):1521-4.
- Siissalo S, Zhang H, Stilgenbauer E, Kaukonen AM, Hirvonen J, Finel M. (2008) The expression of most UDP-glucuronosyltransferases (UGTs) is increased significantly during Caco-2 cell differentiation, whereas UGT1A6 is highly expressed also in undifferentiated cells. *Drug Metab Dispos* 36(11):2331-6.
- Singh R, Wu B, Tang L, Hu M (2011) Uridine diphosphate glucuronosyltransferase isoform-dependent regiospecificity of glucuronidation of flavonoids. *J Agric Food Chem* 59(13):7452-64.
- Singh R, Wu BJ, Tang L, Liu ZQ, Hu M (2010) Identification of the Position of Mono-O-Glucuronide of Flavones and Flavonols by Analyzing Shift in Online UV Spectrum (Amax) Generated from an Online Diode-arrayed Detector. *J Agric Food Chem* 58(17):9384-9395
- Smith PA, Sorich MJ, Low LS, McKinnon RA, Miners JO (2004) Towards integrated ADME prediction: past, present and future directions for modelling metabolism by UDP-glucuronosyltransferases. *J Mol Graph Model* 22(6):507-17.

- Smith PA, Sorich MJ, McKinnon RA, Miners JO (2003) In silico insights: chemical and structural characteristics associated with uridine diphosphate glucuronosyltransferase substrate selectivity. *Clin Exp Pharmacol Physiol* 30(11):836-840.
- Soars MG, Ring BJ, Wrighton SA (2003) The effect of incubation conditions on the enzyme kinetics of udp-glucuronosyltransferases. *Drug Metab Dispos* 31(6):762-7.
- Sorich MJ, Miners JO, McKinnon RA, Smith PA (2004) Multiple pharmacophores for the investigation of human UDP-glucuronosyltransferase isoform substrate selectivity. *Mol Pharmacol* 65(2):301-8.
- Sorich MJ, Smith PA, McKinnon RA, Miners JO (2002) Pharmacophore and quantitative structure activity relationship modelling of UDP-glucuronosyltransferase 1A1 (UGT1A1) substrates. *Pharmacogenetics* 12(8):635-645.
- Sorich MJ, Smith PA, Miners JO, Mackenzie PI, McKinnon R (2008) Recent advances in the in silico modelling of UDP glucuronosyltransferase substrates. *Curr Drug Metab* 9(1):60-9.
- Starlard-Davenport A, Xiong Y, Bratton S, Gallus-Zawada A, Finel M, Radomska-Pandya A (2007) Phenylalanine(90) and phenylalanine(93) are crucial amino acids within the estrogen binding site of the human UDP-glucuronosyltransferase 1A10. *Steroids* 72(1):85-94.
- Sten T, Bichlmaier I, Kuuranne T, Leinonen A, Yli-Kauhialuoma J, Finel M (2009) UDP-glucuronosyltransferases (UGTs) 2B7 and UGT2B17 display converse specificity in testosterone and epitestosterone glucuronidation, whereas UGT2A1 conjugates both androgens similarly. *Drug Metab Dispos* 37(1):417-23.
- Stone AN, Mackenzie PI, Galetin A, Houston JB, Miners JO (2003) Isoform selectivity and kinetics of morphine 3- and 6-glucuronidation by human udp-glucuronosyltransferases: evidence for atypical glucuronidation kinetics by UGT2B7. *Drug Metab Dispos* 31(10):1086-9.
- Strassburg CP (2008) Pharmacogenetics of Gilbert's syndrome. *Pharmacogenomics* 9:703-715.
- Sun H, Zhang L, Chow EC, Lin G, Zuo Z, Pang KS (2008) A catenary model to study transport and conjugation of baicalein, a bioactive flavonoid, in the Caco-2 cell monolayer: demonstration of substrate inhibition. *J Pharmacol Exp Ther* 326(1):117-26.
- Takaoka Y, Ohta M, Takeuchi A, Miura K, Matsuo M, Sakaeda T, Sugano A, Nishio H (2010) Ligand orientation governs conjugation capacity of UDP-glucuronosyltransferase 1A1. *J.Biochem* 148(1):25-8.
- Tang L, Singh R, Liu Z, Hu M (2009) Structure and concentration changes affect characterization of UGT isoform-specific metabolism of isoflavones. *Mol Pharm* 6(5):1466-82.
- Tang L, Ye L, Singh R, Wu B, Lv C, Zhao J, Liu Z, Hu M (2010) Use of glucuronidation fingerprinting to describe and predict mono- and dihydroxyflavone metabolism by recombinant UGT isoforms and human intestinal and liver microsomes. *Mol Pharm* 7(3):664-79.
- Tukey RH, Strassburg CP (2000) Human UDP-glucuronosyltransferases: metabolism, expression, and disease. *Annu Rev Pharmacol Toxicol* 40:581-616.
- Uchaipichat V, Mackenzie PI, Guo XH, Gardner-Stephen D, Galetin A, Houston JB, Miners JO (2004) Human udp-glucuronosyltransferases: isoform selectivity and kinetics of 4-methylumbelliferone and 1-naphthol glucuronidation, effects of organic solvents, and inhibition by diclofenac and probenecid. *Drug Metab Dispos* 32(4):413-423.
- Van Der Spoel D, Lindahl E, Hess B, Groenhof G, Mark AE, Berendsen HJ (2005) GROMACS: fast, flexible and free. *J Comput Chem* 26:1701 – 1718.

- Villeneuve L, Girard H, Fortier LC, Gagné JF, Guillemette C (2003) Novel functional polymorphisms in the UGT1A7 and UGT1A9 glucuronidating enzymes in Caucasian and African-American subjects and their impact on the metabolism of 7-ethyl-10-hydroxycamptothecin and flavopiridol anticancer drugs. *J Pharmacol Exp Ther* 307(1):117-28.
- Volak LP, Court MH (2010) Role for protein kinase C delta in the functional activity of human UGT1A6: implications for drug-drug interactions between PKC inhibitors and UGT1A6. *Xenobiotica* 40(5):306-18.
- Wang JF, Chou KC (2010) Molecular modeling of cytochrome P450 and drug metabolism. *Curr Drug Metab* 11(4):342-6.
- Wang SW, Kulkarni KH, Tang L, Wang JR, Yin T, Daidoji T, Yokota H, Hu M (2009) Disposition of flavonoids via enteric recycling: UDP-glucuronosyltransferase (UGT) 1As deficiency in Gunn rats is compensated by increases in UGT2Bs activities. *J Pharmacol Exp Ther* 329(3):1023-31.
- Wei DG, Yang GF, Wan J and Zhan CG (2005) Binding model construction of antifungal 2-aryl-4-chromanones using CoMFA, CoMSIA, and QSAR analyses. *J Agric Food Chem* 53(5):1604-1611.
- Williamson G, Barron D, Shimo K, Terao J (2005) In vitro biological properties of flavonoid conjugates found in vivo. *Free Radic Res* 39(5):457-69.
- Wishart DS (2007) Improving early drug discovery through ADME modelling: an overview. *Drugs R D* 8(6):349-62.
- Wong CC, Meini W, Glatt HR, Barron D, Stalmach A, Steiling H, Crozier A, Williamson G (2010) In vitro and in vivo conjugation of dietary hydroxycinnamic acids by UDP-glucuronosyltransferases and sulfotransferases in humans. *J Nutr Biochem* 21(11):1060-8.
- Wong YC, Zhang L, Lin G, Zuo Z (2009) Structure-activity relationships of the glucuronidation of flavonoids by human glucuronosyltransferases. *Expert Opin Drug Metab Toxicol* 5(11):1399-1419.
- Wu B, Kulkarni K, Basu S, Zhang S, Hu M (2011) First-pass metabolism via UDP-glucuronosyltransferase: a barrier to oral bioavailability of phenolics. *J Pharm Sci* 100(9):3655-81.
- Xiong Y, Bernardi D, Bratton S, Ward MD, Battaglia E, Finel M, Drake RR, Radominska-Pandya A (2006) Phenylalanine 90 and 93 are localized within the phenol binding site of human UDP-glucuronosyltransferase 1A10 as determined by photoaffinity labeling, mass spectrometry, and site-directed mutagenesis. *Biochemistry* 45(7):2322-32.
- Yin H, Bennett G, Jones JP (1994) Mechanistic studies of uridine diphosphate glucuronosyltransferase. *Chem Biol Interact* 90(1):47-58.
- Zakim D, Dannenberg AJ (1992) How does the microsomal membrane regulate UDP-glucuronosyltransferases? *Biochem Pharmacol* 43(7):1385-93.
- Zhang C, Bitto E, Goff RD, Singh S, Bingman CA, Griffith BR, Albermann C, Phillips GN, Jr and Thorson JS (2008) Biochemical and structural insights of the early glycosylation steps in calicheamicin biosynthesis. *Chem Biol* 15:842-853.
- Zhang D, Zhang D, Cui D, Gambardella J, Ma L, Barros A, Wang L, Fu Y, Rahematpura S, Nielsen J, Donegan M, Zhang H, Humphreys WG (2007) Characterization of the UDP glucuronosyltransferase activity of human liver microsomes genotyped for the UGT1A1*28 polymorphism. *Drug Metab Dispos* 35:2270-80.
- Zhang L, Lin G, Zuo Z (2006) Position preference on glucuronidation of mono-hydroxyflavones in human intestine. *Life Sci* 78(24):2772-80.

- Zhou J, Tracy TS, Remmel RP (2011) Correlation between Bilirubin Glucuronidation and Estradiol-3-Glucuronidation in the Presence of Model UGT1A1 Substrates/Inhibitors. *Drug Metab Dispos* 39:322-9.
- Zhou J, Zhang J, Xie W (2005) Xenobiotic nuclear receptor-mediated regulation of UDP-glucuronosyl-transferases. *Curr Drug Metab* 6(4):289-98.
- Zhou Q, Zheng Z, Xia B, Tang L, Lv C, Liu W, Liu Z, Hu M (2010) Use of isoform-specific UGT metabolism to determine and describe rates and profiles of glucuronidation of wogonin and oroxylin A by human liver and intestinal microsomes. *Pharm Res* 27(8):1568-83.